Ghent University
Faculty of Pharmaceutical Sciences

EXPLORING THE RELATION BETWEEN THE INTRACELLULAR FATE AND BIOLOGICAL ACTIVITY OF NUCLEIC ACID NANOPARTICLES

STUDIE NAAR DE RELATIE TUSSEN HET INTRACELLULAIR GEDRAG EN DE BIOLOGISCHE ACTIVITEIT VAN NUCLEÏNEZUUR NANOPARTIKELS

Katrien Remaut
Pharmacist

Thesis submitted to obtain the degree of
Doctor in Pharmaceutical Sciences

Proefschrift voorgedragen tot het bekomen van de graad van
Doctor in de Farmaceutische Wetenschappen

2007

Dean:
Prof. Dr. Apr. Jean Paul Remon

Promoters:
Prof. Dr. Apr. Stefaan De Smedt
Prof. Dr. Apr. Jo Demeester

Laboratory of General Biochemistry and Physical Pharmacy

Gent, 4 april 2007

De promotoren

Prof. Dr. Apr. Jo Demeester

Prof. Dr. Apr. Stefaan De Smedt

De auteur

Apr. Katrien Remaut

DANKWOORD

Na jaren van wetenschappelijk onderzoek is eindelijk het moment aangebroken waarop ik vele mensen mag bedanken die, rechtstreeks of onrechtstreeks, hebben bijgedragen tot het tot stand komen van dit proefschrift.

Vooreerst had ik graag mijn promotoren Prof. Dr. Stefaan De Smedt en Prof. Dr. Jo Demeester bedankt om me de kans te geven een doctoraat aan te vatten aan het Labo Algemene Biochemie en Fysische Farmacie. Tijdens het vierde jaar van mijn studies kwam ik reeds bij jullie terecht voor het uitvoeren van een onderzoeksstage. Een goed jaar later kreeg ik de kans om te beginnen aan mijn 'eigen' onderzoeksproject met een 'eigen' bureau en (mits wat vertraging) een 'eigen' computer. Dit 'eigen' project bleek toch meer te vereisen dan het uitvoeren van een min of meer afgelijnde onderzoeksstage, maar na enkele maanden van artikels doorworstelen en het verkennen van het nieuwe onderzoeksdomein kon het wetenschappelijk onderzoek echt van start gaan. Stefaan, gedurende vele jaren kon ik rekenen op je niet aflatende enthousiasme en begeleiding. Je leerde me de koe bij de horens te vatten en steeds opnieuw op zoek te gaan naar dat 'one good idea'. Als geen ander slaag je erin om contacten te leggen met de 'groten der aarde' en je studenten uit te sturen over deze aardbol, steeds nieuwsgierig naar wat ze hebben bijgeleerd bij hun terugkomst. Jo, je was als tweede begeleider in de doctoraats-tandem misschien minder betrokken in de rechtstreekse begeleiding van mijn onderzoeksproject. Toch zijn er heel wat zaken waarvoor ik je wens te bedanken. Als hoofd van het labo heb je een cruciale rol in het leggen van de fundamenten waarop het wetenschappelijk onderzoek is gebouwd. Zonder jouw algemeen 'management' van het labo was er van onderzoeksinstrumenten zelfs geen sprake. Het aanvragen van kredieten, het spijzen van de labokas, de aankoop van nieuwe instrumenten (met extra garantie!), stuk voor stuk zijn ze onmisbaar voor de goede werking van het labo. Bovendien kregen we als doctoraatsstudent steeds de kans om interessante congressen bij te wonen, zowel binnen als buiten Europa. En laten we zeker onze jaarlijkse labo-uitstap niet vergeten. Bedankt hiervoor. Een persoonlijk woordje van dank is zeker op zijn plaats voor de mogelijkheid die je me gaf om gedurende twee extra jaren mijn onderzoek tot een goed einde te brengen. Het zou een moeilijke klus geweest zijn zonder deze blijk van vertrouwen die je in me had.

I would also like to take the opportunity to thank Prof. Dr. Rainer Pepperkok from the Advanced Light Microscopy Facility at the EMBL in Heidelberg. Rainer, you gave me the opportunity to come to the EMBL up to three times to benefit from the unbelievably productive research environment. For two months I was isolated with my oligonucleotides, the FCS instrument and the silence of the night, as the instrument was too occupied during

the day. I learned a lot about myself and my research project, and although it was sometimes a demanding period, I wouldn't want to have missed it!

Uiteraard was ik niet de enige die op het labo rondliep om zijn of haar doctoraat tot een goed einde te brengen. Er zijn bijgevolg verschillende mede-doctoraatsstudenten die ik wens te bedanken voor de leuke momenten, zowel binnen als buiten het labo. De meeste tijd bracht ik ongetwijfeld door met mijn bureau-genoten Kevin en Tinneke. Dankzij Tinneke nam mijn kennis van het programma Word significant toe, wat dit doctoraat natuurlijk alleen maar ten goede komt. Kevin op zijn beurt wijdde me in in de wereld van de pixels en de beeldverwerking, onontbeerlijk bij de verwerking van de vele celfoto's. Ons concentratie- en stiltegebied werd op de gepaste tijdstippen onderbroken voor een luchtige babbel of anekdote, al dan niet gevolgd door een lachsalvo. Ik verdenk er Kevin trouwens van om stiekem aandachtig te luisteren als Tinneke en ik het weer eens hadden over de strijk-, opruim- en zoekcapaciteiten van onze 'ideale mannen' thuis.

Een deur meer naar links bevindt zich mijn ex-FCS partner Bart. Bedankt om me in de startblokken te krijgen door me de geheimen en de beperkingen van het FCS instrument te leren kennen. Nu heb je, in vervanging van Jurgen, de rol van 'laboduizendpoot' op je genomen. Geen moeite of vraag is je te veel en je deur staat steeds open voor iedereen. Indien er een prijs zou bestaan voor de meest verdienstelijke labo-persoonlijkheid denk ik dat je zeker een nominatie verdient.

De 'polyvalente zaal' wordt sinds enkele jaren bevolkt door Roos, Lies, Bruno en Ine. Dat deze zaal haar naam niet gestolen heeft, blijkt uit de vele persoons-verschuivingen en bureau-herindelingen die er zich gedurende de afgelopen jaren hebben afgespeeld. De naam 'polyvalent' weerspiegelt zich ook in de verschillende zaken waarvoor je in jullie bureau-knooppunt terecht kon, van koetjes en kalfjes over nuttige onderzoekstips tot heus crisis-overleg. Een speciaal woordje van dank is ook op zijn plaats voor Roos, dankzij wie we nu over een heus bacterie-lokaal beschikken. Ook mag ik er niet aan denken hoe ik nu nog mijn figuren zou maken als je me de basisprincipes van het programma Coreldraw niet had getoond.

Door de exponentiële groei van het labo zagen we Niek, Koen, Farzaneh, Stefaan D., Kevin B. en Barbara hun eigen bureau-eiland oprichten in onze nieuw-veroverde labolokalen. Bij deze wens ik Barbara nog eens te bedanken om als thesisbegeleider me de gevaren en geneugten van het wetenschappelijk onderzoek te leren kennen. Ook Koen en Farzaneh nemen een speciale plaats in als ex-stagiairs tijdens mijn eigen onderzoek. Ik kan toch zeggen dat Koen een belangrijke rol gespeeld heeft bij het tot stand komen van het begrip 'R/G ratio', wat toch vele malen in dit proefschrift aan bod komt. Bij deze zou ik ook Sofie wensen te bedanken, met wie ik kon kennismaken op weg naar het bureau-eiland voor het stellen van mijn vele vragen, en die algauw een aangename 'infiltrant' bleek te zijn voor de

dagelijkse middagpauzes. Verder wens ik onze nieuwste aanwinsten Dries en Marie-Luce te bedanken voor de korte, maar toch al leuke tijd dat we hebben samengewerkt. Naast de mede-onderzoeksstudenten, waren er ook nog mijn stagiairs Karlien, Annika, Fleur, Farzaneh, Koen, Ine D., Philippe, Maria, Marta en Elke die elk, in meer of mindere mate, hebben bijgedragen aan dit werk.

Een speciaal woordje van dank gaat uit naar ons secretariaatsteam Katharine en Bruno. Dank zij jullie hoefden we ons geen zorgen te maken over vliegtuig, trein, hotel of registratie wanneer we, vaak maar net op tijd, kwamen melden dat we weer eens op congres gingen. Ook wanneer we achteraf onze uitgaven en briefjes kwamen binnenbrengen, konden we erop rekenen dat alles door jullie deskundig werd geSAPt. Jullie hulp in het papieren doolhof wordt enorm geäpprecieerd.

Een bijzonder woord van dank gaat uit naar mijn ouders. Reeds van kleinsaf was de ‘onderzoeks-spirit’ aanwezig in mijn leefomgeving. Het eerste doctoraat dat ik heb kunnen bijwonen, kwam dan ook heel vroeg, toen ik als ongeboren kindje de proefschriftverdediging van mijn moeder kon aanhoren. Ook mijn vader schakelde me reeds vroeg in in het wetenschappelijk onderzoek. Als ik eens een dagje ziek was mocht ik mee naar het labo, waar ik gekleurde plastieken doosjes mocht opvullen met de bijpassende gekleurde plastieken tipjes. Het is pas nu, vele jaren later, dat ik besef wat ik eigenlijk aan het doen was… Ook tijdens mijn studies kon ik steeds op jullie rekenen om me te stimuleren wanneer nodig of gewoon om te zien dat jullie best wel trots waren op jullie dochter. Uiteraard kon ik ook steeds rekenen op jullie steun bij die andere mijlpalen in mijn leven, zoals de start van mijn eigen ‘huisje, tuintje, boompje’. Natuurlijk wens ik ook mijn broer niet te vergeten, wiens onnozele buien menig examenperiode een vrolijke toets hebben gegeven. Tenslotte zijn er nog de vele vrienden en familie buiten de werkomgeving. Jullie zijn reeds vele jaren ‘omnipresent’ in mijn leefwereld en dit mag nog vele jaren zo blijven!

Als laatst, maar zeker niet het minst, wens ik mijn man Wim te bedanken. Dankzij jou kregen de figuren in dit proefschrift de juiste kleur en plaats, had ik plots een voorblad en curriculum, bleken de referenties geen fouten meer te bevatten en noem maar op... Maar eigenlijk wens ik je vooral te bedanken voor wie je bent en wat je voor mij iedere dag opnieuw betekent. Jij zorgt ervoor dat ik na een goede of minder goede dag steeds kan thuiskomen in een liefdevolle omgeving. Onze vele hilarische momenten samen zorgen ervoor dat ik met plezier door het leven ga. Ook zou ik graag ons kleintje hier in mijn buik willen bedanken voor de vele kleine schopjes tijdens het schrijven van dit proefschrift. En zoals het leven eens voor mij begon zet het zich nu voor jou weer verder. Het eerste doctoraat dat je zal kunnen bijwonen, komt dan ook heel vroeg, wanneer je als ongeboren kindje de proefschriftverdediging van je mama zal kunnen aanhoren… De herhaling, zou je papa zeggen, is nooit ver weg.

TABLE OF CONTENTS

LIST OF ABBREVIATIONS AND SYMBOLS

ATP:	Adenosinetriphosphate
BSA:	Bovine Serum Albumin
CLSM:	Confocal Laser Scanning Microscopy
DLS:	Dynamic Light Scattering
DMEM:	Dulbecco's Modified Eagle's Medium
DNA:	Desoxyribonucleic Acid
DNase I:	Desoxyribonuclease I
DNase II:	Desoxyribonuclease II
DOPE:	Dioleoylphosphatidylethanolamine
DOTAP:	N-(1-(2,3-dioleoyloxy)propyl)-N,N,N-trimethylammoniumchloride
DSPE-PEG:	Distearoylphosphatidylethanolamine Polyethyleneglycol
DTT:	Dithiothreitol
EDTA:	Ethylenediaminetetraacetic Acid
EGTA:	Ethyleneglycoltetraacetic Acid
ELISA:	Enzyme Linked Immunosorbent Assay
FBS:	Fetal Bovine Serum
FCS:	Fluorescence Correlation Spectroscopy
FCCS:	Fluorescence Cross-correlation Spectroscopy
FDA:	Food and Drug Administration
FFS:	Fluorescence Fluctuation Spectroscopy
FRET:	Fluorescence Resonance Energy Transfer
GFP:	Green Fluorescent Protein
GTP:	Guanosinetriphosphate
HEPES:	4-(2-hydroxyethyl)-1-piperazineethanesulfonic Acid
ICAM-1:	Intracellular Adhesion Molecule 1
kDa:	Kilodalton
LP :	Liposomes
LPXs:	Lipoplexes
mRNA:	Messenger RNA
NGS:	Normal Goat Serum
NLS:	Nuclear Localization Signal
NPC:	Nuclear Pore Complex
N/P ratio:	Nitrogen to Phosphate Ratio
OC:	Open Circular
ONs:	Oligonucleotides

PAGE:	Polyacrylamide Gel Electrophoresis
PAM:	Polyamidoamine
PBS:	Phosphate Buffered Saline
pDNA:	plasmid DNA
pDMAEMA:	poly(2-dimethylamino)ethylmethacrylate
PEI:	Polyethyleneimine
PEG:	Polyethyleneglycol
PEG-LP:	Pegylated Liposomes
PEG-LPXs:	Pegylated Lipoplexes
PEG-PEI:	Polyethyleneglycol-Polyethyleneimine
PLL:	Poly-L-Lysine
PO20-LPXs:	Lipoplexes containing 20 mer Phosphodiester Oligonucleotides
PO40-LPXs:	Lipoplexes containing 40 mer Phosphodiester Oligonucleotides
PS20-LPXs:	Lipoplexes containing 20 mer Phosphothioate Oligonucleotides
PO-ONs:	Phosphodiester Oligonucleotides
PO20-ONs:	20 mer Phosphodiester Oligonucleotides
PO40-ONs :	40 mer Phosphodiester Oligonucleotides
PO40-PEG-LPXs:	Pegylated Lipoplexes containing 40 mer Phosphodiester Oligonucleotides
PS-ONs:	Phosphothioate Oligonucleotides
PS20-ONs:	20 mer Phosphothioate Oligonucleotides
PS20-PEG-LPXs:	Pegylated Lipoplexes containing 20 mer Phosphothioate Oligonucleotides
R/G ratio:	Ratio of the Red to Green Fluorescence
RNA:	Ribonucleic Acid
RNase H:	Ribonuclease H
SC:	Supercoiled
SDS:	Sodiumdodecylsulfate
siRNA:	Small Interfering RNA
SPT:	Single Particle Tracking
RISC:	RNA Induced Silencing Complex
TAT:	Transactivator of Transcription Protein from Human Immunodeficiency Virus-1
TBE:	Buffer based on Tris, Boric Acid and EDTA
TFO:	Triple Helix Forming Oligonucleotides
TNF-α:	Tumor Necrosis Factor - α
TRITC:	Tetramethylrhodamineisothiocyanate

D:	Diffusion Coefficient
F_G:	Green Fluorescence Intensity
F_R:	Red Fluorescence Intensity
λ_{ex}:	Excitation Wavelenght
λ_{em}:	Emission Wavelenght
N:	Number of Molecules
N_g:	Number of Green Labeled Molecules
N_r:	Number of Red Labeled Molecules
N_{gr}:	Number of Double-Labeled Green and Red Molecules
T:	Percentage of Molecules in Triplet State
τ_T:	Triplet Relaxation Time
τ_t:	Diffusion Time
ω_1:	Radius of the FCS Detection Volume
ω_2:	Half the Height of the FCS Detection Volume

GENERAL INTRODUCTION, AIMS AND OUTLINE OF THIS THESIS

GENERAL INTRODUCTION, AIMS AND OUTLINE OF THIS THESIS

Advances in biotechnology have lead to an accelerated discovery of macromolecular therapeutics such as peptides, proteins and polynucleotides. These macromolecules can be targeted against a variety of diseases, each requiring delivery to a well defined compartment of the body. Antisense oligonucleotides (ONs) and plasmid DNA (pDNA) show potential in the treatment of a wide variety of inherited and acquired genetic disorders, viral infections and cancer. Gene therapy aims to deliver these nucleic acids to cells to introduce novel genes or repair malfunctioning genes. Naked nucleic acids, however, are often prone to degradation before reaching their target site, or do not reach their target site at all. Therefore, they need the use of advanced drug delivery systems, such as viral or non-viral vectors. In general, viral vectors provide high transfection efficiencies but suffer from the limited size of the genetic material they can carry. Also, they can induce severe immune responses. Non-viral vectors are advantageous over viral vectors in that they are less expensive, easier and safer to make and more suitable for long time storage. They can also deliver much larger pieces of DNA. When compared to viral vectors, however, the current transfection efficiencies of non-viral vectors are far from optimal.

Non-viral vectors, such as cationic liposomes and cationic polymers, spontaneously form interpolyelectrolyte complexes with the negatively charged nucleic acids. These nanoparticles, which are respectively called lipoplexes and polyplexes, encounter different extra- and intracellular barriers during the delivery process. First of all, the nanoparticles should reach the target tissue, which, depending on the therapeutic application, could be the liver, the lung epithelium, muscle cells, tumor cells and so on. Once they have reached their target site, the nanoparticles mostly enter the cells by endocytosis. Following endocytosis, the nanoparticles are present in the endosomal compartment and should escape into the cytoplasm of the cells to avoid degradation in the lysosomes. Next, the nucleic acids mostly have to leave their pharmaceutical carriers before a therapeutic effect can be obtained. Furthermore, as the nucleic acid sequence is essential for their therapeutic effect, they should remain intact in the intracellular environment. Finally, the nucleic acids should reach their intracellular target, which can be situated in the cytoplasm (in the case of ONs) or in the nucleus (in the case of pDNA) of the cells.

The current generation of non-viral vectors in gene delivery are designed to facilitate entry into the cells and escape of the nucleic acids from the endosomal compartments. For successful nucleic acid delivery, the carriers should also protect the nucleic acids against enzymatic degradation by nucleases in the bloodstream and inside the cells. Viral vectors have evolved to optimally cross the biological barriers in order to deliver their DNA material. When compared to viral vectors, however, non-viral vectors are far less efficient in crossing the extracellular and intracellular space. Increasing attention has been paid to elucidate which of the above mentioned barriers limit the transfection efficiency of non-viral vectors the most. We believe that analyzing the different steps in the delivery process is crucial to allow optimization of the current generation of non-viral gene delivery systems. Unfortunately, the intracellular fate of the delivered nucleic acids is not very well known, mainly because of a lack of suitable methods that allow characterization of these critical steps in living cells.

In this thesis, we aimed to elucidate the role of the intracellular degradation of the nucleic acids in limiting their therapeutic effect. Because of the limited methods that allow to follow the on site degradation of nucleic acids in living cells, we additionally aimed to evaluate the use of an advanced light microscopy technique, namely Fluorescence Correlation Spectroscopy (FCS), for that purpose.

Chapter 1 gives an overview of the cationic lipids and cationic polymers that were used in this thesis to bind the nucleic acids. Also, the different intracellular barriers that are encountered by these non-viral vectors are discussed in more detail. A brief introduction on the basic principles of FCS is also given. In **Chapter 2**, the use of FCS to follow the degradation of naked antisense ONs was evaluated. Therefore, both nuclease resistant phosphothioate and nuclease sensitive phosphodiester ONs were fluorescently labeled and their integrity was followed both in buffer and in living cells. These fluorescently labeled ONs were subsequently complexed with non-pegylated and pegylated cationic liposomes in **Chapter 3** and with non-pegylated and pegylated polymers (polyethyleneimine) in **Chapter 4**, in order to elucidate the protection of the ONs against enzymatic degadation as offered by these carriers. When possible, the physicochemical properties of the carriers were correlated with the observed protection efficiency. In **Chapter 5** and **Chapter 6**, the relationship between the intracellular behavior of respectively non-pegylated and pegylated lipoplexes and their biological activity was investigated upon delivery of the antisense ONs to human lung epithelium cells. Special attention was given to the time and place of the intracellular degradation of the delivered ONs. Finally, in **Chapter 7**, we aimed to elucidate why supercoiled plasmid DNA appeared to be the best topology to generate gene expression upon delivery by non-pegylated cationic liposomes.

Chapter 1

INTRACELLULAR BARRIERS TO OLIGONUCLEOTIDE AND PLASMID DNA DELIVERY

Parts of this chapter are submitted as:

Remaut, K.; Sanders, N. N.; De Geest, B. G.; Braeckmans, K.; Demeester, J.; De Smedt, S. C. *Mat. Sci. Eng. R*.

and are in press:

Remaut, K.; Lucas, B.; Raemdonck, K.; Braeckmans, K.; Demeester, J.; De Smedt, S. C. *J. Control. Release*

ABSTRACT

Gene therapy aims to deliver DNA-based therapeutics such as antisense oligonucleotides (ONs), plasmid DNA (pDNA) and small interfering RNA (siRNA) to introduce novel genes or down-regulate malfunctioning genes. However, many problems remain to be resolved before gene therapy can become a standard clinical practice. The success of gene therapy is largely dependent on the development of a vector that can selectively, efficiently and safely deliver the DNA-based therapeutics to the target cells. On their delivery route, the vectors encounter different barriers. Indeed, they should be taken up by the cells, escape from the endosomal compartment, traffick through the cytoplasm and cross the nuclear membrane. Which of these barriers mainly limit the delivery process is currently not well understood and, very likely, depends strongly on the composition of the non-viral vector. In this chapter, we briefly discuss the nature of the DNA-based therapeutics and the non-viral gene delivery systems that were used in this thesis. Also, the different intracellular barriers that are encountered by these non-viral vectors are discussed in more detail. Finally, we introduce the reader to the basic principles of Fluorescence Correlation Spectroscopy (FCS), as this was the method of choice throughout this thesis to elucidate the effect of degradation of the DNA-based therapeutics on their transfection efficiency.

Chapter 1

Intracellular Barriers to Oligonucleotide and Plasmid DNA Delivery

DNA-BASED THERAPEUTICS

Antisense Oligonucleotides

The aim of the antisense strategy is simply to down-regulate the expression of disease-causing proteins by the inhibition of gene expression. Protein synthesis requires transcription from DNA into mRNA and its translation into protein. Antisense ONs are short (12-28 nucleotides), synthetic strands of DNA that are complementary or antisense to a target sequence, designed to halt the production of proteins at the level of transcription, translation or splicing of the mRNA. The first strategy, namely blocking the transcription, can be achieved by triple helix forming ONs (TFOs). TFOs hybridize in the major groove of DNA by Hoogsteen bonding and prevent DNA read-out by preventing the binding of transcription factors, inhibiting the duplex unwinding or by inducing mutations in the targeted gene [1]. The second strategy, namely blocking the translation, is more commonly used and is generally referred to as the 'antisense' strategy. Antisense ONs bind to their complementary target mRNA in a sequence specific manner through Watson-Crick hydrogen bonding. This can inhibit gene expression by several mechanisms, including translation arrest mediated by blockade of ribosomal read-through and hydrolysis of mRNA by recruitment of RNase H [2]. For an antisense ON to hybridize with its target mRNA, it must find an accessible sequence, which is at least in part a function of the mRNA physical structure. Indeed, mRNA is not a single-stranded random coil but displays a secondary and tertiary structure, which may render large parts of the mRNA inaccessible towards interaction with the matching antisense ONs. Selection of active antisense molecules still remains largely a matter of trial and error, although the use of computer-predictive folding of mRNA has helped to identify hybridization-accessible sites and thus the design of antisense ONs. The abundance and half-life of the target mRNA should also be considered when selecting a gene target. Indeed, the effect of the reduced protein expression will only be apparent after significant turnover of the pre-

existing endogenous protein pool. Therefore, antisense ONs targeted at mRNAs with a short half-life are expected to be more successful in decreasing the level of the corresponding protein.

The first generation of antisense ONs contained phosphodiester linkages (PO-ONs) (Figure 1A). PO-ONs are capable to recruit and activate RNase H, but are sensitive to nucleases and show relatively short half-lives. To overcome this problem, a variety of chemically modified ONs have been developed. The most frequently used chemically modified ONs are the phosphothioate ONs (PS-ONs) in which one of the non-bridging oxygens is replaced by a sulphur (Figure 1B). PS-ONs exhibit a long half-life in vitro and in vivo and retain the ability to recruit RNase H to degrade PS-ONs/mRNA hybrids [3]. A disadvantage of the PS-linkage is its affinity for proteins, which can cause non-sequence-specific antisense effects [4]. Second generation antisense ONs were developed to overcome the disadvantageous properties of the phosphothioates, but frequently the modification of the nucleotides and/or changes in the backbone reduced or eliminated the RNase H recognition of the DNA/RNA duplex [5]. Indeed, only phosphodiester, phosphothioate and chimeric ONs can activate RNase H.

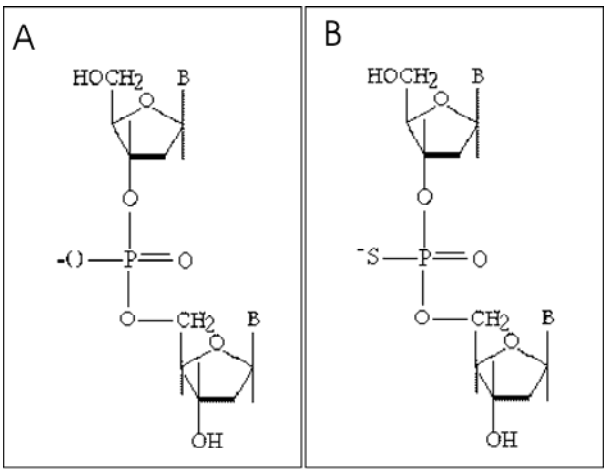

Figure 1. Chemical structure of antisense ONs with (A) a phosphodiester or (B) a phosphothioate backbone.

There are several antisense ONs in phase II or III clinical trials [6]. However, only few of them have made it to the market. Vitravene™ is the first antisense ON that was approved by European authorities in 1999, to treat an inflammatory viral infection of the eye that is caused by cytomegalovirus [7]. A major problem that still prevents the use of antisense therapy is the inefficient delivery of ONs into cells. Therefore, suitable delivery systems need to be developed, as naked ONs only poorly cross cellular membranes [8]. The aims for optimal delivery of ONs are to increase cellular uptake, improve exit from the endosomal compartment and to direct targeting to a particular site of action. Also, the required time frame of delivery needs to match the biological half-life of the target protein and the desired level of knock-down.

Plasmid DNA

Recombinant plasmids are high molecular weight, double-stranded DNA constructs, engineered to contain adventitious genes encoding specific proteins. Plasmid DNA (pDNA) molecules can be considered as pro-drugs that upon cellular internalization make use of the DNA transcription and translation apparatus to synthesize the desired protein. Gene therapy in this case involves the use of pDNA to introduce transgenes to cells that lack the ability to produce the desired protein or to correct functionally incompetent copies of a certain protein [1]. In its early stage of development, pDNA-based gene therapy was attempted to correct inheritable disorders resulting from a single gene defect, such as the cystic fibrosis transmembrane conductance regulator gene in Cystic Fibrosis. In addition to disease treatment, pDNA can be used as a DNA vaccine for genetic immunization. Suicide gene therapy, in which gene expression leads to the convertment of a separately administered non-toxic prodrug into a chemotoxic drug, is another rapidly emerging strategy for cancer treatment. A pDNA-based therapeutic that is currently on the market is Gendicine, which acts by inserting the p53 gene into tumor cells, thereby stimulating cell death [9].

In addition to the transgene of interest, pDNA typically contains several regulatory signals such as promotor and enhancer sequences that play an important role in regulating gene expression. Promotor sequences offer recognition sites for the RNA polymerase to initiate the transcription process, while enhancer sequences can enhance the transcription of the gene of interest by as much as several hundred times. Like antisense ONs, the cellular uptake of naked pDNA molecules remains a very inefficient process. Delivery of pDNA is further reduced by its high molecular weight compared to shorter antisense ONs. Also, pDNA cannot be chemically modified to increase the resistance towards enzymatic degradation. Various types of synthetic vectors have been developed for gene transfer [10]. Among the non-viral vectors, cationic lipid- and cationic polymer-based systems have been the most extensively studied, both for antisense ONs and pDNA delivery. The general features of the non-viral gene delivery systems as used in this thesis are discussed below.

NON-VIRAL GENE DELIVERY SYSTEMS

Liposomes as Nucleic Acids Carriers

Liposomes have emerged as one of the most versatile tools for the delivery of DNA therapeutics. When dispersed in an aqueous medium, phospholipids, which consist of a hydrophilic polar head group and a hydrophobic hydrocarbon tail, form bilayered structures,

called liposomes. Liposomes are spherical, self-closed structures formed by one or more lipid bilayers with an aqueous phase inside and between the lipid bilayers [11]. While multilamellar liposomes consist of a number of phospholipid bilayers and have a size typically ranging from about 200 to 800 nm, unilamellar liposomes consist of a single phospholipid bilayer and are above (large unilamellar vesicles) or below (small unilamellar vesicles) 200 nm in size. For DNA delivery, the nucleic acids are encapsulated into the liposomes' interior or bound to the liposomes' surface by electrostatic interactions. A variety of cationic, anionic and synthetically modified lipids and combinations thereof have been used to deliver a wide range of DNA-based therapeutics. The poor encapsulation efficiencies of the negatively charged nucleic acids in anionic liposomes has prevented their widespread use. Cationic liposomes, however, have been successful for achieving biological effects in cell culture. The first successful in vitro transfection with a cationic lipid was described in 1987, by Felgner *et al.* [12]. Due to their relative high efficiency, cationic lipids have been the most widely studied of the synthetic vectors. The effectiveness of the lipoplexes depends on the type and nature of the cationic lipid, the cell type, the type of nucleic acid (e.g. nucleic acids chemistry and lenght) and the method of formation of the lipoplexes.

Cationic liposomes generally consist of a mixture of zwitterionic and positively charged lipids. Upon mixing cationic liposomes with the negatively charged nucleic acids, spontaneously so-called lipoplexes are formed through electrostatic interactions. Over the last few years, progress has been made in elucidating the structures of lipoplexes. Interaction between DNA and cationic lipids is a self-assembly process that is triggered by DNA-mediated fusion of liposomes, resulting in lipid-bilayers with the DNA sandwiched in between [13]. While the positive charge on the polar head group of the cationic lipids is important for binding the negatively charged nucleic acids, the features of the alkyl chains play an important role in the organization of the lipoplexes. To promote the endosomal escape of lipoplexes, a cone-like lipid (with a small head group and expanding alkyl chains) should be incorporated in the liposomes. Cone-like lipids, such as the neutral dioleoylphosphatidylethanolamine (DOPE) can adopt a hexagonal phase that disturbs the endosomal membrane thereby provoking endosomal escape [14]. The general structure of liposomes is depicted in Figure 2, together with the commonly used cationic lipid N-(1-(2,3-dioleoyloxy)propyl)-N,N,N-trimethylammoniumchloride (DOTAP) and the neutral lipid DOPE.

While a positive surface charge is favorable for gene transfer efficiency in vitro, upon systemic application, the charged particles interact with blood components and non-target tissue, triggering toxic effects and reducing circulation times and targeting ability [15]. A common approach for masking the surface charge is to coat the lipoplexes with a hydrophilic polymer such as polyethyleneglycol (PEG). This 'pegylation' of lipoplexes prevents their aggregation, lowers their toxicity and increases the circulation time in the bloodstream [16].

Unfortunately, as discussed below, shielding appears to reduce the cell transfection activity. Besides the pegylation of the lipoplexes' surface, also sugars, peptides and proteins are often bound to the surface in an effort to target them to specific cells.

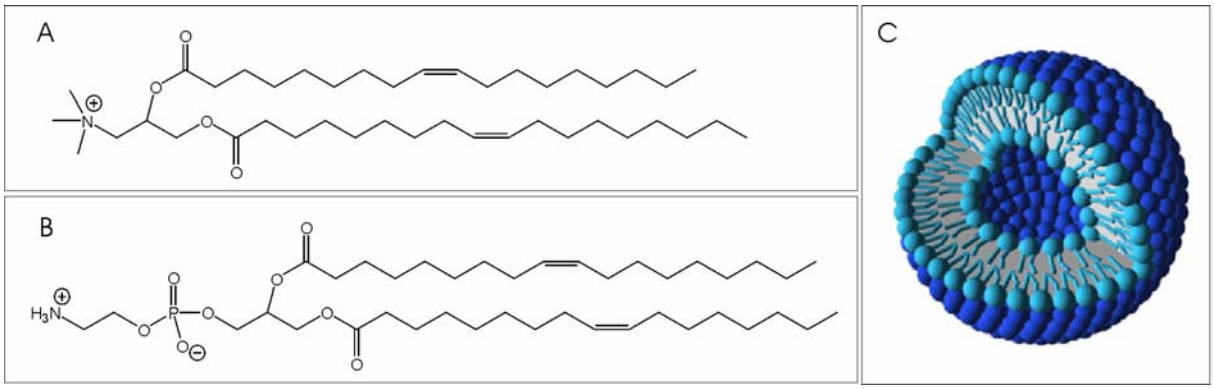

Figure 2. Chemical structure of (A) the cationic lipid DOTAP, (B) the neutral lipid DOPE and (C) an unilamellar liposome.

Polymers as Nucleic Acids Carriers

Another class of synthetic vectors that have been actively studied are cationic polymer-based gene delivery systems [17]. Like cationic lipids, cationic polymers self-assemble with the negatively charged DNA into so-called polyplexes due to electrostatic interactions. Each polyplex often contains several DNA molecules along with many polymer chains. Many different types of polymers have been evaluated as gene delivery vehicles, like cationic polymethacrylates, cationic polypeptides and cationic celluloses [17-20]. In this thesis, polyethyleneimine (PEI) was used as the cationic polymer of choice for gene delivery, as PEI has been reported to exhibit superior transfection efficiencies in many different types of cells [21].

The repeating unit of PEI consists of two carbon atoms followed by a protonatable nitrogen atom. PEI is available in a linear and branched conformation and in a wide variety of molecular weights (Figure 3). At physiological pH, a fraction of the amine groups carries a positive surface charge, which allows binding and condensing the negatively charged DNA. The unprotonated amines give PEI the attribute of serving as an effective buffer over a wide variety of pH ranges, which is believed to be important to PEI's success as a gene delivery vehicle by providing PEI with its endosomolytic properties. Due to its high charge density, PEI seems to compact DNA more efficiently than cationic lipids. The high charge density, however, also seems to be involved in the cytotoxicity of PEI. Both the molar mass and the backbone structure of PEI (being linear or branched) influence the transfection efficiency and cytotoxicity of the PEI/DNA polyplexes [22;23]. Also, the ratio of PEI nitrogens to DNA phosphates (N/P ratio) at which the polyplexes are prepared influences the condensation of

the DNA, the transfection efficiency of the resulting polyplexes and their cell toxicity. Conflicting information is available regarding the structural requirements and the molecular weight of PEI necessary for efficient gene delivery. Indeed, the transfection efficiencies of PEI polymers have been reported to decrease [24] or increase [25] with increasing molecular weight. On the contrary, Von Harpe *et al.* concluded that there was no correlation between the physicochemical properties of a wide variety of commercially available PEIs and the observed transfection efficiencies [26].

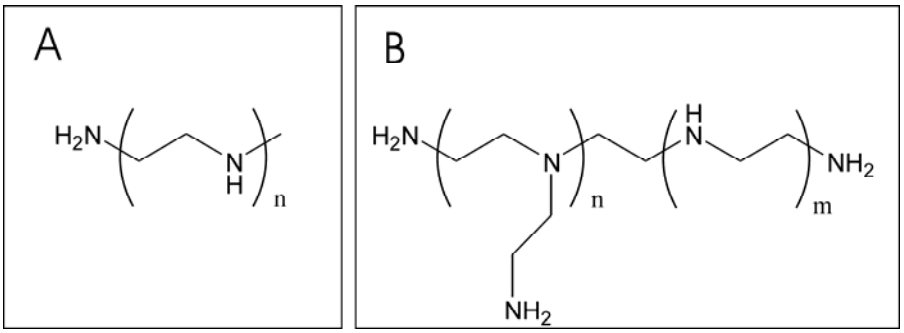

Figure 3. Chemical structure of polyethyleneimine polymers with (A) a linear or (B) a branched backbone.

As for cationic liposomes, adsorption of negatively charged serum proteins can cause aggregation and rapid clearance of the polyplexes from the bloodstream. Pegylation of the DNA/polycation polyplexes has been used to improve the solubility, reduce cytotoxicity, prevent aggregation and improve circulation times in the bloodstream [27]. Unfortunately, pegylation may lower the transfection efficiency of the polyplexes by preventing the cellular uptake or the endosomal escape properties, as discussed below. Besides PEG, PEI can be coupled with different ligands such as antibodies, folate and transferrin with the purpose of cell targeting.

INTRACELLULAR BARRIERS TO OLIGONUCLEOTIDE AND PLASMID DNA DELIVERY

Once DNA nanoparticles have reached their target cells, they have to gain access to the intracellular environment. Furthermore, they have to deliver the nucleic acids to the required compartment of the cell, namely the cytoplasm in the case of ONs and siRNA and the nucleus in the case of pDNA. On their delivery route, DNA nanoparticles encounter different barriers as they have to be taken up by the cells, escape from the endosomal compartment, traffick through the cytoplasm and cross the nuclear membrane. In addition,

the nucleic acids should be released at the most appropriate time and location in the cells and remain intact in the intracellular environment. Each of these steps will be discussed below.

Endocytosis: the Major Uptake Route

The cell is the smallest unit of life in our body. It can be seen as a complex organization of multiple intracellular structures that constantly receives and interprets signals from the environment in order to function and stay alive. The cytosol, in which the nucleus and a variety of organelles are embedded, is protected from the outside environment by a bilayer lipid plasmamembrane. Due to the complex organization of mammalian cells, it comes as no surprise that the income and output of molecules is highly organized. The traffick of newly synthesized molecules to their final destination (e.g. the lysosomes, the golgi apparatus, the extracellular space,…) is organized by different biosynthetic pathways. Likewise, the income of extracellular molecules is organized by endocytic pathways.

The plasmamembrane consists of a lipid bilayer which poses the first barrier in reaching the intracellular environment. Due to their negative charge, naked DNA molecules do not efficiently cross the plasmamembrane. Therefore, they rely on the use of a gene delivery system to gain access to the intracellular environment. Most of the time, DNA nanoparticles such as lipoplexes and polyplexes enter the cells by endocytosis (Figure 4, 1a and 1b). Sometimes, they can enter cells via fusion with the plasmamembrane with direct delivery of the DNA nanoparticles (Figure 4, 1c) or naked DNA (Figure 4, 1d) into the cytoplasm, thus avoiding the endolysosomal compartment. This fusion can occur due to the intrinsic properties of the DNA nanoparticles (e.g. a lipid bilayer around the DNA nanoparticles may facilitate their fusion with the plasmamembrane), or by the incorporation of cell penetrating peptides, such as TAT, into the DNA nanoparticles [28]. The term endocytosis encompasses multiple methods of internalization such as clathrin-dependent endocytosis, clathrin-independent endocytosis, macropinocytosis and phagocytosis. The endocytic pathways control the transport of incoming molecules and determine their fate, such as recycling to the plasmamembrane, secretion in the extracellular space or delivery to specific compartments in the cytoplasm such as the lysosomes, the endoplasmatic reticulum and the golgi apparatus. Endocytosis is essentially the invagination of the plasmamembrane with the formation of endosomal vesicles. This invagination occurs at specific domains in the plasmamembrane, characterized by a specific lipid and/or protein composition for the different endocytic pathways.

In clathrin-dependent endocytosis, this specific domain is characterized by the presence of clathrin and is called a ‘coated pit’ [29]. Invagination at these coated pits, which

cover some 0.5-2% of the plasmamembrane surface, results in the formation of clathrin-coated vesicles. These vesicles loose their clathrin coat upon internalization and fuse with each other or with pre-existing endosomal compartments to form 'early endosomes'. Early endosomes can either recycle their cargo to the extracellular environment or mature to late endosomes, accompanied by a decrease in pH from neutral to pH 5.9-6.0. Late endosomes on their turn deliver their cargo to the lysosomes, accompanied by an additional pH drop from pH 6.0 to 5.0. The average time to mature from early to late endosomes is reported to be 5 minutes, while late endosomes progress to lysosomes in the range of 30 minutes [30]. Rejman *et al.* found that particles of < 200 nm are taken up via the clathrin-dependent pathway [31]. Also, targeting to specific receptors, which are mostly internalized by clathrin-dependent endocytosis, should enhance uptake via this specific endocytic pathway. Examples of ligands that target to specific receptors are transferrin [32], asialoglycoproteins (targeting to hepatocytes) [33], epidermal growth factor [34] and folic acid [35] (targeting to cancer cells), low density lipoprotein [36] and so on.

Clathrin-independent endocytosis can be subdivided into lipid-raft mediated endocytosis and caveolae, both characterized by cholesterol and sphingolipid enriched domains in the plasmamembrane. These lipid domains are additionally associated with caveolin-1 in the case of caveolae. Caveolar vesicles are continuously docking on and fusing with at least two endocytic compartments, namely caveosomes and early endosomes. Caveosomes differ from early endosomes by their neutral pH and deliver their cargo to different intracellular organelles such as the endoplasmatic reticulum or the golgi apparatus. It has been suggested that the clathrin-independent pathway leads to more efficient transfection by DNA nanoparticles since it limits delivery to the lysosomes. Due to the potential fusion with early endosomes, however, cargo taken up by the clathrin-independent pathway can switch to the clathrin-dependent pathway, resulting in recycling to the extracellular space or eventual delivery to the lysosomes [37-39]. It has been suggested that larger particles (200 – 500 nm) enter the cells through caveolae/lipid-raft mediated endocytosis [31]. Particles larger than 500 nm would then preferably enter the cells via macropinocytosis, a mechanism of endocytosis in which large droplets of fluid are trapped underneath extensions (ruffles) of the cell surface. Phagocytosis is restricted to specialized cells, such as macrophages that function to clear large pathogens or cell debris from the circulation.

So far there are only few studies that connect the entry mechanism of lipoplexes and/or polyplexes with the observed transfection efficiencies. Zuhorn *et al.* found that lipoplex-mediated transfection occurs through the cholesterol-dependent clathrin-mediated pathway of endocytosis, rather than through a simple fusion with the plasmamembrane [40]. These observations were confirmed by Rejman *et al.* who found that DOTAP lipoplexes were

internalized by cells solely by means of clathrin-mediated endocytosis [41;42]. Lipid-based DNA nanoparticles will thus be delivered to the lysosomes, unless they are able to escape from the endosomal vesicles. In contrast to lipoplexes, PEI polyplexes were found to be internalized both by clathrin-mediated endocytosis and by caveolae. However, only the caveolae-dependent route resulted in effective transfection [41;42]. Von Gersdorff *et al.*, however, found that the internalization route resulting in successful gene expression depended on both the cell line and the PEI polyplex type used [43]. They also found that the most successful route for gene expression is not necessarily the most utilized internalization route of DNA nanoparticles. Indeed, linear PEI polyplexes were internalized for 70% by clathrin-independent endocytosis and for 30% by clathrin-dependent endocytosis, while only the latter resulted in gene expression.

Escape from the Endosomes and Release of the Nucleic Acids

After internalization by a specific endocytic pathway, DNA nanoparticles are present in endosomal vesicles from which they should escape in order to exert a therapeutic effect. The mechanisms of endosomal escape differ between lipid-based and polymer-based DNA nanoparticles and are discussed below.

Lipid-Based DNA Nanoparticles

A possible mechanism for endosomal escape of lipid-based DNA nanoparticles has been proposed by Zelphati and Szoka [44-47]. According to these authors, lipid contact occurs between cationic lipids from the lipoplex and anionic lipids from the inner face of the endosomal membrane resulting in flip-flop of anionic lipids from the cytoplasmic face of the endosomal membrane. These anionic lipids laterally diffuse into the lipoplex and form a charge neutralized ion-pair with the cationic lipids from the lipoplexes, resulting in destabilization of the lipoplexes and displacement of the negatively charged nucleic acids with their release into the cytoplasm of the cells. Recently, Gordon *et al.* demonstrated that anionic lipids in the endosomal membrane are not a primary prerequisite to trigger nucleic acids release [48]. On the contrary, neutral helper lipids in the delivery system, such as DOPE, appear to play a crucial role in improving the endosomal escape by promoting the transition of the lipoplexes from the lamellar phase to the inverted hexagonal phase resulting in the destabilization of the endosomal membrane [14;49]. Therefore, the presence of DOPE in a liposome formulation can be considered as an important trigger for endosomal escape with release of the nucleic acids in the cytoplasm of the transfected cells.

As discussed above, pegylation of the liposomes ‘guides’ lipoplexes in a more effective way through the extracellular compartments of the body. Pegylation, however, appears to lower the transfection efficiency of lipoplexes at the intracellular level. This

decrease in transfection has been attributed to a decreased interaction of pegylated lipoplexes with cellular membranes and, subsequently, lower uptake of the pegylated lipoplexes by the cells [50]. However, other groups showed that the cellular uptake of pegylated lipoplexes was unaltered and suggested that pegylation interferes at the step of endosomal escape [51;52]. As for non-pegylated lipoplexes, pegylated lipoplexes have to escape from the endosomal compartment and release their nucleic acids in the cytoplasm of the cells. At this stage, however, the PEG-chains prevent close contact between the lipids from the pegylated lipoplexes and the endosomal membrane. Also, the incorporation of PEG-lipids stabilizes the lamellar phase of the lipoplexes so that DOPE is not able to destabilize the endosomal membrane. The nucleic acids thus remain entrapped in the endosomal compartment, precluding their delivery to the nucleus.

Lipid mixing thus seems to be an important parameter to allow for endosomal escape. To overcome the inhibitory effect of pegylation, reversible pegylation has been considered by several groups. In this approach, the PEG-lipids are removed in the endosomal compartment in order to expose the endosomal escape properties of the lipoplexes. To be able to remove the PEG-chains on the liposomes' surface, two strategies are commonly used. One approach makes use of PEG-lipids where a pH sensitive group links the PEG to the lipid. The PEG-chains are then removed in the endosomal compartment due to acidic-catalyzed hydrolysis [53-55]. Another approach is the use of exchangeable PEG-lipids such as PEG-ceramides that simply diffuse out of the lipoplexes as a function of time [56]. The rate of PEG-ceramide removal from the lipoplexes depends on the size of the PEG moiety as well as on the acyl chain length, with shorter acyl chains resulting in more rapid deshielding. When the amount of PEG-chains at the surface has decreased sufficiently, lipid mixing between the cationic liposomes and the endosomal membrane can occur, resulting in endosomal escape and release of the nucleic acids in the cytoplasm of the cells. An important aspect of cationic lipid-mediated delivery is that the nucleic acids are released in the cytoplasm as such, without the additional need to dissociate from their carrier (Figure 4, 3b and 3d). As a result, the naked DNA molecules become susceptible to cytoplasmic nucleases as soon as endosomal escape has occurred (Figure 4, 6a and 6b).

Polymer-Based DNA Nanoparticles

As mentioned above, a wide variety of cationic polymers are under investigation for the delivery of nucleic acids. Some polycations have an intrinsic endosomolytic activity, while others need the co-addition or covalent coupling of 'helper molecules' to induce the endosomal escape [57]. Polymers with an intrinsic endosomolytic activity, like polyamidoamine dendrimers (PAM), poly(2-dimethylamino)ethylmethacrylate (pDMAEMA) and PEI, mostly have a high charge density and a highly branched structure, with the potential to be

protonated. At physiological pH, not all of the protonatable units of such polymers are protonated. Upon acidification of the endosomal compartment, however, the polymers become extensively protonated, inducing their endosomolytic activity. In general, these polymers are believed to escape from the endosomes via the proton sponge mechanism [22;58]. The buffering capacity of the polymers causes protons to be pumped in the endosomes, accompanied with an influx of Cl- ions. This builds up the osmotic pressure with the accumulation of water in the endosomes. Also, because of repulsion between the protonated amine groups, swelling of the polymer can occur. This swelling of the polymer in combination with the osmotic swelling eventually causes the endosomes to rupture, with release of the polyplexes in the cytosol of the cells as such (Figure 4, 3a and 3c). Clearly, this is in contrast to lipoplexes where the nucleic acids are believed to be released at the step of endosomal escape. In theory, all polyplexes based on polymers containing basic groups with buffering capacity between pH 7 and 5 (in other words with a pK_a at or below physiological pH) should be able to escape from the endosomes via the proton sponge mechanism. However, Funhoff *et al.* demonstrated that endosomal escape is not always enhanced by polymers buffering at low pH [59]. Also, the proton sponge theory has recently been doubted by Godbey *et al.* who found that lysosomes were not buffered during transfection with polyplexes formed with PEI [60]. Forrest *et al.* also found that acidification of endosomes still occurred when transfection experiments with PEI polyplexes were conducted. They concluded, however, that the proton sponge theory is still valid, but that acidification is a part of this process [61]. On the other hand, Sonawane *et al.* clearly demonstrated the enhanced Cl^- accumulation and swelling of the endosomes with the strongly buffering PEI and PAM, but not with the non-buffering poly-L-lysine (PLL) [62].

Cationic polymers without intrinsic endosomal escape properties, such as PLL, are devoid of a hydrophobic domain and cannot fuse and/or destabilize the endosomal membrane. Therefore, they require the co-addition or covalent coupling of fusogenic or endosome-disruptive molecules to induce their endosomal escape. These endosomotropic agents, which can be synthetic or virus-derived, mostly depend on the lowering of the endosomal pH for their activity, exposing more hydrophobic regions for interaction with the lipid bilayers from the endosomal membrane. Molecules with endosomal escape properties include polyethylacrylic acid and polypropylacrylic acid as well as virus-derived fusogenic peptides such as hemagglutinin HA-2 from the influenza virus [57;63].

As for lipoplexes, shielding of the polyplexes with PEG-chains is advantageous on the extracellular level, but can lower the endosomal escape. Therefore, the use of removable PEG-chains is also recommended in the case of pegylated polyplexes [64]. Acid-triggered deshielding of polyplexes can be achieved via cleavage of hydrozone-linked PEG or acetal-

linked PEG [65]. Other chemical linkages that may possess pH-dependent hydrolysis include vinyl ethers and orthoesters.

Depending on the endosomal escape mechanism, the nucleic acids reach the cytosol in 'naked' form (Figure 4, 3b and 3d) or while still encapsulated in a nanoparticle (Figure 4, 3a and 3c). In the latter case, the protection of the DNA against enzymatic degradation is expected to be maintained in the cytoplasm. On the other hand, most likely, an additional step of dissociation of the DNA from its carrier is needed to be able to establish a therapeutic effect (Figure 4, 4a and 4b). It has been suggested that PEI/DNA complexes can enter the nucleus as an associated complex [66]. Also, the dissociation of pDNA from PEI appears unnecessary to establish a therapeutic effect [67;68]. Itaka *et al.*, however, found that linear PEI, which released its pDNA more easily, showed a higher transfection efficiency than branched PEI that formed more stable complexes [69]. Also Bertschinger *et al.* demonstrated that branched PEIs have higher affinity for DNA than linear PEIs [70]. For PLL/DNA polyplexes, again low-molecular-weight PLL polymers that released DNA more easily yielded better transfection efficiencies [71]. These examples demonstrate that vector unpacking is a potential barrier for polyplex-mediated nucleic acid delivery.

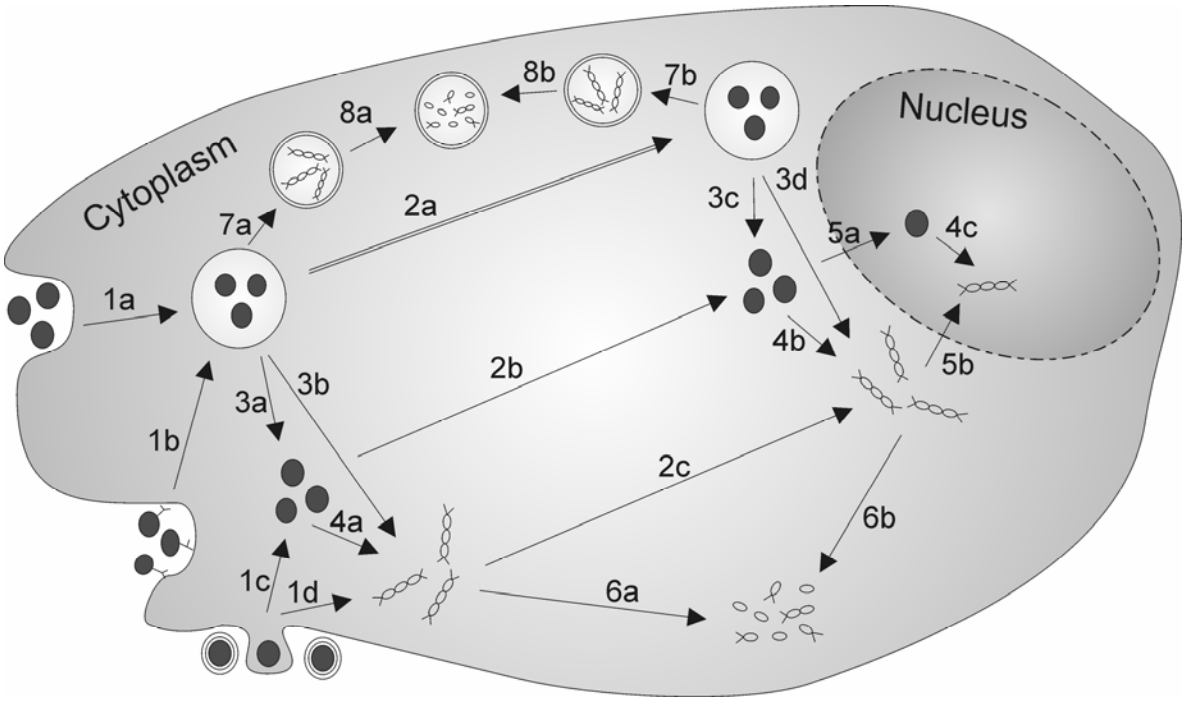

Figure 4. Possible intracellular pathways and barriers as encountered by DNA nanoparticles. (1) Cellular entry, (2) intracellular transport, (3) endosomal escape of DNA nanoparticles or naked nucleic acids, (4) release of nucleic acids from the DNA nanoparticles, (5) nuclear entry of DNA nanoparticles or naked nucleic acids, (6) intracellular degradation of naked nucleic acids and (7, 8) release and degradation of the nucleic acids in the endosomal compartment.

Traveling Through the Cytosol

The Intracellular Transport Machinery

The cytoplasm is a viscous compartment containing a scaffold of filaments termed the cytoskeleton. The filaments divide into three types: actin filaments (7 nm), microtubules (25 nm) and intermediate filaments (12 nm). These filaments are dynamic and can assemble and disassemble according to molecular cues. It appears that the composition of the cytoskeleton makes free diffusion of macromolecules limited [72;73]. Therefore, most likely, DNA nanoparticles have to make use of the efficient intracellular transport mechanisms to reach their target site. The transport system in cells is composed of two main components, namely the actin filaments and the microtubules [74].

Actin filaments are build up from actin monomers that have polymerized after binding ATP. Actin monomers bind to the plus, barbed end of the growing filaments and dissociate from the minus, pointed end. Additional crosslinking and branching of actin filaments allows cells to form specialized structures such as microvilli, stress fibers, ruffles, cortical actin, lamellipodia and filopodia. Underlying the plasmamembrane we find the cortical actin, a dense layer of branched actin filaments, which can serve as a barrier for incoming viral and non-viral particles. For trafficking, cargo can travel along the actin filaments using the myosin family of motor proteins, which generally move towards the plus end of the actin filaments while hydrolizing ATP [75]. Alternatively, cargo can attach to the growing end of a polymerizing actin filament, which generates directional propulsion. In general, actin filaments are more involved in short, non-directed movement.

Microtubules are assembled of α- and β-tubulin dimers that organize into hollow, cylindrical filaments while hydrolyzing GTP. The plus ends of microtubules are pointed towards the plasmamembrane, while the minus ends are anchored to the microtubule organizing center adjacent to the nucleus. Microtubules play an important role in cell division and the intracellular trafficking of organelles and other cargo, using the dynein and kinesin families of motor proteins for movement. Dyneins move cargo towards the minus end of the microtubules (e.g. towards the nucleus), while kinesins move cargo towards the plus end of the microtubules (e.g. towards the plasmamembrane) [76;77]. Motors that move towards both minus- and plus-ends of microtubules have not been identified in nature. In contrast to actin filaments, microtubules are associated with long, directed movement in cells.

Intracellular Transport of DNA Nanoparticles

Microtubules and the kinesin and dynein motor proteins are responsible for the trafficking of endosomal vesicles [76]. Therefore, incoming nanoparticles can traffick the cytoplasm while still present in the endosomal vesicles (Figure 4, 2a). The direction in which

the 'endosomal nanoparticles' move depends on which motor proteins are working on the endosomes, while the distance of cytoplasmic traveling depends on the time during which the motor proteins remain attached to the endosomal vesicles. Endosomes can also move bidirectionally, switching between the kinesin and dynein motor proteins on a time scale of once a minute [76]. Of course, the distance traveled is also dependent on the time of endosomal escape, making it more likely to reach the nucleus when the nanoparticles do not escape from the endosomes too soon after entry. On the other hand, since endosomal vesicles are trafficked to the lysosomes, endosomal escape of the cargo at the appropriate time (e.g. traveled to the perinuclear region but not yet fused with lysosomes), remains important for cargo that is not resistant to the destructive lysosomal environment.

Apart from in endosomal vesicles, DNA nanoparticles can diffuse to the perinuclear region as such (Figure 4, 2b). Passive diffusion through the cytoplasm, which is crowded with cell organelles and the actin and microtubules network, is expected to be limited. Directed transport of DNA nanoparticles by hijacking the dynein motors could be an interesting strategy to traffic from the cell periphery to the cell nucleus [33]. Dynein has a head group, which binds the microtubules and a tale for binding of cargo. Which parameters determine recognition of cargo, such as DNA nanoparticles, by dynein remain unclear. Wang *et al.* demonstrated that coupling of cytoplasmic dynein to anionic latex beads stimulated their microtubules-assisted transport to the nucleus, demonstrating that dynein is indeed an interesting target for directed transport of DNA nanoparticles [78].

Recently, real-time multiple particle tracking using video microscopy has gained interest to elucidate the intracellular transport of non-viral gene delivery systems [79]. Bausinger *et al.* found that PEI/DNA polyplexes exhibit three different kinds of intracellular transport: ad random diffusion, active diffusion using the actin cytoskeleton and, most importantly, active diffusion to the cell nucleus within the endosomal vesicles using the microtubules [80]. Also, Suh *et al.* observed that PEI/DNA polyplexes achieved rapid perinuclear accumulation due to their active transport along the microtubules [81]. In the perinuclear region, however, most of the particles were immobile, with only limited access to the nuclear interior.

Intracellular Transport of Naked Nucleic Acids

Free DNA that is present in the cytoplasm can either passively diffuse or be actively transported to the nucleus (Figure 4, 2c). Lukacs *et al.* found that the diffusion of small nucleic acid fragments (<250 bp) in the cytoplasm was only modestly slowed down when compared with that in saline but was greatly reduced when larger DNA fragments such as pDNA were used [73]. Later on Dauty *et al.* found that the actin cytoskeleton, which has a mesh size of about 150 nm, was the principal determinant of this size-dependent DNA

mobility in the cytoplasm [72]. Small nucleic acid fragments like oligonucleotides and siRNA have no difficulties in reaching and entering the nucleus [82-84]. Free plasmids, however, show only limited diffusion from the injection site. It has recently been shown that, apart from passive diffusion, free pDNA can utilize the microtubules network to traffick to the nucleus, probably using the dynein motor proteins [85]. Also, molecules bearing nuclear localization signals (NLSs) arrive at the nuclear membrane by active transport along the microtubules, evoked by NLS recognition of the dynein motor proteins [86]. This demonstrates that NLSs have not only an important function in nuclear import, but can also help to concentrate the NLS-bearing cargo at the perinuclear region before nuclear import takes place.

Breaking Through the Nuclear Membrane

The nucleus is separated from the cytoplasm by a lipid bilayer membrane. The outer membrane is continuous with the endoplasmatic reticulum, while the inner membrane lies within the nucleus. On several locations throughout the nuclear envelope, the outer and inner membrane fuse, forming channels that connect the cytoplasm and the nucleoplasm. These channels are called the nuclear pore complexes (NPCs) and play an important role in transport into and out of the cell nucleus. The NPCs contain an aqueous channel of about 9 nm that allows passive diffusion of small molecules up to 40 kDa. For larger molecules, an energy and signal-dependent mechanism is required, enlarging the NPCs to about 40 nm [87]. This active transport is mediated by nuclear localization signals (NLSs) and specific carrier molecules such as members from the importine-β family. Molecules destined for nuclear import either bear their own NLSs or are recognized by endogenous NLSs. NLS containing cargo binds in the cytoplasm to the importine-α subunit of an importine-α/β dimer. Alternatively, the NLS containing cargo can directly bind to importine-β, without the need for the importine-α adaptor molecule. Then, the construct docks via the importine-β subunit to the cytoplasmic face of the NPCs, followed by translocation through the NPCs into the nucleus. Binding of the nuclear RanGTP to the importine-β subunit releases the importine-α/NLS-cargo in the nuclear environment, where the NLS-cargo is released from the importine-α subunit. The importine-α and -β subunits are then recycled back to the cytoplasm to mediate a new round of nuclear import [88-90].

For small nucleic acids like ONs, the nuclear envelope poses no barrier. Upon microinjection in the cytoplasm, free ONs can indeed rapidly accumulate in the nuclear environment [82;83]. When delivered by DNA nanoparticles, most likely dissociation of the ONs from the carrier is needed before nuclear entry can occur. In the case of cationic lipids, as discussed above, this dissociation occurs at the step of endosomal escape [91;92]. For cationic polymers, an additional dissociation step in the cytoplasm will be required. It has indeed

been shown that PEI improves the antisense activity of a phosphodiester but not of a phosphothioate ON, because the latter was not able to dissociate from the PEI polymers due to the stronger binding [93].

Several studies have pointed out that the nuclear membrane is an important barrier for larger DNA fragments such as pDNA [94-96]. pDNA can reach the nuclear envelope in a free form or while being complexed to the DNA nanoparticles. DNA nanoparticles that are small enough could gain access to the nuclear environment via the NPCs, postponing the need for dissociation of the nucleic acids from the nanoparticles (Figure 4, 5a). In all other cases, an additional dissociation step is required before nuclear accumulation of the nucleic acids can take place. Microinjection experiments have demonstrated that only 0.1% of the cytoplasmic plasmids are able to reach the nuclear interior in non-dividing cells [97]. Nuclear accumulation of pDNA is, however, greatly enhanced during cell division when the nuclear envelope is temporarily broken down [98;99]. In non-dividing cells, pDNA needs a NLS to gain access to the nuclear interior via the NPCs [100]. Therefore, coupling of NLSs to pDNA has been an attractive, although not so successful, strategy to increase nuclear transport [101]. NLS peptides can also be coupled to the DNA nanoparticles instead of to the pDNA. In this case, however, the benefit from the NLS is lost when release of the nucleic acids from the DNA nanoparticles occurs. Apart from the need for a NLS, DNA size also plays an important role in nuclear delivery, making it easier for smaller DNA fragments [102;103]. Indeed, DNA with a size up to 1 kb can enter the nucleus rather efficiently after coupling of a NLS peptide [104], while for larger DNA fragments coupling of NLSs has not always been successful [105].

Surviving the Intracellular Environment

Degradation of therapeutic DNA is believed to be one of the factors limiting gene and oligonucleotide therapy, since the destruction of incoming genes translates into a loss of gene expression. Glasspool-Malone *et al.* demonstrated that the co-administration of the nuclease inhibitor aurintricarboxylic acid greatly enhanced the transfection efficiency of naked pDNA administered to macaque and murine test animals [106]. Also, Ross *et al.* reported an enhanced gene transfection in cells transfected in the presence of the acidic nuclease inhibitor DMI-2 [107]. Degradation of nucleic acids can occur in the cytoplasm or in the endosomal compartment (Figure 4, 6 and 8). Lechardeur *et al.* estimated the apparent half-life of double-stranded DNA in the cytosol of HeLa cells between 50-90 minutes while Pollard *et al.* showed that the delivery of pDNA in COS-7 and A549 cells was prevented by Ca^{2+}-sensitive nucleases [108;109]. Clearly, when using DNA nanoparticles to deliver pDNA, the time and place of release of the nucleic acids will play an important role in generating a therapeutic outcome. Ideally, the delivery system should release the pDNA close to the

nuclear membrane. Since the translocation of the pDNA to the cell nucleus is greatly enhanced upon cell division, the time between release of the pDNA and cell division should be as short as possible to avoid excessive degradation of the pDNA in the waiting period before cell division occurs. Therefore, delivery systems where the release of pDNA is triggered by cell division could greatly enhance the transfection efficiency. Another approach could be to develop delivery systems that become entrapped in the cell nucleus during cell division and release their pDNA directly in the cell nucleus afterwards (Figure 4, 4c).

Also ONs are exposed to intracellular degradation. In 1991, Leonetti *et al.* microinjected fluorescently labeled antisense ONs in the cytoplasm of cells and found that the ONs accumulated in the nucleus within the first minutes after injection [82]. The fluorescence signal could be detected for over 20 hours for a PS-ON, whereas it disappeared within 3 hours for a PO-ON, which was attributed to its degradation. The first intracellular study focusing on the degradation of ONs was performed by Uchiyama *et al.* using Fluorescence Resonance Energy Transfer (FRET) [110]. They found that a PO-ON was degraded within 60 minutes, whereas a PS-ON remained intact. Both for antisense ONs and pDNA delivery, the use of suitable delivery vehicles that protect the nucleic acids against enzymatic degradation could enhance the therapeutic efficiency. In order to develop such delivery vehicles, it is important to gain knowledge on the time and place of degradation of the nucleic acids in living cells. Studies focusing on this intracellular degradation in 'real-time' are scarce, mainly because of the limited amount of available methods that allow characterization of this critical step in living cells. In this thesis, we aimed to elucidate the role of the intracellular degradation of the nucleic acids in limiting their therapeutic effect. Therefore, we evaluated the use of an advanced light microscopy technique, namely Fluorescence Correlation Spectroscopy (FCS). The basic principles of FCS are briefly discussed below.

THEORETICAL ASPECTS OF FLUORESCENCE CORRELATION SPECTROSCOPY

Experimental Setup

Fluorescence Correlation Spectroscopy (FCS), which is a light microscopy based technique, was introduced in the early 1970s as a non invasive method to study interactions on the single molecule level [111-113]. The basic concept of FCS is to keep the number of fluorescently labeled molecules low enough, so that each of them contributes substantially to

the measured fluorescence signal. By using a small focal volume, only a few fluorescent molecules are detected at any time. In these circumstances, diffusion of fluorescent molecules in and out of the focal volume leads to fluorescence fluctuations that give information on respectively the average number of fluorescent molecules present in the focal volume and their diffusion coefficient. In single-color FCS, the fluorescence fluctuations of only one type of fluorophore are monitored, while in dual-color FCS the fluorescence fluctuations of two spectrally different fluorophores are detected simultaneously with separate detectors.

During the 90s, the size of the focal volume was further reduced to less than 1 femtoliter by combining FCS with confocal detection. Figure 5 shows a schematic representation of a typical FCS instrument. The incoming laser light is reflected by a triple chroic mirror and is focused to a small diffraction limited spot in the sample by a high numerical aperture objective lens. Emission light coming from the sample passes the triple chroic mirror and is split by a subsequent dichroic mirror into a green and a red component that is detected by respectively the 'green' and 'red' detector of the FCS instrument. A pinhole in front of the detectors blocks all light coming from outside the focal region. By combining the focused laser beam and the confocal pinhole, the fluorescence coming from only a small volume will be detected, which is usually referred to as the 'confocal detection volume'. The use of ultrasensitive avalanche photodiode detectors allow detecting the fluorescence of single molecules. Single molecules diffusing into and out of the confocal detection volume induce fluorescence fluctuations (Figure 5B). The duration of the fluctuations is determined by the degree of mobility of the diffusing species and the size of the confocal detection volume. From the fluorescence fluctuations, an auto- and/or cross-correlation curve (see following sections) can be derived (Figure 5C). Both the average number of molecules in the focal volume as well as their diffusion characteristics can then be calculated by fitting of an appropriate model to the experimental auto- and/or cross-correlation curves.

Nowadays, FCS instruments are mostly available as add-on modules to confocal laser scanning microscopes (CLSMs). A CLSM allows high-resolution imaging of the fluorescent sample and accurate positioning in 3-D of the FCS focal volume. After selection of the point of interest, the laser beam of the CLSM is parked at that location and the fluorescence fluctuations are recorded for a certain period of time. The powerful combination of both instruments makes it possible to study molecule dynamics in small regions of living cells.

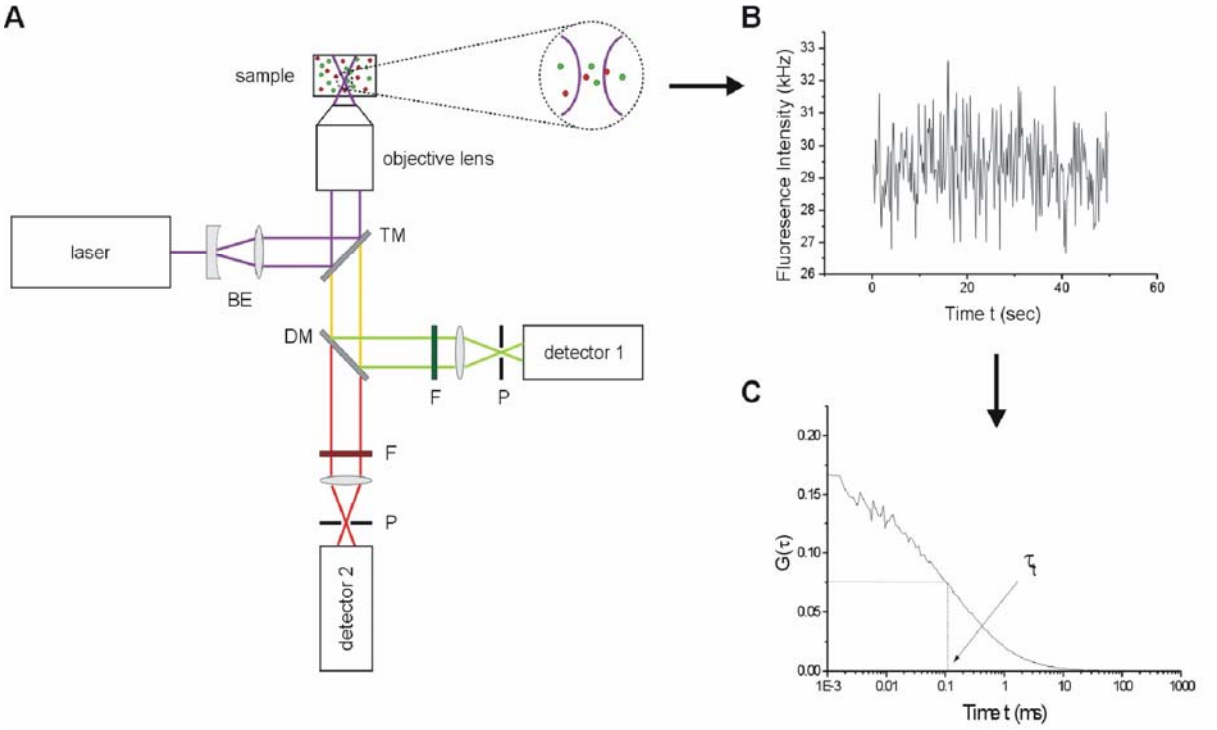

Figure 5. (A) Schematic setup of the FCS instrument. The excitation light from the laser is reflected by a triple chroic mirror (TM) into the objective lens of the microscope. The light emitted by the fluorescent molecules in the excitation volume passes through the objective lens and the triple chroic mirror, to be split by the subsequent dichroic mirror (DM) into a red and a green component. The intensity of the emitted red and green light is measured by respectively the red and green detector. A pinhole (P) in front of the detector blocks the out-of-focus fluorescence. (B) Diffusion of molecules in and out of the confocal volume causes fluorescence intensity fluctuations. (C) From these fluorescence intensity fluctuations an auto-correlation curve can be derived from which the diffusion time τ_t (i.e. the time to pass through the confocal volume) and the amount *N* of the fluorescent molecules can be calculated.

Auto-correlation Analysis

FCS basically monitors fluorescence intensity fluctuations caused by the diffusion of fluorescently labeled molecules through the detection volume of a CLSM (Figure 5B). The diffusion speed of the fluorescent molecules directly determines the average residence time and the frequency of leaving and reentering the focal volume. This is reflected in the frequency and duration of single fluctuations in the fluorescence intensity measurements: fast diffusion results in a high frequency of short lasting fluctuations and vice versa. To be able to reliably calculate the diffusion coefficient from the fluorescence fluctuations, it is necessary to analyze a large number of fluctuations by calculating a fluorescence fluctuation auto-correlation function. Auto-correlation analysis is performed by multiplying the fluorescence intensity fluctuations with themselves at different delay times τ, and averaging this product in a statistical manner over a large number of fluctuation events:

$$G(\tau) = \frac{\langle \delta F(t) * \delta F(t+\tau) \rangle}{\langle F(t) \rangle^2}$$

where $\delta F(t) = F(t) - \langle F(t) \rangle$ denotes the fluorescence intensity fluctuations. The average is calculated over the different time points *t* available in the experimental fluctuation profile. The resulting auto-correlation curve G(τ) then decays from a large value at τ = 0 to zero for large decay times τ (Figure 5C). The average residence time of the fluorescent molecules in the confocal detection volume can be determined as the time $\tau_{1/2}$ at which the amplitude of the auto-correlation curve has decayed to 50% of its original value. In other words, the auto-correlation curve generated from slowly diffusing molecules will decay more slowly when compared to rapidly diffusing molecules. In addition, the amplitude of the auto-correlation curve is inversely proportional to the number of fluorescent molecules that reside on average in the confocal detection volume.

In order to more accurately determine the number of molecules (*N*) in the confocal volume and their characteristic diffusion time (τ_t), the auto-correlation curve can be fitted with a single-species (eq. 1) or dual-species (eq. 2) model:

$$G(\tau) = \frac{1}{N} * \left(1 - T + T * \exp\left(\frac{-t}{\tau_T}\right)\right) * \frac{1}{1 + \frac{t}{\tau_t}} * \frac{1}{\sqrt{1 + \left(\frac{\omega_1}{\omega_2}\right)^2 \left(\frac{t}{\tau_t}\right)}} \qquad \text{eq. 1}$$

$$G(\tau) = \frac{1}{N} * \left(1 - T + T * \exp\left(\frac{-t}{\tau_T}\right)\right) * \left(\frac{y}{\left(1 + \frac{t}{\tau_{t1}}\right) * \sqrt{1 + \left(\frac{\omega_1}{\omega_2}\right)^2 \left(\frac{t}{\tau_{t1}}\right)}} + \frac{1-y}{\left(1 + \frac{t}{\tau_{t2}}\right) * \sqrt{1 + \left(\frac{\omega_1}{\omega_2}\right)^2 \left(\frac{t}{\tau_{t2}}\right)}}\right) \qquad \text{eq. 2}$$

where $2\omega_1$ and $2\omega_2$ represent the diameter and the height of the detection volume, respectively. *T* represents the percentage of molecules in triplet state and τ_T represents the triplet relaxation time. For the dual-species model (eq. 2), there are *N*y* molecules with diffusion time τ_{t1} and *N*(1-y)* molecules with diffusion time τ_{t2}. The diffusion coefficient *D* can be calculated from the characteristic diffusion time according to equation 3:

$$D = \frac{\omega_1^2}{4\tau_t} \qquad \text{eq.3}$$

Apart from a single-species or dual-species fit, the auto-correlation curve G(τ) can be fitted to other models such as a triple-species fit or anomalous diffusion. These models were, however, not used in the FCS experiments and will therefore not be discussed in this thesis. For a detailed review on FCS theory, we refer the interested reader elsewhere [114-117].

A common application of auto-correlation analysis is to study the interaction of fluorescently labeled molecules with non-labeled substrates, based upon a change in the diffusion characteristics of the fluorescently labeled molecules upon binding to their reaction partner. Since, generally, there will be two diffusing subpopulations (a bound and unbound fraction), this application requires the use of the dual-species model (Eq. 2). It should be noted that the minimal difference in diffusion coefficients between both subpopulations should be at least a factor of two in order to be distinguishable by FCS [118]. Assuming globular molecules, the diffusion coefficient *D* is proportional to $1/(M)^{1/3}$, where M is the molecular weight [119]. This implies that the molecular weight of the bound and unbound molecules should differ by at least a factor of 8 [120], to be able to use auto-correlation analysis for studying the association and/or dissociation kinetics of fluorescent labeled molecules with their reaction partner.

Cross-correlation Analysis

To overcome the above described limitation of auto-correlation analysis for studying reaction kinetics between partners of equal size, dual-color cross-correlation spectroscopy (FCCS) has been developed [121]. In dual-color FCCS, both reaction partners are labeled with spectrally different fluorophores (e.g. a green and red fluorophore). When both partners interact, a new double-labeled reaction product is formed. The two differently colored fluorophores are excited by independent laser lines. The light emitted in the common confocal detection volume is split onto two separate detectors. When both types of molecules are moving independently, there will be no correlation between the fluctuations of each color. However, when they interact and are moving together through the detection volume, (a fraction of) the fluctuations will occur synchronized in both detectors. From both the green and the red fluorescence fluctuation profiles, an auto-correlation curve can be derived, which gives information on the number of green (N_g + N_{gr}) or red-labeled (N_r + N_{gr}) molecules and their diffusion behavior, with N_g and N_r being the number of single-labeled green or red molecules and N_{gr} being the number of double-labeled green and red molecules. Alternatively, cross-correlation of the green and red detector signals gives rise to a cross-correlation curve from which information on the diffusion behavior (τ_t) and number (N_{gr}) of the double-labeled molecules can be derived by fitting of the cross-correlation curve with

equation 4 [121]. Let it be noted that the amplitude of the cross-correlation curve is proportional to the number of double-labeled molecules N_{gr}.

$$G(\tau) = \frac{N_{gr}}{\left(N_g + N_{gr}\right) * \left(N_r + N_{gr}\right)} * \frac{1}{1 + \frac{t}{\tau_t}} * \frac{1}{\sqrt{1 + \left(\frac{\omega_1}{\omega_2}\right)^2 \left(\frac{t}{\tau_t}\right)}} \qquad \text{eq. 4}$$

A limitation of FCCS lies in the assumption that no fluorescence enhancement or quenching occurs upon interaction of the two fluorescently labeled molecules. Also, the experimental realization of a FCCS setup is more demanding, since the confocal volumes of both channels should be of equal size and perfectly overlapping. Calibration and alignment of the FCCS system can be done as described by Schwille *et al.* [121].

FCS to Study the Behavior of Non-Viral Gene Delivery Systems

Since FCS became a commercially available technique in the late nineties, FCS has been used to explore the barriers in the delivery process of nucleic acids [122]. Auto-correlation analysis was used to examine the molecular movement of ONs and RNA in the nuclei of living cells [123;124], the self-assembling process of lipoplexes and polyplexes [125-127], the hydrolysis of DNA by several enzymes [128] and the intracellular fate of PEI and PEI/DNA complexes [129]. Furthermore, cross-correlation analysis has been used to study the degradation of ONs in buffer [121;130] and the release of DNA from cationic lipid vesicles in buffer [131]. In living cells, cross-correlation analysis is complicated due to experimental difficulties such as photobleaching, autofluorescence, light absorption and scattering leading to a low signal to noise ratio [120;132-134]. Consequently, only limited studies can be found which applied cross-correlation analysis in the intracellular environment. Bacia *et al.* studied the endocytic pathway of the cholera toxin A and B subunits in live cells using FCCS [135] and reviewed the application of FCCS in living cells recently [136].

Studying the complexation and dissociation behavior of non-viral gene delivery systems in living cells by auto- or cross-correlation analysis is a very difficult task. As the complexes usually consist of a large number of nucleic acid molecules and a large number of carrier molecules, each being fluorescently labeled, the complexes contain many fluorophores. Consequently, passage of the complexes through the detection volume of the FCS instrument causes very bright intensity peaks in the fluorescence fluctuation profiles that complicate classical auto- and cross-correlation analysis. Our group has come up with alternative means to examine the complexation and dissociation behavior of nucleic acid containing complexes by applying a statistical method to study the occurrence of such peaks

objectively [137;138]. In this context, since correlation analysis is not performed anymore, the term FCS is usually replaced by FFS (fluorescence fluctuation spectroscopy). Our group has applied single-color FFS to study the association and dissociation of fluorescently labeled ONs with non-labeled cationic polymers in buffer [139-141] and demonstrated that dual-color FCS is a valuable tool to study the association and dissociation of fluorescently labeled ONs and fluorescently labeled cationic polymers and liposomes, both in buffer [142;143] and in living cells [144;145].

Apart from FCS, the intracellular processing of nucleic acid containing complexes is often visualized by conventional fluorescence (confocal) microscopy. One can use fluorescent dyes of different colors simultaneously to differently stain the nucleic acids, their carriers, cellular compartments and so on. The intracellular behavior can then be evaluated by the absence or presence of co-localization of the different fluorescent dyes. The accuracy of co-localization studies is, however, limited by the resolution of the microscope setup, which is about ~170 nm. In some cases, this fundamental limit can be overcome by using fluorescence resonance energy transfer (FRET) [146]. FRET can occur between two fluorescent molecules, termed a donor and acceptor, that are in very close proximity (typically < 10 nm) of each other. The acceptor fluorophore must have an excitation spectrum that is (partly) overlapping with the emission spectrum of the donor fluorophore. When the donor molecule is excited, it can transfer a part of its energy non-radiatively to the acceptor molecule [147]. This leads to quenching of the donor fluorescence and, if the acceptor is a fluorophore, the emission of acceptor fluorescence. Since the FRET efficiency is inversely proportional to the 6th power of the intermolecular distance, it is a very sensitive marker to probe molecular interactions in the 1-10 nm range. FRET can be detected with (confocal) fluorescence microscopy by measuring the decrease in donor fluorescence and/or the increase in acceptor fluorescence [148]. In the context of nucleic acid delivery, FRET (confocal) microscopy has been used to study the intracellular dissociation of lipoplexes [44] and polyplexes [69]. In these studies, FRET occurred as long as the nucleic acids were compacted in the complexes, while it disappeared when the nucleic acids were released. FRET microscopy has also been used to study the hybridization [149] and degradation [110] of ONs. In the latter case, the ONs were double-labeled with a donor and an acceptor fluorophore and the degradation of the ONs was followed by an increase in donor fluorescence and a decrease in acceptor fluorescence. As will be described in the next chapters of this thesis, we evaluated the use of FRET and FCS as a sensitive method to study the (intracellular) degradation of double-labeled ONs. By following the ratio of acceptor to donor fluorescence as a function of time with the sensitive detectors of the FCS instrument, it was possible to determine the relative resistance against nucleases both in buffer and in living cells.

REFERENCES

(1) Patil, S. D.; Rhodes, D. G.; Burgess, D. J. DNA-based therapeutics and DNA delivery systems: a comprehensive review. *AAPS J.* **2005**, 7, 61-77.

(2) Sazani, P.; Kole, R. Therapeutic potential of antisense oligonucleotides as modulators of alternative splicing. *J. Clin. Invest.* **2003**, 112, 481-486.

(3) Woolf, T. M.; Jennings, C. G. B.; Rebagliati, M.; Melton, D. A. The stability, toxicity and effectiveness of unmodified and phosphorothioate antisense oligodeoxynucleotides in Xenopus oocytes and embryos. *Nucleic Acids Res.* **1990**, 18, 1763-1769.

(4) Brown, D. A.; Kang, S. H.; Gryaznov, S. M.; Dedionisio, L.; Heidenreich, O.; Sullivan, S.; Xu, X.; Nerenberg, M. I. Effect of phosphorothioate modification of oligodeoxynucleotides on specific protein-binding. *J. Biol. Chem.* **1994**, 269, 26801-26805.

(5) Agrawal, S. Importance of nucleotide sequence and chemical modifications of antisense oligonucleotides. *Biochim. Biophys. Acta* **1999**, 1489, 53-68.

(6) Holmlund, J. T. Applying antisense technology - Affinitak (TM) and other antisense oligonucleotides in clinical development. *Ann. NY Acad. Sci.* **2003**, 1002, 244-251.

(7) Jabs, D. A.; Griffiths, P. D. Fomivirsen for the treatment of cytomegalovirus retinitis. *Am. J. Ophthalmol.* **2002**, 133, 552-556.

(8) Akhtar, S.; Hughes, M. D.; Khan, A.; Bibby, M.; Hussain, M.; Nawaz, Q.; Double, J.; Sayyed, P. The delivery of antisense therapeutics. *Adv. Drug Deliver. Rev.* **2000**, 44, 3-21.

(9) Peng, Z. H. Current status of gendicine in China: Recombinant human Ad-p53 agent for treatment of cancers. *Hum. Gene Ther.* **2005**, 16, 1016-1027.

(10) Liu, F.; Huang, L. Development of non-viral vectors for systemic gene delivery. *J. Control. Release* **2002**, 78, 259-266.

(11) Torchilin, V. P. Recent advances with liposomes as pharmaceutical carriers. *Nat. Rev. Drug Discov.* **2005**, 4, 145-160.

(12) Felgner, P. L.; Gadek, T. R.; Holm, M.; Roman, R.; Chan, H. W.; Wenz, M.; Northrop, J. P.; Ringold, G. M.; Danielsen, M. Lipofection - A highly efficient, lipid-mediated DNA-transfection procedure. *Proc. Natl. Acad. Sci. USA* **1987**, 84, 7413-7417.

(13) Oberle, V.; Bakowsky, U.; Zuhorn, I. S.; Hoekstra, D. Lipoplex formation under equilibrium conditions reveals a three-step mechanism. *Biophys. J.* **2000**, 79, 1447-1454.

(14) Zuhorn, I. S.; Bakowsky, U.; Polushkin, E.; Visser, W. H.; Stuart, M. C. A.; Engberts, J. B. F. N.; Hoekstra, D. Nonbilayer phase of lipoplex-membrane mixture determines endosomal escape of genetic cargo and transfection efficiency. *Mol. Ther.* **2005**, 11, 801-810.

(15) Audouy, S. A. L.; De Leij, L. F. M. H.; Hoekstra, D.; Molema, G. In vivo characteristics of cationic liposomes as delivery vectors for gene therapy. *Pharm. Res.* **2002**, 19, 1599-1605.

(16) Meyer, O.; Kirpotin, D.; Hong, K.; Sternberg, B.; Park, J. W.; Woodle, M. C.; Papahadjopoulos, D. Cationic liposomes coated with polyethylene glycol as carriers for oligonucleotides. *J. Biol. Chem.* **1998**, 273, 15621-15627.

(17) Park, T. G.; Jeong, J. H.; Kim, S. W. Current status of polymeric gene delivery systems. *Adv. Drug Deliver. Rev.* **2006**, 58, 467-486.

(18) Pack, D. W.; Hoffman, A. S.; Pun, S.; Stayton, P. S. Design and development of polymers for gene delivery. *Nat. Rev. Drug Discov.* **2005**, 4, 581-593.

(19) Kakizawa, Y.; Kataoka, K. Block copolymer micelles for delivery of gene and related compounds. *Adv. Drug Deliver. Rev.* **2002**, 54, 203-222.

(20) Merdan, T.; Kopecek, J.; Kissel, T. Prospects for cationic polymers in gene and oligonucleotide therapy against cancer. *Adv. Drug Deliver. Rev.* **2002**, 54, 715-758.

(21) Boussif, O.; Lezoualch, F.; Zanta, M. A.; Mergny, M. D.; Scherman, D.; Demeneix, B.; Behr, J. P. A Versatile Vector for Gene and Oligonucleotide Transfer Into Cells in Culture and In-Vivo - Polyethylenimine. *Proc. Natl. Acad. Sci. USA* **1995**, 92, 7297-7301.

(22) Godbey, W. T.; Wu, K. K.; Mikos, A. G. Poly(ethylenimine) and its role in gene delivery. *J. Control. Release* **1999**, 60, 149-160.

(23) Wightman, L.; Kircheis, R.; Rossler, V.; Carotta, S.; Ruzicka, R.; Kursa, M.; Wagner, E. Different behavior of branched and linear polyethylenimine for gene delivery in vitro and in vivo. *J. Gene Med.* **2001**, 3, 362-372.

(24) Kunath, K.; von Harpe, A.; Fischer, D.; Peterson, H.; Bickel, U.; Voigt, K.; Kissel, T. Low-molecular-weight polyethylenimine as a non-viral vector for DNA delivery: comparison of physicochemical properties, transfection efficiency and in vivo distribution with high-molecular-weight polyethylenimine. *J. Control. Release* **2003**, 89, 113-125.

(25) Godbey, W. T.; Wu, K. K.; Mikos, A. G. Size matters: Molecular weight affects the efficiency of poly(ethylenimine) as a gene delivery vehicle. *J. Biomed. Mater. Res.* **1999**, 45, 268-275.

(26) von Harpe, A.; Petersen, H.; Li, Y. X.; Kissel, T. Characterization of commercially available and synthesized polyethylenimines for gene delivery. *J. Control. Release* **2000**, 69, 309-322.

(27) Sung, S. J.; Min, S. H.; Cho, K. Y.; Lee, S.; Min, Y. J.; Yeom, Y. I.; Park, J. K. Effect of polyethylene glycol on gene delivery of polyethylenimine. *Biol. Pharm. Bull.* **2003**, 26, 492-500.

(28) Gupta, B.; Levchenko, T. S.; Torchilin, V. P. Intracellular delivery of large molecules and small particles by cell-penetrating proteins and peptides. *Adv. Drug Deliver. Rev.* **2005**, 57, 637-651.

(29) Mousavi, S. A.; Malerod, L.; Berg, T.; Kjeken, R. Clathrin-dependent endocytosis. *Biochem. J.* **2004**, 377, 1-16.

(30) Watson, P.; Jones, A. T.; Stephens, B. Intracellular trafficking pathways and drug delivery: fluorescence imaging of living and fixed cells. *Adv. Drug Deliver. Rev.* **2005**, 43-61.

(31) Rejman, J.; Oberle, V.; Zuhorn, I. S.; Hoekstra, D. Size-dependent internalization of particles via the pathways of clathrin-and caveolae-mediated endocytosis. *Biochem. J.* **2004**, 377, 159-169.

(32) Qian, Z. M.; Li, H. Y.; Sun, H. Z.; Ho, K. Targeted drug delivery via the transferrin receptor-mediated endocytosis pathway. *Pharmacol. Rev.* **2002**, 54, 561-587.

(33) Hamm-Alvarez, S. F. Targeting endocytosis and motor proteins to enhance DNA persistence. *Pharm. Sci. Technol. To.* **1999**, 2, 190-196.

(34) Johnston, J. B.; Navaratnam, S.; Pitz, M. W.; Maniate, J. M.; Wiechec, E.; Baust, H.; Gingerich, J.; Skliris, G. P.; Murphy, L. C.; Los, M. Targeting the EGFR pathway for cancer therapy. *Curr. Med. Chem.* **2006**, 13, 3483-3492.

(35) Stephenson, S. M.; Low, P. S.; Lee, R. J. Folate receptor-mediated targeting of liposomal drugs to cancer cells. *Method. Enzymol.* **2004**, 387, 33-50.

(36) Desmidt, P. C.; Vanberkel, T. J. C. Ldl-Mediated Drug Targeting. *Crit. Rev. Ther. Drug.* **1990**, 7, 99-120.

(37) Kirkham, M.; Parton, R. G. Clathrin-independent endocytosis: New insights into caveolae and non-caveolar lipid raft carriers. *BBA-Mol. Cell Res.* **2005**, 1745, 273-286.

(38) Nabi, I. R.; Le, P. U. Caveolae/raft-dependent endocytosis. *J. Cell Biol.* **2003**, 161, 673-677.

(39) Pelkmans, L. Secrets of caveolae- and lipid raft-mediated endocytosis revealed by mammalian viruses. *BBA-Mol. Cell Res.* **2005**, 1746, 295-304.

(40) Zuhorn, I. S.; Kalicharan, R.; Hoekstra, D. Lipoplex-mediated transfection of mammalian cells occurs through the cholesterol-dependent clathrin-mediated pathway of endocytosis. *J. Biol. Chem.* **2002**, 277, 18021-18028.

(41) Rejman, J.; Bragonzi, A.; Conese, M. Role of clathrin- and caveolae-mediated endocytosis in gene transfer mediated by lipo- and polyplexes. *Mol. Ther.* **2005**, 12, 468-474.

(42) Rejman, J.; Conese, M.; Hoekstra, D. Gene transfer by means of lipo- and polyplexes: Role of clathrin and caveolae-mediated endocytosis. *J. Liposome Res.* **2006**, 16, 237-247.

(43) von Gersdroff, K.; Sanders, N. N.; Vandenbroucke, R.; De Smedt, S. C.; Wagner, E.; Ogris, M. The internalization route resulting in successful gene expression depends on both cell line and polyethylenimine polyplex type. *Mol. Ther.* **2006**, 14, 745-753.

(44) Zelphati, O.; Szoka, F. C., Jr. Mechanism of oligonucleotide release from cationic liposomes. *Proc. Natl. Acad. Sci. USA* **1996**, 93, 11493-11498.

(45) Szoka, F. C., Jr.; Xu, Y.; Zelphati, O. How are nucleic acids released in cells from cationic lipid-nucleic acid complexes? *J. Liposome Res.* **1996**, 567-587.

(46) Zelphati, O.; Szoka, F. C., Jr. Intracellular distribution and mechanism of delivery of oligonucleotides mediated by cationic lipids. *Pharm. Res.* **1996**, 13, 1367-1372.

(47) Zelphati, O.; Szoka, F. C., Jr. Cationic liposomes as an oligonucleotide carrier: mechanism of action. *J. Liposome Res.* **1997**, 7, 31-49.

(48) Gordon, S. P.; Berezhna, S.; Scherfeld, D.; Kahya, N.; Schwille, P. Characterization of interaction between cationic lipid-oligonucleotide complexes and cellular membrane lipids using confocal imaging and fluorescence correlation spectroscopy. *Biophys. J.* **2005**, 88, 305-316.

(49) Fattal, E.; Couvreur, P.; Dubernet, C. "Smart" delivery of antisense oligonucleotides by anionic pH-sensitive liposomes. *Adv. Drug Deliver. Rev.* **2004**, 56, 931-946.

(50) Deshpande, M. C.; Davies, M. C.; Garnett, M. C.; Williams, P. M.; Armitage, D.; Bailey, L.; Vamvakaki, M.; Armes, S. P.; Stolnik, S. The effect of poly(ethylene glycol) molecular architecture on cellular interaction and uptake of DNA complexes. *J. Control. Release* **2004**, 97, 143-156.

(51) Song, L. Y.; Ahkong, Q. F.; Rong, Q.; Wang, Z.; Ansell, S.; Hope, M. J.; Mui, B. Characterization of the inhibitory effect of PEG-lipid conjugates on the intracellular delivery of plasmid and antisense DNA mediated by cationic lipid liposomes. *Biochim. Biophys. Acta* **2002**, 1558, 1-13.

(52) Shi, F.; Wasungu, L.; Nomden, A.; Stuart, M. C. A.; Polushkin, E.; Engberts, J. B. F. N.; Hoekstra, D. Interference of poly(ethylene glycol)-lipid analogues with cationic-lipid-mediated delivery of oligonucleotides; role of lipid exchangeability and non-lamellar transitions. *Biochem. J.* **2002**, 366, 333-341.

(53) Masson, C.; Garinot, M.; Mignet, N.; Wetzer, B.; Mailhe, P.; Scherman, D.; Bessodes, M. pH-sensitive PEG lipids containing orthoester linkers: new potential tools for nonviral gene delivery. *J. Control. Release* **2004**, 99, 423-434.

(54) Guo, X.; Szoka, F. C. Steric stabilization of fusogenic liposomes by a low-pH sensitive PEG-diortho ester-lipid conjugate. *Bioconjug. Chem.* **2001**, 12, 291-300.

(55) Boomer, J. A.; Inerowicz, H. D.; Zhang, Z. Y.; Bergstrand, N.; Edwards, K.; Kim, J. M.; Thompson, D. H. Acid-triggered release from sterically stabilized fusogenic liposomes via a hydrolytic DePEGylation strategy. *Langmuir* **2003**, 19, 6408-6415.

(56) Rejman, J.; Wagenaar, A.; Engberts, J. B. F. N.; Hoekstra, D. Characterization and transfection properties of lipoplexes stabilized with novel exchangeable polyethylene glycol-lipid conjugates. *BBA-Biomembr.* **2004**, 1660, 41-52.

(57) Cho, Y. W.; Kim, J. D.; Park, K. Polycation gene delivery systems: escape from endosomes to cytosol. *J. Pharm. Pharmacol.* **2003**, 55, 721-734.

(58) Bieber, T.; Meissner, W.; Kostin, S.; Niemann, A.; Elsasser, H. Intracelullar route and transcriptional competence of polyethylenimine-DNA complexes. *J. Control. Release* **2002**, 82, 441-454.

(59) Funhoff, A. M.; van Nostrum, C. F.; Koning, G. A.; Schuurmans-Nieuwenbroek, N. M. E.; Crommelin, D.; Hennink, W. Endosomal escape of polymeric gene delivery complexes is not always enhanced by polymers buffering at low pH. *Biomacromolecules* **2004**, 5, 32-39.

(60) Godbey, W. T.; Barry, M. A.; Saggau, P.; Wu, K. K.; Mikos, A. G. Poly(ethylenimine)-mediated transfection: A new paradigm for gene delivery. *J. Biomed. Mater. Res.* **2000**, 51, 321-328.

(61) Forrest, M. L.; Pack, D. W. On the kinetics of Polyplex endocytic trafficking: implications for gene delivery vector design. *Mol. Ther.* **2002**, 6, 57-65.

(62) Sonawane, N. D.; Szoka, F. C.; Verkman, A. S. Chloride accumulation and swelling in endosomes enhances DNA transfer by polyamine-DNA polyplexes. *J. Biol. Chem.* **2003**, 278, 44826-44831.

(63) Wagner, E.; Plank, C.; Zatloukal, K.; Cotten, M.; Birnstiel, M. L. Influenza-virus hemagglutinin HA-2 N-terminal fusogenic peptides augment gene-transfer by transferrin polylysine DNA complexes - Toward a synthetic virus-like gene-transfer vehicle. *Proc. Natl. Acad. Sci. USA* **1992**, 89, 7934-7938.

(64) Walker, G. F.; Fella, C.; Pelisek, J.; Fahrmeir, J.; Boeckle, S.; Ogris, M.; Wagner, E. Toward synthetic viruses: Endosomal pH-triggered deshielding of targeted polyplexes greatly enhances gene transfer in vitro and in vivo. *Mol. Ther.* **2005**, 11, 418-425.

(65) Meyer, M.; Wagner, E. pH-responsive shielding of non-viral gene vectors. *Expert Opin. Drug Delivery* **2006**, 3, 563-571.

(66) Godbey, W. T.; Wu, K. K.; Mikos, A. G. Tracking the intracellular path of poly(ethylenimine)/DNA complexes for gene delivery. *Proc. Natl. Acad. Sci. USA* **1999**, 96, 5177-5181.

(67) Pollard, H.; Remy, J. S.; Loussouarn, G.; Demolombe, S.; Behr, J. P.; Escande, D. Polyethylenimine but not cationic lipids promotes transgene delivery to the nucleus in mammalian cells. *J. Biol. Chem.* **1998**, 273, 7507-7511.

(68) Honore, I.; Grosse, S.; Frison, N.; Favatier, F.; Monsigny, M.; Fajac, I. Transcription of plasmid DNA: Influence of plasmid DNA/polyethylenimine complex formation. *J. Control. Release* **2005**, 107, 537-546.

(69) Itaka, K.; Harada, A.; Yamasaki, Y.; Nakamura, K.; Kawaguchi, H.; Kataoka, K. In situ single cell observation by fluorescence resonance energy transfer reveals fast intra-cytoplasmic delivery and easy release of plasmid DNA complexed with linear polyethylenimine. *J. Gene Med.* **2004**, 6, 76-84.

(70) Bertschinger, M.; Backliwal, G.; Schertenleib, A.; Jordan, M.; Hacker, D. L.; Wurm, F. M. Disassembly of polyethylenimine-DNA particles in vitro: implications for polyethylenimine-mediated DNA delivery. *J. Control. Release* **2006**, 116, 96-104.

(71) Schaffer, D. V.; Fidelman, N. A.; Dan, N.; Lauffenburger, D. A. Vector unpacking as a potential barrier for receptor-mediated polyplex gene delivery. *Biotechnol. Bioeng.* **2000**, 67, 598-606.

(72) Dauty, E.; Verkman, A. S. Actin cytoskeleton as the principal determinant of size-dependent DNA mobility in cytoplasm. *J. Biol. Chem.* **2005**, 280, 7823-7828.

(73) Lukacs, G. L.; Haggie, P.; Seksek, O.; Lechardeur, D.; Freedman, N.; Verkman, A. S. Size-dependent DNA mobility in cytoplasm and nucleus. *J. Biol. Chem.* **2000**, 275, 1625-1629.

(74) Campbell, E. A.; Hope, T. J. Role of the cytoskeleton in nuclear import. *Adv. Drug Deliver. Rev.* **2003**, 55, 761-771.

(75) Anderson, J. L.; Hope, T. J. Intracellular trafficking of retroviral vectors: obstacles and advances. *Gene Ther.* **2005**, 12, 1667-1678.

(76) Murray, J. W.; Wolkoff, A. W. Roles of the cytoskeleton and motor proteins in endocytic sorting. *Adv. Drug Deliver. Rev.* **2003**, 55, 1385-1403.

(77) King, S. M. The dynein microtubule motor. *BBA-Mol. Cell Res.* **2000**, 1496, 60-75.

(78) Wang, Z. H.; Sheetz, M. P. One-dimensional diffusion on microtubules of particles coated with cytoplasmic dynein and immunoglobulins. *Cell Struct. Funct.* **1999**, 24, 373-383.

(79) Suh, J.; Dawson, M.; Hanes, J. Real-time multiple-particle tracking: Applications to drug and gene delivery. *Adv. Drug Deliver. Rev.* **2005**, 57, 63-78.

(80) Bausinger, R.; von Gersdorff, K.; Braeckmans, K.; Ogris, M.; Wagner, E.; Brauchle, C.; Zumbusch, A. The transport of nanosized gene carriers unraveled by live-cell imaging. *Angew. Chem. Int. Edit.* **2006**, 45, 1568-1572.

(81) Suh, J.; Wirtz, D.; Hanes, J. Efficient active transport of gene nanocarriers to the cell nucleus. *Proc. Natl. Acad. Sci. USA* **2003**, 100, 3878-3882.

(82) Leonetti, J. P.; Mechti, N.; Degols, G.; Gagnor, C.; Lebleu, B. Intracellular distribution of microinjected antisense oligonucleotides. *Proc. Natl. Acad. Sci. USA* **1991**, 88, 2702-2706.

(83) Chin, D. J.; Green, G. A.; Zon, G.; Szoka, F. C., Jr.; Straubinger, R. M. Rapid nuclear accumulation of injected oligodeoxyribonucleotides. *New Biologist* **1990**, 2, 1091-1100.

(84) Raemdonck, K.; Remaut, K.; Lucas, B.; Sanders, N. N.; Demeester, J.; De Smedt, S. C. In situ analysis of single-stranded and duplex siRNA integrity in living cells. *Biochemistry* **2006**, 45, 10614-10623.

(85) Vaughan, E. E.; Dean, D. A. Intracellular trafficking of plasmids during transfection is mediated by microtubules. *Mol. Ther.* **2006**, 13, 422-428.

(86) Salman, H.; Abu-Arish, A.; Oliel, S.; Loyter, A.; Klafter, J.; Granek, R.; Elbaum, M. Nuclear localization signal peptides induce molecular delivery along microtubules. *Biophys. J.* **2005**, 89, 2134-2145.

(87) van der Aa, M. A. E. M.; Mastrobattista, E.; Oosting, R. S.; Hennink, W. E.; Koning, G. A.; Crommelin, D. J. A. The nuclear pore complex: The gateway to successful nonviral gene delivery. *Pharm. Res.* **2006**, 23, 447-459.

(88) Goerlich, D. Transport into and out of the cell nucleus. *EMBO J* **1998**, 17, 2721-2727.

(89) Nigg, E. A. Nucleocytoplasmic transport: Signals, mechanisms and regulation. *Nature* **1997**, 779-787.

(90) Goerlich, D.; Mattaj, I. W. Nucleocytoplasmic transport. *Science* **1996**, 1513-1518.

(91) Marcusson, E. G.; Bhat, B.; Manoharan, M.; Bennett, C. F.; Dean, N. M. Phosphorothioate oligodeoxyribonucleotides dissociate from cationic lipids before and entering the nucleus. *Nucleic Acids Res.* **1998**, 26, 2016-2023.

(92) Remaut, K.; Lucas, B.; Braeckmans, K.; Sanders, N. N.; Demeester, J.; De Smedt, S. C. Delivery of phosphodiester oligonucleotides: Can DOTAP/DOPE liposomes do the trick? *Biochemistry* **2006**, 45, 1755-1764.

(93) Dheur, S.; Dias, N.; Van Aerschot, A.; Herdewijn, P.; Bettinger, T.; Remy, J. S.; Helene, C.; Saison-Behmoaras, E. T. Polyethylenimine but not cationic lipid improves antisense activity of 3'-capped phosphodiester oligonucleotides. *Antisense Nucleic Acid Drug Dev.* **1999**, 9, 515-525.

(94) Tachibana, R.; Harashima, H.; Ide, N.; Ukitsu, S.; Ohta, Y.; Suzuki, N.; Kikuchi, H.; Shinohara, Y.; Kiwada, H. Quantitative analysis of correlation between number of nuclear plasmids and gene expression activity after transfection with cationic liposomes. *Pharm. Res.* **2002**, 19, 377-381.

(95) Escriou, V.; Carrière, M.; Bussone, F.; Wils, P.; Scherman, D. Critical assessment of the nuclear import of plasmid during cationic lipid-mediated gene transfer. *J. Gene Med.* **2001**, 3, 179-187.

(96) Remaut, K.; Sanders, N. N.; Fayazpour, F.; Demeester, J.; De Smedt, S. C. Influence of plasmid DNA topology on the transfection properties of DOTAP/DOPE liposomes. *J. Control. Release* **2006**, 115, 335-343.

(97) Abdelhady, H. G.; Allen, S.; Davies, M. C.; Roberts, C. J.; Tendler, S. J. B.; Williams, P. M. Direct real-time molecular scale visualisation of the degradation of condensed DNA complexes exposed to DNase I. *Nucleic Acids Res.* **2003**, 31, 4001-4005.

(98) Brunner, S.; Sauer, T.; Carotta, S.; Cotten, M.; Saltik, M.; Wagner, E. Cell cycle dependence of gene transfer by lipoplex, polyplex and recombinant adenovirus. *Gene Ther.* **2000**, 7, 401-407.

(99) Mortimer, I.; Tam, P.; MacLachlan, I.; Graham, R. W.; Saravolac, E. G.; Joshi, P. B. Cationic lipid-mediated transfection of cells in culture requires mitotic activity. *Gene Ther.* **1999**, 6, 403-411.

(100) Wilson, G. L.; Dean, B. S.; Wang, G.; Dean, D. A. Nuclear import of plasmid DNA in digitonin-permeabilized cells requires both cytoplasmic factors and specific DNA sequences. *J. Biol. Chem.* **1999**, 274, 22025-22032.

(101) Boulikas, T. Nuclear localization signal peptides for the import of plasmid DNA in gene therapy. *Int. J. Oncol.* **1997**, 301-309.

(102) Kreiss, P.; Cameron, B.; Rangara, R.; Mailhe, P.; Aguerre, C. O.; Airiau, M.; Scherman, D.; Crouzet, J.; Pitard, B. Plasmid DNA size does not affect the physicochemical properties of lipoplexes but modulates gene transfer efficiency. *Nucleic Acids Res.* **1999**, 27, 3792-3798.

(103) Darquet, A. M.; Rangara, R.; Kreiss, P.; Schwartz, B.; Naimi, S.; Delaere, P.; Crouzet, J.; Scherman, D. Minicircle: An improved DNA molecule for in vitro and in vivo gene transfer. *Gene Ther.* **1999**, 6, 209-218.

(104) Ludtke, J. J.; Zhang, G.; Sebestyen, M. G.; Wolff, J. A. A nuclear localization signal can enhance both the nuclear transport and expression of 1 kb DNA. *J. Cell Sci.* **1999**, 112, 2033-2041.

(105) van der Aa, M. A. E. A.; Koning, G. A.; d'Oliveira, C.; Oosting, R. S.; Wilschut, K. J.; Hennink, W. E.; Crommelin, D. J. A. An NLS peptide covalently linked to linear DNA does not enhance transfection efficiency of cationic polymer based gene delivery systems. *J. Gene Med.* **2005**, 7, 208-217.

(106) Glasspool-Malone, J.; Steenland, P. R.; McDonald, R. J.; Sanchez, R. A.; Watts, T. L.; Zabner, J.; Malone, R. W. DNA transfection of macaque and murine respiratory tissue is greatly enhanced by use of a nuclease inhibitor. *J. Gene Med.* **2002**, 4, 323-332.

(107) Ross, G. F.; Bruno, M. D.; Uyeda, M.; Suzuki, K.; Nagao, K.; Whitsett, J. A.; Korfhagen, T. R. Enhanced reporter gene expression in cells transfected in the presence of DMI-2, an acid nuclease inhibitor. *Gene Ther.* **1998**, 5, 1244-1250.

(108) Lechardeur, D.; Sohn, K. J.; Haardt, M.; Joshi, P. B.; Monck, M.; Graham, R. W.; Beatty, B.; Squire, J.; O'Brodovich, H.; Lukacs, G. L. Metabolic instability of plasmid DNA in the cytosol: a potential barrier to gene transfer. *Gene Ther.* **1999**, 6, 482-497.

(109) Pollard, H.; Toumaniantz, G.; Amos, J. L.; Avet-Loiseau, H.; Guihard, G.; Behr, J. P.; Escande, D. Ca2+-sensitive cytosolic nucleases prevent efficient delivery to the nucleus of injected plasmids. *J. Gene Med.* **2001**, 3, 153-164.

(110) Uchiyama, H.; Hirano, K.; Kashiwasake-Jibu, M.; Taira, K. Detection of Undegraded Oligonucleotides *in Vivo* by Fluorescence Resonance Energy Transfer. *J. Biol. Chem.* **1996**, 271, 380-384.

(111) Elson, E. S.; Magde, D. Fluorescence correlation spectroscopy. I. Conceptual basis and theory. *Biopolymers* **1974**, 13, 1-27.

(112) Magde, D.; Webb, W. W.; Elson, E. Thermodynamic fluctuations in a reacting system - Measurement by Fluorescence Correlation Spectroscopy. *Phys. Rev. Lett.* **1972**, 29, 705-708.

(113) Magde, D.; Elson, E. L.; Webb, W. W. Fluorescence Correlation Spectroscopy. 2. Experimental Realization. *Biopolymers* **1974**, 13, 29-61.

(114) Rigler R, Elson ES: Fluorescence correlation spectroscopy. Theory and applications. New York, Springer, 2001.

(115) Krichevsky, O.; Bonnet, G. Fluorescence correlation spectroscopy: the technique and its applications. *Rep. Prog. Phys.* **2002**, 65, 251-297.

(116) Elson, E. L. Fluorescence correlation spectroscopy measures molecular transport in cells. *Traffic* **2001**, 2, 789-796.

(117) Chen, Y.; Muller, J. D.; Berland, K. M.; Gratton, E. Fluorescence fluctuation spectroscopy. *Methods* **1999**, 19, 234-252.

(118) Meseth, U.; Wohland, T.; Rigler, R.; Vogel, H. Resolution of fluorescence correlation measurements. *Biophys. J.* **1999**, 76, 1619-1631.

(119) Rarbach, M.; Kettling, U.; Koltermann, A.; Eigen, M. Dual-color fluorescence cross-correlation spectroscopy for monitoring the kinetics of enzyme-catalyzed reactions. *Methods* **2001**, 24, 104-116.

(120) Bacia, K.; Schwille, P. A dynamic view of cellular processes by in vivo fluorescence auto- and cross-correlation spectroscopy. *Methods* **2003**, 29, 74-85.

(121) Schwille, P.; Meyer-Almes, F.; Rigler, R. Dual-Color Fluorescence Cross-Correlation spectroscopy for multicomponent diffusional analysis in solution. *Biophys. J.* **1997**, 72, 1878-1886.

(122) De Smedt, S. C.; Remaut, K.; Lucas, B.; Braeckmans, K.; Sanders, N. N.; Demeester, J. Studying biophysical barriers to DNA delivery by advanced light microscopy. *Adv. Drug Deliver. Rev.* **2005**, 57, 191-210.

(123) Politz, J. C.; Browne, E. S.; Wolf, D. E.; Pederson, T. Intranuclear diffusion and hybridization state of oligonucleotides measured by fluorescence correlation spectroscopy in living cells. *Proc. Natl. Acad. Sci. USA* **1998**, 95, 6043-6048.

(124) Pederson, T. Movement and localization of RNA in the cell nucleus. *FASEB J.* **1999**, 13, S238-S242.

(125) Jurkiewicz, P.; Okruszek, A.; Hof, M.; Langner, M. Associating oligonucleotides with positively charged liposomes. *Cell. Mol. Biol. Lett.* **2003**, 8, 77-84.

(126) Adjimatera, N.; Kral, T.; Hof, M.; Blagbrough, I. S. Lipopolyamine-mediated single nanoparticle formation of calf thymus DNA analyzed by fluorescence correlation spectroscopy. *Pharm. Res.* **2006**, 23, 1564-1573.

(127) Clamme, J. P.; Azoulay, J.; Mély, Y. Monitoring of the formation and dissociation of PEI/DNA complexes by two photon fluorescence correlation spectroscopy. *Biophys. J.* **2003**, 84, 1960-1968.

(128) Kinjo, M.; Nishimura, G.; Koyama, T.; Mets, U.; Rigler, R. Single-molecule analysis of restriction DNA fragments using fluorescence correlation spectroscopy. *Anal. Biochem.* **1998**, 260, 166-172.

(129) Clamme, J. P.; Krishnamoorthy, G.; Mély, Y. Intracellular dynamics of the gene delivery vehicle polyethylenimine during transfection: investigation by two-photon fluorescence correlation spectroscopy. *BBA-Biomembr.* **2003**, 1617, 52-61.

(130) Kettling, U.; Koltermann, A.; Schwille, P.; Eigen, M. Real-time enzyme kinetics monitored by dual-color fluorescence cross-correlation spectroscopy. *Proc. Natl. Acad. Sci. USA* **1998**, 95, 1416-1420.

(131) Berezhna, S.; Schaefer, S.; Heintzmann, R.; Jahnz, M.; Boese, G.; Deniz, A.; Schwille, P. New effects in polynucleotide release from cationic lipid carriers revealed by confocal imaging, fluorescence cross-correlation spectroscopy and single particle tracking. *BBA-Biomembr.* **2005**, 1669, 193-207.

(132) Schwille, P. Fluorescence correlation spectroscopy and its potential for intracellular applications. *Cell Biochem. Biophys.* **2001**, 34, 383-408.

(133) Schwille, P.; Haupts, U.; Maiti, S.; Webb, W. W. Molecular dynamics in living cells observed by fluorescence correlation spectroscopy with one- and two-photon excitation. *Biophys. J.* **1999**, 77, 2251-2265.

(134) Gennerich, A.; Schild, D. Fluorescence correlation spectroscopy in small cytosolic compartments depends critically on the diffusion model used. *Biophys. J.* **2000**, 79, 3294-3306.

(135) Bacia, K.; Majoul, I. V.; Schwille, P. Probing the endocytic pathway in live cells using Dual-Color Fluorescence Cross-Correlation analysis. *Biophys. J.* **2002**, 83, 1184-1193.

(136) Bacia, K.; Kim, S. A.; Schwille, P. Fluorescence cross-correlation spectroscopy in living cells. *Nat. Methods* **2006**, 3, 83-89.

(137) Van Craenenbroeck, E.; Vercammen, J.; Matthys, G.; Beirlent, J.; Marot, C.; Hoebeke, J.; Strobbe, R.; Engelborghs, Y. Heuristic statistical analysis of fluorescence fluctuation data with bright spikes: Application to ligand binding to the human serotonin receptor expressed in Escherichia coli cells. *Biol. Chem.* **2001**, 382, 355-361.

(138) Van Craenenbroeck, E.; Matthys, G.; Beirlant, J.; Engelborghs, Y. A statistical analysis of fluorescence correlation data. *J. Fluoresc.* **1999**, 9, 325-331.

(139) Van Rompaey, E.; Sanders, N. N.; De Smedt, S. C.; Demeester, J. Complex formation between cationic polymethacrylates and oligonucleotides. *Macromolecules* **2000**, 33, 8280-8288.

(140) Van Rompaey, E.; Engelborghs, Y.; Sanders, N.; De Smedt, S. C.; Demeester, J. Interactions between oligonucleotides and cationic polymers investigated by fluorescence correlation spectroscopy. *Pharm. Res.* **2001**, 18, 928-936.

(141) Van Rompaey, E.; Chen, Y.; Muller, J. D.; Gratton, E.; Van Craenenbroeck, E.; Engelborghs, Y.; De Smedt, S. C.; Demeester, J. Fluorescence fluctuation analysis for the study of interactions between oligonucleotides and polycationic polymers. *Biol. Chem.* **2001**, 382, 379-386.

(142) Lucas, B.; Van Rompaey, E.; De Smedt, S. C.; Demeester, J.; Van Oostveldt, P. Dual-color FFS to study the complexation between poly-l-lysine and oligonucleotides. *Macromolecules* **2002**, 35, 8152-8160.

(143) Lucas, B.; Remaut, K.; Braeckmans, K.; Haustraete, J.; De Smedt, S. C.; Demeester, J. Studying pegylated DNA complexes by dual color fluorescence fluctuation spectroscopy. *Macromolecules* **2004**, 37, 3832-3840.

(144) Lucas, B.; Remaut, K.; Sanders, N. N.; Braeckmans, K.; De Smedt, S. C.; Demeester, J. Towards a better understanding of the dissociation behavior of liposome-oligonucleotide complexes in the cytosol of cells. *J. Control. Release* **2005**, 103, 435-450.

(145) Lucas, B.; Remaut, K.; Sanders, N. N.; Braeckmans, K.; De Smedt, S. C.; Demeester, J. Studying the intracellular dissociation of polymer-oligonucleotide complexes by dual color fluorescence fluctuation spectroscopy and confocal imaging. *Biochemistry* **2005**, 44, 9905-9912.

(146) Periasamy, A. Imaging the dynamic events: FRET microscopy. *Biophys. J.* **2001**, 80, 161A-161A.

(147) Jares-Erijman, E. A.; Jovin, T. M. FRET imaging. *Nature Biotechnol.* **2003**, 21, 1387-1395.

(148) Gordon, G. W.; Berry, G.; Liang, X. H.; Levine, B.; Herman, B. Quantitative fluorescence resonance energy transfer measurements using fluorescence microscopy. *Biophys. J.* **1998**, 74, 2702-2713.

(149) Sixou, S.; Szoka, F. C., Jr.; Green, G. A.; Giusti, B.; Zon, G.; Chin, D. J. Intracellular oligonucleotide hybridization detected by fluorescence resonance energy transfer (FRET). *Nucleic Acids Res.* **1994**, 22, 662-668.

Chapter 2

FRET-FCS AS A TOOL TO EVALUATE THE STABILITY OF OLIGONUCLEOTIDES AFTER INTRACELLULAR DELIVERY

Parts of this chapter were published in:

Remaut, K.; Lucas, B.; Braeckmans, K.; Sanders, N. N.; De Smedt, S. C.; Demeester, J. *J. Control. Release* **2005**, 103, 259-271.

ABSTRACT

In this chapter, we studied the use of a dual-color Fluorescence Correlation Spectroscopy (FCS) instrument to follow the intracellular degradation of single-stranded, double-labeled oligonucleotides (ONs). The degradatioan of the ONs was studied by following the disappearance of Fluorescence Resonance Energy Transfer (FRET) between the rhodamine green and Cy5 fluorophores attached to respectively the 3' and 5' end of the ONs. The green and red fluorescence intensities upon rhodamine green excitation were monitored using the ultrasensitive detectors of the FCS instrument. The ratio of the red to green fluorescence (R/G ratio) as obtained from such FRET-FCS measurements gave accurate information on the integrity of the ONs, without the need for additional auto- or cross-correlation analysis of the registered fluorescence intensity fluctuations. Intracellular measurements revealed that most of the 40 mer phosphodiester ONs were degraded before they entered the nucleus. For the 20 mer phosphodiester ONs, this degradation occurred more slowly, and both intact and degraded ONs entered the nucleus. For the 20 mer phosphothioate ONs, no intracellular degradation was observed during the measured time period. The sensitive detection of the intracellular fluorescence by the FCS setup will be particularly useful in situations where the expected fluorescence is too low to be detected by FRET-imaging as may occur after intracellular delivery of ONs by cationic carriers.

Chapter 2

FRET-FCS as a Tool to Evaluate the Stability of Oligonucleotides after Intracellular Delivery

INTRODUCTION

Antisense oligonucleotides (ONs) are being widely investigated to down-regulate genes of interest. They have already been proved efficient in treating viral infections such as the human immunodeficiency virus type 1 [1], the hepatitis B virus [2] and the human cytomegalovirus [3]. Also, utilization of antisense ONs for the treatment of cancer is believed to be possible [4]. Antisense drugs act by specifically binding to the target mRNA or DNA, which results in inhibition of the target translation or transcription. In spite of this simple action mechanism, different barriers still limit the antisense activity. Indeed, before the ONs can reach their target site, they first have to cross the cellular membrane, escape from the endosomal compartment, leave their pharmaceutical carriers (i.e. the delivery system) and hybridize to the target sequence. In all these processes, degradation of the antisense drug is highly undesirable. Regrettably, the intracellular fate of antisense ONs remains rather unknown, also because of the limited methods that allow characterization of these critical steps in living cells.

An important tool to study interactions between molecules is Fluorescence Resonance Energy Transfer (FRET). In FRET, an excited donor fluorophore can lead to the emission signal from an acceptor fluorophore because of a distance-dependent energy transfer between the donor and the acceptor. Therefore, FRET can be used to monitor virtually any process that changes the distance between the donor and acceptor. Uchiyama *et al.* [5] used FRET-imaging to study the degradation of single-stranded ONs, double-labeled with a donor and acceptor fluorophore. Upon injection in sea urchin eggs, the decrease of the acceptor to donor fluorescence ratio showed that a phosphodiester ON was degraded within 60 minutes, whereas the phosphothioate ON remained intact. In FRET-imaging, the

amount of FRET is monitored using a conventional fluorescence or confocal microscope, followed by image analysis. However, when interacting molecules have to be studied at very low (e.g. nanomolar) concentrations, the (intracellular) fluorescence could become too low to allow FRET-imaging. Therefore, a more sensitive detection of the fluorescence could expand the possibilities of intracellular FRET measurements.

A promising tool to measure intracellularly the fluorescence of lowly concentrated molecules is Fluorescence Correlation Spectroscopy (FCS) [6]. Compared to a fluorescence microscope, a FCS setup makes use of much more sensitive avalanche photo diode detectors which can even register the fluorescence of single molecules. Basically, FCS monitors the fluorescence fluctuations as the fluorescent molecules move in and out the detection volume (typically some femtoliters) of a microscope. From the fluorescence intensity fluctuations information is obtained on the amount of molecules in the detection volume and their diffusion coefficient. In dual-color FCS, the fluorescence of two spectrally different fluorophores is measured by two (separate) detectors and also the amount of double-labeled molecules can be derived. Some studies were reported in which dual-color FCS was used to follow the hybridization of single-stranded ONs and the degradation of the double-labeled hybridization products [7-10]. Our research group applied dual-color FCS to investigate the interactions between ONs and their pharmaceutical carriers [11;12]. In cells however, the fluorescence fluctuation analysis is complicated [13;14] and using dual-color FCS, only one intracellular study has been reported so far [15].

In this chapter we wondered whether the intracellular degradation of lowly concentrated ONs could be monitored by FRET using a dual-color FCS setup to measure the fluorescence. The degradation of single-stranded, double-labeled (Cy5 and rhodamine green) ONs, giving FRET between the two labels, was studied both in buffer, cytosolic cell extract and living cells. We found that the green and the red fluorescence intensities as registered by the detectors of the dual-color FCS instrument can provide us within seconds with information on the integrity of the ONs. Furthermore, these fluorescence intensities could be easily determined in living cells, giving us the possibility to follow the intracellular fate of ONs, without the need for additional auto- and cross-correlation analysis of the intracellular fluorescence intensity fluctuations.

MATERIALS AND METHODS

Oligonucleotides

Fluorescently labeled 20 mer phosphodiester (PO20-ONs), 20 mer phosphothioate (PS20-ONs) (5'-CCC-CCA-CCA-CTT-CCC-CTC-TC-3') and 40 mer phosphodiester oligonucleotides (PO40-ONs) (5'-GCC-GTC-TCT-GAC-TGC-TGA-TGA-CTA-CTA-TCG-TAT-AGT-GCG-G-3') were purchased from Eurogentec (Seraing, Belgium). All ONs were double-labeled with a rhodamine green fluorophore at the 3' end and a Cy5 fluorophore at the 5' end. Also, single-labeled (rhodamine green or Cy5) PO20-ONs were used. The ONs were PAGE-purified and the presence of both dyes was controlled by Maldi-Tof Mass Spectrometry by the supplier. The concentration of the ONs stock solutions as given by the supplier was verified by absorption measurements at 260 nm (1 OD_{260} = 33 µg ONs). Labeling efficiencies were calculated from absorption measurements at 500 nm (~ rhodamine green, ε = 54 000 $l.mol^{-1}.cm^{-1}$) and 647 nm (~ Cy5, ε = 250 000 $l.mol^{-1}.cm^{-1}$) and revealed that over 85% of the ONs bore the two labels.

Fluorescence Emission Scans

Fluorescence emission scans were taken on an Aminco Bowman Series 2 Spectrofluorimeter to determine the FRET efficiency of the ONs. The excitation wavelengths used for rhodamine green and Cy5 were 488 nm and 647 nm, respectively. The emission wavelengths were 532 nm and 671 nm. The ONs were diluted in 'degradation buffer' (20 mM HEPES, 110 mM potassium acetate and 2 mM magnesium acetate, pH 7.4) to a final concentration of 100 nM. As a control sample, a mixture of 100 nM single-labeled 3' rhodamine green and 100 nM single-labeled 5' Cy5 PO20-ONs was used. Emission spectra were recorded from 510 to 750 nm with the excitation wavelength set to 488 nm, before and after addition of 1 unit DNase I solution (Pulmozyme®, 1 units/µL, Genentech) to 700 µL ON solution. In all experiments the background fluorescence of the degradation buffer used was negligible.

The FRET efficiency of the ONs was determined as the extent of rhodamine green fluorescence quenching using eq. 1, with F_1 being the fluorescence intensity at 532 nm of the double-labeled ONs upon excitation at 488 nm and F_2 being the fluorescence intensity at 532 nm of the control sample (in which no FRET occurs).

$$Q = \left(1 - \left(F_1 / F_2\right)\right) * 100 \qquad \text{eq. 1}$$

Fluorescence Correlation Spectroscopy (FCS)

Theoretical Concept

For details about the theoretical concept of FCS, we would like to refer to Chapter 1 of this thesis and references 6 (single-color FCS) and 10 (dual-color FCS). Briefly, FCS makes use of ultrasensitive avalanche photodiode detectors to monitor fluorescence intensity fluctuations caused by the diffusion of fluorescently labeled molecules through the excitation volume of a microscope. From these fluorescence intensity fluctuations an auto-correlation curve can be derived which allows calculating the amount of fluorescent molecules in the detection volume and their diffusion coefficient. In dual-color FCS the interaction between two molecules labeled with spectrally different fluorophores is monitored (e.g. green and red fluorophore). Apart from an auto-correlation curve, a cross-correlation curve can be derived which gives information on the amount of double-labeled molecules and their diffusion coefficient. While the amplitude of the auto-correlation curve is inversely proportional to the amount of fluorescently labeled molecules in the detection volume (regardless of whether they are single or double-labeled), the amplitude of the cross-correlation curve is proportional to the amount of double-labeled molecules.

Experimental Setup

Dual-color FCS experiments were performed on a dual-color FCS setup installed on a MRC1024 Bio-Rad confocal laser scanning microscope. An inverted microscope (Eclipse TE300D, Nikon, Japan) was used, which was equipped with a water immersion objective lens (Plan Apo 60X, NA 1.2, collar rim correction, Nikon, Japan). The 488 nm and 647 nm lines of a krypton-argon laser (Biorad, Cheshire, UK) were used and fluorescence intensity fluctuations were recorded on a digital ALV 5000/E correlator. The system was calibrated as described by Schwille *et al.* [10] to optimize the overlap of the excitation and detection volumes and to determine the size of the detection volume. Briefly, a 20 nM rhodamine green solution was excited using 488 nm laser light. The fluorescence emission is mainly detected by the green detector but also partially reaches the red detector. Due to this 'crosstalk' an auto-correlation curve can be generated from both the green and the red detector. If the detection volumes of the green and the red detector are of the same size, both auto-correlation curves should have the same amplitude. If additionally the green and red detection volume overlap, the generated cross-correlation curve should also have the same amplitude as the auto-correlation curves.

Auto- and Cross-correlation analysis

For determination of the diffusion behaviour, 50 µL of ONs solution was placed in a glass-bottomed 96 well plate (certified DNase/RNase free, Greiner Bio-one, lot 03170175,

Frickenhausen, Germany) and the laser beam (488 nm, 647 nm or a combination of both) was focused at 50 µm above the bottom of the wells. The ONs concentrations ranged between 5 and 10 nM. Fluorescence intensity fluctuations were recorded for 3 x 30 seconds with laser excitation set to 488 nm, 647 nm or both. The recorded auto- and/or cross-correlation curves $G(\tau)$ were analyzed in Origin™ (Microcal software, Northampton, USA) using equation 1 or 4 as described in Chapter 1 of this thesis. From the diffusion time τ_t the diffusion coefficient *D* was calculated using equation 3 (see Chapter 1).

R/G ratio as Obtained from FRET-FCS Measurements

In FRET-FCS measurements, the green (rhodamine green) and red (Cy5) fluorescence intensities were recorded for 2 seconds with both detectors of the dual-color FCS instrument, with laser excitation set to 488 nm. From these fluorescence intensities, the ratio of the red to the green fluorescence (R/G ratio) was calculated. No additional auto- or cross-correlation analysis were performed.

For FRET-FCS measurements on degrading ONs, the ONs were diluted to a concentration of 0.7 µM in degradation buffer (for DNase I) or an acidic buffer (for DNase II) (40 mM acetic acid and 60 mM potassium acetate, pH 4.7). Subsequently, 4 µL of 100x, 500x or 2000x diluted DNase I or 4 µL DNase II (4.7 units/µL, Sigma) was added. The solutions with a total volume of 40 µL were incubated at 37°C. At different time points 2 µL was removed and diluted with 198 µL TBE buffer (10.8 g/L Tris base, 5.5 g/ L boric acid and 0.58 g/L EDTA) to stop the degradation. On these solutions (final concentration of 7 nM), the R/G ratio was determined. For the FRET-FCS measurements in cytosolic cell extract, the ONs were incubated at 37°C with an equal volume of cell lysate and diluted with TBE to the appropriate concentration (between 5 and 10 nM).

When performing intracellular FRET-FCS, first a confocal image of the microinjected cell was taken and the detection volume was positioned in the cytoplasm or the nucleus of the cell. Then, the green and red fluorescence intensities were recorded (for 2 seconds) with laser excitation set to 488 nm. Laser excitation was kept at a low level (1% of the maximum laser power (0.3 mW) at the focal plane) to prevent cell damaging and photobleaching. For real-time monitoring of the intracellular degradation, the green and red fluorescence intensities were recorded (for 2 seconds) in the nucleus at different time points.

Cell Culture and Microinjection Experiments

Vero cells were cultured in Dulbecco's modified Eagle's medium (DMEM) without phenol red (Gibco, Merelbeke, Belgium) containing 2 mM glutamine, 10% heat deactivated fetal bovine serum (FBS) and 1% penicillin-streptomycin at 37°C in a humidified atmosphere containing 5% CO_2. For intracellular FRET-FCS measurements, cells were seeded on petri

dishes with in the center a 150 µm thick glass bottomed circle (Part No. PG-1.5-14-F, Glass bottom No. 1.5, MatTek Corporation) at 10^4 cells/cm². The cells were incubated between 24 and 48 hours before starting the microinjection experiments.

Microinjection experiments were performed with a Femtojet® microinjector and an Injectman® NI 2 micromanipulator (Eppendorf). All injections were performed in the cytoplasm of the cells, using 2 µM ONs. Immediately after injection, FRET-FCS measurements were carried out as described earlier in the Fluorescence Correlation Spectroscopy section.

Preparation of Cytosolic Cell Extract

Cell extract was derived from Vero cells at 90% confluency following the Clontech Cytosolic Extraction Procedure. Briefly, cells were collected after centrifugation and suspended in a hypotonic lysis buffer containing protease inhibitors (10 mM HEPES pH 7.9, 1.5 mM $MgCl_2$ and 10 mM KCl + 1 µM Leupeptine, 0.5 mM Pefabloc SC, 1 mM DTT and 0.5 mM EGTA). After 15 minutes swelling on ice, cells were centrifuged again and resuspended in 2 times the cell pellet volume of lysis buffer + protease inhibitors. This cell suspension was drawn into a narrow-gauge syringe and rapidly ejected. Lysis occurred by repeating the drawing and ejection procedure 10 times. The disrupted cell suspension was then centrifuged for 20 minutes at 11 000 g and the supernatant was stored at –80°C.

The presence of lysosomal enzymes was determined by assessing the hexosaminidase activity. 10 µL of cytosolic extract was incubated overnight with 60 µL substrate solution (7.5 mM p-nitrophenyl-N-acetyl-β-D-glucosaminide and 0.1 mM citric acid, pH 5) at 37°C. After addition of 90 µL 'stop solution' (10 mM EDTA and 100 mM glycine, pH 10.5) the absorbance was measured at 405 nm. As a control, the cytosolic cell extract was heated to 100°C to destroy all enzymatic activity. These tests revealed that the obtained cytosolic cell extract contained lysosomal enzymes (data not shown).

RESULTS AND DISCUSSION

Oligonucleotide Degradation as Revealed from Fluorescence Emission Scans

Emission spectra were taken from 510 to 750 nm to determine the FRET efficiency of the double-labeled ONs (Figure 1A). All double-labeled ONs displayed FRET as can be seen by the decrease in the rhodamine green fluorescence (at 532 nm) and the increase in the Cy5 fluorescence (at 671 nm) when compared to the control sample. FRET efficiencies as

calculated from the rhodamine green quenching using eq. 1 equaled 84%, 66% and 44% for the PO40-ONs, PS20-ONs and PO20-ONs respectively. Clearly, the PO40-ONs give the best FRET efficiency. At first sight this may seem contradictory since one would expect the FRET efficiency to decrease when the distance between the fluorophores increases. However, probably the PO40-ONs are more flexible compared to the PO20-ONs and PS20-ONs and take a shape that brings the two fluorophores closer together.

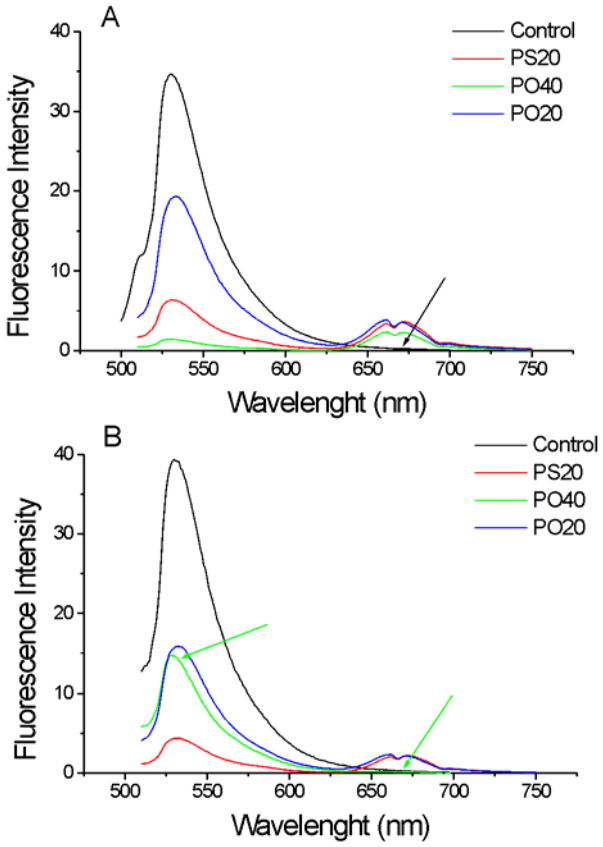

Figure 1. Fluorescence emission scans of the double-labeled ONs. The 'control sample' is a mixture of 100 nM single-labeled rhodamine green PO20-ONs and 100 nM single-labeled Cy5 PO20-ONs. Excitation wavelength was set to 488 nm. All ONs concentrations equaled 100 nM. (A) Before addition of DNase I. The FRET efficiency was calculated to be 66% (PS20-ONs), 84% (PO40-ONs) and 44% (PO20-ONs). The control showed no FRET (indicated by the arrow). (B) After addition of 1 unit DNase I to the ONs solutions. There is a 10-fold increase in the PO40-ONs' rhodamine green emission and a corresponding decrease in the Cy5 emission (indicated by the arrows) showing the degradation of the PO40-ONs. The PS20-ONs and PO20-ONs emission scans remain unchanged.

Emission scans were taken again after addition of 1 unit DNase I to the ONs solutions (Figure 1B). For the PO40-ONs, the rhodamine green emission increased 10-fold together with a corresponding decrease in the Cy5 fluorescence, demonstrating the degradation of the PO40-ONs. Indeed, when the ON-strand is degraded, the donor and acceptor fluorophore can move freely, the close proximity of the fluorophores is lost and FRET no longer occurs. Apparently, DNase I does not degrade the PS20-ONs and the PO20-ONs. As

for the PS20-ONs, this can be explained by the increased nuclease resistance due to the phosphothioate backbone. In the case of the PO20-ONs, however, this cannot be the reason. However, it has been reported that the DNase I endonuclease has the highest affinity for DNA with mixed-sequence regions [16]. Cytidine and guanosine-rich regions or consecutive adenosines or thymidines seriously lower the cleavage probabilities. As the PO20-ONs contain two cytidine-rich regions, this probably explains the resistance towards DNase I.

Oligonucleotide Degradation as Revealed from FRET-FCS Measurements

We are interested to monitor the stability of ONs in living cells, even at low concentrations. As shown above, the elimination of FRET upon degradation of the ONs results in an increase in the rhodamine green fluorescence and a decrease in the Cy5 fluorescence after excitation at 488 nm. Therefore, a major aim of this chapter is to evaluate whether the degradation of double-labeled, single-stranded ONs can be observed from the donor (green) and acceptor (red) fluorescence intensities as registered by the separate detectors of a dual-color FCS instrument.

The ratio of the red to green fluorescence (R/G ratio) before and after addition of different desoxyribonucleases to the ON solutions are summarized in Figure 2. As already discussed above, each intact ON showed FRET, which can be seen by the high R/G ratio (black bars). From the initial R/G ratios, a FRET efficiency order of PO40-ONs > PS20-ONs > PO20-ONs appears, which is in agreement with the FRET efficiency order as determined from the fluorescence emission scans. Also in agreement with the results from the fluorimetric scans, addition of DNase I leads only to the degradation of the PO40-ONs (gray bars), which can be seen by the drop of the R/G ratio due to the disappearance of FRET. Upon incubation with DNase II (light gray bars), both the PO40-ONs and PO20-ONs degrade. So where the cytidine-rich regions of the PO20-ONs lower the splicing probability of the DNase I enzyme, this does not influence the DNase II enzyme which is indeed reported to cleave DNA without an apparent sequence specificity [17]. After addition of cytosolic cell extract (white bars), again the PO40-ONs and PO20-ONs degrade. Probably this again results from DNase II or DNase II-like enzymes which are found intracellularly. With all desoxyribonucleases the PS20-ONs stay intact, which demonstrates the nuclease resistance of ONs with a phosphothioate backbone. The graphs insert in Figure 2 shows the degradation of the ONs visualized with PAGE gel electrophoresis. It can be seen that a drop in the R/G ratio corresponds to the disappearance of the ONs on gel, demonstrating the applicability of the R/G ratio to predict the degradation of the ONs.

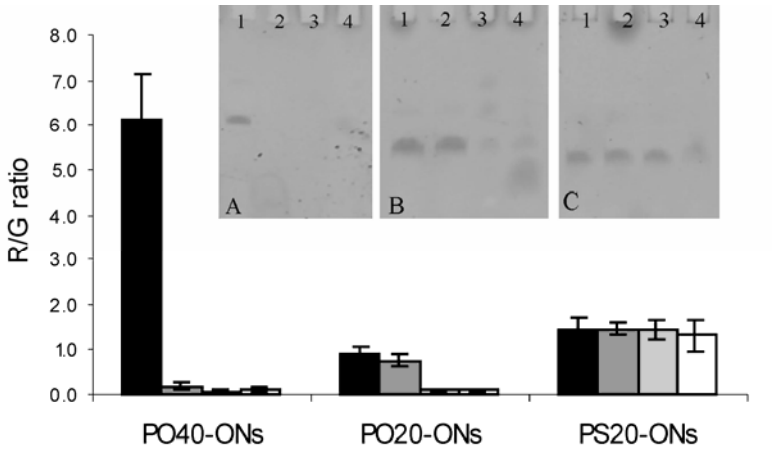

Figure 2. Degradation of the ONs in the presence of DNase I, DNase II or cytosolic cell extract. Ratio of the red (~ Cy5) to the green (~ rhodamine green) emission as obtained from the fluorescence intensity fluctuations registered by the FCS setup. Laser excitation was 488 nm. Measurements were performed in buffer (black bars), after addition of 1 unit DNase I (gray bars), 20 units DNase II (light gray bars) or cytosolic cell extract (white bars) to 200 µL of the ONs solutions. Values are the mean as obtained from four independent solutions. Graph insert: polyacrylamide gel electrophoresis on (A) PO40-ONs, (B) PO20-ONs and (C) PS20-ONs. The wells contain 100 ng ON (lane 1), 100 ng ON + 1 unit DNase I (lane 2), 100 ng ON + 20 units DNase II (lane 3) or 100 ng ON + cytosolic cell extract (lane 4). The incubation times were 1 hour for the DNase I enzyme and cytosolic cell extract and 8 hours for the DNase II enzyme.

Oligonucleotide Degradation as Revealed from the Auto- and Cross-correlation Analysis of the Fluorescence Fluctuations

Based on theoretical considerations outlined below one can argue that auto-correlation analysis can only be used to distinguish between fully intact and fully degraded ONs. Assuming $D \sim 1/(MG)^{1/3}$ [7], a 8-fold change in molecular weight corresponds to a 2-fold change in diffusion coefficient, being the minimal change in mobility which is well-distinguishable by FCS. With the molecular weight of for example the PO20-ONs being 6924 g/mol, the molecular weight of the degradation products should be maximally 865 g/mol to double the diffusion coefficient. With the average molecular weight per nucleotide being 330 g/mol, this corresponds to degradation products consisting of only 2 to 3 nucleotides before a distinguishable change in diffusion coefficient is obtained. Clearly, this makes auto-correlation analysis less attractive to study the degradation when compared to the disappearance of the FRET signal, which is already achieved from the moment that both fluorophores are separated, regardless of the molecular weight of the degradation products formed.

Cross-correlation analysis represents an alternative in reactions where the expected changes in diffusion coefficient are minimal. Nevertheless, the amplitude of the cross-correlation curve is only proportional to the amount of double-labeled ONs if no fluorescence enhancement or quenching of the fluorophores occurs upon interaction. However, this was

not the case as FRET occurs. Although Kohl *et al.* [18] demonstrated that FRET efficiencies between 30-60% can be tolerated if properly corrected for in the data analysis, cross-correlation analysis of the fluorescence fluctuations could also only be used to distinguish between fully intact or fully degraded ONs.

Table 1. Diffusion times of the PO20-ONs before and after addition of different desoxyribonucleases. Diffusion times τ_t (ms) were determined from the auto-correlation curves after excitation with respectively 488 nm ($\tau_{g,\,488}$) and 647 nm ($\tau_{r,\,647}$). When possible, $\tau_{r,\,488}$, being the diffusion time of the red labeled components upon excitation at 488 nm, was also determined. τ_{cc} represents the diffusion time determined from the cross-correlation curve. The diffusion time of rhodamine green was 0.21 ± 0.02 ms in our FCS setup and corresponds to a diffusion coefficient of 2.8 x 10^{-10} m²/s. * ND: not determinable.

	$\tau_{g,\,488}$	$\tau_{r,\,488}$	$\tau_{r,647}$	τ_{cc}
Buffer	0.52 ± 0.05	0.57 ± 0.07	0.53 ± 0.02	0.56 ± 0.08
DNase I	0.58 ± 0.08	0.57 ± 0.09	0.53 ± 0.02	0.50 ± 0.10
DNase II	0.29 ± 0.02	ND*	0.29 ± 0.02	ND*
Cell lysate	0.30 ± 0.02	ND*	0.30 ± 0.02	ND*

As an example, the diffusion times for the PO20-ONs are depicted in Table 1. The auto- and cross-correlation curves from which these diffusion times were calculated are depicted in Figure 3. When the ONs are intact (in buffer and in the presence of DNase I), the auto-correlation curves from the green and red detector upon excitation with respectively 488 nm (~ rhodamine green) and 647 nm (~ Cy5) are of good quality and almost completely overlap (Figure 3, green and red line). Also, due to FRET, it is possible to generate a proper auto-correlation curve for the Cy5 fluorophores upon excitation at 488 nm (Figure 3, gray line). Fitting of these auto-correlation curves with a single-species model is possible, leading to the diffusion times $\tau_{g,\,488}$ (~ rhodamine green), $\tau_{r,\,647}$ and $\tau_{r,\,488}$ (~ Cy5), which were all equal (Table 1). The diffusion time calculated from the cross-correlation curve (τ_{cc} ~ double-labeled ONs) equals the diffusion times from the auto-correlation curves, showing that the solutions consist of double-labeled ONs. However, calculating the amount of double-labeled ONs from the generated cross-correlation curve (Figure 3, blue line) was not possible, as FRET disturbed the cross-correlation analysis.

When the ONs degrade (in the presence of DNase II and cytosolic cell extract), single-labeled degradation products are formed and a cross-correlation curve can no longer be recorded (Figure 3, graph insert, blue line). Hence, τ_{cc} cannot be determined. Also, the

auto-correlation curve generated from the red detector upon excitation at 488 nm has become very noisy (Figure 3, graph insert, gray line). Therefore, the diffusion time of the Cy5-labeled degradation products cannot be determined upon excitation at 488 nm ($\tau_{r,\ 488}$) since FRET no longer occurs. Good quality auto-correlation curves can be generated from the green and red detector upon excitation at respectively 488 nm and 647 nm (Figure 3, graph insert, green and red line). From the calculated diffusion times $\tau_{g,\ 488}$ (~ rhodamine green) and $\tau_{r,\ 647}$ (~ Cy5) it can be seen that shorter degradation products were formed, which move more rapidly through the excitation volume of the FCS instrument (Table 1).

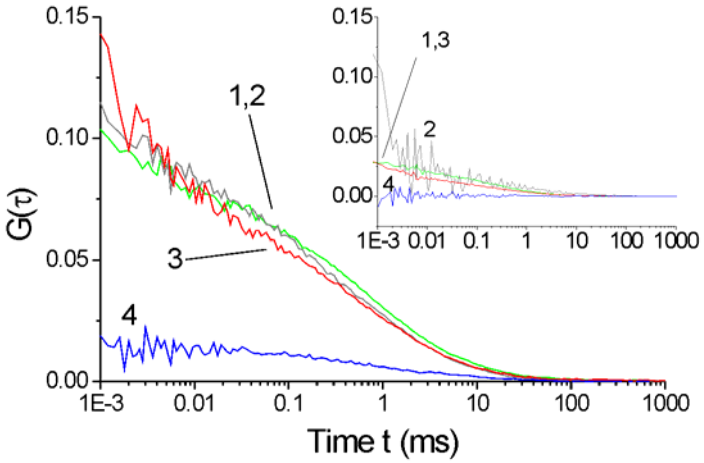

Figure 3. Auto- and cross-correlation curves of the PO20-ONs. Line 1 (green) is the auto-correlation curve obtained from the green detector upon excitation at 488 nm (~ rhodamine green), line 2 (gray) is the auto-correlation curve obtained from the red detector upon excitation at 488 nm (~ Cy5, excitation due to FRET), line 3 (red) is the auto-correlation curve obtained from the red detector upon excitation at 647 nm (~ Cy5, 'direct' excitation) and line 4 (blue) is the cross-correlation curve obtained from the fluorescence intensities registered by the green and the red detector upon excitation at 488 and 647 nm. The graph insert represents the auto-correlation curves after degradation of the PO20-ONs.

In Vitro Time Dependent Degradation of the ONs

In the following experiments, we wondered whether the ratio of the red to the green fluorescence intensities as registered with the FCS setup upon excitation at 488 nm (R/G ratio) allows to monitor the time dependent degradation of the ONs. First, the change in the R/G ratio was evaluated upon mixing different amounts of intact and degraded PO40-ONs, mimicking the transition from fully intact to fully degraded ONs. Figure 4 shows that upon mixing a higher percentage of degraded PO40-ONs, the R/G ratio decreases and reaches a value of 8% of the initial value when the solution consists of only degraded PO40-ONs.

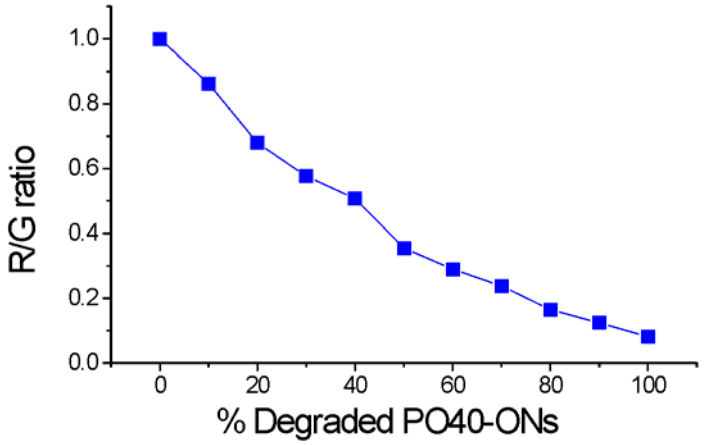

Figure 4. Relation between the amount of intact ONs and the R/G ratio. Ratio of the red to green fluorescence intensities (R/G ratio) as measured by the dual-color FCS module of solutions prepared by mixing different amounts of intact and degraded PO40-ONs. The x-axis indicates the percentage of degraded PO40-ONs. Laser excitation was set to 488 nm. To normalize the R/G ratio we considered the R/G ratio for the intact PO40-ONs to be 1.

Subsequently, the R/G ratios for the PS20-ONs, PO20-ONs and PO40-ONs were monitored when bringing them in contact with DNase I, DNase II or cytosolic cell extract (Figure 5). For incubation with 0.04 units DNase I (Figure 5A), the R/G ratio decreases rapidly for the PO40-ONs (triangle) and degradation is completed within the first 15 minutes. When comparing the R/G ratios with those in Figure 4, one can estimate the amount of intact and degraded ONs present. Already within 2 minutes, a R/G ratio of 0.35 is revealed, corresponding to approximately 50% degraded ONs. Additionally, the PO40-ONs solution was incubated with 0.008 units (diamond) and 0.002 units (cross) DNase I. As expected, the R/G ratio decreases more slowly when a lower enzyme concentration is used. For 0.008 units DNase I, 50% degradation is reached after 30 minutes reaction time and for 0.002 units DNase I, still 80% of the ONs are intact after 90 minutes incubation. For the PO20-ONs (circle) and PS20-ONs (square), the R/G ratio remains within 90% of the initial value, again confirming the resistance of these ONs towards degradation by DNase I.

The R/G ratios after incubation of the ONs with DNase II were followed for 8 hours (Figure 5B). Again, the R/G ratio for the PO40-ONs drops within the first 15 minutes and the stability of the PS20-ONs is demonstrated. For the PO20-ONs however, although rather slow, it is clear that the degradation occurs in the presence of DNase II.

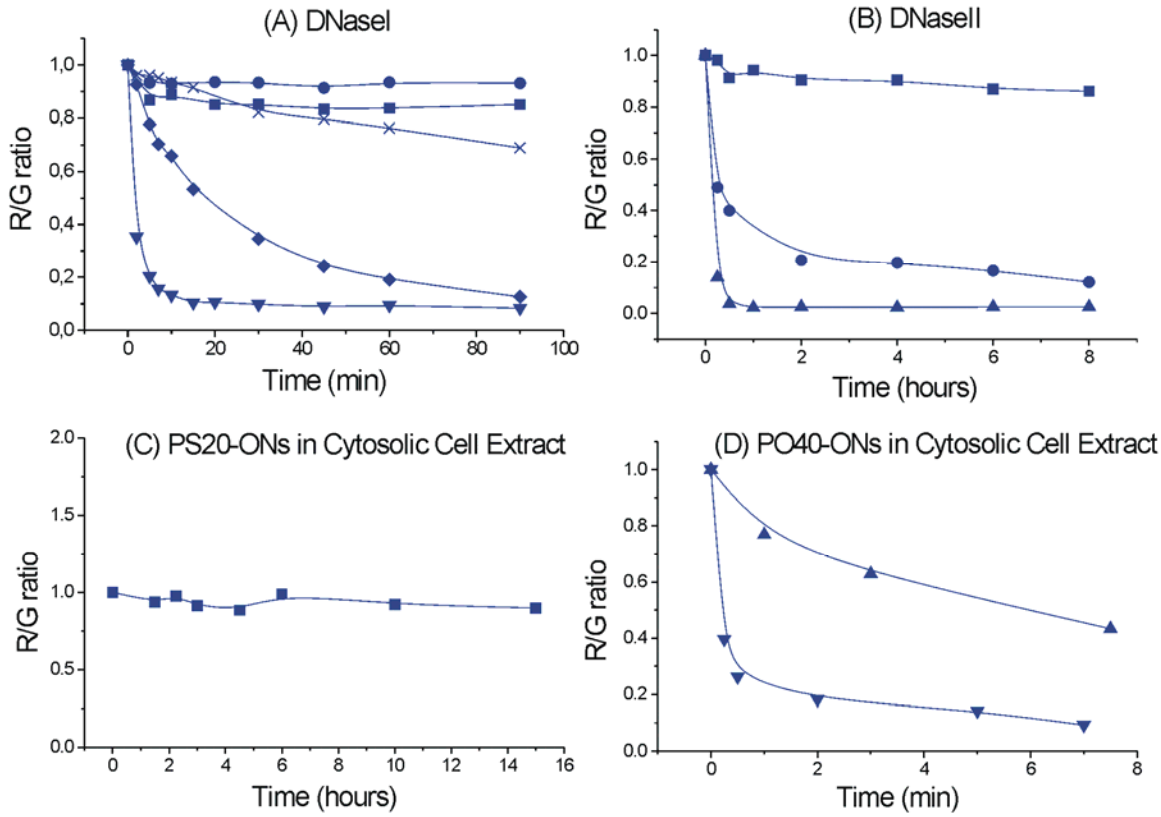

Figure 5. Time dependent degradation of the ONs in the presence of DNase I, DNase II and cytosolic cell extract. FRET-FCS measurements were performed with laser excitation set to 488 nm. To normalize the R/G ratio we considered the R/G ratio for the intact ONs to be 1. (A) PO20-ONs (circle), PS20-ONs (square) and PO40-ONs (triangle) incubated with 0.04 units DNase I and PO40-ONs incubated with 0.008 units (diamond) or 0.002 units (cross) of DNase I. (B) PO20-ONs (circle), PS20-ONs (square) and PO40-ONs (triangle) incubated with 20 units DNase II. (C) PS20-ONs incubated with an equal volume of cytosolic cell extract. (D) PO40-ONs incubated with an equal volume of undiluted (down triangle) or 1/10 diluted (up triangle) cytosolic cell extract.

Finally, the ONs were incubated in cytosolic cell extract. For the PS20-ONs, the R/G ratio did not decrease significantly during the 15 hours of incubation time (Figure 5C). This demonstrates the high resistance of the PS20-ONs towards degradation by cytosolic nucleases when compared to its phosphodiester analogue. Indeed, the R/G ratio for the PO20-ONs decreases immediately upon addition of cytosolic cell extract (data not shown). This is also the case for the PO40-ONs (Figure 5D). For the undiluted cytosolic cell extract (down triangle) the R/G ratio decreases very rapidly in the first two minutes of incubation while the degradation is slowed down when 1/10 diluted cytosolic cell extract is used (up triangle).

Although not within the scope of this chapter, these results point out that monitoring the R/G ratio as a function of time shows potential to study the kinetics of enzymatic reactions that result in the splicing (or coupling) of a donor and an acceptor fluorophore on the molecules under investigation.

Real-time Monitoring of the ON Degradation in Living Cells

The use of FRET-FCS in living cells was evaluated by injecting intact and degraded PO40-ONs into the cytoplasm of Vero cells (Figure 6). Both intact and degraded ONs accumulate in the nucleus, a behavior that has been reported previously [19]. Due to FRET, the Cy5 fluorescence can be detected upon excitation at 488 nm for the intact PO40-ONs, but not for the degraded PO40-ONs (Figure 6A-B, picture 3). From FRET-FCS measurements, a R/G ratio > 1.5 was determined for the intact PO40-ONs both in the cytoplasm and the nucleus (Figure 6A), while for the degraded PO40-ONs the R/G ratios equaled 0.3 and 0.2 respectively (Figure 6B). This demonstrates that the R/G ratios measured by the dual-color FCS setup appear to be a reliable parameter to distinguish intact from degraded ONs, even in living cells.

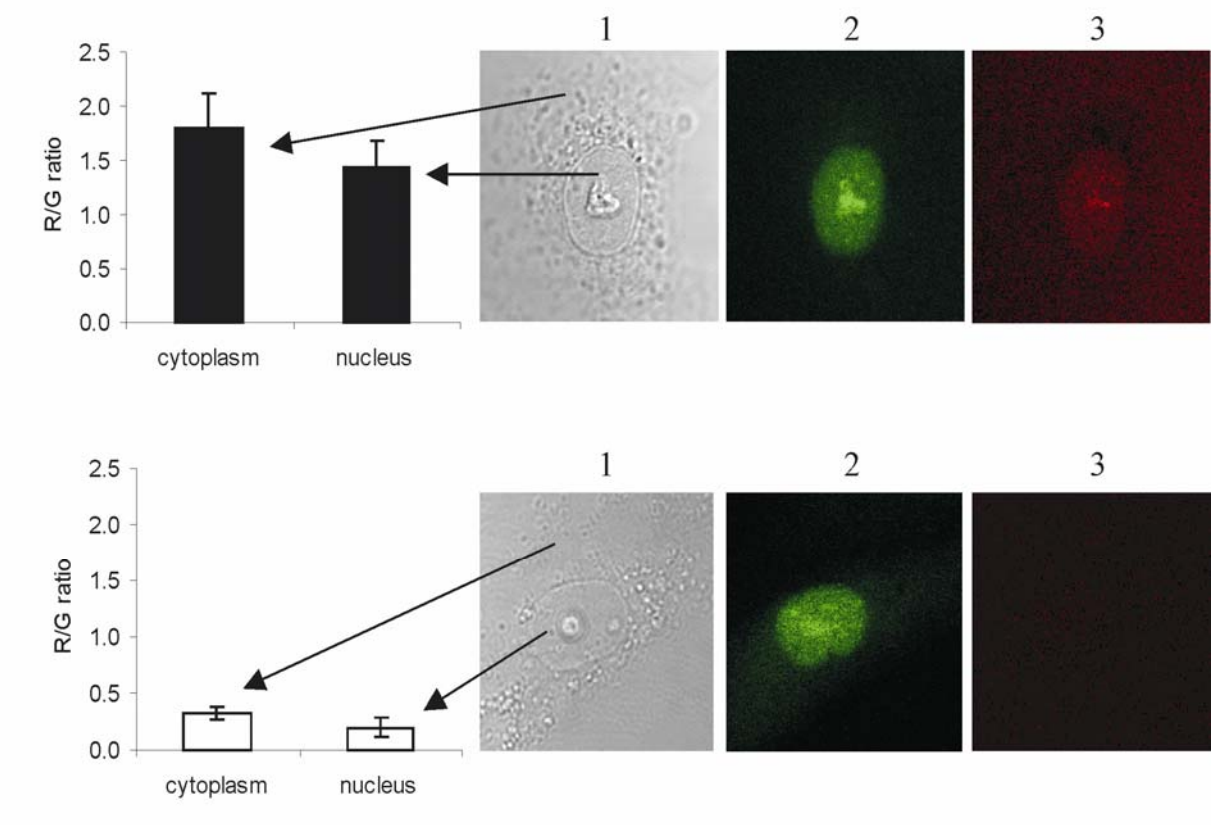

Figure 6. Intracellular applicability of the R/G ratio. R/G ratio measured in the cytoplasm or nucleus of Vero cells after microinjection of (A) intact or (B) degraded PO40-ONs in the cytoplasm of the cells. Laser excitation was set to 488 nm. The transmission image (1), rhodamine green (donor) fluorescence (2) and Cy5 (acceptor) fluorescence (3) are also shown.

Subsequently, the intact ONs were injected in the cytoplasm of Vero cells and at different time points the rhodamine green and Cy5 fluorescence intensities were recorded in the nucleus after excitation at 488 nm. With these settings, only intact ONs can contribute to the measured red fluorescence. In contrast, the measured green fluorescence may come

from both intact and degraded ONs. The measured fluorescence intensities and the calculated R/G ratios of the injected ONs are summarized in Figure 7.

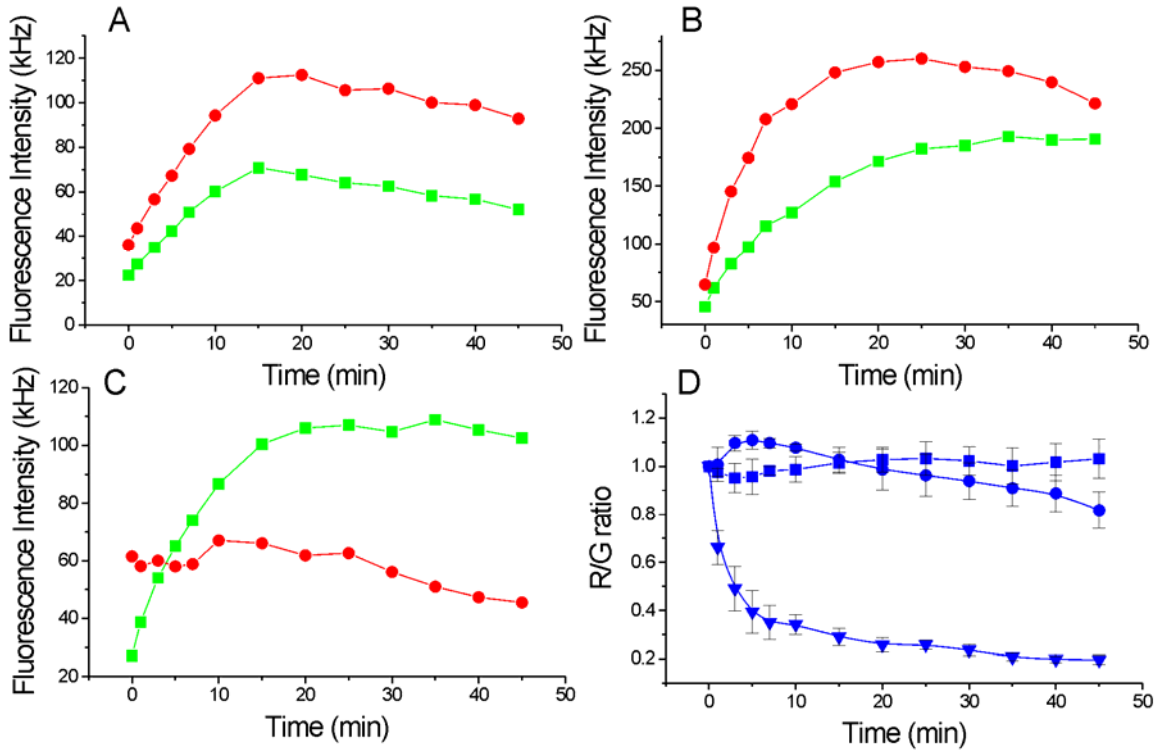

Figure 7. Time dependent intracellular degradation of the ONs. Fluorescence intensities measured by the green (square) and red (circle) detector of the dual-color FCS setup in the nucleus of Vero cells injected in the cytoplasm with (A) PS20-ONs, (B) PO20-ONs and (C) PO40-ONs. Laser excitation was set to 488 nm. (D) Normalized R/G ratios for the PS20-ONs (square), PO20-ONs (circle) and PO40-ONs (triangle).

For the PS20-ONs, both the green and red fluorescence intensities increase during the first 15 minutes after injection, corresponding to the nuclear accumulation of the intact PS20-ONs (Figure 7A). Indeed, as long as intact ONs are entering the nucleus, FRET causes an equal increase in both the green and the red fluorescence. After this initial accumulation, the PS20-ONs seems to redistribute in the cell, as observed from a slow decay in both the green and red nuclear fluorescence intensities. This is in agreement with previously reported behavior of PS-ONs to continuously shuttle between the cytoplasm and the nucleus [20]. It can be seen from the R/G ratios (Figure 7D, square) that there was no significant degradation of the PS20-ONs during the measured time period since the R/G ratio remains around its initial value.

Also for the PO20-ONs, an increase in the green and red fluorescence intensities can be observed in the first 15 minutes (Figure 7B). Again this demonstrates that intact ONs are entering the nucleus. However, a decrease in the R/G ratio is observed starting from 10 minutes after the injection, demonstrating the degradation of the PO20-ONs (Figure 7D,

circle). It should be noted that the degradation of the PO20-ONs as measured in living cells is much slower when compared to cytosolic cell extract. Since the hexosaminidase test revealed that the cytosolic cell extract contained lysosomal enzymes, it is most likely that DNase II-like enzymes present in the lysosomal compartment are responsible for this rapid degradation. Upon microinjection, the ONs are directly delivered to the cytosol which contains DNase I or DNase I-like enzymes but very little DNase II. This could explain why the degradation in the cytosol occurs much slower, since the buffer experiments mentioned above also showed that not DNase I but mostly DNase II is responsible for the degradation of the PO20-ONs.

The green and red fluorescence intensities of a cell injected with the intact PO40-ONs are shown in Figure 7C. Interestingly, only the green fluorescence intensity increases during the first 20 minutes after injection. Apparently, the PO40-ONs undergo a very rapid cytoplasmic degradation: even within minutes after injection only degraded ONs accumulate in the nucleus. Also from the R/G ratios, the rapid degradation of the PO40-ONs is clear (Figure 7D, triangle). The R/G ratio indeed drops within the first 15 minutes and shows that the majority of the ONs are degraded within the first 15 minutes after injection. These results are consistent with the buffer measurements, which also showed that the PO40-ONs are very susceptible towards DNase I degradation. Interestingly, the red fluorescence intensity remains at its initial value during the first 20 minutes, indicating that the intact PO40-ONs that reached the nucleus are not degraded in the nucleus within this time. This observation was confirmed by direct microinjection of the PO40-ONs in the nucleus of the cells, where indeed no significant degradation of the PO40-ONs was observed (data not shown).

These measurements show that monitoring the intracellular fluorescence intensities by the FCS instrument can be easily used to follow the fate of microinjected ONs. Where the fluorescence intensities give information on the amount and distribution of the ONs, the calculated R/G ratios can provide us with information on the integrity of the ONs. The short measurement times (2 seconds) and low laser excitation prevent photobleaching and cell photodamaging effects. Also, with these settings, the autofluorescence of the cells equaled 3 kHz, being 10-40 fold lower than the fluorescence intensities coming from the ONs. Therefore the R/G ratios could be monitored over a long time period without introducing artifacts. This in contrast to conventional FCS measurements, where in general the fluorophores should generate high counts per molecule, preferentially at low laser excitation power. In cells, however, most fluorophores exhibit reduced counts per molecule when compared to buffer. Optimization of the intracellular counts per molecule can be achieved by using longer illumination times and/or higher laser power, but also increases the risk of disturbing photobleaching and cell photodamaging effects [21]. Since in the FRET-FCS measurements used in this chapter auto- or cross-correlation analysis is not required, the

illumination time and laser power are less critical and can be minimized to reduce unwanted side effects.

CONCLUSIONS AND OUTLOOK

Because of the straightforward design and action mechanism, antisense ONs show great potential as therapeutic drugs, although intracellular barriers still limit the antisense activity. Many researchers focus on developing delivery systems to protect the ONs, while others try to improve the resistance of the antisense ONs towards nucleases by chemical modifications of the ON backbone. There are only few studies dealing with the turnover of antisense ONs in the cytoplasm and nucleus of cells, partially due to the limited methods applicable on living cells.

In this chapter we evaluated the use of a dual-color FCS setup to study the intracellular degradation of single-stranded ONs labeled with rhodamine green at the 3' end and Cy5 at the 5' end. For the intact ONs, FRET occurred between the two labels: both green and red fluorescence was detected upon rhodamine green excitation. Upon degradation of the ONs, the rhodamine green fluorescence increased, while the Cy5 fluorescence decreased. We showed that the ratio of the red to the green fluorescence (R/G ratio), as measured by the two detectors of the dual-color FCS setup, provides us within seconds with information on the integrity of the ONs. In vitro measurements showed that phosphothioate ONs were resistant to degradation with DNase I, DNase II and cytosolic cell extract. With regard to ONs with a phosphodiester backbone, DNase II (slowly) and cytosolic cell extract (rapidly) degraded both PO20-ONs and PO40-ONs, while the DNase I enzyme only degraded the PO40-ONs. The latter could be attributed to the sequence specific cleavage behavior of the DNase I enzyme, which prefers the mixed-region PO40-ONs over the cytidine-rich PO20-ONs.

Especially, the potential of the dual-color FCS instrument to follow the intracellular degradation of the ONs was demonstrated. Based upon the R/G ratio, the cytoplasmic turnover of the PO40-ONs was estimated between 2-10 minutes. For the PS20-ONs, no degradation was observed during the 45 minutes measuring time. Interestingly, the degradation of the PO20-ONs in the microinjected cells occurred more slowly when compared to the degradation in cytosolic cell extract. Since the cytosolic cell extract contained lysosomal enzymes, this indicates that the DNase II-like enzymes present in the lysosomal compartment are most likely responsible for this rapid degradation. Therefore, avoiding the lysosomal compartment will be of great interest when delivering antisense ONs.

The role of DNase II in lowering the transfection efficiency of non-viral DNA delivery vectors has indeed been reported recently [22]. It should be noted that the end-labeling of the ONs may interfere with the degradation by intracellular exonucleases. As a consequence, the measured degradation time of the double-labeled ONs could be an underestimation of the degradation time of their non-labeled analogues.

Apart from the R/G ratios, the diffusion properties of the intact ONs and their degradation products could be determined, as a FCS setup was used to monitor the fluorescence intensity fluctuations. However, studying the degradation of the ONs based on a change in diffusion coefficient does not appear to be the most straightforward way. Especially in living cells an accurate determination of the diffusion coefficient is rather difficult. This highly recommends the use of the R/G ratios to follow the ONs degradation in living cells.

Using the FRET-FCS methodology described in this chapter, we aimed to study whether double-labeled ONs which are complexed to cationic liposomes and cationic polymers, frequently used to deliver antisense ONs, are adequately protected against degradation. Therefore, the double-labeled ONs were complexed to non-pegylated and pegylated cationic liposomes and non-pegylated and pegylated polyethyleneimine and the protection against enzymatic degradation was followed by the use of FRET-FCS, as described in Chapter 3 and Chapter 4, respectively.

ACKNOWLEDGEMENTS

Katrien Remaut is a Research Assistant of the Research Foundation - Flanders. The financial support of this institute is acknowledged with gratitude. The Ghent University (UG-BOF) and Research Foundation - Flanders (G.0310.02) supported this project through instrumentation credits and financial support. Koen Raemdonck is gratefully acknowledged for his assistance in the practical experiments. Norbert Opitz (Max Planck Institute for Molecular Physiology, Dortmund, Germany) is acknowledged for the installation of the FCS-module on the MRC-1024. The authors would also like to thank Prof. Dr. Dieter Deforce (Ghent University) for the use of the PAGE system.

REFERENCES

(1) Lisziewicz, J.; Sun, D.; Metelev, V.; Zamecnik, P.; Gallo, R. C.; Agrawal, S. Long term treatment of human immunodeficiency virus infected cells with antisense oligonucleotide phosphorothioates. *Proc. Natl. Acad. Sci. USA* **1993**, 90, 3860-3864.

(2) Jensen, K. D.; Kopeckova, P.; Kopecek, J. Antisense oligonucleotides delivered to the lysosome escape and actively inhibit the Hepatitis B virus. *Bioconjug. Chem.* **2002**, 13, 975-984.

(3) Jabs, D. A.; Griffiths, P. D. Fomivirsen for the treatment of cytomegalovirus retinitis. *Am. J. Ophthalmol.* **2002**, 133, 552-556.

(4) Wang, H.; Cai, Q.; Zeng, X.; Yu, D.; Agrawal, S.; Zhang, R. Antitumor activity and pharmacokinetics of a mixed-backbone antisense oligonucleotide targeted to the RIalpha subunit of protein kinase A after oral administration. *Proc. Natl. Acad. Sci. USA* **1999**, 96, 13989-13994.

(5) Uchiyama, H.; Hirano, K.; Kashiwasake-Jibu, M.; Taira, K. Detection of undegraded oligonucleotides *in vivo* by Fluorescence Resonance Energy Transfer. *J. Biol. Chem.* **1996**, 271, 380-384.

(6) Elson, E. S.; Magde, D. Fluorescence correlation spectroscopy. I. Conceptual basis and theory. *Biopolymers* **1974**, 13, 1-27.

(7) Rarbach, M.; Kettling, U.; Koltermann, A.; Eigen, M. Dual-color fluorescence cross-correlation spectroscopy for monitoring the kinetics of enzyme-catalyzed reactions. *Methods* **2001**, 24, 104-116.

(8) Kettling, U.; Koltermann, A.; Schwille, P.; Eigen, M. Real-time enzyme kinetics monitored by dual-color fluorescence cross-correlation spectroscopy. *Proc. Natl. Acad. Sci. USA* **1998**, 95, 1416-1420.

(9) Koltermann, A.; Kettling, U.; Bieschke, J.; Winkler, T.; Eigen, M. Rapid assay processing by integration of dual-color fluorescence cross-correlation spectroscopy: High throughput screening for enzyme activity. *Proc. Natl. Acad. Sci. USA* **1998**, 95, 1421-1426.

(10) Schwille, P.; Meyer-Almes, F.; Rigler, R. Dual-Color Fluorescence Cross-Correlation spectroscopy for multicomponent diffusional analysis in solution. *Biophys. J.* **1997**, 72, 1878-1886.

(11) Lucas, B.; Remaut, K.; Braeckmans, K.; Haustraete, J.; De Smedt, S. C.; Demeester, J. Studying pegylated DNA complexes by dual color fluorescence fluctuation spectroscopy. *Macromolecules* **2004**, 37, 3832-3840.

(12) Van Rompaey, E.; Engelborghs, Y.; Sanders, N.; De Smedt, S. C.; Demeester, J. Interactions between oligonucleotides and cationic polymers investigated by fluorescence correlation spectroscopy. *Pharm. Res.* **2001**, 18, 928-936.

(13) Gennerich, A.; Schild, D. Fluorescence correlation spectroscopy in small cytosolic compartments depends critically on the diffusion model used. *Biophys. J.* **2000**, 79, 3294-3306.

(14) Brock, R.; Hink, M. A.; Jovin, T. M. Fluorescence correlation microscopy of cells in the presence of autofluorescence. *Biophys. J.* **1998**, 75, 2547-2557.

(15) Bacia, K.; Majoul, I. V.; Schwille, P. Probing the endocytic pathway in live cells using Dual-Color Fluorescence Cross-Correlation analysis. *Biophys. J.* **2002**, 83, 1184-1193.

(16) De Meester I, De Smedt SC: Deoxyribonuclease I, in Lauwers A, Scharpé S (eds): Pharmaceutical enzymes. New York, Marcel Dekker Inc., 1997, pp 285-304.

(17) Evans, C. J.; Aguilera, R. J. DNase II: genes, enzymes and function. *Gene* **2003**, 322, 1-15.

(18) Kohl, T.; Heinze, K. G.; Kuhlemann, R.; Koltermann, A.; Schwille, P. A protease assay for two-photon crosscorrelation and FRET analysis based solely on fluorescent proteins. *Proc. Natl. Acad. Sci. USA* **2002**, 99, 12161-12166.

(19) Chin, D. J.; Green, G. A.; Zon, G.; Szoka, F. C. J.; Straubinger, R. M. Rapid nuclear accumulation of injected oligodeoxyribonucleotides. *New Biologist* **1990**, 2, 1091-1100.

(20) Lorenz, P.; Misteli, T.; Baker, B. F.; Bennett, C. F.; Spector, D. L. Nucleocytoplasmic shuttling: A novel in vivo property of antisense phosphorothioate oligodeoxynucleotides. *Nucleic Acids Res.* **2000**, 28, 582-592.

(21) Schwille, P. Fluorescence correlation spectroscopy and its potential for intracellular applications. *Cell Biochem. Biophys.* **2001**, 34, 383-408.

(22) Howell, D. P.; Krieser, R. J.; Eastman, A.; Barry, M. A. Deoxyribonuclease II is a lysosomal barrier to transfection. *Mol. Ther.* **2003**, 8, 957-963.

Chapter 3

PROTECTION OF OLIGONUCLEOTIDES AGAINST NUCLEASES BY PEGYLATED AND NON-PEGYLATED LIPOSOMES

Parts of this chapter were published in:

Remaut, K.; Lucas, B.; Braeckmans, K.; Sanders, N. N.; Demeester, J.; De Smedt, S. C. *J. Control. Release* **2005**, 110, 212-226.

ABSTRACT

Antisense oligonucleotides (ONs), complexed to carriers such as cationic liposomes, inhibit the production of proteins. The biochemical and biophysical phenomena that govern the extent of this inhibition are still not fully understood. Major biological barriers limiting a pronounced antisense effect are the cellular entry and endosomal escape of the ONs containing liposomes, the release of the ONs from the liposomes and the extra- and intracellular degradation of the ONs. In this chapter we focus on the latter barrier and evaluate, by the FRET-FCS technique described in Chapter 2, to what extent phosphodiester ONs (PO-ONs) complexed to DOTAP/DOPE liposomes, are protected against degradation by nucleases. Liposomes studied were either with or without a polyethyleneglycol (PEG) moiety at the surface. Using non-pegylated liposomes the PO-ONs were initially adequately protected when exposed to DNase I. Indeed, in the mechanism for lipoplex formation as suggested by others, the ONs become trapped between lipid bilayers and are therefore shielded from the environment. However, after a few hours the PO-ONs no longer stayed intact. This was explained by a gradual fusion of the lipoplexes in time thereby spontaneously releasing PO-ONs. Using pegylated liposomes, a substantial fraction of the PO-ONs degraded immediately after exposing the complexes to DNase I. Based on experimental evidence we suggest that the presence of the PEG-chains influences lipoplex formation so that the ONs are not trapped between lipid bilayers and therefore remain accessible to the DNase I enzyme.

Chapter 3

Protection of Oligonucleotides Against Nucleases by Pegylated and Non-Pegylated Liposomes

INTRODUCTION

Antisense oligonucleotides (ONs) are being widely investigated for the down-regulation of genes [1]. To inhibit protein production, the ONs have to reach the cytoplasm or nucleus of the cells where they act by specific binding to the target mRNA or DNA. In spite of this simple action mechanism, different barriers still limit the antisense activity. Actually, before the ONs can reach their target site, they first have to cross the cellular membrane, escape from the endosomal compartment, leave their pharmaceutical carriers (i.e. the delivery system) and hybridize to the target sequence [2].

Rapid degradation of phosphodiester ONs (PO-ONs) is known to be one of the factors limiting their success as therapeutics. One approach to improve antisense activity is to develop ONs with increased nuclease resistance so that intracellular degradation should not be an issue [3]. However, modification of the ON backbone often induces undesirable features. The first generation of chemically modified ONs, namely phosphothioate ONs (PS-ONs), are known to frequently exhibit non-specific, non-antisense effects, generally attributed to their increased non-specific protein binding when compared to their phosphodiester analogues [4]. The second and third generation antisense compounds all work to some extent but have one or more problems such as solubility, delivery issues, lack of RNase H activation or simply the cost of synthesis [5].

Another approach to improve the antisense activity of ONs is the development of suitable delivery systems [2;6]. The delivery system, often composed of cationic lipids or cationic polymers, is designed to help the ONs to enter the cell and escape from the endosomes. Clearly, in cases where degradable PO-ONs are used, the protection of the ONs against nucleases, given by their carrier, becomes an important aspect. Ideally, the

delivery system should protect the complexed ONs during the different steps of the trafficking pathway. In general, cationic carriers are believed to protect the complexed ONs against degradation. However, we, among others, have observed that some carriers can establish an antisense effect with degradable PO-ONs, while other carriers fail [7;8]. The lack of antisense activity has been attributed to insufficient ON protection against nucleases with the carriers used, although no direct proof of this hypothesis was given.

There are few studies that relate the biophysical properties of carrier/ON complexes to the obtained antisense effect. In an attempt to better understand the intracellular behavior of carrier/ON complexes, our laboratory uses Fluorescence Correlation Spectroscopy (FCS) [9]. We have already used FCS to monitor the complexation behavior (association/dissociation) between ONs and cationic polymers or lipids, both in buffer and in living cells [10-14]. Also, in Chapter 2, we demonstrated that the FCS-setup allows following the intracellular degradation of fluorescently double-labeled ONs when Fluorescence Resonance Energy Transfer (FRET) occurs between the two fluorophores [15]. In this approach, which we have termed FRET-FCS, the detectors of the dual-color FCS instrument register the acceptor and donor fluorescence upon donor excitation. The ratio of the acceptor to donor fluorescence (R/G ratio) gave accurate information on the integrity of the ONs, since the R/G ratio decreases when degradation proceeds.

In this chapter, we aimed to determine the ON protection against nucleases when the ONs are complexed to either pegylated or non-pegylated cationic liposomes. Therefore, the ONs containing liposomes were dispersed in a DNase I solution and the degradation of the ONs was investigated by FRET-FCS.

MATERIALS AND METHODS

Materials

A 40 mer phosphodiester oligonucleotide (PO40-ONs) (5'-GCC-GTC-TCT-GAC-TGC-TGA-TGA-CTA-CTA-TCG-TAT-AGT-GCG-G-3'), double-labeled with a rhodamine green (λ_{ex} = 488 nm, λ_{em} = 532 nm) fluorophore at the 3' end and a Cy5 (λ_{ex} = 647 nm, λ_{em} = 670 nm) fluorophore at the 5' end was used. The ONs were purchased from Eurogentec (Seraing, Belgium) and were PAGE-purified by the supplier. The concentration of the ONs stock solutions as given by the supplier was additionally checked by absorption measurements at 260 nm (1 OD_{260} = 33 µg ONs/mL).

The cationic phospholipid DOTAP (N-(1-(2,3-dioleoyloxy)propyl)-N,N,N-trimethyl-ammoniumchloride), the neutral phospholipid DOPE (dioleoylphosphatidylethanolamine) and

the pegylated, neutral phospholipid DSPE-PEG (distearoylphosphatidylethanolamine (polyethyleneglycol2000)) were purchased from Avanti® Polar Lipids (Alabaster, AL, USA). Sodium dodecylsulfate (SDS) was purchased from Sigma (St Louis, MO, USA).

Human lung carcinoma cells (A549 cells, ATCC number: CCL-185) (DSMZ, Braunschweig, Germany) were cultured in Dulbecco's modified Eagle's medium (DMEM) without phenol red (Gibco, Merelbeke, Belgium) containing 2 mM glutamine, 10% heat deactivated fetal bovine serum (FBS) and 1% penicillin-streptomycin. Cells were prophylactically treated against mycoplasma with Plasmocin (Invivogen, Cayla, France). Any remaining contamination by mycoplasma was determined using a mycoplasma PCR detection kit (Venorgem, Minerva Biolabs GmbH, Berlin, Germany) and revealed that the cells were mycoplasma free.

Preparation of Liposomes

The non-pegylated liposomes contained DOTAP and DOPE in a 1:1 molar ratio. For the pegylated liposomes 5 mol % DSPE-PEG was incorporated. The lipids were dissolved in a 1:1 (volume) mixture of chloroform:methanol. Subsequently, the solution of lipids was placed in a round-bottomed flask and the solvents were evaporated under vacuum at 30°C. The resulting lipid film was further dried under a flow of nitrogen for 30 minutes. The lipid film was then resuspended in HEPES buffer (20 mM at pH 7.4) at a final concentration of 5 mM DOTAP and stored overnight at 4°C to allow liposome formation. The resulting liposomes were extruded at room temperature through a polycarbonate membrane with a pore size of 0.1 µm, using the Avanti Polar Lipids mini-extruder. The hydrodynamic size and zeta potential of the resulting cationic liposomes was routinely checked by respectively dynamic light scattering (DLS, Malvern 4700, Malvern, Worcestershire, UK) and surface potential measurements (Zetasizer 2000, Malvern, Worcestershire, UK), as previously described [16]. The hydrodynamic diameter and zeta potential of the non-pegylated liposomes equaled respectively 126 ± 7 nm and +45 ± 4 mV. The pegylated liposomes had a similar hydrodynamic diameter (128 ± 6 nm) and a lower zeta potential (+18 ± 3 mV) due to the presence of the PEG-chains.

Preparation of Liposome/ONs Complexes

Upon mixing positively charged liposomes with negatively charged ONs, spontaneously liposome/ONs complexes (lipoplexes) are formed. The lipoplexes were prepared by mixing equal volumes of a liposome dispersion and an ON solution. The resulting dispersion was vortexed for 10 seconds and the lipoplexes were allowed to equilibrate for 30 minutes at room temperature prior to use. The concentration of the

liposomes was dependent on the desired +/- ratio, being the ratio of the number of positive charges (originating from the liposomes) to the number of negative charges (originating from the ONs). Lipoplexes with +/- ratios of 2.5, 5 and 10 were used. The +/- ratio of the lipoplexes was calculated assuming that 1 µg of ONs contains 3.43 nmol negative charges.

Fluorescence Correlation Spectroscopy (FCS)

Experimental Setup

Dual-color FCS experiments were performed on a dual-color FCS-setup installed on a MRC1024 Bio-Rad confocal laser scanning microscope. An inverted microscope (Eclipse TE300, Nikon, Japan) was used, which was equipped with a water immersion objective lens (Plan Apo 60X, NA 1.2, collar rim correction, Nikon, Japan). The laser beam was focused at about 50 µm above the bottom of the glass-bottom 96-well plate (Grainer Bio-one, Frickenhausen, Germany), which contained the samples. The 488 nm and the 647 nm laser beams of a krypton-argon laser (Bio-Rad, Cheshire, UK) were used and the fluorescence intensity fluctuations were recorded on a digital ALV 5000/E correlator. To verify whether the excitation volumes and the detection volumes optimally overlapped, the system was calibrated as described by Schwille *et al.* [17].

Theoretical Background

For details on the theoretical background of FCS, we would like to refer to Chapter 1 of this thesis and Schwille *et al.* [18] and Hess *et al.* [19]. Briefly, an FCS instrument registers fluorescence intensity fluctuations caused by the diffusion of fluorescently labeled molecules through the detection volume of a microscope. From these fluorescence intensity fluctuations an auto-correlation curve can be derived, which allows calculating the amount of fluorescent molecules in the detection volume and their diffusion coefficient. In dual-color FCS, two spectrally different fluorophores are used. The (green and red) fluorescence intensity fluctuations of the double-labeled (green and red) molecules can then be measured simultaneously using the green and red detector of the dual-color FCS instrument.

Dual-color FCS measurements were done on lipoplexes composed of non-labeled cationic liposomes and double-labeled PO40-ONs. The green and red fluorescence fluctuations were recorded for 4 intervals of 50 seconds while exciting the lipoplexes at 488 nm. When possible, auto-correlation analysis was done as described in Chapter 1. The auto-correlation curves $G(\tau)$ were analyzed using a single-species fit (equation 1, see Chapter 1) or a dual-species fit (equation 2, see Chapter 1) to calculate the amount of molecules N in the detection volume and their diffusion time τ_t, being the average time the fluorescently labeled molecules need to migrate through the detection volume of the FCS instrument. The

auto-correlation curves were always analyzed using both equations and the non-sense analysis was disregarded based on the appearance of the residual of the fit (or if the dual-species fit revealed that more than 95% of the species moved with a diffusion coefficient similar to the one obtained with eq.1). From the diffusion time τ_t the diffusion coefficient D was calculated using equation 3 (see Chapter 1).

FCS on Liposomes/ON Complexes

Figure 1A schematically illustrates on which type of samples FCS measurements were done.

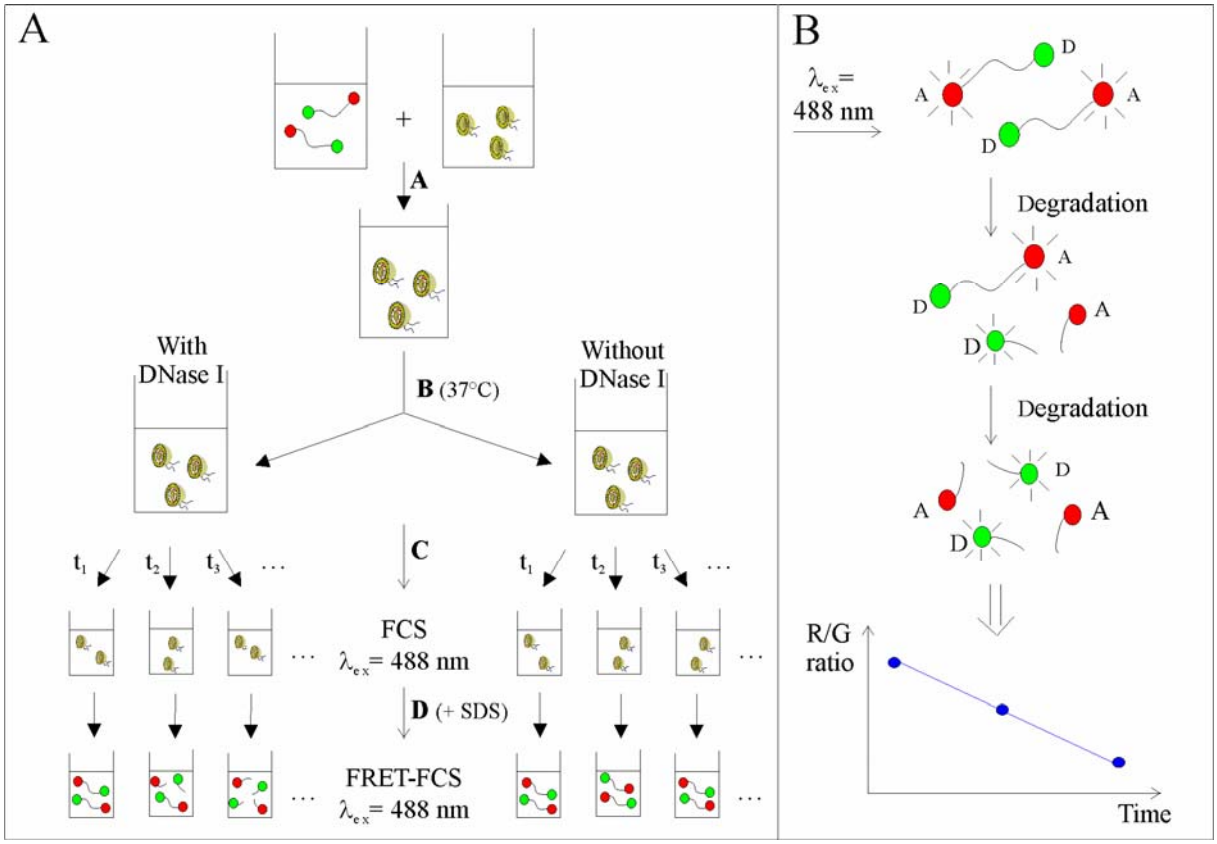

Figure 1. A. Schematic representation of the conducted experiments. (A) Complexes were prepared from fluorescently double-labeled PO40-ONs with pegylated or non-pegylated liposomes. (B) These ON/liposome dispersions were incubated at 37°C with and without 0.2 Units DNase I enzyme. (C) After the appropriate incubation times (t_1, t_2, t_3, ...) a 50 µL aliquot was removed and the DNase I activity was inhibited by adding 50 µL TBE buffer. On these dispersions, FCS measurements were performed with laser excitation set to 488 nm. (D) Then, PO40-ONs molecules were released from the lipoplexes by adding 2 µL 1% SDS. On those solutions, FRET-FCS measurements were performed to determine the R/G ratio, which is a measure for the amount of intact PO40-ONs, released from the complexes by SDS. Laser excitation was set to 488 nm. B. Schematic representation of the R/G ratio of the double-labeled ONs. In intact ONs, FRET occurs: upon excitation at 488 nm of the rhodamine green (donor, D, green) fluorophore, also the Cy5 (acceptor, A, red) fluorophore emits light. When degradation proceeds, FRET no longer occurs and only the rhodamine green fluorophore emits light. Hence, the R/G ratio decreases when the degradation proceeds.

500 µL of non-pegylated liposomes or pegylated liposomes (64, 32 or 16 µM for obtaining a +/- ratio of respectively 10, 5 or 2.5) was mixed with 500 µL of double-labeled PO40-ONs (160 nM) (Figure 1A, step A). The liposomes and ONs solutions were prepared in 'degradation buffer' (20 mM HEPES, 110 mM potassium acetate and 2 mM magnesium acetate, pH 7.4) to ensure the activity of the DNase I enzyme. After 30 minutes, the lipoplex dispersion was incubated at 37°C both with and without 0.2 Units DNase I (Pulmozyme®, 1 units/µL, Genentech) (Figure 1A, step B). At different time intervals, 50 µL of the lipoplex dispersion was removed and mixed with 50 µL EDTA-enriched TBE buffer (10.8 g/L tris base, 5.5 g/L boric acid and 3.7 g/L EDTA) to stop the DNase I activity. This 100 µL sample was transferred to a 96-well plate and FCS measurements were performed (Figure 1A, step C). After the FCS measurements, 2 µL 1% SDS solution was added to the well in order to induce the release of the ONs from the liposomes (Figure 1A, step D). On this solution, FRET-FCS measurements were performed: the rhodamine green and Cy5 fluorescence intensities were recorded with the dual-color FCS instrument upon excitation at 488 nm and the ratio of the red to green fluorescence (R/G ratio) was calculated. The R/G ratio is, as illustrated in Figure 1B, a measure for the amount of intact ONs [15].

RESULTS AND DISCUSSION

FCS on ONs Containing LPXs

Upon mixing negatively charged ONs with positively charged liposomes, lipoplexes (LPXs) are spontaneously formed. As outlined below, using fluorescently double-labeled ONs, the LPXs could be detected by FCS.

Figure 2A shows the fluorescence fluctuations measured on a solution of free double-labeled ONs upon excitation of the rhodamine green fluorophore at 488 nm. FRET clearly occurs since the fluorescence of the Cy5 acceptor (red line) is higher than the fluorescence of the rhodamine green donor (green line). The calculated R/G ratio for the intact PO40-ONs equaled 6 ± 0.3. Figure 2B shows the auto-correlation curve as derived from the red fluorescence fluctuations together with the single-species fit (equation 1, see Chapter 1). From this auto-correlation curve, the presence of 195 ± 4 molecules with a diffusion coefficient of $1.12 \pm 0.08 * 10^{-10}$ m²/s was calculated (Table 1). From the residuals of the fit (Figure 2C) it can be seen that a satisfactory fit was obtained using a single-species fit. A slight improvement of the fit was obtained by a dual-species fit (equation 2, see Chapter 1, residuals of the fit in Figure 2D), but more than 95% of the species moved with a diffusion coefficient similar to the one as calculated by a single-species fit. The latter together with the

fact that the solution of free PO40-ONs contains only 1 species, namely the ONs, made us disregard the dual-species fit.

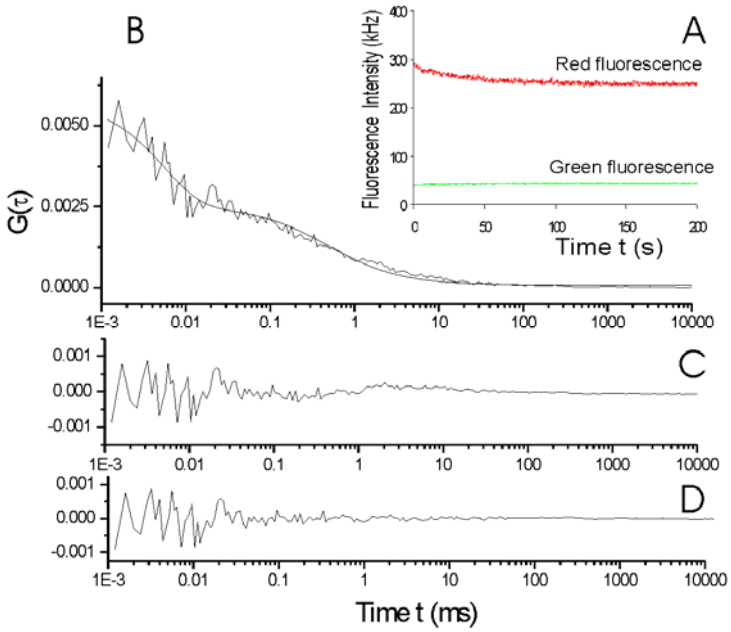

Figure 2. (A) Fluorescence intensity fluctuations of free PO40-ONs as measured by the green (green line) and red (red line) detector of the FCS instrument. (B) From the red fluorescence fluctuations an auto-correlation curve was obtained that was best fitted with a single-species fit. (C) and (D) show the residuals of the fit after fitting the auto-correlation data with respectively a single-species fit or a dual-species fit. Laser excitation was set to 488 nm.

Figure 3 shows the fluorescence fluctuations as obtained on a solution of double-labeled ONs complexed with non-pegylated liposomes, upon excitation of the rhodamine green fluorophore at 488 nm. When compared to free ONs (Figure 2A), two observations can be made.

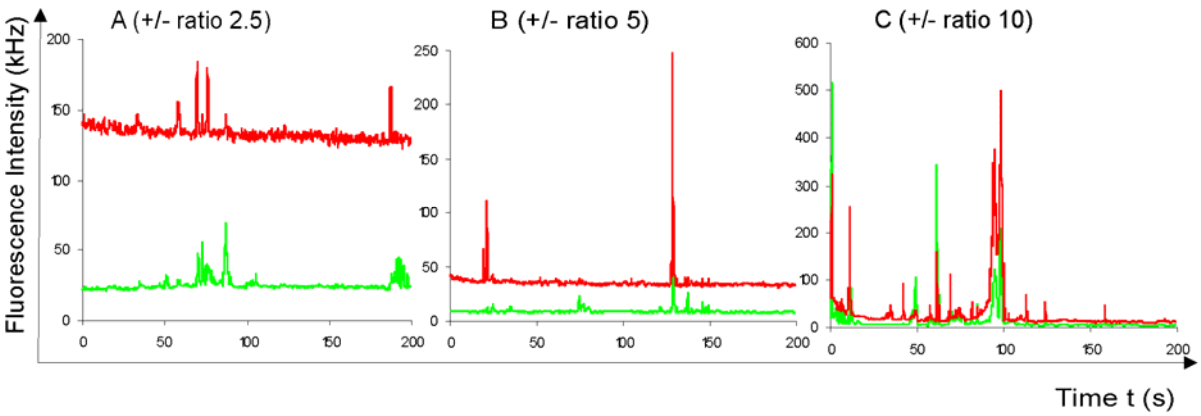

Figure 3. Fluorescence intensity fluctuations of non-pegylated lipoplexes as measured by the green (green line) and red (red line) detector of the FCS instrument. Lipoplexes were prepared with (A) a +/- ratio of 2.5, (B) a +/- ratio of 5 and (C) a +/- ratio of 10. Laser excitation was set to 488 nm.

First, highly intense fluorescence peaks occur in the fluorescence fluctuation profiles. When the +/- ratio is increased, the highly intense fluorescence peaks occur more frequently and the peak height increases. Second, the background fluorescence (i.e. the average fluorescence in between the peaks) decreases when the +/- ratio increases.

For a +/- ratio of 2.5 and 5, auto-correlation analysis of the background fluorescence was feasible. The obtained auto-correlation curves together with the single-species fit are depicted in Figure 4A. Comparison of the residuals of the fit in Figure 4C (single-species fit) and Figure 4D (dual-species fit) shows that fitting to equation 2 gave only a slight improvement. Additionally, more than 95% of the species moved with a diffusion coefficient similar to the one obtained with a single-species fit. Also, the diffusion coefficient of the additional component was found to be poorly reproducible and thus the dual-species fit was disregarded. Fitting to equation 1 revealed a diffusion coefficient of respectively $1.18 \pm 0.15 * 10^{-10}$ m²/s and $1.09 \pm 0.11 * 10^{-10}$ m²/s for LPXs with a +/- ratio of 2.5 and 5 (Table 1). This is consistent with the diffusion of free PO40-ONs, indicating that the background fluorescence comes from free ONs. This can additionally be seen from the overlap of the normalized auto-correlation curves obtained on a solution of free ONs (blue line), LPXs with a +/- ratio of 2.5 (green line) and LPXs with a +/- ratio of 5 (red line) (Figure 4B). The amount of free ONs in the detection volume (*N* in equation 1), as calculated from the background fluorescence, equaled 104 ± 3 and 32 ± 1 for a +/- ratio of 2.5 and 5, respectively (Table 1). Since the complexes were prepared with the same ON concentration as in Figure 2 for free PO40-ONs (where *N* equaled 195 ± 4), one can conclude that respectively about 47% and 84% of the ONs are complexed in the lipoplex dispersions of Figure 3A and 3B. For a +/- ratio of 10 (Figure 3C), the presence of successive highly intense fluorescence peaks disturbed the auto-correlation curve and auto-correlation analysis was impaired (graph insert in Figure 4A). However, from the auto-correlation amplitude of 0.3, the number of free ONs was estimated to be 3.5 ± 1, indicating that approximately 98% of the ONs are complexed using a +/- ratio of 10.

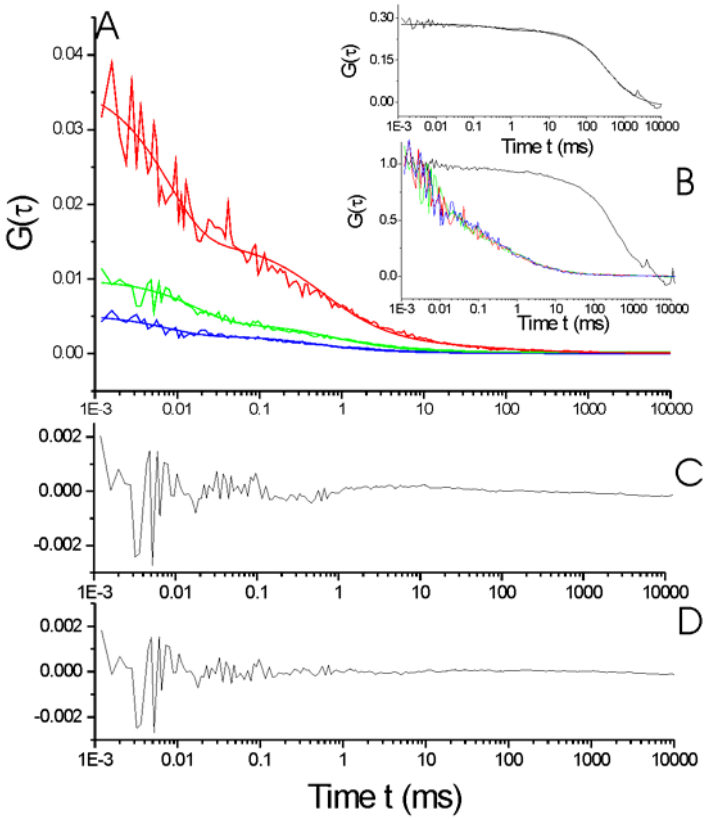

Figure 4. (A) Auto-correlation curves and single-species fit as obtained from the red fluorescence fluctuations of non-pegylated lipoplexes with a +/- ratio of 2.5 (green line), a +/- ratio of 5 (red line) and a +/- ratio of 10 (graph insert, black line). As a comparison, the auto-correlation curve as obtained on a solution of free PO40-ONs is also depicted (blue line). (B) shows the same auto-correlation curves normalized to 1. (C) and (D) show the residuals of the fit after fitting the auto-correlation data of LPXs with a +/- ratio of 2.5 with respectively a single-species fit and a dual-species fit. The appearance of the residuals of the fit of LPXs with a +/- ratio of 5 was similar. Laser excitation was set to 488 nm.

The obtained fluorescence fluctuation profiles for the LPXs are consistent with the diffusion of 'multimolecular' complexes bearing numerous ONs, each ON being labeled with the rhodamine green and Cy5 fluorophore. Indeed, large, multimolecular complexes give rise to highly intense fluorescence bursts each time such a complex passes the detection volume of the FCS instrument. In between the diffusion of complexes, free ONs move in and out of the detection volume and background fluorescence can be measured, which is clearly distinguishable from the fluorescence peaks. After increasing the +/- ratio, more ONs are complexed, indicated by a decrease in fluorescence background and an increase in the height and frequency of the fluorescence peaks. It should be noted that when SDS, which induces the disintegration of the LPXs, is added to the complexes, the background fluorescence returns to the level of free PO40-ONs as in Figure 2A. Also, fluorescence peaks are no longer detected, consistent with the induced release of the ONs from the LPXs (data not shown). After SDS release, the calculated R/G ratio for respectively a +/- ratio of 2.5, 5

and 10 equaled 5.7 ± 0.2, 5.8 ± 0.3 and 5.8 ± 0.2, in agreement with the R/G ratio as determined from Figure 2A. It is important to notice that the R/G ratio can only be accurately determined after SDS release of the PO40-ONs from the LPXs. When the ONs are complexed, the background fluorescence becomes ill-defined with increasing +/- ratios. As a result, the calculated R/G ratios are associated with larger error bars and deviate from the actual R/G ratio of intact ONs after SDS release (Table 1).

Table 1. FCS measurements of free PO40-ONs and PO40-ONs complexed to non-pegylated (LPX) and pegylated (PEG-LPX) liposomes with a +/- ratio of 2.5, 5 and 10. All samples were excited at 488 nm. F_G and F_R represent the average background fluorescence intensity as measured by respectively the green and red detector of the dual-color FCS instrument. The R/G ratio, e.g. the ratio from the red to green fluorescence, was calculated from these fluorescence intensities. From auto-correlation analysis of the red fluorescence intensities, the amount of molecules *N* and their diffusion coefficient *D* was calculated. *single-species fit of the background fluorescence (fluorescence peaks omitted), #dual-species fit of the fluorescence fluctuations (fluorescence peaks included), N.D. not determinable.

	F_G (kHz)	F_R (kHz)	R/G ratio	N	D (10^{-10} m²/s)	
free PO40-ONs*	42.7 ± 0.9	258.0 ± 10	6 ± 0.3	195 ± 4	1.12 ± 0.08	
LPX2.5*	23.7 ± 1.1	131.4 ± 6.0	5.5 ± 0.4	104 ± 3	1.18 ± 0.15	
LPX5*	8.4 ± 0.3	34.7 ± 1.1	4.1 ± 0.2	32 ± 1	1.09 ± 0.11	
LPX10*	5.0 ± 0.8	17.4 ± 5.0	2.9 ± 0.9	3.5 ± 1	N.D.	
PEG-LPX2.5#	38.4 ± 0.4	198.3 ± 2.9	5.2 ± 0.1	104 ± 5	1.06 ± 0.18 0.022 ± 0.004	50% 50%
PEG-LPX5#	28.6 ± 0.3	144.7 ± 3.1	5.1 ± 0.1	64 ± 2	1.20 ± 0.16 0.018 ± 0.003	53% 47%
PEG-LPX10#	16.1 ± 1.9	66.2 ± 7.7	4.1 ± 0.7	45 ± 1	1.12 ± 0.18 0.025 ± 0.004	64% 36%

FCS on ONs Containing PEG-LPXs

Next, we measured the fluorescence fluctuations of double-labeled PO40-ONs complexed with pegylated liposomes upon excitation at 488 nm (Figure 5). Again two observations were made. First, the green and the red detector of the FCS instrument detected fluorescence peaks. In contrast to the LPXs (Figure 3), the peaks in the fluorescence fluctuation profiles appeared more frequently, were narrower and showed a more uniform height. A second observation in Figure 5 was that the average fluorescence decreases with an increasing +/- ratio. This again reflects that at a higher +/- ratio more ONs become complexed. In contrast to LPXs, it was, however, not possible to accurately

determine the background fluorescence since the fluorescence peaks appeared too frequently, indicating the continuous presence of PEG-LPXs in the detection volume of the FCS instrument. It should be noted that also for PEG-LPXs, the addition of SDS restored the red and green fluorescence to the level of free PO40-ONs as in Figure 2A. Also, fluorescence peaks were no longer detected, consistent with the induced release of the ONs from the PEG-LPXs (data not shown).

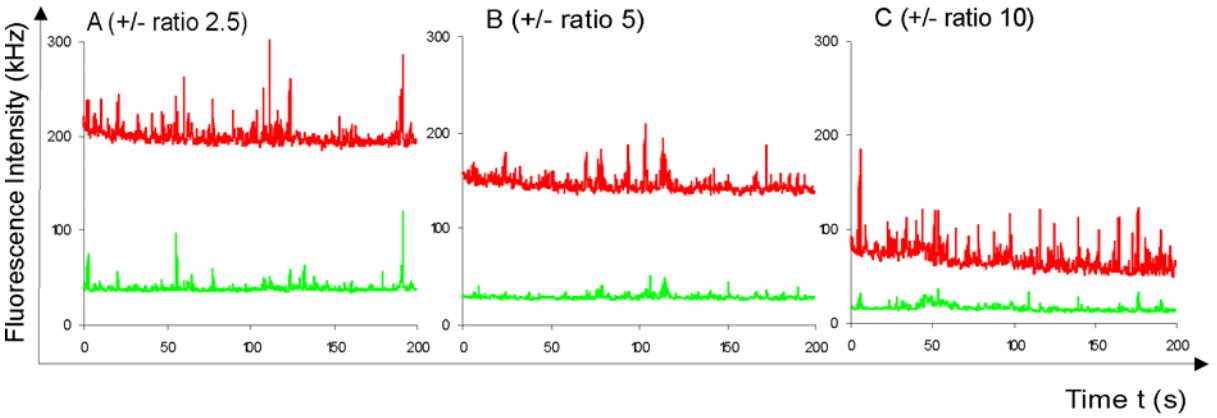

Figure 5. Fluorescence intensity fluctuations of pegylated lipoplexes as measured by the green (green line) and red (red line) detector of the FCS instrument. Pegylated lipoplexes were prepared with (A) a +/- ratio of 2.5, (B) a +/- ratio of 5 and (C) a +/- ratio of 10. Laser excitation was set to 488 nm.

In contrast to LPXs, the more uniform fluorescence peaks originating from the PEG-LPXs did not disturb the auto-correlation analysis. Therefore, auto-correlation analysis was performed on the fluorescence fluctuations with the fluorescence peaks included. The obtained auto-correlation curves together with the dual-species fit are depicted in Figure 6A. Comparison of the residuals of the fit using equation 1 (Figure 6B) versus equation 2 (Figure 6C) shows that fitting of the auto-correlation curves was best performed with the dual-species fit, indicating the presence of two species with a distinct diffusion coefficient (Table 1). For a +/- ratio of 2.5, 104 ± 5 particles were calculated from which 50% (N_1 = 52 ± 2.5) had a diffusion coefficient D_1 of $1.06 \pm 0.18 * 10^{-10}$ m²/s, consistent with diffusion of free ONs. The second species ($N_2 = 52 \pm 2.5$) diffused more slowly ($D_2 = 0.022 \pm 0.004 * 10^{-10}$ m²/s) reflecting the diffusion of the PEG-LPXs through the detection volume of the FCS instrument. This value agreed well with the diffusion coefficient of $0.018 * 10^{-10}$ m²/s found for DOTAP/ONs vesicles by Merkle *et al.*, using two photon FCS [20]. Again, the ON concentration used in the preparation of the PEG-LPXs equaled the ON concentration as used in Figure 2A. When compared to free PO40-ONs ($N_3 = 195 \pm 4$), 143 ± 6.5 (N_3-N_1) ONs were complexed in 52 ± 2.5 (N_2) complexes, being an average of 2.8 ± 0.2 ONs per complex. Using the same approach as for a +/- ratio of 2.5, an average of 5.4 ± 0.2 and 10.3 ± 0.7 ONs per complex was calculated for the PEG-LPXs with a +/- ratio of 5 and 10, respectively.

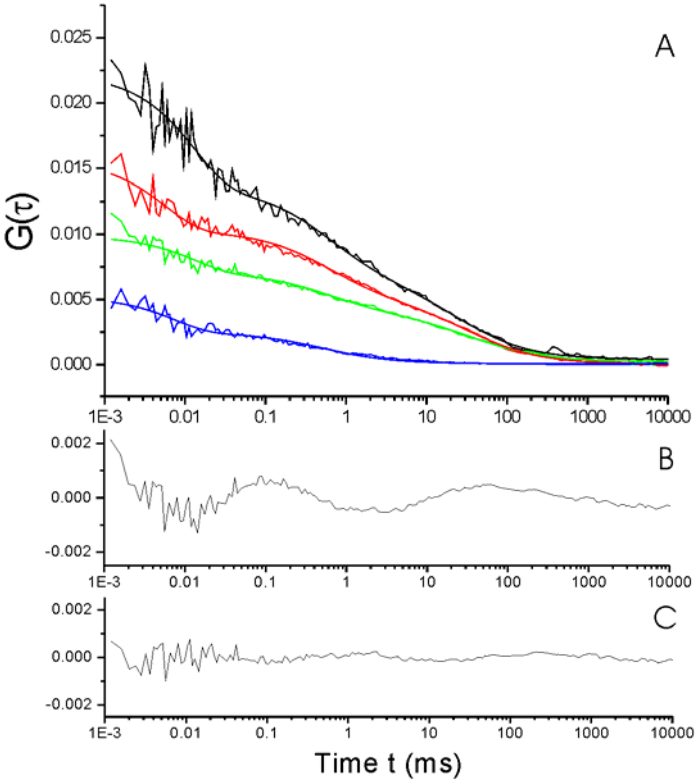

Figure 6. (A) Auto-correlation curves and dual-species fit as obtained from the red fluorescence fluctuations of pegylated lipoplexes with a +/- ratio of 2.5 (green line), a +/- ratio of 5 (red line) and a +/- ratio of 10 (black line). As a comparison, the auto-correlation curve and single-species fit as obtained on a solution of free PO40-ONs is also depicted (blue line). (B) and (C) show the residuals of the fit after fitting the auto-correlation data of PEG-LPXs with a +/- ratio of 2.5 with respectively a single-species fit and a dual-species fit. The appearance of the residuals of the fit of PEG-LPXs with a +/- ratio of 5 and 10 was similar. Laser excitation was set to 488 nm.

Once again, the obtained fluorescence fluctuation profiles for the PEG-LPXs are consistent with the diffusion of 'multimolecular' complexes bearing numerous ONs through the detection volume. However, when compared to LPXs (Figure 3), where the free ONs (~ background fluorescence) could be well separated from the lipoplexes which occasionally diffuse through the detection volume of the FCS instrument (~ dissimilar fluorescence peaks), the fluorescence fluctuation profile of PEG-LPXs suggests a more frequent presence of PEG-LPXs in the detection volume (~ successive fluorescence peaks) which appear to contain an equal amount of ONs (~ uniform peak height).

The question now raised is how best to explain the difference in fluorescence fluctuation profiles of LPXs and PEG-LPXs. It is well known that pegylation of lipoplexes prevents their aggregation, whereas non-pegylated lipoplexes can fuse to form large aggregates [21]. Due to the aggregation of LPXs, large multimolecular complexes are formed, bearing various amounts of ONs. The passage of such a complex through the detection volume of the FCS instrument results in highly intense fluorescence bursts, as seen from the non-uniform broad peaks. Also, the largest aggregates will sediment and will therefore no

longer pass through the detection volume of the FCS instrument, which could explain the lower amount of fluorescence peaks in Figure 3. For PEG-LPXs, the PEG-chains prevent complex aggregation. Consequently, the complexes do not sediment and remain homogeneously distributed. This causes complexes to be present in the detection volume of the FCS instrument most of the time, explaining the regular appearance of fluorescence peaks in Figure 5. The lack of aggregation could also explain why PEG-LPXs seem to contain a more consistent amount of ONs as suggested from the uniform peak height in the fluctuation profile.

ON Protection Against Nucleases by LPXs

In general it is believed that cationic liposomes protect complexed ONs against degradation by nucleases. We examined to what extent ONs complexed to liposomes are actually protected against degradation by nucleases. Although PAGE could be used for this purpose, the concentration of ONs needed to detect degraded ONs could be quite extensive (and expensive). Therefore we preferred to use FRET-FCS to determine the extent of ON degradation in LPXs and PEG-LPXs incubated with DNase I, as illustrated schematically in Figure 1B.

Figure 7A shows the R/G ratio as obtained for PO40-ONs released by SDS from non-pegylated lipoplexes after they were exposed to DNase I for various times (i.e. after step D in Figure 1A). The R/G ratio obtained from LPXs incubated in a solution without DNase I does not decrease, which was expected since no degradation can occur. When the LPXs were incubated in a solution containing DNase I, the R/G ratio decreases: the longer the exposure of the LPXs to DNase I, the lower the R/G ratio of PO40-ONs released by SDS. In the LPXs with a +/- ratio of 2.5 and 5, the ONs seem to be completely degraded when the LPXs are exposed to DNase I for about 12 hours. The LPXs with a +/- ratio of 10 offer better ON protection during the first 12 hours of incubation, however, the ONs become almost completely degraded after 18 hours incubation time. These results suggest that over time, the DNase I enzyme has access to and degrades the PO40-ONs.

One question is whether or not the ON degradation occurs inside the complexes, i.e. when the ONs are associated to the liposomes. To address this question we took a closer look at the amount of free ONs in the lipoplex dispersions, spontaneously released as a function of time. As we used an FCS instrument, which can detect single molecules, the number of free ONs in the LPX dispersions as obtained in Figure 1A, step C, (i.e. before PO40-ONs release induced by SDS) could be easily calculated from the amplitude of the auto-correlation curves or by fitting to equation 1 (auto-correlation data not shown, but similar as in Figure 4).

Figure 7B shows the amount of spontaneously released ONs in the dispersion of non-pegylated lipoplexes. For all +/- ratios studied, the amount of spontaneously released ONs starts to increase after 4 hours incubation time. For a +/- ratio of 2.5 and 5, all ONs seem to be released upon 12 hours incubation time, exactly the time in Figure 7A at which all PO40-ONs are degraded. Similarly, for a +/- ratio of 10, maximum release is obtained after 18 hours incubation time, again being the time after which Figure 7A shows that all ONs are degraded. Combining Figure 7A and 7B, one comes to the conclusion that not the complexed ONs, but rather the spontaneously released ONs become degraded by the DNase I enzyme.

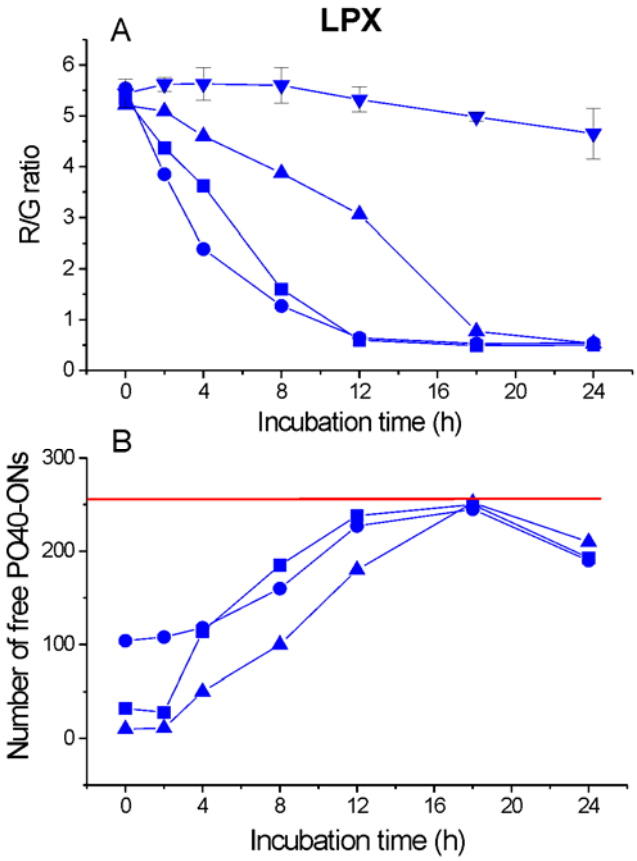

Figure 7. (A) R/G ratio of PO40-ONs released by SDS from non-pegylated lipoplexes with a +/- ratio of 2.5 (circle), 5 (square) and 10 (up triangle). The x-axis represents the time during which the LPXs were incubated with 0.2 Units DNase I. As a control, LPXs to which no DNase I was added were used (down triangle). Laser excitation was set to 488 nm and the green and red detector of the dual-color FCS instrument recorded the fluorescence intensities. (B) Number of free PO40-ONs as spontaneously released from non-pegylated lipoplexes with a +/- ratio of 2.5 (circle), 5 (square) and 10 (triangle). The x-axis represents the time during which the LPXs were incubated with 0.2 Units DNase I. The amount of free PO40-ONs was calculated from the background fluorescence intensities as measured by the red detector upon excitation at 647 nm (~ Cy5). In this way, the amount of calculated free ONs is independent from the possible degradation of the ONs. A line is drawn at the level of full PO40-ONs release. It should be noted that the same amount of spontaneously released PO40-ONs was observed when the LPXs were incubated without the DNase I enzyme.

One should then wonder why a gradual release of ONs from the LPXs occurs. It has been observed previously that lipid contact and membrane mixing in a lipoplex dispersion can trigger lipoplex aggregation and contents leakage [22;23]. So each time fusion between lipoplexes occurs, part of the ONs are released. As can be seen in Figure 7B, the amount of spontaneously released ONs reaches the level of free ONs before complexation with the liposomes. This means that full release of the complexed ONs may occur when using DOTAP/DOPE liposomes if the LPxs are able to aggregate during a prolonged period of time. The disassembly of the LPXs as a function of time could also be observed from the fact that the release of ONs was accompanied by a decrease in the amount of highly intense fluorescence peaks (~ lipoplexes) in the fluorescence fluctuation profiles and an increase in the average fluorescence background (~ free ONs). As an example, this phenomenon is depicted in Figure 8 for LPXs with a +/- ratio of 10, respectively 4, 8 and 18 hours after incubation with the DNase I enzyme. Note that after 18 hours the released ONs are degraded, since the green fluorescence is now higher than the red fluorescence due to the disappearance of FRET. This gradual release of ONs was also observed for LPXs that were incubated without DNase I. In this case, however, the released ONs remained intact.

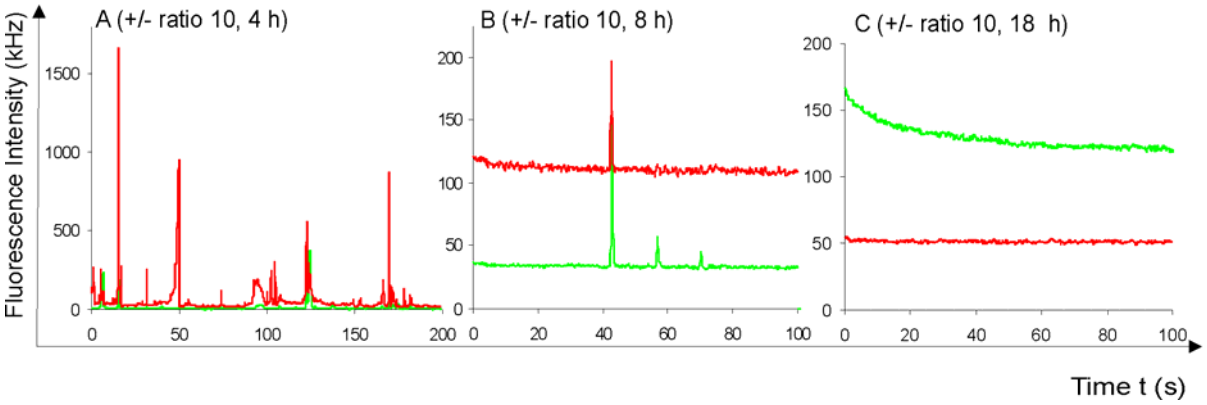

Figure 8. Fluorescence intensity fluctuations of non-pegylated lipoplexes with a +/- ratio of 10 as measured by the green (green line) and red (red line) detector of the FCS instrument. The LPXs were incubated with 0.2 units DNase I for (A) 4 hours, (B) 8 hours and (C) 18 hours. Laser excitation was set to 488 nm.

ON Protection Against Nucleases by PEG-LPXs

Figure 9A shows the R/G ratio as obtained on PO40-ONs released by SDS from pegylated lipoplexes after being exposed to DNase I for various lengths of time. Again, the R/G ratio obtained for PEG-LPXs that were incubated in a solution without DNase I remained rather constant, indicating that in this control experiment the ONs were not degraded. In the presence of DNase I, for all +/- ratios, there is a significant drop in the R/G ratio during the first 2 hours of incubation. This indicates that, initially, there is a substantial fraction of the ONs that is accessible to the DNase I enzyme. After this initial degradation the R/G ratio

remains rather constant (as in the control sample without DNase I). Apparently, no significant further degradation of the remaining intact PO40-ONs occurs, even not after 24 hours incubation time.

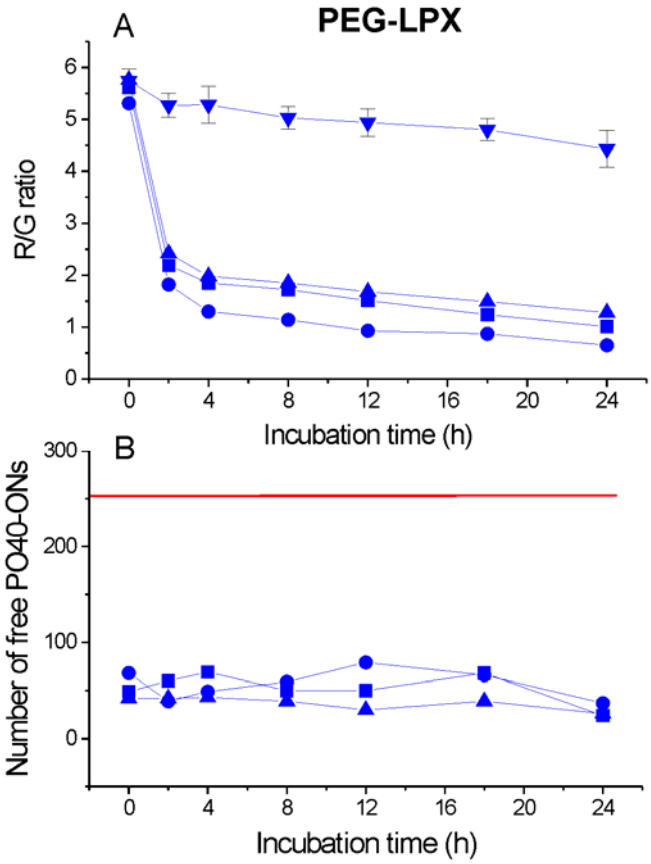

Figure 9. (A) R/G ratio of PO40-ONs released by SDS from pegylated lipoplexes with a +/- ratio of 2.5 (circle), 5 (square) and 10 (up triangle). The x-axis represents the time during which the PEG-LPXs were incubated with 0.2 Units DNase I. As a control, PEG-LPXs to which no DNase I was added were used (down triangle). Laser excitation was set to 488 nm and the green and red detector of the dual-color FCS instrument recorded the fluorescence intensities. (B) Number of free PO40-ONs as spontaneously released from pegylated lipoplexes with a +/- ratio of 2.5 (circle), 5 (square) and 10 (triangle). The x-axis represents the time during which the PEG-LPXs were incubated with 0.2 Units DNase I. The amount of free PO40-ONs was calculated from the fluorescence intensities as measured by the red detector upon excitation at 647 nm (~ Cy5). In this way, the amount of calculated free ONs is independent from the possible degradation of the ONs. A line is drawn at the level of full PO40-ONs release. It should be noted that the same amount of spontaneously released PO40-ONs was observed when the PEG-LPXs were incubated without the DNase I enzyme.

As for the LPXs, we took a closer look at the amount of spontaneously released ONs in the PEG-LPX dispersions as a function of the incubation time (Figure 9B). The number of free ONs in the PEG-LPX dispersions as obtained in Figure 1A, step C, (i.e. before PO40-ONs release induced by SDS) was calculated by fitting the obtained auto-correlation curves to equation 2 and determination of the number of species 1 (*N*y*) that had a diffusion coefficient 1 that corresponds to the diffusion of free ONs (auto-correlation data not shown, but similar as in Figure 6). Interestingly, a longer incubation of the PEG-LPXs did not result in

a spontaneous release of the ONs. Apparently, the ONs remain attached to the PEG-LPXs. It can be expected that the presence of the PEG-chains provides a steric hindrance and prevents lipid contact between the different PEG-LPXs. Consequently, PEG-LPX aggregation and contents leakage do not take place. This was also clearly reflected in the FCS measurements, where consecutive similar fluorescence peaks remained to exist even after 24 hours incubation time, independent on the +/- ratio of the PEG-LPXs (Figure 10). From the green and red fluorescence intensities it can also be seen that the R/G ratio upon 24 hours incubation time is only slightly increased upon increasing the +/- ratio from 2.5 over 5 to 10.

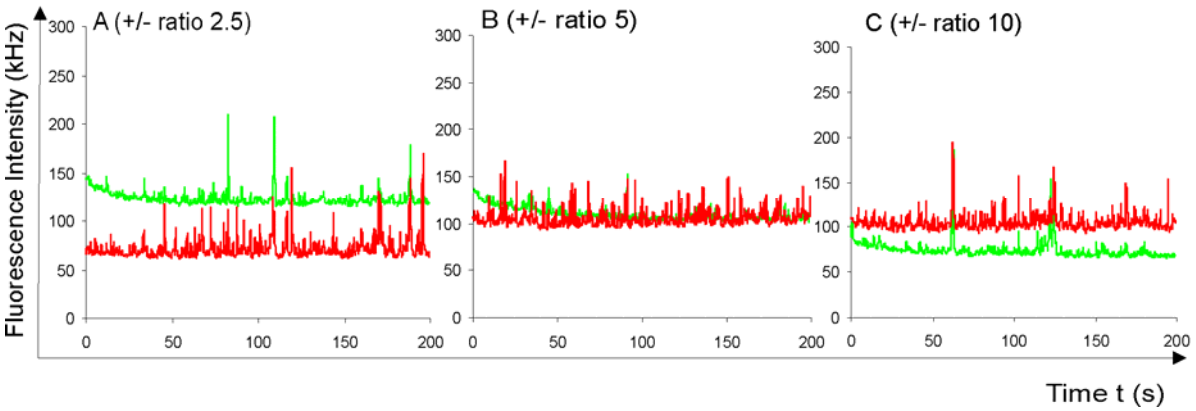

Figure 10. Fluorescence intensity fluctuations of pegylated lipoplexes as measured by the green (green line) and red (red line) detector of the FCS instrument upon incubation with 0.2 units DNase I for 24 hours. The PEG-LPXs were prepared with (A) a +/- ratio of 2.5, (B) a +/- ratio of 5 and (C) a +/- ratio of 10. Laser excitation was set to 488 nm.

Explanation of the Protective Properties of LPXs and PEG-LPXs Based upon their Structural Properties

It should be noted that the initial decrease in the R/G ratio for PEG-LPXs in Figure 9A is more pronounced than observed for LPXs in Figure 7A. Since this reflects the immediate degradation of uncomplexed ONs, one could argue that more free (uncomplexed) ONs are present in the PEG-LPX dispersion than in the LPX dispersion. However, the initial amount of free, uncomplexed ONs did not differ significantly between LPXs and PEG-LPXs as can be seen when the first data points in Figure 7B and Figure 9B are compared. This indicates that for PEG-LPXs, apparently also a large fraction of the complexed ONs are accessible to the DNase I enzyme. A possible explanation can be found in the mechanism for lipoplex formation as proposed by others [24-26] (Figure 11A). When mixing negatively charged ONs with positively charged non-pegylated liposomes, the ONs bind to the surface of the liposomes due to electrostatic interactions. In the case of non-pegylated liposomes, these 'ON coated' liposomes subsequently 'bridge' neighbouring cationic liposomes. Thereby the

liposomes fuse and the ONs become entrapped between lipid bilayers originating from the individual cationic non-pegylated liposomes (Figure 11A, step 1 and 2). This process may repeat several times, resulting in the formation of multilamellar liposomes/ON particles (lipoplexes) that contain the ONs on the inside (Figure 11A, step 3). The ONs are thus shielded from the environment and expected to be protected against enzymatic degradation. This hypothesis is in agreement with our observation that when using non-pegylated liposomes, not the complexed, but rather the spontaneously released ONs are accessible to the DNase I enzyme.

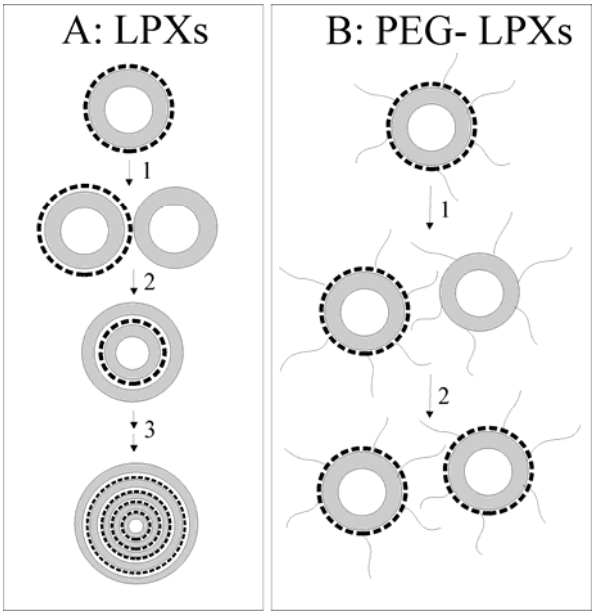

Figure 11. Mechanism proposed for the formation of (A) non-pegylated lipoplexes and (B) pegylated lipoplexes. The gray band represents the lipid bilayer from the liposomes, while the black band represent the ONs.

In contrast to non-pegylated lipoplexes rather few studies, if any, describe the mechanism behind the formation of pegylated lipoplexes. The initial degradation of the complexed ONs, however, suggests that in the PEG-LPXs the ONs are present on the outside, rather than on the inside. In Figure 11B we propose a mechanism for the formation of PEG-LPXs that can account for these observations. As occurs in the formation of LPXs, first the anionic ONs will bind to the cationic surface of the pegylated liposomes due to electrostatic interactions (Figure 11B, step 1). However, the presence of the PEG-chains on the surface of the pegylated liposomes is expected to prevent close contact between different 'ON coated' PEG-LPXs, hindering the fusion of pegylated liposomes and thus the formation of multilamellar particles. Hence, the ONs are not entrapped between lipid bilayers originating from the individual pegylated liposomes, but remain unprotected at the surface of the pegylated liposomes, still susceptible towards enzymatic degradation (Figure 11B, step 2). This could explain why not only the free ONs, but also part of the ONs associated to the

outer surface of the PEG-LPXs, can be degraded by the DNase I enzyme. To verify this hypothesis, the surface charge of the non-pegylated and pegylated liposomes was measured, before and after complexation with negatively charged ONs at a +/- ratio of 2.5, 5 and 10.

Zeta Potential and Hydrodynamic Diameter of LPXs and PEG-LPXs

Figure 12A shows the zeta potential and hydrodynamic diameter of non-pegylated liposomes before and after complexation with negatively charged ONs. At a +/- ratio of 5 and 10 the zeta potential equaled the value of the cationic liposomes without ONs. This indicates that the surface of the LPXs consists of cationic liposomes, with most of the negatively charged ONs inside the LPXs. This agrees with the mechanism of lipoplex formation as proposed in Figure 11A, where the negatively charged ONs become sandwiched between lipid bilayers from the positively charged DOTAP/DOPE liposomes. At a +/- ratio of 2.5, the zeta potential decreased when compared to the cationic liposomes. This indicates that the amount of cationic liposomes with this +/- ratio is not sufficient to capture all negatively charged ONs inside the LPXs. Also, the lower surface charge and thus the lower electrical repulsion between the lipoplexes at a +/- ratio of 2.5 encourages aggregate formation, which can be seen by the larger hydrodynamic diameter when compared to lipoplexes with a +/- ratio of 5 and 10.

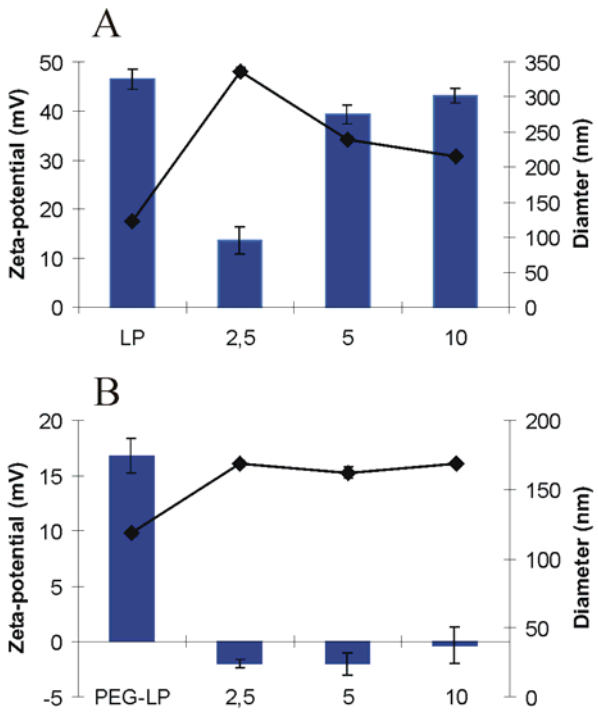

Figure 12. The zeta potential (bars) and hydrodynamic diameter (line) of liposome/ONs complexes prepared with (A) non-pegylated and (B) pegylated liposomes with a +/- ratio of 2.5, 5 and 10. The first data point represents the zeta potential and hydrodynamic diameter of respectively non-pegylated (LP) and pegylated (PEG-LP) liposomes before complexation.

Figure 12B shows the zeta potential and hydrodynamic diameter of pegylated liposomes before and after complexation with negatively charged ONs. Independent on the +/- ratio, the positively charged liposomes turn neutral to slightly negative when ONs are added to the solution. This indicates that the negatively charged ONs are attached to the surface of the pegylated liposomes without being covered by a second layer of positively charged pegylated liposomes, what agrees with the proposed mechanism for the formation of PEG-LPXs as depicted in Figure 11B. With this zeta potential, normally, aggregate formation would be expected due to the rather low electrical repulsion between different PEG-LPXs. However, from the hydrodynamic diameter it can be seen that the PEG-LPXs all display equal small sizes. This, again, can be explained by the presence of the PEG-chains at the surface of the pegylated liposomes, which prevent aggregate formation.

CONCLUSIONS AND OUTLOOK

In this chapter, we used the FRET-FCS technique as described in Chapter 2 to contribute to a better understanding of the protection of antisense ONs against nucleases by pegylated and non-pegylated DOTAP/DOPE liposomes.

Both pegylated and non-pegylated liposomes were able to complex an increasing number of ONs when a higher +/- ratio was used. When exposed to DNase I, initially, the non-pegylated lipoplexes offered a good protection of ONs against enzymatic degradation. However, due to lipoplex aggregation and subsequent ON release, the protection against enzymatic degradation was overcome during longer incubation times. We suggest that not the complexed, but rather the spontaneously released ONs are accessible to the DNase I enzyme, which agrees with the mechanism of lipoplex formation as proposed by others [24-26]. One way to prolong the protection of ONs against enzymatic degradation would therefore be to prevent the aggregation between different LPXs, e.g. by the incorporation of PEG-chains at the liposomes' surface. Complexes prepared from pegylated liposomes indeed remained stable over a prolonged period of time, without aggregate formation or spontaneous release of the ONs (e.g. even after 24 hours the FCS profile had not changed). However, when the PEG-LPXs were exposed to nucleases, initially a significant amount of the complexed ONs was degraded. We obtained experimental evidence that the presence of the PEG-chains influences lipoplex formation so that the ONs are not sandwiched between different lipid bilayers, but remain unprotected at the surface of the PEG-LPXs. To circumvent this rapid degradation, 'post-pegylation' should be considered, in which the incorporation of PEG-chains takes place after the initial lipoplex formation. In that way, the good complexation

properties of non-pegylated liposomes, in which the ONs are shielded from the environment, would be combined with the prolonged stability of the pegylated lipoplexes. This chapter showed that FCS and FRET-FCS are capable tools to investigate characteristics such as complexation behavior and ON protection against nucleases of cationic lipid-based carriers used in antisense delivery. In the next chapter, we evaluated whether the FRET-FCS technique could also be used to determine the protective properties of cationic polymer-based carriers used in gene delivery, such as polyethyleneimine (PEI). Also, as FRET-FCS is readily applicable on living cells, we evaluated in Chapter 5 and Chapter 6 respectively, whether FRET-FCS could be used to give further insight into the relationship between the intracellular fate and degradation of ONs when delivered by the LPXs and PEG-LPXs as used in this chapter and the observed antisense activity.

ACKNOWLEDGEMENTS

Katrien Remaut is a Research Assistant of the Research Foundation - Flanders (Belgium). Niek Sanders and Kevin Braeckmans are Postdoctoral Fellows of the Research Foundation - Flanders (Belgium). The financial support of this institute is acknowledged with gratitude. The Ghent University (UG-BOF) and Funds for Scientific Research-Flanders (G.0310.02) supported this project through instrumentation credits and financial support. Dr. N. Opitz (Max Planck Institute for Molecular Physiology, Dortmund, Germany) is acknowledged for the installation of the FCS-module on the MRC-1024 Bio-Rad confocal laser-scanning microscope.

REFERENCES

(1) Sazani, P.; Kole, R. Therapeutic potential of antisense oligonucleotides as modulators of alternative splicing. *J. Clin. Invest.* **2003**, 112, 481-486.

(2) Shi, F.; Hoekstra, D. Effective intracellular delivery of oligonucleotides in order to make sense of antisense. *J. Control. Release* **2004**, 97, 189-209.

(3) Agrawal, S. Importance of nucleotide sequence and chemical modifications of antisense oligonucleotides. *Biochim. Biophys. Acta* **1999**, 1489, 53-68.

(4) Brown, D. A.; Kang, S. H.; Gryaznov, S. M.; Dedionisio, L.; Heidenreich, O.; Sullivan, S.; Xu, X.; Nerenberg, M. I. Effect of phosphorothioate modification of oligodeoxynucleotides on specific protein-binding. *J. Biol. Chem.* **1994**, 269, 26801-26805.

(5) Hogrefe, R. I. An antisense oligonucleotide primer. *Antisense Nucleic Acid Drug Dev.* **1999**, 9, 351-357.

(6) Akhtar, S.; Hughes, M. D.; Khan, A.; Bibby, M.; Hussain, M.; Nawaz, Q.; Double, J.; Sayyed, P. The delivery of antisense therapeutics. *Adv. Drug Deliver. Rev.* **2000**, 44, 3-21.

(7) Lucas, B.; Van Rompaey, E.; Remaut, K.; Sanders, N.; De Smedt, S.; Demeester, J. On the biological activity of anti-ICAM-1 oligonucleotides complexed to non-viral carriers. *J. Control. Release* **2004**, 96, 207-219.

(8) Dheur, S.; Dias, N.; Van Aerschot, A.; Herdewijn, P.; Bettinger, T.; Remy, J. S.; Helene, C.; Saison-Behmoaras, E. T. Polyethylenimine but not cationic lipid improves antisense activity of 3'-capped phosphodiester oligonucleotides. *Antisense Nucleic Acid Drug Dev.* **1999**, 9, 515-525.

(9) De Smedt, S. C.; Remaut, K.; Lucas, B.; Braeckmans, K.; Sanders, N. N.; Demeester, J. Studying biophysical barriers to DNA delivery by advanced light microscopy. *Adv. Drug Deliver. Rev.* **2005**, 57, 191-210.

(10) Lucas, B.; Remaut, K.; Braeckmans, K.; Haustraete, J.; De Smedt, S. C.; Demeester, J. Studying pegylated DNA complexes by dual color fluorescence fluctuation spectroscopy. *Macromolecules* **2004**, 37, 3832-3840.

(11) Van Rompaey, E.; Engelborghs, Y.; Sanders, N.; De Smedt, S. C.; Demeester, J. Interactions between oligonucleotides and cationic polymers investigated by fluorescence correlation spectroscopy. *Pharm. Res.* **2001**, 18, 928-936.

(12) Van Rompaey, E.; Chen, Y.; Muller, J. D.; Gratton, E.; Van Craenenbroeck, E.; Engelborghs, Y.; De Smedt, S.; Demeester, J. Fluorescence fluctuation analysis for the study of interactions between oligonucleotides and polycationic polymers. *Biol. Chem.* **2001**, 382, 379-386.

(13) Lucas, B.; Remaut, K.; Sanders, N. N.; Braeckmans, K.; De Smedt, S. C.; Demeester, J. Towards a better understanding of the dissociation behavior of liposome-oligonucleotide complexes in the cytosol of cells. *J. Control. Release* **2005**, 103, 435-450.

(14) Lucas, B.; Remaut, K.; Sanders, N. N.; Braeckmans, K.; De Smedt, S. C.; Demeester, J. Studying the intracellular dissociation of polymer-oligonucleotide complexes by dual color fluorescence fluctuation spectroscopy and confocal imaging. *Biochemistry* **2005**, 44, 9905-9912.

(15) Remaut, K.; Lucas, B.; Braeckmans, K.; Sanders, N. N.; De Smedt, S. C.; Demeester, J. FRET-FCS as a tool to evaluate the stability of oligonucleotide drugs after intracellular delivery. *J. Control. Release* **2005**, 103, 259-271.

(16) Lucas, B.; Van Rompaey, E.; De Smedt, S. C.; Demeester, J.; Van Oostveldt, P. Dual-color FFS to study the complexation between poly-l-lysine and oligonucleotides. *Macromolecules* **2002**, 35, 8152-8160.

(17) Schwille, P.; Meyer-Almes, F.; Rigler, R. Dual-Color Fluorescence Cross-Correlation spectroscopy for multicomponent diffusional analysis in solution. *Biophys. J.* **1997**, 72, 1878-1886.

(18) Schwille, P. Fluorescence correlation spectroscopy and its potential for intracellular applications. *Cell Biochem. Biophys.* **2001**, 34, 383-408.

(19) Hess, S. T.; Huang, S.; Heikal, A. A.; Webb, W. W. Biological and chemical applications of fluorescence correlation spectroscopy: a review. *Biochemistry* **2002**, 41, 697-705.

(20) Merkle, D.; Lees-Miller, S. P.; Cramb, D. T. Structure and dynamics of lipoplex formation examined using two-photon fluorescence cross-correlation spectroscopy. *Biochemistry* **2004**, 43, 7263-7272.

(21) Meyer, O.; Kirpotin, D.; Hong, K.; Sternberg, B.; Park, J. W.; Woodle, M. C.; Papahadjopoulos, D. Cationic liposomes coated with polyethylene glycol as carriers for oligonucleotides. *J. Biol. Chem.* **1998**, 273, 15621-15627.

(22) Tarahovsky, Y. S.; Koynova, R.; MacDonald, R. C. DNA release from lipoplexes by anionic lipids: Correlation with lipid mesomorphism, interfacial curvature, and membrane fusion. *Biophys. J.* **2004**, 87, 1054-1064.

(23) Guo, X.; Mackay, J. A.; Szoka, F. C. Mechanism of pH-triggered collapse of phosphatidylethanolamine liposomes stabilized by an ortho ester polyethyleneglycol lipid. *Biophys. J.* **2003**, 84, 1784-1795.

(24) Zelphati, O.; Szoka, F. C., Jr. Cationic liposomes as an oligonucleotide carrier: mechanism of action. *J. Liposome Res.* **1997**, 7, 31-49.

(25) Pedroso de Lima, M. C.; Simoes, S.; Pires, P.; Faneca, H.; Düzgünes, N. Cationic lipid-DNA complexes in gene delivery: from biophysics to biological applications. *Adv. Drug Deliver. Rev.* **2001**, 47, 277-294.

(26) Weisman, S.; Hirsch-Lerner, D.; Barenholz, Y.; Talmon, Y. Nanostructure of cationic lipid-oligonucleotide complexes. *Biophys. J.* **2004**, 87, 609-614.

Chapter 4

PROTECTION OF OLIGONUCLEOTIDES AGAINST NUCLEASES BY PEGYLATED AND NON-PEGYLATED POLYETHYLENEIMINE

Parts of this chapter are in press:

Remaut, K.; Lucas, B.; Raemdonck, K.; Braeckmans, K.; Demeester, J.; De Smedt, S. C. *Biomacromolecules*

ABSTRACT

In the previous chapter we demonstrated that FRET-FCS could be used to investigate characteristics such as the complexation behavior and protection of oligonucleotides (ONs) against nucleases by cationic lipid-based carriers frequently used in antisense delivery. Besides cationic lipids, also cationic polymers can be used in gene delivery. Among the cationic polymers, polyethyleneimine (PEI) is a promising candidate for delivery of ONs. In this chapter we aimed to investigate whether ONs are differently protected against enzymatic degradation in respectively PEI and polyethyleneglycol-polyethyleneimine (PEG-PEI) polyplexes. Using the FRET-FCS technique as described in Chapter 2, we found that PEI/ON polyplexes remain to protect the ONs they carry over a prolonged period of time, while in PEG-PEI/ON polyplexes the degradation of the ONs slowly proceeds. We attribute this to the observation that PEI appears to compact the ONs more firmly in the polyplexes' core when compared to PEG-PEI, which apparently also results in a better protection against enzymatic degradation. These observations may also influence the efficiency of PEI-based ON delivery *in vivo,* where pegylation is an attractive strategy to enhance the stability of the polyplexes in the bloodstream.

Chapter 4

Protection of Oligonucleotides Against Nucleases by Pegylated and Non-Pegylated Polyethyleneimine

INTRODUCTION

Currently a variety of carriers are under investigation for the delivery of nucleic acids such as plasmid DNA (pDNA). Viral vectors provide high transfection efficiencies for pDNA but suffer from the limited size of the pDNA they can carry. Also, they can induce severe immune responses. Non-viral vectors, such as cationic polymers [1] and cationic liposomes [2] are advantageous over viral vectors in that they are less expensive, easier and safer to make and more suitable for long time storage. They can also deliver much larger pieces of pDNA when compared to viral methods [3]. Cationic lipids as well as cationic polymers spontaneously form interpolyelectrolyte complexes with the negatively charged nucleic acids. These DNA complexes are respectively called lipoplexes and polyplexes. The current transfection efficiencies of non-viral vectors are, however, far from optimal. Despite their low efficiency, non-viral vectors retain high interest due to their favorable safety profile and ease of manufacturing.

Non-viral carriers are, besides for the delivery of pDNA, also investigated for the delivery of antisense oligonucleotides (ONs). Antisense ONs show potential in the treatment of a wide variety of genetic and viral disorders. The principle of antisense is based on the specific inhibition of unwanted gene expression by blocking mRNA activity. This is achieved by a sequence-specific binding of the ONs to their complementary target mRNA, which results in blocking or degradation of the target sequence. Before the ONs can down-regulate a targeted gene expression, they have to reach the intracellular environment. The non-viral carriers should help the ONs to enter the cells and to escape from the endosomal compartment. Generally speaking, the ON/carrier complexes should exhibit a net positive charge to enhance the binding to the negatively charged cell membrane, which can be

accomplished by varying the ratio of the cationic carrier to the negatively charged ONs [4]. Also, the complexes should preferably have a small, uniform size distribution (< 200 nm) to facilitate endocytosis [5]. For successful ONs delivery, the carriers should also protect the ONs against enzymatic degradation by the nucleases in the blood and the cells.

Among the cationic polymers, polyethyleneimine (PEI) is a promising candidate for non-viral gene delivery [6;7]. The repeating unit of PEI consists of two carbon atoms followed by one nitrogen atom (Figure 1). Because of the amine groups, PEI carries a positive surface charge which allows binding and condensing the negatively charged DNA. Both the molar mass and the backbone structure of PEI (being linear or branched) influence the transfection efficiency and cytotoxicity of the PEI/DNA polyplexes [8;9]. Conflicting information is available regarding the structural requirements and the molecular weight of PEI necessary for efficient gene delivery. Kunath *et al.* reported that low molecular weight PEI is better for transfection when compared to PEI with a high molecular weight [10]. In contrast, Godbey *et al.* found a higher transfection efficiency with increasing molecular weight [11]. Von Harpe *et al.* studied the transfection efficiency of a wide variety of commercially available PEIs and although he found vast differences in transfection efficiencies, he found no correlation between the physicochemical properties of the PEIs and their transfection efficiency [12].

In vitro, the use of unmodified PEI-based polyplexes comes with problems of cytotoxicity, biocompatibility and solubility. *In vivo,* non-specific protein adsorption, aggregation and rapid blood clearance can be added to the list. Approaches for improving the solubility of PEI-based polyplexes include grafting of PEI with nonionic water-soluble polymers such as polyethyleneglycol (PEG). Furthermore, this pegylation reduces the cytotoxicity and prolongs the stability and circulation of the polyplexes in the bloodstream [13;14]. Also for cationic lipids, pegylation is an attractive strategy to prevent aggregation of the lipoplexes and opsonization by the reticulo endothelial system. In the previous chapter, we indeed found that the pegylated lipoplexes were stable over a prolonged period of time, whereas the non-pegylated lipoplexes were liable to aggregation. However, we also investigated the protection of ONs while being complexed to the non-pegylated and pegylated liposomes and found that pegylation influenced the lipoplex formation so that the ONs remain unprotected at the surface of the lipoplexes, prone to enzymatic degradation. On the contrary, non-pegylated lipoplexes contained the ONs on the inside, inaccessible to nuclease attack [15].

In this chapter, we wondered whether pegylation of PEI influences the complexation with ONs. To truly investigate the influence of pegylation, PEI and PEG-PEI with an identical PEI segment (branched, 2 kDa) were used (Figure 1). We especially aimed to investigate whether ONs are differently protected against enzymatic degradation in respectively PEI and PEG-PEI polyplexes. Following our previous work, in which we used Fluorescence

Correlation Spectroscopy (FCS) to monitor the association and dissociation between ONs and cationic polymers and cationic liposomes [16-20], we used FCS to study the PEI/ON and PEG-PEI/ON polyplexes. We demonstrated in Chapter 2 and Chapter 3 respectively, that the FCS-setup allows to follow the enzymatic degradation of fluorescently double-labeled ONs, both naked and complexed to cationic lipids [15;21]. In this chapter, fluorescently double-labeled ONs were complexed to PEI and PEG-PEI polymers and their protection against enzymatic degradation was followed by FCS.

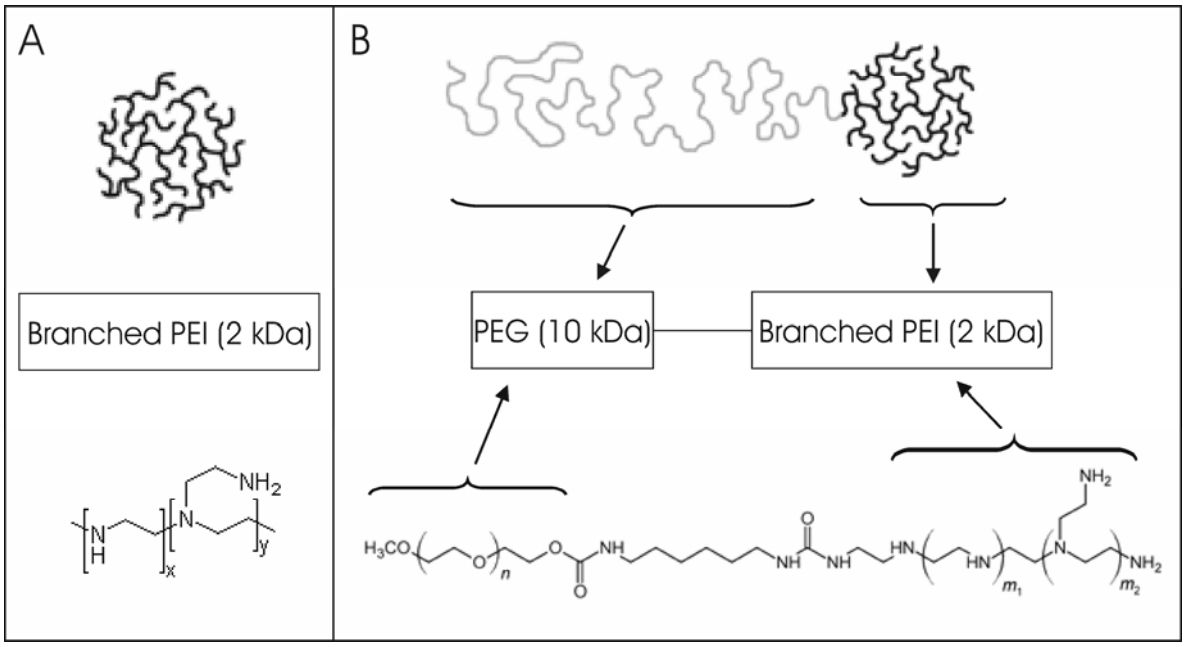

Figure 1. Schematic representation of (A) branched PEI and (B) PEG-PEI as used in this chapter. The molar mass of the branched PEI was 2 kDa. The PEG-PEI (12 kDa) consists of one branched PEI segment (2 kDa) and one PEG segment (10 kDa).

MATERIALS AND METHODS

Materials

Double-labeled 40 mer phosphodiester oligonucleotides (ONs) (5' GCC-GTC-TCT-GAC-TGC-TGA-TGA-CTA-CTA-TCG-TAT-AGT-GCG-G 3'; 13388,1 g/mol) were purchased from Eurogentec (Seraing, Belgium) and were purified by polyacrylamide gel electrophoresis (PAGE) by the supplier. The ONs were double-labeled with a rhodamine green fluorophore at the 3' end (λ_{ex} = 488 nm, λ_{em} = 532 nm) and a Cy5 fluorophore at the 5' end (λ_{ex} = 647 nm, λ_{em} = 670 nm).

Non-pegylated branched polyethyleneimine (PEI, 2 kDa) was purchased from Sigma (St. Louis, USA) (Figure 1A). Polyethyleneglycol-polyethyleneimine (PEG-PEI) was synthesized by the University of Nebraska Medical Center as described by Vinogradov *et al.*, by coupling an activated PEG to the branched PEI of 2 kDa that was purchased from Sigma (Figure 1B) [22]. The total content of nitrogen of the PEI and PEG-PEI was respectively 23.3 and 3.75 µmol/mg polymer. The weight average molecular weight M_w of the PEG-PEI was determined to be 12 kDa by static light scattering (e.g. one PEG-segment of 10 kDa and one branched PEI segment of 2 kDa per PEG-PEI).

DNase I (Pulmozyme®, 1 unit/µL) was kindly provided by NV Roche, Brussels, Belgium. Dextran sulfate was purchased from Sigma (St Louis, USA). The molar mass and sulfate content, as provided by the supplier, equaled respectively 500 kDa and 2.3 sulfate groups per glucosyl residue. A stock solution of 10 µg/µL was prepared in 20 mM HEPES buffer, pH 7.4.

Preparation of PEI/ON and PEG-PEI/ON Polyplexes

The N/P ratio of the polyplexes is defined as the molar ratio of the total number of nitrogen atoms in the PEI-segment of the polymer to the number of DNA phosphates. Polyplexes with different N/P ratios were prepared by adding a cationic polymer solution to an equal volume of an ON solution, followed by vortexing the dispersion for 10 seconds. Every polymer and ON solution was prepared in the so called 'degradation buffer' (2 mM magnesium acetate, 110 mM potassium acetate and 20 mM HEPES, pH 7.4). In this buffer it is known that the enzyme DNase I is active [23]. The polyplexes were allowed to equilibrate at room temperature for 30 minutes prior to use. The hydrodynamic size and zeta potential of the polyplexes was routinely checked by respectively dynamic light scattering (DLS, Malvern 4700, Malvern, Worcestershire, UK) and surface potential measurements (Zetasizer 2000, Malvern, Worcestershire, UK), as previously described [16].

Gel Electrophoresis Measurements on the Polyplex Dispersions and ONs Degradation

To study the complexation between ONs and respectively PEI and PEG-PEI by agarose gel electrophoresis, 5 µL of the ON solution (60 µg/mL) was mixed with 5 µL of a PEI respectively PEG-PEI solution (the concentration of PEI respectively PEG-PEI being dependent on the desired N/P ratio). The polyplexes were allowed to equilibrate for 30 minutes at room temperature before further use. To study the displacement of the ONs from the polyplexes an increasing amount of dextran sulfate was added to the dispersions. All samples were diluted with degradation buffer to a total volume of 30 µL. Also, 5 µL was taken

from each sample and diluted with degradation buffer to a total volume of 50 µL to perform FCS measurements. Before loading the remaining samples on the agarose gel, 5 µL of 50% sucrose was added.

The degradation of the ONs, upon exposure of the polyplexes to DNase I, was studied by polyacrylamide gel electrophoresis (PAGE) as follows. 2 µL of the ON solution (150 µg/mL) was mixed with 2 µL of the PEI respectively PEG-PEI solution (resulting in polyplexes with a N/P ratio of 10). After equilibration, the samples were diluted with degradation buffer to a total volume of 12 µL. Then, the samples were incubated, respectively with or without 0.2 units of DNase I for 30 hours. After the desired incubation time, 5 µL 10x EDTA-enriched TBE buffer was added (10.8 g/L tris base, 5.5 g/L boric acid and 3.7 g/L EDTA) to inhibit DNase I. Subsequently, 5 µL of dextran sulfate (10 µg/µL) was added to release the ONs from the polyplexes before loading the samples on the polyacrylamide gel. Also, from these dispersions 5 µL was removed and diluted with degradation buffer to a total volume of 50 µL to perform FCS measurements. Before loading the remaining samples on the polyacrylamide gel, 5 µL of 50% sucrose was added.

FCS Measurements on the Polyplex Dispersions and ONs Degradation

Dual-color FCS measurements were performed on polyplexes composed of non-labeled cationic PEI or PEG-PEI polymers and fluorescently double-labeled ONs. A dual-color FCS-setup installed on a MRC1024 Bio-Rad confocal laser scanning microscope was used. An inverted microscope (Eclipse TE300, Nikon, Japan) was used, which was equipped with a water immersion objective lens (Plan Apo 60X, NA 1.2, collar rim correction, Nikon, Japan). To verify whether the excitation volumes and the detection volumes optimally overlapped, the system was calibrated as described by Schwille *et al.* [24]. The laser beam was focused at about 50 µm above the bottom of the glass-bottom 96-well plate (Grainer Bio-one, Frickenhausen, Germany), which contained the samples. The 488 nm and the 647 nm laser beams of a krypton-argon laser (Bio-Rad, Cheshire, UK) were used and the green and red fluorescence intensity fluctuations were recorded on a digital ALV 5000/E correlator while exciting the polyplexes at 488 or 647 nm for 5 intervals of 50 seconds. To evaluate the integrity of the ONs, the ratio of the red to the green fluorescence (R/G ratio) was calculated after release of the ONs from the polyplexes by dextran sulfate upon excitation at 488 nm.

For FCS measurements in Figure 2, 100 µL of 200 nM ONs in degradation buffer was incubated respectively with and without 1 unit DNase I at 37°C for 4 hours. Then, 100 µL 2x EDTA-enriched TBE buffer was added to the Eppendorf tubes to inhibit the DNase I. Mixtures of intact and degraded ONs were prepared by mixing 50/0, 40/10, 30/20, 20/30, 10/40 and 0/50 µL of intact/degraded ONs. For FCS measurements in Figure 6 and 7, 50 µL

samples were obtained from the gel electrophoresis experiments as described above. To follow the degradation of the complexed ONs as a function of time (Figure 8), polyplexes were prepared by mixing 200 µL 1 µM ONs with 200 µL polymer solution (respectively 0.0087 or 0.0174 µg/µL PEI and 0.054 or 0.107 µg/µL PEG-PEI to obtain a N/P ratio of 5 or 10). After 30 minutes equilibration, the polyplex dispersions were diluted with degradation buffer to a total volume of 1000 µL and subsequently divided into two aliquots of 500 µL. To one 500 µL aliquot 1 µL (1 unit) DNase I was added. The two aliquots were further divided into Eppendorf tubes containing each 50 µL polyplex dispersion and incubated at 37°C. After the desired incubation time, 50 µL 2x EDTA-enriched TBE buffer was added to the Eppendorf tubes to inhibit the DNase I. On these samples, FCS measurements were performed respectively before and after addition of 20 or 10 µL dextran sulfate (10 µg/µL) to release the ONs from respectively the PEI and PEG-PEI polyplexes.

RESULTS

FRET to Study the Degradation of Fluorescently Double-Labeled ONs

As reported in Chapter 2, in the intact ONs used in this chapter Fluorescence Resonance Energy Transfer (FRET) occurs between the rhodamine green fluorophore at the 3' end and the Cy5 fluorophore at the 5' end [21]. Upon excitation at 488 nm laser light, the energy is transferred from the rhodamine green (donor fluorophore) to the Cy5 (acceptor fluorophore). This turns the ONs more red fluorescent while they become less green fluorescent. Figure 2 shows the green and red fluorescence intensities (as measured by the detectors of the FCS instrument upon excitation at 488 nm laser light) of solutions containing a mixture of intact and degraded ONs. At higher amounts of degraded ONs, the solutions become less red fluorescent but more green fluorescent. Hence, the ratio of the red to green fluorescence (R/G ratio) decreases as a function of the amount of degraded ONs. Indeed, degradation of the ONs by endonucleases increases the distance between the fluorophores so that FRET no longer occurs [21]. Therefore, the R/G ratio can be used to monitor the integrity of the double-labeled ONs.

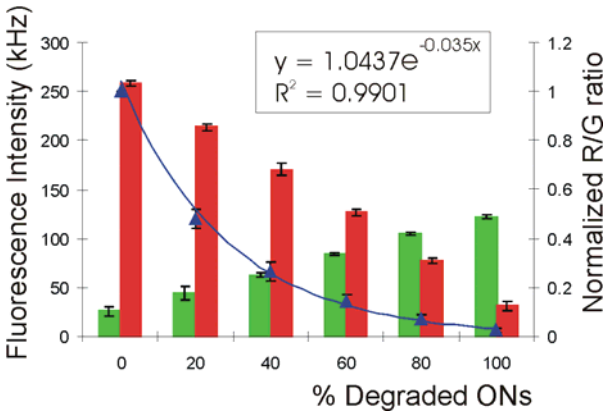

Figure 2. Green (green bars) and red (red bars) fluorescence of solutions composed of intact and degraded double-labeled ONs. The total (intact + degraded) ON concentration of all solutions was equivalent to 100 nM of intact ON. The red and green fluorescence was measured by the detectors of the FCS instrument with laser excitation set to 488 nm. The R/G ratio is also depicted (triangle). Values represent the average ± standard deviation of three independent experiments.

Association of ONs with PEI and PEG-PEI

The association of ONs with PEI and PEG-PEI as a function of the N/P ratio, was first studied by agarose gel electrophoresis. As Figure 3 shows, up to a N/P ratio of 1, free (uncomplexed) ONs migrate in the agarose gel thus indicating that the amount of cationic polymer is not sufficient to bind all the negatively charged ONs. At a N/P ratio of 2.5 a large amount of the ONs appears to be bound to the PEI and PEG-PEI, indicating that the amount of PEI and PEG-PEI is sufficient to bind all the ONs.

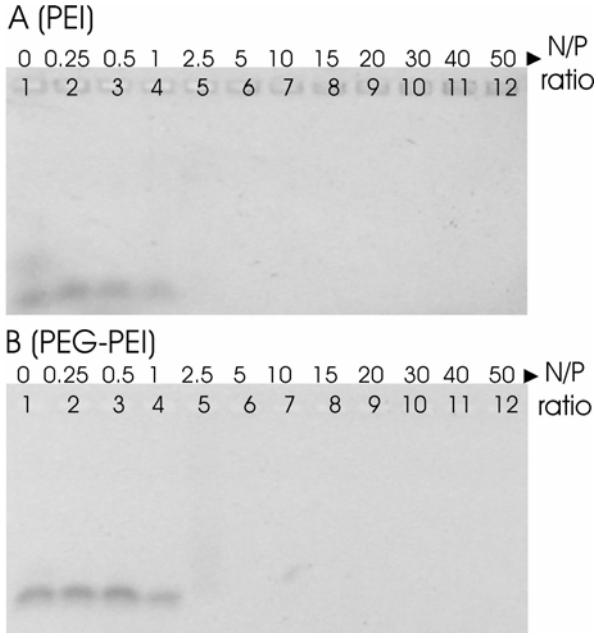

Figure 3. Gel electrophoresis on (A) PEI/ON and (B) PEG-PEI/ON dispersions. Lane 1: free ONs. Lane 2-12: PEI or PEG-PEI/ON polyplexes with the N/P ratio as depicted above each lane. The amount of ONs in each lane was 300 ng. This experiment was repeated three times with newly prepared samples, showing the same results as depicted.

Figure 4 shows the fluorescence fluctuation profiles of respectively free and complexed double-labeled ONs as measured by FCS upon excitation at 488 nm. FRET clearly occurs in the free ONs (Figure 4A) since the red fluorescence (acceptor fluorophore) is much higher than the green fluorescence (donor fluorophore). From the fluorescence intensities, a R/G ratio of 11.3 ± 0.6 was obtained. When PEI, respectively PEG-PEI, is added to the ONs the red fluorescence decreases significantly (Figure 4B and C). Also, 'fluorescence peaks' are visible in the red fluorescence fluctuations of the PEG-PEI/ON dispersions (Figure 4C) but not in the fluorescence fluctuations of the PEI/ON dispersions (Figure 4B). Both observations will be interpreted and explained in the Discussion section.

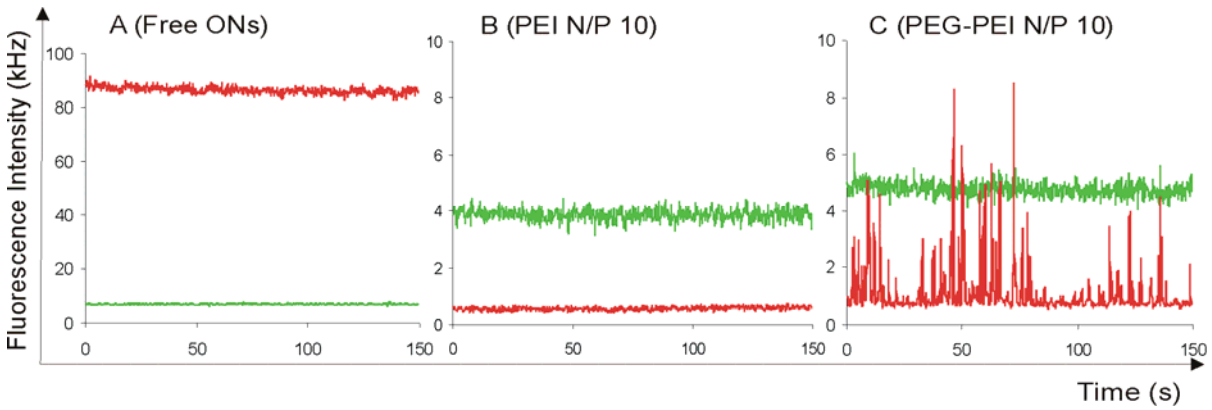

Figure 4. Representative FCS measurements on (A) free ONs, (B) PEI/ON dispersions and (C) PEG-PEI/ON dispersions. The green (green line) and red (red line) fluorescence intensity fluctuations were recorded by the FCS instrument with laser excitation set to 488 nm. The N/P ratio of the polyplexes was 10.

Dissociation of PEI/ON and PEG-PEI/ON Polyplexes

When negatively charged dextran sulfate is added to the polyplex dispersions, it is expected that it will compete with the ONs for binding to the PEI and PEG-PEI polymers, thereby possibly displacing the ONs from the polyplexes. As Figure 5 shows, this was indeed observed by gel electrophoresis. Release of the ONs from both PEI (Figure 5A) and PEG-PEI (Figure 5B) starts from lane 5, containing 1 µg dextran sulfate. It can be seen, however, that a greater amount of dextran sulfate is required for complete release of the ONs from PEI versus PEG-PEI based polyplexes. Indeed, while 3 µg dextran sulfate seems to be sufficient to fully displace the ONs from the PEG-PEI based polyplexes, complete release of the ONs from the PEI based polyplexes only occurs as from lane 9-10, containing 30-60 µg dextran sulfate.

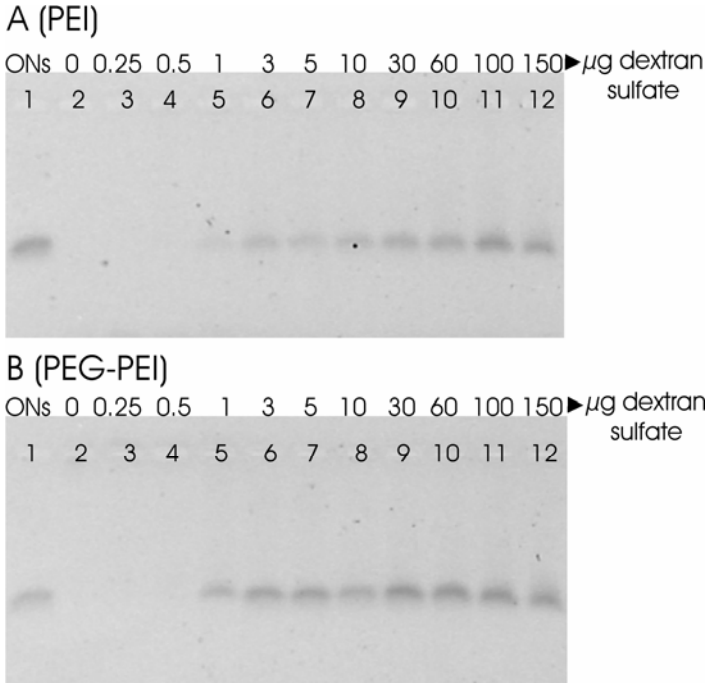

Figure 5. Gel electrophoresis on (A) PEI/ON and (B) PEG-PEI/ON dispersions. Lane 1: free ONs. Lane 2-12: PEI or PEG-PEI/ON polyplexes (N/P ratio of 10) to which increasing amounts of dextran sulfate were added as depicted above each lane in µg. The amount of ONs in each lane was 300 ng. This experiment was repeated three times with newly prepared samples, showing the same results as depicted.

The dextran sulfate containing dispersions, as analyzed by gel electrophoresis in Figure 5, were further measured by FCS as described in the Materials and Methods section. The average fluorescence intensities upon excitation of the polyplex/dextran sulfate dispersions at 488 nm, and the corresponding R/G ratio, are depicted in Figure 6. Free ONs show higher red than green fluorescence due to FRET, which results in a R/G ratio of around 11 (Figure 6 A and B, sample 1). Upon complexation, the ONs significantly loose their green and red fluorescence which is due to the quenching of the fluorophores (see Discussion section). Accordingly, the R/G ratio of the complexed ONs dropped to 0.2 ± 0.1 (Figure 6 A and B, sample 2).

Figure 6A, samples 3-12 show the outcome of the FCS measurements on PEI/ON dispersions containing increasing amounts of dextran sulfate. We can clearly see that the green and red fluorescence increases as a function of the amount of dextran sulfate, which indicates the gradual release of the ONs from the polyplexes. In agreement with the gel electrophoresis experiment in Figure 5A, the release starts from sample 5 containing 1 µg dextran sulfate. It takes however up to 150 µg dextran sulfate to fully release the ONs from the PEI/ON polyplexes (Figure 6A, sample 12). Importantly, upon adding increasing amounts of dextran sulfate to the PEI/ON dispersions not only the fluorescence intensities, but also the R/G ratio gradually recovers until the value as measured for free ONs (Figure 6A, sample 1).

As Figure 6B shows, adding dextran sulfate to PEG-PEI/ON dispersions also increases the green and red fluorescence. Although not visible on the agarose gel in Figure 5B, FCS measurements point out that the release of ONs from the polyplexes starts from sample 4, containing 0.5 µg dextran sulfate. The addition of 1 µg dextran sulfate releases all the ONs, accompanied by a full recovery of the R/G ratio (Figure 6B, sample 5). This is in clear contrast to the PEI/ON dispersions in Figure 6A, where the ONs were only gradually released upon adding increasing amounts of dextran sulfate. Apparently, the ONs become more easily displaced from the PEG-PEI/ON polyplexes than from the PEI/ON polyplexes.

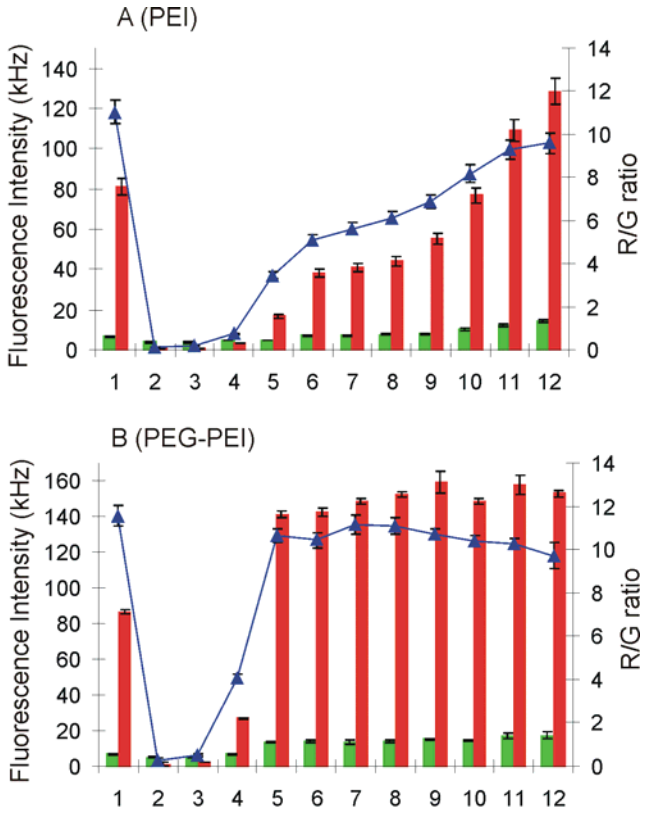

Figure 6. FCS measurements on (A) PEI/ON and (B) PEG-PEI/ON dispersions. The green (green bar) and red (red bar) fluorescence intensity fluctuations were recorded by the FCS instrument with laser excitation set to 488 nm. The samples as measured by FCS were composed of a fraction of the samples 1-12 used in Figure 5 as described in the Materials and Methods section. Accordingly, lane 1 contains free ONs and lane 2-12 contain PEI or PEG-PEI/ON polyplexes (N/P ratio of 10) to which respectively 0, 0.25, 0.5, 1, 3, 5, 10, 30, 60, 100, and 150 µg dextran sulfate was added. The R/G ratio is also depicted (triangle). Values represent the average ± standard deviation of three FCS measurements per sample.

Protection of ONs Against Enzymatic Degradation by PEI and PEG-PEI

Figure 7 shows the result of polyacrylamide gel electrophoresis on respectively free and complexed ONs that were incubated with or without 0.2 units of DNase I. Comparing lanes 2 and 3 shows that the degradation products run further on the gel. Lanes 4 and 6 contain respectively PEI and PEG-PEI based polyplexes that were incubated at 37°C for 30

hours without DNase I. After the 30 hours of incubation, dextran sulfate was added to release the ONs from the polyplexes. It seems that only intact ONs are released from both types of polyplexes. Lanes 5 and 7 contain respectively PEI and PEG-PEI based polyplexes that were incubated for 30 hours with DNase I. After inhibition of the DNase I and release of the ONs by adding dextran sulfate, it can be seen that the ONs that were complexed to PEI predominantly stayed intact, while a large fraction of the ONs that were complexed to PEG-PEI were degraded.

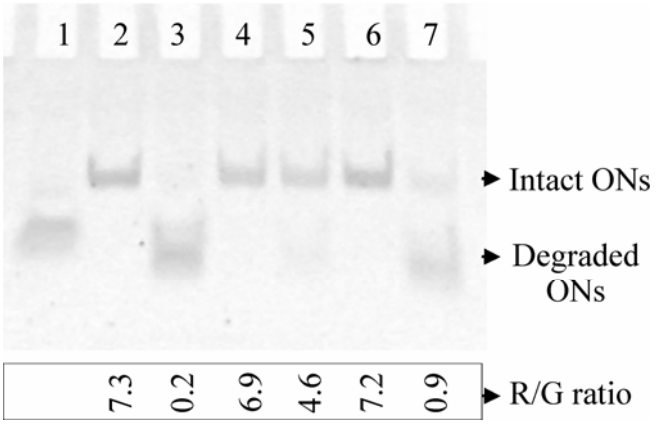

Figure 7. Gel electrophoresis on free ONs, PEI/ON and PEG-PEI/ON dispersions. (Lane 1) bromophenolblue marker, (lanes 2-3) free ONs respectively without and with 0.2 units DNase I, (lanes 4-5) PEI polyplexes respectively without and with 0.2 units DNase I and (lanes 6-7) PEG-PEI polyplexes respectively without and with 0.2 units DNase I. The N/P ratio of the polyplexes was 10. The samples were incubated at 37°C for 30 hours. Before loading the samples on the gel, the DNase I activity was inhibited with EDTA-enriched TBE buffer and the ONs were released from the polyplexes by adding dextran sulfate. For lanes 2-7, the R/G ratio (as determined by FCS on a fraction of the samples) is also depicted. Each lane (except for lane 1) contained 300 ng ONs. This experiment was repeated three times with newly prepared samples, showing the same results as depicted.

The samples as analyzed by gel electrophoresis in Figure 7 were also measured by FCS. From the R/G ratio, as depicted at the bottom of Figure 7, the amount of degraded ONs could be calculated using the equation $y = 1.0437e^{-0.035x}$ in which y is the normalized R/G ratio and x is the percentage of degraded ONs. This equation was determined from an exponential fit ($R^2 = 0.9901$) of the normalized R/G ratio as a function of the percentage of degraded ONs as depicted in Figure 2. For the samples in lanes 2, 4 and 6, 98 ± 2% of the ONs remained intact. From the free ONs in lane 3, only 0.5 ± 0.1% remained intact upon incubation with the DNase I enzyme. When the ONs were complexed to PEI or PEG-PEI (lanes 5 and 7), respectively 82 ± 5% and 38 ± 4% of the ONs survived the incubation with the DNase I enzyme.

We examined the degradation kinetics of the ONs complexed to PEI and PEG-PEI in more detail with the FCS instrument (Figure 8). Therefore, as described in the Materials and Methods section, we measured the R/G ratio of the ONs (upon excitation at 488 nm) after release of the ONs by dextran sulfate from the polyplexes that were incubated with DNase I for a certain period of time. Again, from the R/G ratio, the amount of degraded ONs was calculated using the equation $y = 1.0437e^{-0.035x}$ in which y is the normalized R/G ratio and x is the percentage of degraded ONs.

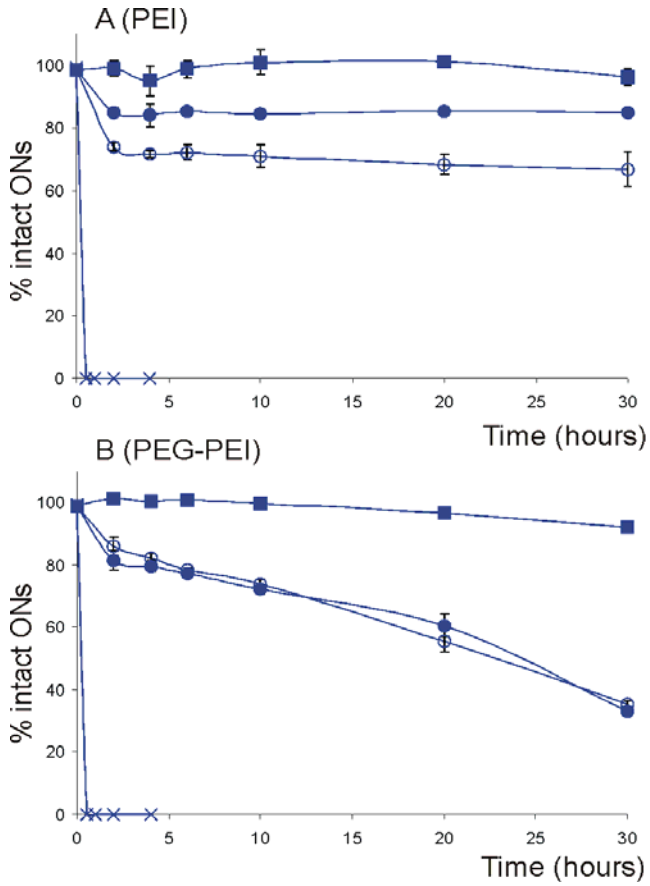

Figure 8. Percentage of ONs remaining intact after incubating (A) PEI/ON polyplexes and (B) PEG-PEI/ON polyplexes with DNase I, as measured by FCS. The percentage of intact ONs was calculated from the R/G ratio, after inhibition of the DNase I with EDTA-enriched TBE buffer and subsequent release of the ONs from the polyplexes using dextran sulfate. Laser excitation was set to 488 nm. (squares) polyplexes incubated without DNase I (average ± standard deviation of the N/P ratio 5 and 10), (open circles) polyplexes with a N/P ratio of 5 incubated with 1 unit of DNase I, (closed circles) polyplexes with a N/P ratio of 10 incubated with 1 unit of DNase I and (crosses) naked ONs incubated with 1 unit of DNase I. Values represent the average ± standard deviation of two samples per time point. When no error bars appear, they were smaller than the symbol.

When PEI/ON and PEG-PEI/ON polyplexes were incubated without DNase I, the amount of intact ONs only slightly decreased to respectively 96 ± 3% and 93 ± 1% after 30 hours of incubation, indicating that almost no degradation occurred (Figure 8, squares). For PEI/ON polyplexes with a N/P ratio of 5, 26 ± 2% of the ONs were degraded after a couple of

hours. Upon longer incubation times the degradation slowly proceeded: 33 ± 5% of the ONs were degraded after 30 hours (Figure 8A, open circles). For PEI/ON polyplexes with a N/P ratio of 10 initially only 15 ± 1% of the ONs became degraded while a longer incubation with DNase I did not further degrade the ONs (Figure 8A, closed circles).

For PEG-PEI/ON polyplexes the protection of the ONs seemed independent on the N/P ratio of the polyplexes (Figure 8B, open and closed circles). Initially, also 14 ± 3% of the ONs become degraded. In contrast to PEI/ON polyplexes, more ONs become degraded upon longer incubation with DNase I. Indeed, after 30 hours 66 ± 2% of the ONs are degraded. It should be noted that when free ONs were incubated with DNase I under the same circumstances, complete degradation was already achieved within 30 minutes (Figure 8 A and B, crosses).

Hydrodynamic Size and Zeta Potential of PEI/ON and PEG-PEI/ON Polyplexes

Figure 9 shows the hydrodynamic size and zeta potential of PEI/ON and PEG-PEI/ON polyplexes with a N/P ratio of 5 and 10. PEG-PEI polyplexes are respectively 170 ± 13 nm and 203 ± 9 nm for a N/P ratio of 5 and 10. PEI polyplexes are about three times larger, with respectively 570 ± 33 nm and 627 ± 34 nm for a N/P ratio of 5 and 10. Depending on the N/P ratio, the PEI polyplexes are neutral to slightly positive, while the PEG-PEI polyplexes are neutral to slightly negative.

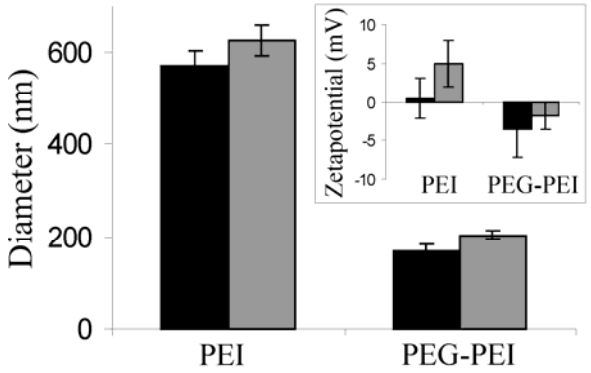

Figure 9. Hydrodynamic size and zeta potential measurements (graph insert) on PEI/ON and PEG-PEI/ON dispersions. (Black bars) N/P ratio of 5 and (gray bars) N/P ratio of 10. Values represent the average ± standard deviation of three independent experiments.

DISCUSSION

A better understanding of the physicochemical properties and biological behavior of cationic polymers is expected to provide valuable knowledge for the future design of highly efficient nucleic acid delivery systems. The *in vitro* transfection efficiency of cationic polymer/nucleic acid polyplexes depends, however, on a large variety of factors such as cell type, confluency of cells, the way the complexes are formed as well as their composition, the composition of the incubation medium, the time of incubation and so on [25]. This complicates the search for optimal nucleic acid delivery systems and necessitates screening of new candidates under various experimental conditions. Physicochemical properties such as the size and charge of carrier/DNA complexes are routinely checked by respectively dynamic light scattering and zeta potential measurements. To what extent the carriers protect the nucleic acids against enzymatic degradation is mostly investigated by agarose (in the case of pDNA) and polyacrylamide (in the case of ONs) gel electrophoresis. This requires, however, a sufficient amount of complexes and thus a sufficient amount of cationic carriers to be able to visualize the degradation of the nucleic acids, which may be an issue for cationic carriers that are expensive or difficult to synthesize. In this chapter, we used FCS as a tool to gain insight in the protection of ONs against enzymatic degradation when complexed to cationic polymers. FCS is advantageous in that it can be done in very small sample volumes (microliters) in the nanomolar concentration range. The low concentrations used are a major advantage when studying scarce DNA and polymer material. Also, the small sample volume required makes the technique suitable for measurements in rare media (e.g. cytosolic lysates) and living cells.

First, we studied the association and dissociation behavior of PEI/ON and PEG-PEI/ON polyplexes. From a gel retardation assay (Figure 3), we observed that both PEI and PEG-PEI upon mixing with ONs spontaneously form complexes at a N/P ratio of 2.5 and higher. From gel electrophoresis, one would thus conclude that the PEG-chains in PEG-PEI did not influence the complexation behavior when compared to PEI, an observation that has been reported before in the complex formation with plasmid DNA [13]. This could result from the fact that for the PEG-PEI, as used in this chapter, there is only about one PEG-chain per cationic PEI segment (Figure 1B), thus lowering the chance that the PEG-chains would shield the cationic charges on the PEI backbone.

FCS measurements, however, did reveal some differences between PEI and PEG-PEI with regard to the complexation of ONs (compare Figures 4B and 4C). Both with PEI and PEG-PEI, a drastic decrease in the green and red fluorescence of the ONs occurred upon complexation, which we attribute to the quenching of the fluorophores due to the compaction

of the ONs in the polyplexes. Probably, PEI and PEG-PEI interfere with the emitted photons through scattering or blockage (absorption) when the ONs are present in the polyplexes' core. Clearly, electrostatic interactions between the anionic ONs and the cationic PEI segment of PEI and PEG-PEI drive the complex formation. The polyplexes consist of a core of cationic segments (partially) neutralized by ON strands, additionally surrounded by a shell of neutral PEG-chains in the case of PEG-PEI. In the core, the ONs are tightly packed so that the fluorophores they are carrying are quenched. The compaction of the ONs in the core of the PEG-PEI based polyplexes appears, however, different from that in the PEI based polyplexes. Indeed, highly intense fluorescence peaks are visible in the red fluorescence fluctuation profiles of the PEG-PEI polyplexes (Figure 4C). Such a high peak is due to the movement of a PEG-PEI/ON complex containing multiple ONs (and thus multiple fluorophores) through the detection volume of the FCS instrument. In other words, it indicates the presence of multiple ONs in a PEG-PEI/ON complex. It is very likely that PEI/ON complexes also contain multiple ONs. Such highly intense fluorescence peaks could, however, not be observed with PEI/ON polyplexes (Figure 4B). We attribute this to a stronger quenching of the fluorophores in the PEI based polyplexes when compared to the PEG-PEI based polyplexes. Assuming that the quenching of the fluorophores on the ONs is related to the compaction of the ONs in the polyplexes' core, PEI would thus compact the ONs more firmly than PEG-PEI. In Figures 5 and 6 we determined the amount of dextran sulfate needed to displace the ONs from the polyplexes. Both gel electrophoresis and FCS measurements pointed out that the ONs were more easily released from the PEG-PEI polyplexes than from the PEI polyplexes. This observation, together with the different quenching of the fluorophores, supports the hypothesis that the ONs are compacted more tightly by PEI than by PEG-PEI.

In a next set of experiments we studied the degradation of the ONs complexed to PEI and PEG-PEI upon dispersion of the polyplexes in a DNase I solution. The fluorescently double-labeled ONs used in this thesis show FRET: degradation of the ONs increases the green fluorescence and lowers the red fluorescence. Consequently, a high R/G ratio indicates intact ONs while a low one points out degradation of the ONs [21]. On the one hand, for a solution of free ONs the R/G ratio is representative for the amount of intact free ONs (e.g. Figure 2). On the other hand, upon complexation of the ONs with PEI and PEG-PEI, the fluorescence drops to nearly zero (e.g. Figure 4). Due to this severe quenching, the R/G ratio of the complexed ONs is no longer representative for the amount of intact ONs in the polyplexes. Figure 6 showed that the R/G ratio of the ONs, released from the polyplexes by the addition of dextran sulfate, is restored to its original level. Also, when the ONs are free in solution, it is known that FRET can only occur between the labeled ends of a single ON. With greater compaction of the ONs in the polyplexes, however, it is possible that FRET occurs

between fluorophores of different ONs. Therefore, the R/G ratio of the ONs was only interpreted upon release of the ONs from the polyplexes. In this case, the R/G ratio reflects to what extent the ONs were protected against enzymatic degradation while they were present in the polyplexes. The ONs were released from the polyplexes by adding the negatively charged dextran sulfate. It should be noted that at high amounts of dextran sulfate the green and red fluorescence of the ONs released from the polyplexes (samples 12 in Figure 6A and 6B) are higher than the green and red fluorescence of the ON solution before complexation (samples 1 in Figure 6A and 6B). This increase in fluorescence could not be attributed to the non-fluorescing dextran sulfate, nor were the fluorescence properties of the ONs altered upon the presence of dextran sulfate. Instead, we found that the amount of ONs in the solutions containing dextran sulfate had increased, indicating that dextran sulfate also displaced the ONs that sticked to the bottom of the wells. The R/G ratio is, however, not dependent on the concentration of the ONs in solution, explaining why the R/G ratio before and after complexation is similar. Therefore, the increased fluorescence does not impede the use of the R/G ratio to monitor the degradation of the ONs as a function of time.

Let us now focus on the outcome of the FCS measurements on polyplexes with a N/P ratio of 10 that were incubated with DNase I (Figure 8, closed circles). Initially, PEI and PEG-PEI equally protect the ONs they carry against enzymatic degradation: 15 ± 3% of the ONs degrade during the first 2 hours. One could wonder whether these degraded ONs originate from free (uncomplexed) ONs present in the dispersions, indicating that 15 ± 3% of the ONs remained free in solution. However, Figure 3 clearly shows that no free ONs appear at a N/P ratio of 5 or 10. Therefore, the initial degradation as observed in Figure 8 is highly likely attributed to the enzymatic degradation of ONs while being complexed to the PEI and PEG-PEI polymers. We mentioned before that the complexed ONs are present in the polyionic core of the polyplexes. It seems that for the polyplexes with a N/P ratio of 10, 15 ± 3% of the ONs is still accessible to nucleases, probably as a result of being located at the edge of the polyplexes' core. By analogy, free regions of plasmid DNA strands have been observed to dangle from the polyplexes' core of PEI/DNA polyplexes [26].

Figure 8 clearly shows that pegylation of the PEI based polyplexes has an influence on the protection of the ONs: PEI/ON polyplexes remain to protect the ONs they carry over a prolonged period of time while in PEG-PEI/ON polyplexes the degradation of the ONs slowly proceeds, reaching 66 ± 2% of degraded ONs after 30 hours of incubation. As reported above, PEI appears to compact the ONs more firmly in the polyplexes' core than PEG-PEI. This firm compaction apparently also results in a better protection against enzymatic degradation. Alternatively, PEG-PEI polyplexes exhibit a core-shell structure in which the polyplexes' core is shielded from the environment by a shell of hydrophilic PEG-chains [27].

This PEG-shield may provide an additional (steric) barrier for nuclease attack and may thus contribute to the protection of the ONs. The latter is, however, not supported by the results presented in this chapter. A possible explanation for the worse protection of ONs in PEG-PEI polyplexes is the following. In essence, polyplexes are oppositely charged polyion strands held together by electrostatic interactions. It is expected that polyplexes are subjected to dynamic processes of binding and dissociation of the involved polyelectrolytes. During these 'rearrangements', ONs from the inner part of the polyplexes' core could relocate to the edge of the polyplexes' core, becoming accessible to enzymatic degradation. Since weaker polyelectrolyte interactions seem to exist in the PEG-PEI polyplexes (as indicated from the lesser quenching of the ONs' fluorescence and the easier displacement of the ONs by dextran sulfate), the rearrangements of the ONs in the PEG-PEI/ON polyplexes may be more pronounced when compared to those in PEI/ON polyplexes, leading to more opportunities for DNase I attack. Since the ONs are about 13.3 kDa and the PEI polymers are about 2 kDa, one would expect that 6-7 PEI polymers can bind to a single ON. The ON-binding PEI segment of the PEG-PEI polymers is also 2 kDa, but the PEG-chains (10 kDa) could make it more difficult for 6-7 PEG-PEI polymers to bind to a single ON. This could explain why the ONs more easily 'rearrange' in the PEG-PEI based polyplexes. Another difference between the PEI and PEG-PEI based polyplexes is the size of the particles, with PEG-PEI polyplexes being about 3 times smaller than the PEI polyplexes. This implies that the effective surface area for DNase I attack is larger for the smaller PEG-PEI polyplexes when compared to the larger PEI polyplexes, which could contribute to the more pronounced degradation of the ONs in the PEG-PEI polyplexes. It should be noted that free ONs were fully degraded within the first 30 minutes of incubation with the DNase I enzyme. From this point of view, both PEI and PEG-PEI offer a drastic improvement in the life time of the complexed ONs.

The degradation of the ONs was also followed by PAGE (Figure 7). When analyzed by gel electrophoresis (using Image J) 12% and 72% of the ONs were degraded in respectively PEI and PEG-PEI polyplexes after incubation for 30 hours with DNase I. When the degradation was calculated from the R/G ratio of the same samples that were analyzed by FCS, these values were respectively 18 $\pm$ 5% and 62 $\pm$ 4% at the 30 hours time point. These values agree very well with the degradation that was observed in Figure 8: respectively 15 $\pm$ 3% and 66 $\pm$ 2% of the ONs were degraded after incubation of PEI and PEG-PEI polyplexes with DNase I for 30 hours. This points out that FCS is a valuable alternative for gel electrophoresis to follow the degradation of ONs complexed to cationic carriers.

In literature, there is only one report comparing the stability of ONs complexed to respectively PEI and PEG-PEI. By densitometric analysis of PAGE gels, Brus *et al.* found that PEI and PEG-PEI with molecular weight ranging from 0.8 to 2 kDa equally protected the

complexed ONs with a recovery of 90% of intact ONs [28]. The shorter incubation time (2 hours), lower DNase I concentration (e.g. for free ONs, only 50% degraded under these circumstances) and different N/P ratio (N/P of 20) most likely explain why the degradation was less pronounced when compared to our observations. They also found that PEG-PEI polyplexes with more, but shorter PEG chains protected more efficiently when compared to polyplexes containing fewer PEG chains of a higher molecular weight. Godbey *et al.* found, using gel electrophoresis, that plasmid DNA that was complexed with branched PEI (25 kDa) was not degraded when exposed to at least 25 units of DNase I for 24 hours **[29]**. With regard to other polymers, Harada *et al.* used capillary gel electrophoresis to determine the protective properties of PEG-PLL (pegylated poly-l-lysine) polyplexes and found that after 2 hours of incubation with DNase I respectively 60% and 85% of the ONs were still intact, dependent on the density of the PEG shell [30]. Clearly, these studies demonstrate that the stability of the complexed ONs depends on the polyplexes' characteristics such as the density of the PEG shell. Nevertheless, Fisher *et al.* found that *in vivo,* pegylation of PEI worsened the protection of the ONs after intravenous injection of the polyplexes [14]. Also, the pegylated PEI polyplexes used in this chapter did not offer a better protection when compared to the unpegylated PEI polyplexes, which may suggest that the PEG-PEI did not result in a sufficiently dense PEG-shield to prevent nuclease attack.

The complexation between ONs [17] and plasmid DNA [31;32] with PEI and PEG-PEI has been studied by FCS before, both in buffer and in living cells. This is, however, the first time that FCS was used to obtain more information on the protection that PEI and PEG-PEI polymers offer to complexed ONs. Since PEI and PEG-PEI with an identical PEI segment (branched, 2 kDa) were used, we could truly investigate the effect of pegylation. In conclusion, pegylation lowered the protective properties of the PEI/ON polyplexes, especially at longer incubation times, an observation which may be related to the weaker compaction of the ONs with the PEG-PEI polymers. These observations may also influence the efficiency of PEI-based ON delivery *in vivo,* where pegylation is an attractive strategy to enhance the stability of the polyplexes in the bloodstream.

ACKNOWLEDGEMENTS

The Ghent University (UG-BOF) and FWO-Flanders (G.0310.02) supported this project through instrumentation credits and financial support. Marta Wójtowicz is gratefully acknowledged for here assistance in the practical experiments. Norbert Opitz (Max Planck Institute for Molecular Physiology, Dortmund, Germany) is acknowledged for the installation

of the FCS-module on the MRC-1024. PEG-PEI was a generous gift from Prof. Dr. S. Vinogradov from the University of Nebraska, Medical Center.

REFERENCES

(1) Park, T. G.; Jeong, J. H.; Kim, S. W. Current status of polymeric gene delivery systems. *Adv. Drug Deliver. Rev.* **2006**, 58, 467-486.

(2) Audouy, S.; Hoekstra, D. Cationic lipid-mediated transfection in vitro and in vivo. *Mol. Membr. Biol.* **2001**, 18, 129-143.

(3) Akhtar, S.; Hughes, M. D.; Khan, A.; Bibby, M.; Hussain, M.; Nawaz, Q.; Double, J.; Sayyed, P. The delivery of antisense therapeutics. *Adv. Drug Deliver. Rev.* **2000**, 44, 3-21.

(4) Jaaskelainen, I.; Peltola, S.; Honkakoski, P.; Monkkonen, J.; Urtti, A. A lipid carrier with a membrane active component and a small complex size are required for efficient cellular delivery of anti-sense phosphorothioate oligonucleotides. *Eur. J. Pharm. Sci.* **2000**, 10, 187-193.

(5) Watson, P.; Jones, A. T.; Stephens, B. Intracellular trafficking pathways and drug delivery: fluorescence imaging of living and fixed cells. *Adv. Drug Deliver. Rev.* **2005**, 43-61.

(6) Boussif, O.; Lezoualch, F.; Zanta, M. A.; Mergny, M. D.; Scherman, D.; Demeneix, B.; Behr, J. P. A versatile vector for gene and oligonucleotide transfer into cells in culture and *in vivo* - Polyethylenimine. *Proc. Natl. Acad. Sci. USA* **1995**, 92, 7297-7301.

(7) Godbey, W. T.; Mikos, A. G. Recent progress in gene delivery using non-viral transfer complexes. *J. Control. Release* **2001**, 72, 115-125.

(8) Godbey, W. T.; Wu, K. K.; Mikos, A. G. Poly(ethylenimine) and its role in gene delivery. *J. Control. Release* **1999**, 60, 149-160.

(9) Wightman, L.; Kircheis, R.; Rossler, V.; Carotta, S.; Ruzicka, R.; Kursa, M.; Wagner, E. Different behavior of branched and linear polyethylenimine for gene delivery in vitro and in vivo. *J. Gene Med.* **2001**, 3, 362-372.

(10) Kunath, K.; von Harpe, A.; Fischer, D.; Peterson, H.; Bickel, U.; Voigt, K.; Kissel, T. Low-molecular-weight polyethylenimine as a non-viral vector for DNA delivery: comparison of physicochemical properties, transfection efficiency and in vivo distribution with high-molecular-weight polyethylenimine. *J. Control. Release* **2003**, 89, 113-125.

(11) Godbey, W. T.; Wu, K. K.; Mikos, A. G. Size matters: Molecular weight affects the efficiency of poly(ethylenimine) as a gene delivery vehicle. *J. Biomed. Mater. Res.* **1999**, 45, 268-275.

(12) von Harpe, A.; Petersen, H.; Li, Y. X.; Kissel, T. Characterization of commercially available and synthesized polyethylenimines for gene delivery. *J. Control. Release* **2000**, 69, 309-322.

(13) Sung, S. J.; Min, S. H.; Cho, K. Y.; Lee, S.; Min, Y. J.; Yeom, Y. I.; Park, J. K. Effect of polyethylene glycol on gene delivery of polyethylenimine. *Biol. Pharm. Bull.* **2003**, 26, 492-500.

(14) Fischer, D.; Osburg, B.; Petersen, H.; Kissel, T.; Bickel, U. Effect of poly(ethylene imine) molecular weight and pegylation on organ distribution and pharmacokinetics of polyplexes with oligodeoxynucleotides in mice. *Drug Metab. Dispos.* **2004**, 32, 983-992.

(15) Remaut, K.; Lucas, B.; Braeckmans, K.; Sanders, N. N.; Demeester, J.; De Smedt, S. C. Protection of oligonucleotides against nucleases by pegylated and non-pegylated liposomes as studied by Fluorescence Correlation Spectroscopy. *J. Control. Release* **2005**, 110, 209-223.

(16) Lucas, B.; Van Rompaey, E.; De Smedt, S. C.; Demeester, J.; Van Oostveldt, P. Dual-color FFS to study the complexation between poly-l-lysine and oligonucleotides. *Macromolecules* **2002**, 35, 8152-8160.

(17) Lucas, B.; Remaut, K.; Braeckmans, K.; Haustraete, J.; De Smedt, S. C.; Demeester, J. Studying pegylated DNA complexes by dual color fluorescence fluctuation spectroscopy. *Macromolecules* **2004**, 37, 3832-3840.

(18) Lucas, B.; Remaut, K.; Sanders, N. N.; Braeckmans, K.; De Smedt, S. C.; Demeester, J. Studying the intracellular dissociation of polymer-oligonucleotide complexes by dual color fluorescence fluctuation spectroscopy and confocal imaging. *Biochemistry* **2005**, 44, 9905-9912.

(19) Van Rompaey, E.; Chen, Y.; Muller, J. D.; Gratton, E.; Van Craenenbroeck, E.; Engelborghs, Y.; De Smedt, S.; Demeester, J. Fluorescence fluctuation analysis for the study of interactions between oligonucleotides and polycationic polymers. *Biol. Chem.* **2001**, 382, 379-386.

(20) De Smedt, S. C.; Remaut, K.; Lucas, B.; Braeckmans, K.; Sanders, N. N.; Demeester, J. Studying biophysical barriers to DNA delivery by advanced light microscopy. *Adv. Drug Deliver. Rev.* **2005**, 57, 191-210.

(21) Remaut, K.; Lucas, B.; Braeckmans, K.; Sanders, N. N.; De Smedt, S. C.; Demeester, J. FRET-FCS as a tool to evaluate the stability of oligonucleotide drugs after intracellular delivery. *J. Control. Release* **2005**, 103, 259-271.

(22) Vinogradov, S. V.; Bronich, T. K.; Kabanov, A. V. Self-assembly of polyamine-poly(ethylene glycol) copolymers with phosphorothioate oligonucleotides. *Bioconjug. Chem.* **1998**, 9, 805-812.

(23) Sanders NN, De Smedt SC, Demeester J: Deoxyribonuclease I, in McGrath BM, Walsh G (eds): Therapeutic Enzymes. Boca Raton, Taylor & Francis Group, 2006, pp 97-116.

(24) Schwille, P.; Meyer-Almes, F.; Rigler, R. Dual-Color Fluorescence Cross-Correlation spectroscopy for multicomponent diffusional analysis in solution. *Biophys. J.* **1997**, 72, 1878-1886.

(25) Merdan, T.; Kopecek, J.; Kissel, T. Prospects for cationic polymers in gene and oligonucleotide therapy against cancer. *Adv. Drug Deliver. Rev.* **2002**, 54, 715-758.

(26) Dunlap, D. D.; Maggi, A.; Soria, M. R.; Monaco, L. Nanoscopic structure of DNA condensed for gene delivery. *Nucleic Acids Res.* **1997**, 25, 3095-3101.

(27) Guo, Y.; Sun, Y.; Li, G.; Xu, Y. The molecular structures of poly(ethylene glycol)-modified nonviral gene delivery polyplexes. *Mol. Pharm.* **2004**, 1, 477-482.

(28) Brus, C.; Petersen, H.; Aigner, A.; Czubayko, F.; Kissel, T. Efficiency of polyethylenimines and polyethylenimine-graft-poly (ethylene glycol) block copolymers to protect oligonucleotides against enzymatic degradation. *Eur. J. Pharm. Biopharm.* **2004**, 57, 427-430.

(29) Godbey, W. T.; Barry, M. A.; Saggau, P.; Wu, K. K.; Mikos, A. G. Poly(ethylenimine)-mediated transfection: A new paradigm for gene delivery. *J. Biomed. Mater. Res.* **2000**, 51, 321-328.

(30) Harada, A.; Togawa, H.; Kataoka, K. Physicochemical properties and nuclease resistance of antisense-oligodeoxynucleotides entrapped in the core of polyion complex micelles composed of poly(ethylene glycol)-poly(L-lysine) block copolymers. *Eur. J. Pharm. Sci.* **2001**, 13, 35-42.

(31) Clamme, J. P.; Azoulay, J.; Mély, Y. Monitoring of the formation and dissociation of PEI/DNA complexes by two photon fluorescence correlation spectroscopy. *Biophys. J.* **2003**, 84, 1960-1968.

(32) Clamme, J. P.; Krishnamoorthy, G.; Mély, Y. Intracellular dynamics of the gene delivery vehicle polyethylenimine during transfection: investigation by two-photon fluorescence correlation spectroscopy. *BBA-Biomembr.* **2003**, 1617, 52-61.

Chapter 5

INTRACELLULAR FATE AND BIOLOGICAL ACTIVITY OF ANTISENSE OLIGONUCLEOTIDES DELIVERED BY NON-PEGYLATED LIPOSOMES

Parts of this chapter were published in:

Remaut, K.; Lucas, B.; Braeckmans, K.; Sanders, N. N.; Demeester, J.; De Smedt, S. C. *Biochemistry* **2006**, 45, 1755-1764.

ABSTRACT

Delivering phosphodiester ONs (PO-ONs) remains an attractive but challenging goal in antisense therapy. In Chapter 3, we found that PO-ONs complexed to DOTAP/DOPE liposomes were adequately protected against enzymatic degradation. In this chapter, however, we found that the liposomes fail in generating an antisense effect with PO-ONs, while they succeed with chemically modified ONs like phosphothioate ONs (PS-ONs). Therefore, we aimed to explain the biological activity of PO- and PS-ONs delivered by DOTAP/DOPE liposomes based on a detailed understanding of their cell biological behavior by means of Fluorescence Correlation Spectroscopy and Confocal Laser Scanning Microscopy. We conclude that DOTAP/DOPE liposomes are not suited to deliver PO-ONs due to the release of naked PO-ONs in the cytosol at the time of the endosomal escape of the liposomes and the subsequent rapid degradation of the naked PO-ONs. In the case of PS-ONs, the ONs are not degraded upon release at the time of the endosomal escape of the liposomes, creating a pool of intact, biologically active PS-ONs. This indicates that DOTAP/DOPE liposomes are mainly suitable to deliver nuclease resistant ONs. However, the cells seemed to display an export pathway to remove intact PS-ONs from the cells, limiting the presence of naked PS-ONs in the nucleus to about 8 hours following the delivery.

Chapter 5

Intracellular Fate and Biological Activity of Antisense Oligonucleotides Delivered by Non-pegylated Liposomes

INTRODUCTION

Antisense ONs show potential as therapeutics in the treatment of viral infections and cancer [1]. Oligonucleotide-based therapeutics act by a sequence specific binding to their target mRNA, which results in blocking or degradation of the target sequence. This on its turn results in the down-regulation of the targeted protein expression. Despite this simple mechanism of action and many identified potential targets, only a few oligonucleotide-based therapeutics are actually on the market [2;3].

To improve the efficacy of ONs, chemically modified ONs are explored to minimize the degradation in the body [4]. The synthesis of modified ONs can, however, introduce unwanted side effects [4;5]. Therefore, finding optimal delivery systems ('carriers') for unmodified phospodiester ONs (PO-ONs) remains attractive but very challenging. Generally speaking, optimal carriers for PO-ONs should protect the ONs against enzymatic degradation, enhance their cellular entry and facilitate endosomal escape. The ONs should also be released into the cytoplasm of the cells or should be able to exert an antisense effect while being encapsulated by the carriers. Clearly, the carriers should be sufficiently 'intelligent' to overcome extra- and intracellular barriers to be able to deliver sufficient amounts of intact PO-ONs at their target.

Cationic liposomes are among the most widely investigated carriers for delivery of nucleic acids [6]. Upon mixing cationic liposomes with the negatively charged ONs, spontaneously cationic liposome/ONs complexes (lipoplexes) are formed. In literature as well as in our experiments, cationic liposomes fail in generating an antisense effect with PO-ONs,

while they succeed with the chemically modified phosphothioate ONs (PS-ONs) [7-9]. It is well known that PS-ONs are more resistant towards enzymatic degradation than ONs with a phosphodiester backbone. Therefore a major hypothesis to explain the difference in biological activity is that PS-ONs remain intact while PO-ONs degrade. However, to find better carriers for PO-ONs, one should know when and where in the cells the PO-ONs begin to degrade. Importantly, we should also know whether, besides degradation of the PO-ONs, other intracellular mechanisms are involved in limiting the biological activity. In this chapter we aimed to explain the biological activity of PO- and PS-ONs delivered by liposomes composed of the cationic lipid DOTAP and the neutral helper lipid DOPE, based on a detailed understanding of their intracellular fate. Especially, we focused on the time and place of degradation of the delivered PO- and PS-ONs. Therefore, fluorescently double-labeled ONs, giving FRET between the two labels, were complexed to non-pegylated cationic liposomes and their intracellular distribution and degradation was followed by FCS and CLSM.

MATERIALS AND METHODS

Materials

Anti-intracellular adhesion molecule-1 (Anti-ICAM-1) 20 mer ONs with a phosphodiester backbone (PO20-ONs) or a phosphothioate backbone (PS20-ONs) were used (Isis1939: 5' CCC-CCA-CCA-CTT-CCC-CTC-TC 3'). As a control ON, an ON without anti-ICAM-1 activity was used (5'GAG-ACT-TTC-ACT-TTT-CTC-TA 3'). For the Fluorescence Correlation Spectroscopy (FCS) experiments and confocal imaging, fluorescently double-labeled PO20-ONs and PS20-ONs were used as well as 40 mer phosphodiester ONs without anti-ICAM-1 activity (PO40-ONs; 5'-GCC-GTC-TCT-GAC-TGC-TGA-TGA-CTA-CTA-TCG-TAT-AGT-GCG-G-3'). The ONs were double-labeled with a rhodamine green fluorophore at the 3' end (λ_{ex} = 488 nm, λ_{em} = 532 nm) and a Cy5 fluorophore at the 5' end (λ_{ex} = 647 nm, λ_{em} = 670 nm). All ONs were purchased from Eurogentec (Seraing, Belgium) and were PAGE-purified by the supplier.

The cationic phospholipid DOTAP (N-(1-(2,3-dioleoyloxy)propyl)-N,N,N-trimethyl-ammoniumchloride) and the neutral phospholipid DOPE (dioleoylphosphatidylethanolamine) were purchased from Avanti® Polar Lipids (Alabaster, AL, USA).

Human lung carcinoma cells (A549 cells, ATCC number: CCL-185) (DSMZ, Braunschweig, Germany) were cultured in Dulbecco's modified Eagle's medium (DMEM) without phenol red (Gibco, Merelbeke, Belgium) containing 2 mM glutamine, 10% heat

deactivated fetal bovine serum (FBS) and 1% penicillin-streptomycin at 37°C in a humidified atmosphere containing 5% CO_2.

Preparation of Liposome/ONs Complexes

The liposomes contained DOTAP and DOPE in a 1:1 molar ratio and were prepared as described in Chapter 3. The hydrodynamic size and zeta potential of the resulting cationic liposomes was routinely checked by respectively dynamic light scattering (DLS, Malvern 4700, Malvern, Worcestershire, UK) and surface potential measurements (Zetasizer 2000, Malvern, Worcestershire, UK), as previously described [10] and equaled respectively 126 $\pm$ 7 nm and +45 $\pm$ 4 mV.

Confocal Imaging and Fluorescence Correlation Spectroscopy (FCS)

Confocal imaging and dual-color FCS experiments were performed on a Confocor2 installed on a LSM510 confocal laser scanning microscope (Carl Zeiss, Jena, Germany). The excitation light of an argon ion laser (488 nm, 30 mW) and/or a helium-neon laser (633 nm, 5 mW) was reflected by a dichroic mirror (HFT 488/633) and focused through a Zeiss C-apochromat 40x, NA 1.2 water immersion objective into the sample. The fluorescence emission was recollected by the same objective and split by another dichroic mirror (NFT 635) into the green detector (after passing a 505-550 bandpass filter) or into the red detector (after passing a 650 longpass filter). Detection of the emission light was obtained with photonmultipliers (in the case of confocal imaging) or much more sensitive avalanche photodiodes (in the case of FCS). Confocal detection was ensured by excluding out-of-plane fluorescence with pinholes in front of the detectors (70 µm or 90 µm for respectively the green or the red detector). For FCS measurements, the apparatus was calibrated by measuring the diffusion time of rhodamine green in solution, which equaled 40 $\pm$ 5 µs in this FCS setup and corresponds to a diffusion coefficient of 2.8 x 10^{-10} m²/s.

When performing intracellular FCS measurements, first a LSM510 confocal image of the cell was taken. Then, Confocor2 measuring points were selected on the confocal image in the cytoplasm or the nucleus of the cell and the green and red fluorescence intensities were recorded with laser excitation set to 488 nm (or 633 nm). From these fluorescence intensities, the R/G ratio was calculated. When possible, the calculated auto-correlation curves $G(\tau)$ were analyzed with the Confocor2 software using a single-species (eq. 1) or dual-species (eq. 2) fit according to the Marquardt nonlinear least-squares fit algorithm. Note that these equations are very similar to the ones used for our FCS setup (eq. 1 and eq. 2 in Chapter 1), except that with the commercially available Confocor2 as used in this chapter, the auto-correlation curves decay to 1 instead of 0. Fitting to equation 1 gives information on

the amount of molecules *N* in the detection volume and their diffusion time τ_t, being the average time the fluorescently labeled molecules need to migrate through the detection volume of the FCS instrument.

$$G(\tau) = 1 + \frac{1}{N} * \left(1 - T + T * \exp\left(\frac{-t}{\tau_T}\right)\right) * \frac{1}{\left(1 + \frac{t}{\tau_t}\right) * \sqrt{1 + \left(\frac{\omega_1}{\omega_2}\right)^2 \left(\frac{t}{\tau_t}\right)}} \quad \text{eq.1}$$

$$G(\tau) = 1 + \frac{1}{N} * \left(1 - T + T * \exp\left(\frac{-t}{\tau_T}\right)\right) * \left(\frac{y}{\left(1 + \frac{t}{\tau_{t1}}\right) * \sqrt{1 + \left(\frac{\omega_1}{\omega_2}\right)^2 \left(\frac{t}{\tau_{t1}}\right)}} + \frac{1 - y}{\left(1 + \frac{t}{\tau_{t2}}\right) * \sqrt{1 + \left(\frac{\omega_1}{\omega_2}\right)^2 \left(\frac{t}{\tau_{t2}}\right)}}\right) \quad \text{eq. 2}$$

ω_1 and $2\omega_2$ represent the radius and the height of the detection volume. *T* represents the percentage of molecules in triplet state and τ_T represents the triplet relaxation time. For dual-species fit (eq. 2), there are *N*y* molecules with diffusion time τ_{t1} and *N*(1-y)* molecules with diffusion time τ_{t2}.

Transfection of A549 Cells with ONs Containing DOTAP/DOPE Liposomes

Lipoplexes (LPXs) were prepared by mixing 15 µL of a liposome dispersion (200 µM) and 15 µL of fluorescently double-labeled ONs (2 µM), resulting in a +/- ratio of 5 (being the ratio of the number of positive charges originating from the liposomes, to the number of negative charges originating from the ONs). The resulting dispersion was vortexed for 10 seconds and the lipoplexes were allowed to equilibrate for 30 minutes at room temperature prior to use. Then, 120 µL DMEM was added before transferring the lipoplex dispersion to A549 cells grown to 90% confluency on glass-bottomed cover slips (Part No. PG-1.5-14-F, Glass bottom No. 1.5, MatTek Corporation). After 4 hours incubation at 37°C and 5% CO_2, the cells were washed and incubated further in DMEM containing 2 mM glutamine, 10% heat deactivated FBS and 1% penicillin-streptomycin. Confocal imaging and FCS measurements were performed at 1, 2, 4, 8, and 12 hours after applying the lipoplex dispersion to the A549 cells.

Microinjection

Microinjection experiments were performed with a Femtojet® microinjector and an Injectman® NI 2 micromanipulator (Eppendorf, Hamburg, Germany) coupled to the LSM510

confocal laser scanning microscope. All injections were performed in the cytoplasm of A549 cells. Immediately after injection, FCS measurements were carried out as described above in the Fluorescence Correlation Spectroscopy section. Naked fluorescently double-labeled PO20-ONs (2 µM) or a mixture of fluorescently double-labeled PO20-ONs (2 µM) and non-labeled PO20-ONs (20 µM) were injected. Upon microinjection, the concentration of the injected ONs is expected to be diluted about 30 times, yielding intracellular concentrations of respectively 66 nM and 733 nM.

Antisense Activity of PO20-ONs and PS20-ONs Containing DOTAP/DOPE Liposomes

The antisense activity of non-labeled phosphodiester (PO20-ONs) and phosphothioate (PS20-ONs) anti-ICAM-1 ONs was determined by detecting the ICAM-1 expression on the surface of A549 cells using ELISA. Mycoplasma free A549 cells were plated onto 96-well microtiter plates at 10^4 cells/well. At 90% confluency, the cells were washed three times with phosphate buffered saline (PBS) (Gibco, Merelbeke, Belgium) and free or complexed ONs were added to the cells (0.7 µg ON/well), followed by 4 hours of incubation. Lipoplexes with a +/- ratio of 2.5, 5 and 10 were used, containing non-labeled ONs. Subsequently, the free or complexed ONs were removed and after washing of the cells with PBS, 100 µL culture medium supplemented with 10 ng/mL TNF-α was added to induce overexpression of ICAM-1. After 18 hours of incubation, the ICAM-1 expression was determined as described below. To determine the basal ICAM-1 expression, the cells were incubated for 18 hours with 100 µL culture medium without TNF-α.

ICAM-1 Assay

The cells were fixed for 15 minutes at room temperature with PBS containing 20 mg/mL paraformaldehyde. After washing with PBS, aspecific binding places were blocked by incubating the cells for 1 hour with 2% normal goat serum (NGS) in a 1% bovine serum albumin/PBS (BSA/PBS) solution. The cells were washed with PBS and incubated for 90 minutes at 37°C with mouse anti-human ICAM-1 antibody (ImmunoSource, Zoersel, Belgium) (0.5 µg/mL in 1% BSA/PBS). After washing the cells with PBS, antibody bound to the cell surface was determined by incubating the cells for 1 hour at 37°C with sheep anti-mouse antibody-alkaline phosphatase conjugate (1:1000 dilution in 1% BSA/PBS). After 3 washes, the alkaline phosphatase activity was determined using 100 µL of p-nitrophenylphosphate (10 mg/mL in 0.1 M TRIS pH 8.4). After 30 minutes incubation at 37°C, the absorbance was determined using an ELISA plate reader at 405 nm (Wallac Victor2 multilabel reader, Perkin-Elmer Life Sciences, Boston, MA, USA).

The antisense activity of the anti-ICAM-1 PO20- or PS20-ONs was calculated as the percentage of the ICAM-1 expression when compared to A549 cells that were treated with a control ON using equation 3. In this way, the level of the basal and induced expression of the ICAM-1 protein in A549 cells treated with the control ONs is set to respectively 0% and 100%. As the level of the basal or induced expression can be influenced by the conditions that are applied on the cells, the basal and induced ICAM-1 expression was determined on cells that were treated with the control ONs in the same conditions as were applied for the antisense PO20- or PS20-ONs (e.g. naked or complexed to DOTAP/DOPE liposomes at a +/- ratio of 2.5, 5 or 10).

$$\frac{\left(A_{ON,TNF\alpha} - A_{Control,CM}\right)}{\left(A_{Control,TNF\alpha} - A_{Control,CM}\right)} \times 100 \qquad \text{eq.3}$$

$A_{Control,CM}$ is the absorption of cells treated with naked or complexed control ONs and without TNF-α induction (the basal ICAM-1 expression). $A_{Control,TNF\alpha}$ is the absorption of cells treated with naked or complexed control ONs upon induction with TNF-α (the control TNF-α-induced ICAM-1 expression) and $A_{ON,TNF\alpha}$ is the absorption of cells treated with naked or complexed anti-ICAM-1 ONs upon induction with TNF-α. (the ON-treated TNF-α-induced ICAM-1 expression).

RESULTS

Anti-ICAM-1 Activity of Phosphodiester and Phosphothioate ONs Delivered by DOTAP/DOPE Liposomes

Figure 1 shows the antisense activity obtained with DOTAP/DOPE liposomes containing 20 mer anti-ICAM-1 ONs with either a nuclease sensitive phosphodiester backbone (PO20-ONs) or a nuclease resistant phosphothioate backbone (PS20-ONs). Naked PO20- and PS20-ONs did not show antisense activity. It is indeed well known that naked ONs do not adequately enter cells, which is often attributed to their negative charge. The antisense effect of LPXs with a +/- ratio of 2.5 does not differ significantly from the antisense effect established by naked ONs. In Chapter 3 we showed experimentally that at a +/- ratio of 2.5, only 45% of the ONs were complexed to the cationic liposomes, the other part of the ONs remained free [11]. Apparently, this inadequate complexation resulted in a low biological activity of the LPXs at this +/- ratio, both for PO20- and PS20-ONs. At a +/- ratio of

5 or 10, we showed that the amount of complexed ONs increased to respectively 84% and 98% (see Chapter 3) [11]. In the case of PS20-ONs, increasing the +/- ratio to 5 or 10 resulted in a significant antisense effect. PO20-ONs, however, were not able to down-regulate the targeted protein expression. A major difference between PO-ONs and PS-ONs is the nuclease sensitivity of the backbone. Therefore, intracellular degradation could well be one of the factors limiting the antisense activity of the PO20-ONs. In the following experiments we aimed to figure out whether intracellular degradation is indeed the major barrier towards DOTAP/DOPE liposome-mediated PO-ONs delivery, or whether also other intracellular barriers contribute to the lack of antisense activity. Therefore, the intracellular pathway of fluorescently double-labeled ONs complexed to DOTAP/DOPE liposomes was followed by FCS and confocal imaging.

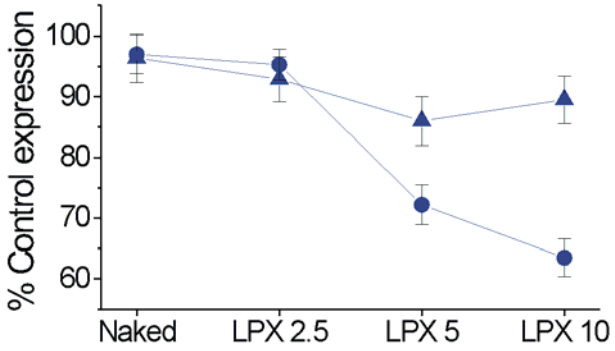

Figure 1. Antisense activity of PO20-ONs (triangle) or PS20-ONs (circle) administered to A549 cells naked or complexed to DOTAP/DOPE liposomes (LPX) at a +/- ratio of 2.5, 5 or 10. The antisense activity was calculated as the percentage of induced ICAM-1 expression when compared to A549 cells that were treated with the corresponding formulation containing the control ONs (e.g. respectively naked or complexed to DOTAP/DOPE liposomes at a +/- ratio of 2.5, 5 or 10) as described in the Materials and Methods section.

Detection of Intact and Degraded ONs by FRET-FCS

In the intact fluorescently double-labeled ONs, Fluorescence Resonance Energy Transfer (FRET) occurs between the rhodamine green (donor) and the Cy5 (acceptor) fluorophore [12]. Consequently, excitation of rhodamine green gives rise to emission by both rhodamine green and Cy5 (Figure 2A). A prerequisite for energy transfer is the close proximity of the donor and acceptor fluorophore. When the ONs degrade, the distance between both fluorophores increases and FRET no longer occurs. In this case, excitation of the rhodamine green does not result anymore in emission by the Cy5 (Figure 2B). As outlined below, FRET can be used to distinguish between intact and degraded ONs.

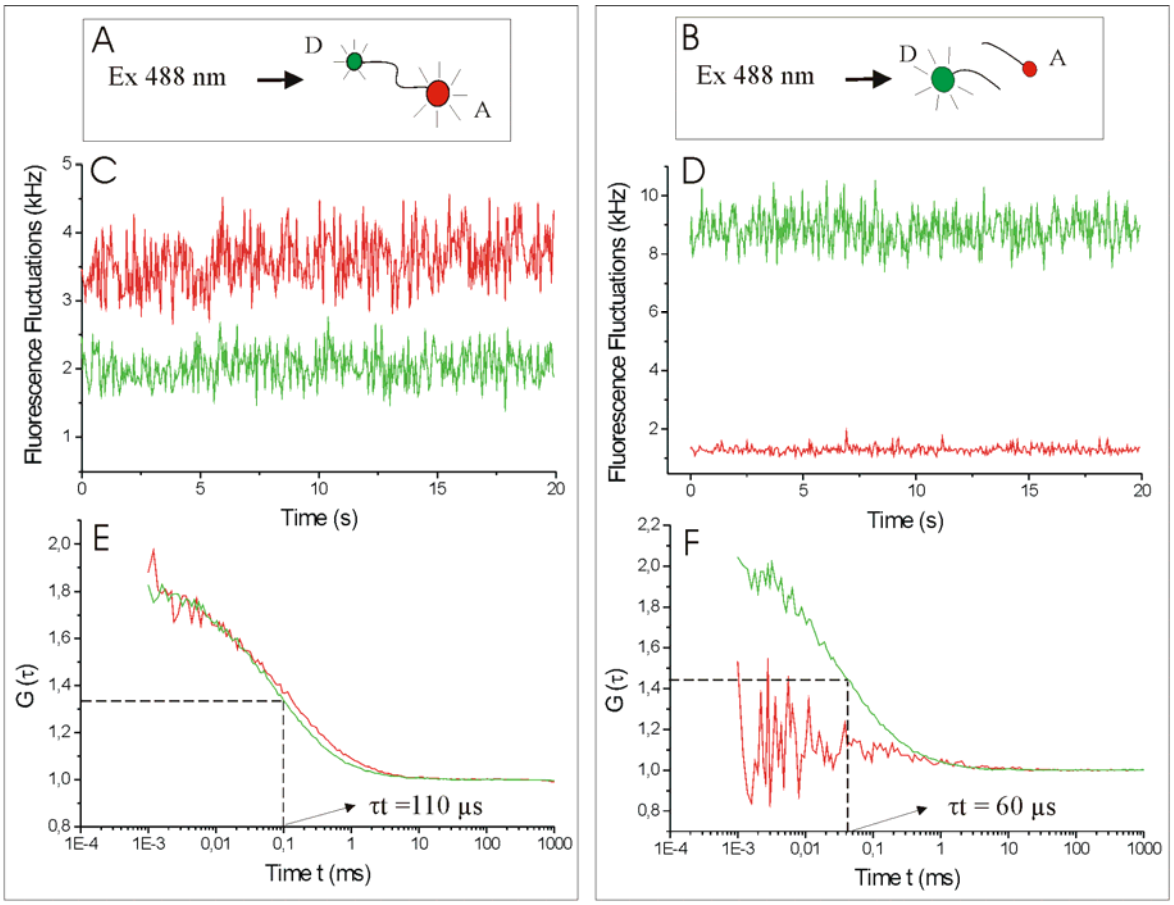

Figure 2. Schematic representation of FCS experiments on (A) intact and (B) degraded double-labeled ONs. In the intact ONs, FRET occurs between rhodamine green (donor, D, green) and Cy5 (acceptor, A, red) upon excitation at 488 nm laser light. (C, D) Fluorescence fluctuations as registered by the green (green line) and red (red line) detector of the FCS instrument in a solution of respectively intact and degraded PO20-ONs. (E, F) Auto-correlation curves as obtained from the fluorescence fluctuations of respectively intact and degraded PO20-ONs. The concentration of the ONs in solution ranged between 5 and 10 nM. PO20-ONs hydrolysis was accomplished by incubating the intact PO20-ONs with 20 units of the DNase II enzyme (4.7 units/µL, Sigma) for 8 hours at 37°C in an acidic buffer (40 mM acetic acid and 60 mM K-acetate, pH 4.7).

Figure 2C shows the fluorescence fluctuations as registered by the green and red detector of the FCS instrument upon excitation of a solution of intact double-labeled PO20-ONs at 488 nm light. Clearly, the fluorescence intensity fluctuates as fluorescently labeled molecules move in and out of the detection volume of the FCS instrument. Due to FRET the ONs are, besides green fluorescent, also red fluorescent. Table 1 shows the 'R/G ratio' which is defined as the ratio of the red to the green fluorescence as measured by the FCS detectors. For the intact double-labeled PO20-ONs used in this thesis, the R/G ratio is higher than 1. Figure 2E shows that proper auto-correlation curves can be derived from both the green and red fluorescence fluctuations. The diffusion time, which is the average time the ONs need to migrate through the detection volume of the FCS instrument, can be calculated by fitting the auto-correlation curves to equation 1 (Table 1).

Figure 2D shows the fluorescence fluctuations as registered by the green and red detector upon excitation of a solution of degraded PO20-ONs at 488 nm. Due to the disappearance of FRET, the Cy5 fluorophores are no longer excitable at 488 nm. This is reflected in a decrease in the red fluorescence intensity in combination with an increase in the green fluorescence intensity, which lowers the R/G ratio (Table 1). Figure 2F shows that a proper auto-correlation curve can be obtained from the green fluorescence fluctuations and a diffusion time can be calculated by fitting to equation 1 (Table 1). In contrast, the red fluorescence fluctuations can no longer be auto-correlated.

Table 1. The fluorescence intensities as measured by the green (F_G) and the red (F_R) detector of the FCS instrument on solutions of intact PS20-ONs, intact and degraded PO20-ONs and intact and degraded PO40-ONs (laser excitation set to 488 nm light). The R/G ratio represents the ratio of the red to green fluorescence. The diffusion times τ_t calculated from the auto-correlation curves obtained from these fluorescence fluctuations are depicted as well (N.D. = not determinable). The concentration of the ONs in solution ranged between 5 and 10 nM. PO20-ONs hydrolysis was accomplished by incubating the intact PO20-ONs with 20 units of the DNase II enzyme (4.7 units/µL, Sigma) for 8 hours at 37°C in an acidic buffer (40 mM acetic acid and 60 mM K-acetate, pH 4.7). PO40-ONs hydrolysis was accomplished by incubating the intact PO40-ONs with 1 unit of the DNase I enzyme (1 unit/µL, Genentech) for 1 hour at 37°C in 'degradation buffer' (20 mM HEPES, 110 mM potassium acetate and 2 mM magnesium acetate, pH 7.4).

	Intact PS-ON	Intact PO20-ON	Degraded PO20-ON	Intact PO40-ON	Degraded PO40-ON
F_R (kHz)	3.4	3.5	1.2	3.7	0.7
F_G (kHz)	1.4	2	8.8	0.7	6.3
R/G ratio	2.4	1.8	0.1	5.2	0.1
Diffusion time τ_t (µs) as calculated from F_R	131 ± 6	125 ± 14	N.D.	207 ± 4	N.D.
Diffusion time τ_t (µs) as calculated from F_G	105 ± 12	110 ± 5	60 ± 5	43 ± 2	60 ± 6

In the case of PO40-ONs, the diffusion time calculated from the green fluorescence fluctuations increases upon degradation of the ONs (Table 1). This may seem contradictory as shorter degradation products are expexted to be formed. However, due to the high FRET efficiency of the PO40-ONs, there remains only little donor fluorescence originating from the intact PO40-ONs. Instead, fluorescence originating from a small fraction of free rhodamine green fluorophores may reach the green detector. Consequently, the diffusion time lies within the range of that of free rhodamine green fluorophores. When the PO40-ONs degrade, the donor fluorescence increases and a diffusion time can be calculated, corresponding to the green labeled degradation products that were formed. As for the PO20-ONs, the red fluorescence fluctuations (upon excitation at 488 nm) can be auto-correlated as long as the

ONs remain intact. The latter together with the R/G ratio allows distinguishing between intact and degraded ONs with the FCS instrument.

Intracellular Fate of PS20-ONs Delivered by Non-pegylated Liposomes

A549 cells were transfected with DOTAP/DOPE liposomes containing fluorescently double-labeled PS20-ONs (PS20-LPXs). At certain time points confocal images were taken and FCS measurements were performed in the nucleus and cytoplasm of the cells with laser excitation set to 488 nm (Figure 3). In that case excitation of the Cy5 fluorophores only occurs if the ONs are still intact.

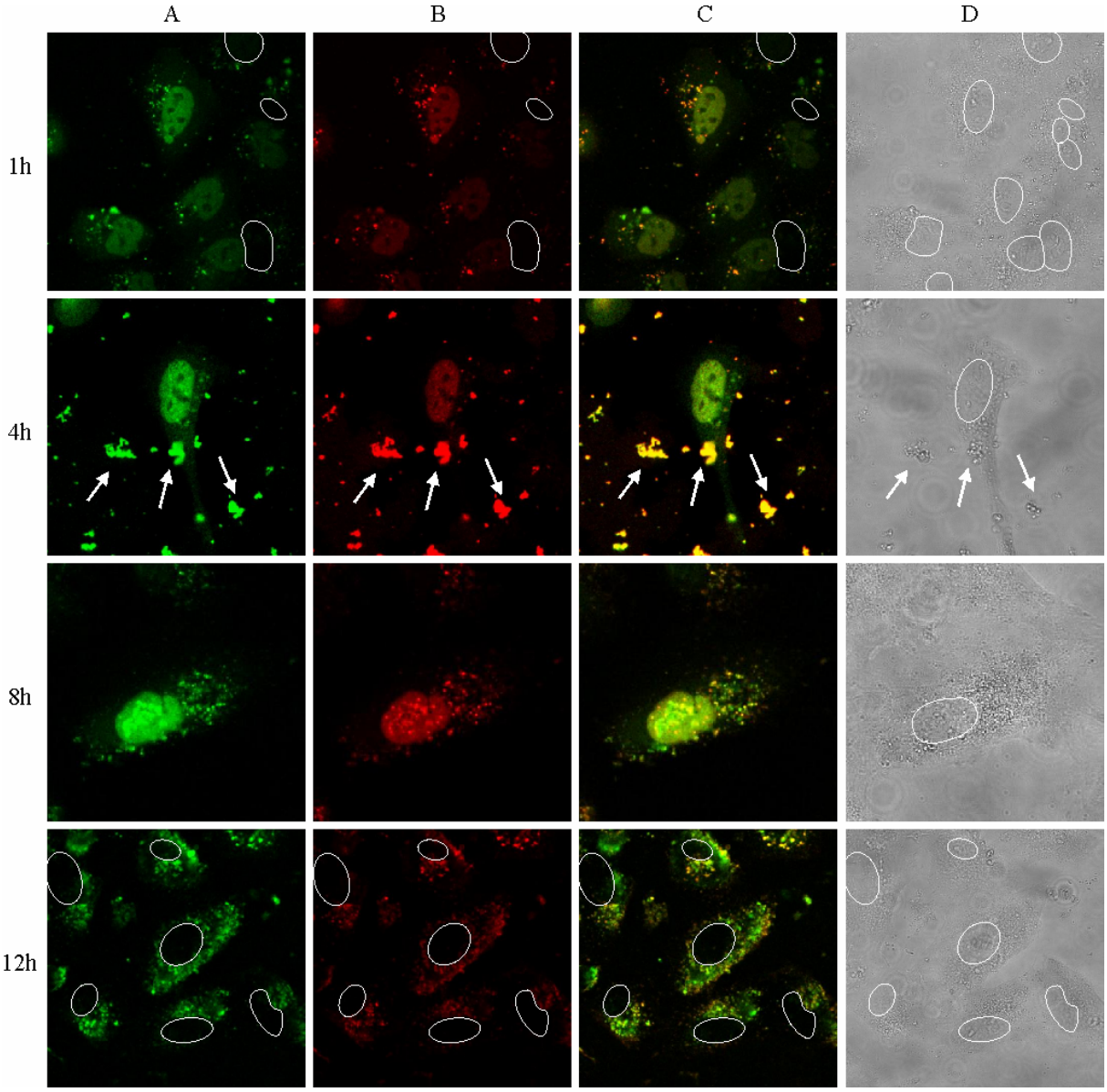

Figure 3. Green (A), red (B) and merged (C) confocal images of A549 cells respectively 1, 4, 8 and 12 hours after transfection with PS20-LPXs. As excitation light of 488 nm was used, the red fluorescence in B comes from Cy5 excitation due to FRET. In the transmission images (D) a circle was drawn around the nucleus (as also around the non-fluorescent nuclei in A, B and C). The arrows point to PS20-LPXs aggregates.

Within 1 hour after adding PS20-LPXs to A549 cells, confocal images showed green fluorescence in the nuclei of most cells (Figure 3A-1h). As the PS20-LPXs themselves are by far too large (~150 nm) to cross the pores of the nuclear membrane, the nuclear fluorescence indicates the entry of free PS20-ONs after being released from the LPXs. Figure 3B-1h shows that also red fluorescence can be detected in the nuclei of most cells, indicating that FRET occurs and thus that the PS20-ONs are intact. From the red and green fluorescence fluctuations in the nucleus, as measured by the FCS detectors (upon excitation at 488 nm), an average R/G ratio of 2.2 ± 0.4 was calculated, which agreed well with the R/G ratio of intact PS20-ONs in buffer (Table 1). Also, proper auto-correlation curves could be generated from both the green and red fluorescence fluctuations (Figure 4). As discussed in Chapter 2 [12], the diffusion time itself (as obtained from the auto-correlation curves) can only be used to distinguish between fully intact and fully degraded double-labeled ONs. Nevertheless, the fact that a proper auto-correlation curve can be derived for the Cy5 fluorophores upon 488 nm excitation points out that FRET still occurs. Therefore, we chose to depict the auto-correlation curves, which were best fitted with a dual-species fit (equation 2), without further discussing the obtained diffusion times. Taken together, the above-mentioned observations clearly show that 1 hour after transfection PS20-ONs were released from the LPXs and stayed intact in the intracellular environment.

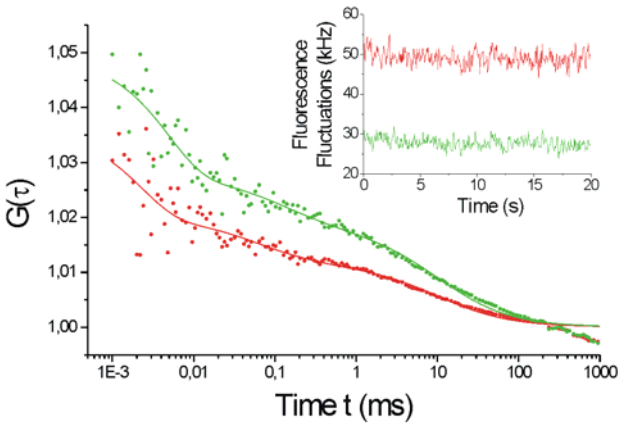

Figure 4. FCS measurements performed in the nucleus of A549 cells 1 hour after transfection with PS20-LPXs with laser excitation set to 488 nm. The graph shows the auto-correlation curves (dotted line) as derived from the green (rhodamine green, donor, green line) and red (Cy5, acceptor, red line) detector of the FCS instrument. The auto-correlation curves were best fitted with a dual-species fit (eq. 2) (solid line). The graph insert shows the green (green line) and red (red line) fluorescence fluctuations from which the auto-correlation curves were derived.

More PS20-LPXs were able to enter the cells and release their ONs upon 4 hours incubation time, as was concluded from the increased nuclear fluorescence intensity (Figure 3-4h). Also, as pointed by the arrows, aggregates of PS20-LPXs became visible in the medium surrounding the cells. It is indeed known that lipoplexes have the tendency to

aggregate into large multimolecular complexes at longer contact times [13]. Figure 3B-4h indicates the presence of FRET in the PS20-LPX aggregates outside the cells as well as in the free PS20-ONs in the nuclei of the cells. Also here, the average R/G ratio of 2.3 ± 0.4 in the nuclei revealed that the PS20-ONs were still intact.

At longer incubation times, the formation of nuclear bodies could be seen in some cells as bright fluorescent spots in the nucleus (Figure 3-8h). This phenomenon has been reported previously for PS-ONs, especially at higher concentrations [14-16]. The nuclear bodies contained intact PS20-ONs, as they were both green and red colored. Also, the R/G ratio of 1.8 ± 0.2 as measured in the nucleus demonstrates that the PS20-ONs were still intact upon 8 hours residence time.

After 12 hours, the nuclear fluorescence largely disappeared (Figure 3-12h). The average fluorescence intensities in the nuclei, as measured by the FCS detectors, equaled the autofluorescence of the nuclei (~ 5 kHz). Since the FCS detectors are much more sensitive than the CLSM detectors and can detect single molecules, this confirms that no PS20-ONs are left in the nuclei of most cells. Importantly, the disappearance of PS20-ONs out of the nuclei correlated with the appearance of punctated structures in the cytoplasm of the cells (Figure 3A-12h). As seen from the red fluorescence in Figure 3B-12h these cytoplasmic granules contain intact PS20-ONs. Now and then highly intense green and red fluorescence peaks simultaneously occurred in the fluorescence fluctuation profiles as measured by the FCS instrument in the cytoplasm of these cells (Figure 5). The fluorescence peaks had an average R/G ratio of 1.6 ± 0.3 and indicate the simultaneous movement of a number of intact PS20-ONs through the detection volume of the FCS instrument. As deduced from the broadness of the peaks in Figure 5, the PS20-ONs containing structures need about 5 to 10 seconds to pass through the detection volume of the FCS instrument, indicating a slow movement in the cytosol.

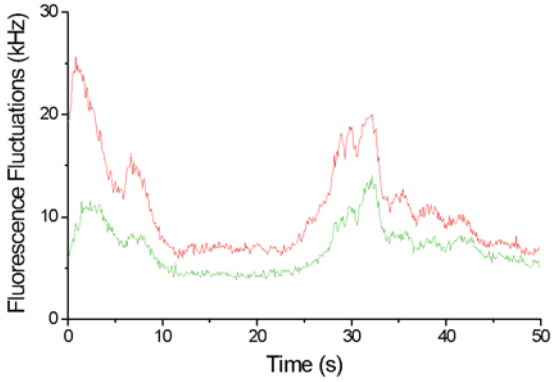

Figure 5. Fluorescence fluctuations as measured by the green (green line) and red (red line) detector of the FCS instrument in the cytoplasm of A549 cells transfected with PS20-LPXs. Laser excitation was set to 488 nm. The average R/G ratio of the fluorescence peaks was 1.6 ± 0.3, indicating intact PS20-ONs.

Intracellular Fate of PO20-ONs Delivered by Non-pegylated Liposomes

A549 cells were transfected with DOTAP/DOPE liposomes containing fluorescently double-labeled PO20-ONs (PO20-LPXs). As for the PS20-LPXs, confocal images of the cells were taken and FCS measurements were performed in the nucleus and cytoplasm of the cells with laser excitation set to 488 nm (Figure 6).

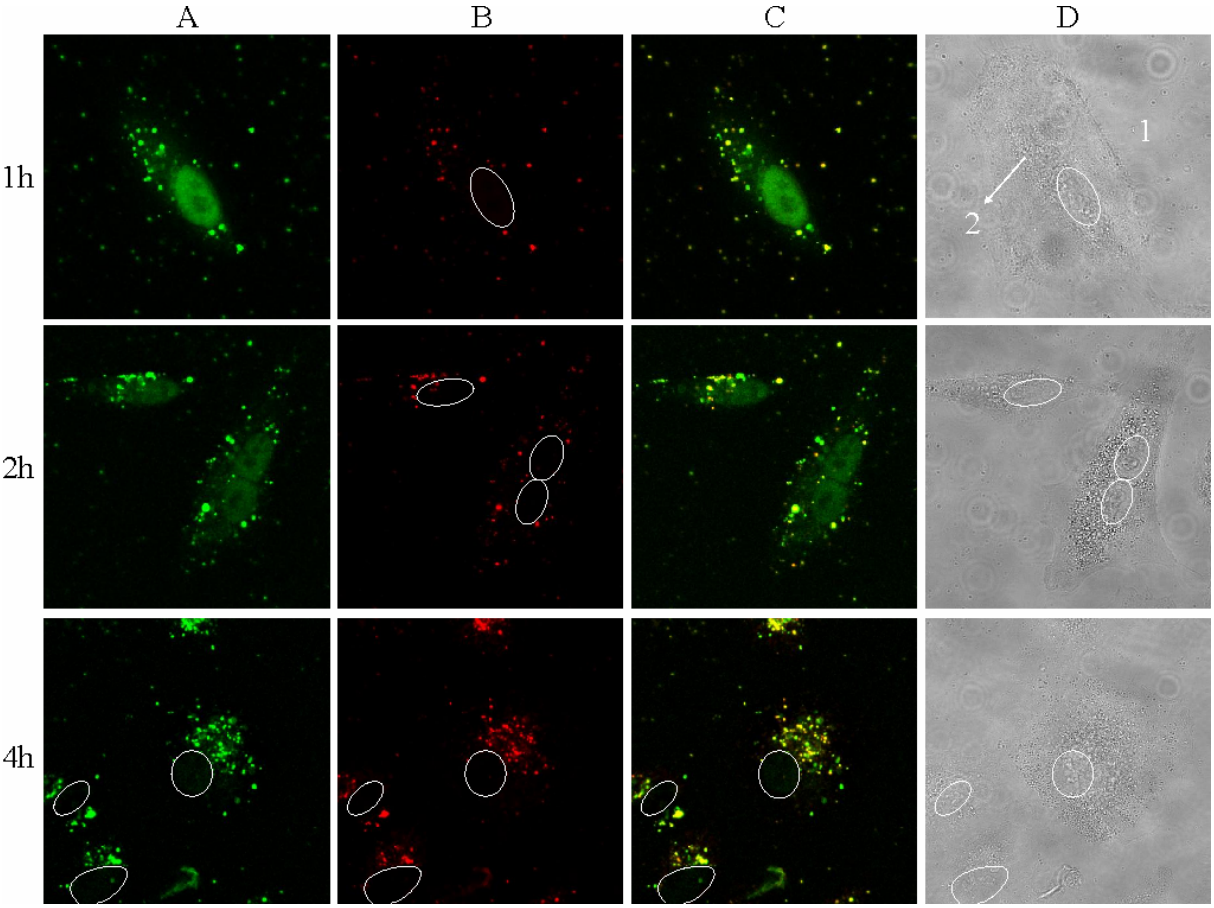

Figure 6. Green (A), red (B) and merged (C) confocal image of A549 cells respectively 1, 2 and 4 hours after transfection with PO20-LPXs. As excitation light of 488 nm was used, the red fluorescence comes from Cy5 excitation due to FRET. In the transmission images (D) a circle was drawn around the nucleus (as also around the non-fluorescent nuclei in A, B and C).

Green fluorescent nuclei were observed in the first hour after transfection (Figure 6A-1h). This demonstrates the entry of PO20-LPXs in the cells and the release of the PO20-ONs from the LPXs, as only free ONs can diffuse through the pores of the nuclear membrane. In contrast to PS20-ONs (Figure 3), no red fluorescence was found in the nuclei upon excitation at 488 nm light (Figure 6B-1h). This suggests that FRET does not occur and indicates that the PO20-ONs present in the nuclei are degraded. FCS measurements in the nuclei revealed an average R/G ratio of 0.3 ± 0.1, showing that the released PO20-ONs that had entered the nuclei were indeed degraded. Also, upon excitation at 488 nm light, the auto-correlation

curve obtained from the nuclear green fluorescence fluctuations (~ rhodamine green) was of good quality (Figure 7, green line) while the red fluorescence fluctuations (~ Cy5) could not be correlated (Figure 7, red line). Nevertheless, red fluorescence could be detected in the PO20-LPXs outside the cells (Figure 6B-1h, region 1) as well as in some PO20-LPXs in the cytoplasm of the cells (Figure 6B-1h, region 2). By positioning the measuring points of the FCS instrument on the fluorescent dots, the R/G ratio of the PO20-LPXs could be determined. The average R/G ratio of the fluorescent dots in region 2 was 1.7 ± 0.2 and confirmed that the DOTAP/DOPE liposomes in the cytosol still contained intact PO20-ONs. This indicates that the degradation of the PO20-ONs occurs after release of the ONs from the LPXs.

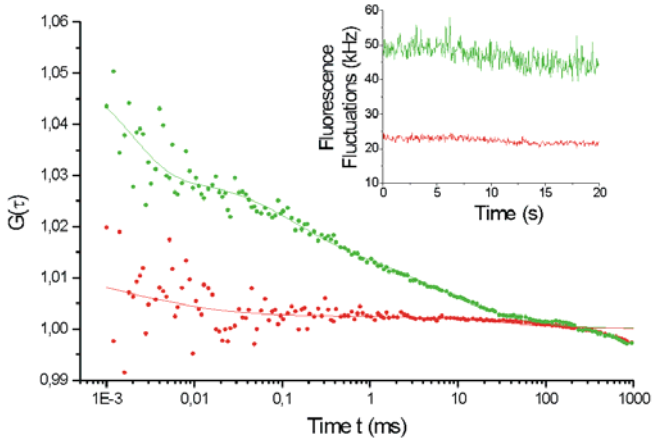

Figure 7. FCS measurements performed in the nucleus of A549 cells 1 hour after transfection with PO20-LPXs with laser excitation set to 488 nm. The graph shows the auto-correlation curves (dotted line) as derived from the green (rhodamine green, donor, green line) and red (Cy5, acceptor, red line) detector of the FCS instrument. The auto-correlation curves were best fitted with a dual-species fit (eq. 2) (solid line). The graph insert shows the green (green line) and red (red line) fluorescence fluctuations from which the auto-correlation curves were derived

The nuclear green fluorescence faded already after 2 hours incubation (Figure 6A-2h) and disappeared upon incubation times longer than 4 hours (Figure 6A-4h). Most likely, as previously observed by Fisher *et al.* [16], the small fluorescent degradation products easily diffuse out of the cells and are therefore no longer detected. However, the red dots in Figure 6B-2h and Figure 6B-4h show that most of the PO20-LPXs in and around the cells still contain intact PO20-ONs, again confirming that degradation mainly occurs after release of the ONs from the LPXs.

.

Intracellular Fate of PO40-ONs Delivered by Non-pegylated Liposomes

Figure 8 shows confocal and transmission images of A549 cells after being transfected with non-pegylated liposomes containing fluorescently double-labeled PO40-ONs (PO40-LPXs). As for the PS20-LPXs and PO20-LPXs, the cells were excited at 488 nm. In that case, the red fluorescence comes from the excitation of the Cy5 fluorophores due to FRET, what can only occur if the ONs are still intact.

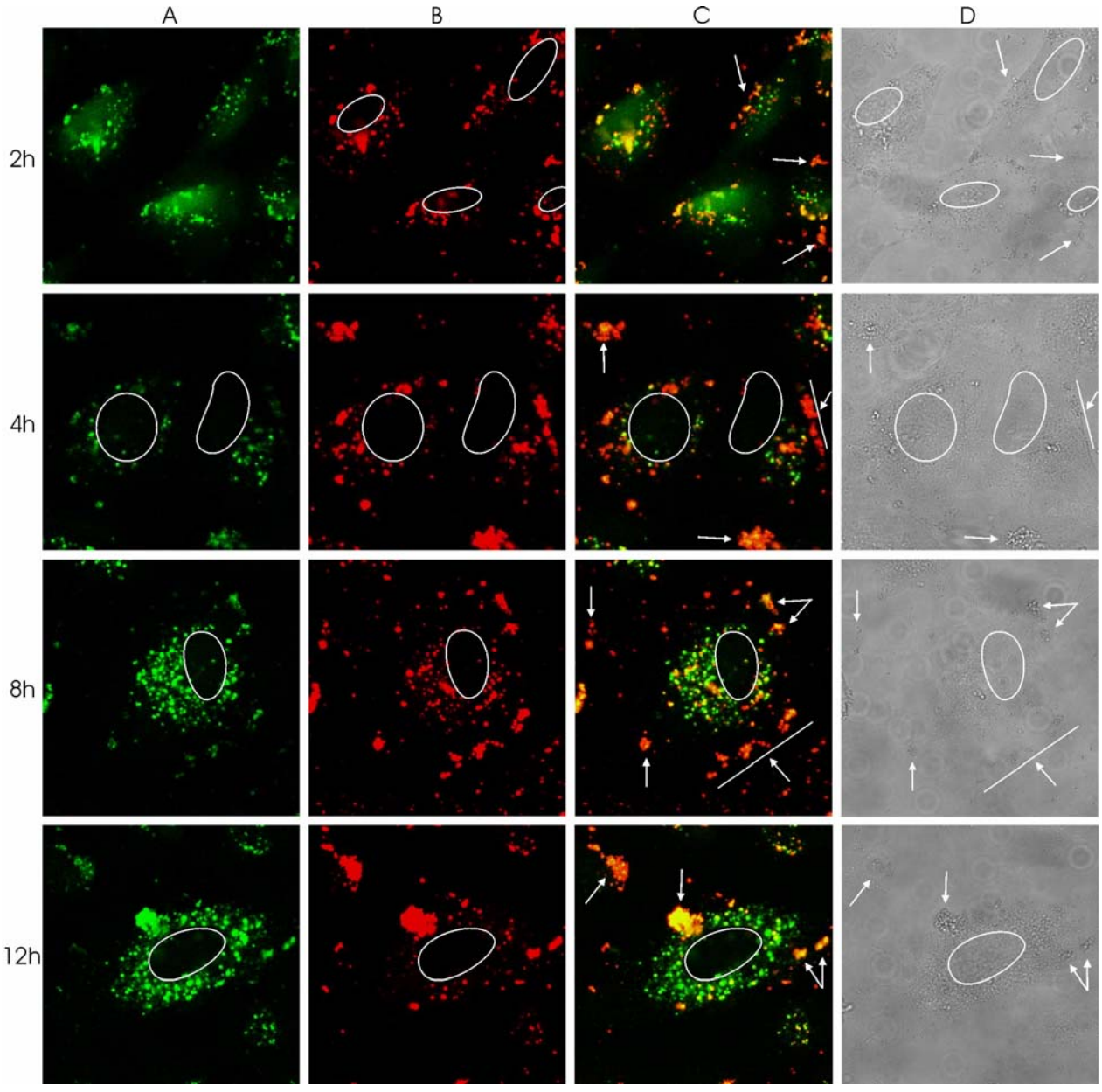

Figure 8. Green (A), red (B) and merged (C) confocal images of A549 cells respectively 2, 4, 8 and 12 hours after transfection with P040-LPXs. As excitation light of 488 nm was used, the red fluorescence in B comes from Cy5 excitation due to FRET. In the transmission images (D) a circle was drawn around the nuclei (as also around the non-fluorescent nuclei in A, B and C). The arrows point to PO40-LPXs that are located outside the cells.

In the first two hours following transfection, green fluorescent nuclei were observed (Figure 8A-2h). As the P040-LPXs themselves are too large to cross the pores of the nuclear membrane, this demonstrates the nuclear accumulation of the free PO40-ONs, released from the DOTAP/DOPE liposomes. Figure 8B-2h shows that red fluorescence could not be detected in the nuclei of the cells, suggesting that FRET does not occur and that the ONs in the nuclei were thus degraded. The average R/G ratio in the nuclei of the transfected cells, as measured by the FCS setup, equaled 0.2 ± 0.1 and confirmed that the PO40-ONs were degraded.

As Figure 8A-4h shows, the green fluorescence in the nuclei faded upon 4 hours incubation time. Also, fluorescence measurements with the very sensitive detectors of the FCS setup pointed out that the nuclear fluorescence intensity did not differ significantly anymore from the autofluorescence of the nuclei (~ 5 – 10 kHz). However, some green and red fluorescent dots could be detected in the cytoplasm of the cells. Also at 8 hours incubation time, nuclear fluorescence could no longer be detected. However, the amount of green fluorescent spots in the cytoplasm of the cells clearly increased (Figure 8A-8h). From the color of the fluorescent spots in Figure 8C-8h it could be deduced that most of the punctated structures in the cytoplasm contained degraded PO40-ONs (green fluorescent spots) while other ones contained intact PO40-ONs (red fluorescent spots) or a mixture of intact and degraded PO40-ONs (yellow fluorescent spots). Similar information was obtained from measurements with the FCS setup: the R/G ratio as measured in the cytoplasm of the cells varied between 0.5 and 4 confirming that some of the cytoplasmic structures contained mostly degraded ONs while other ones were composed of mostly intact ONs.

At 12 hours incubation time (Figure 8A-12h), a large number of green fluorescent spots were still present in the cytoplasm of the cells. However, there were less red fluorescent spots when compared to 8 hours incubation time, indicating that degradation of the PO40-ONs proceeded in these cytoplasmic structures (Figure 8B-12h). It should be noted that the PO40-LPXs located outside the cells (as pointed out by the arrows in the C- and D-images of Figure 8) remained red fluorescent and thus remained to contain intact ONs, irrespective of the incubation time. When FCS measurements were performed on these not endocytosed lipoplexes, the R/G ratio of 5.1 ± 0.6 clearly confirmed that they contained intact PO40-ONs. These observations suggest that the degradation of the complexed ONs only occurred after entry of the PO40-LPXs in the A549 cells.

Degradation of Naked PO20-ONs upon Microinjection in A549 Cells

As described above, FCS measurements and confocal images of A549 cells transfected with DOTAP/DOPE liposomes revealed that PO-ONs were degraded in the

intracellular environment within the first hour following transfection. Also, the data suggested that the degradation occurred after being released from the liposomes. To see whether PO-ONs indeed degrade that rapidly, naked PO-ONs were injected in the cytoplasm of A549 cells and FCS measurements were performed to monitor the degradation. We chose to inject the PO20-ONs, as they contain the sequence for the anti-ICAM-1 activity, while the PO40-ONs are not biologically active.

As observed previously by others, PO20-ONs accumulated in the nuclei of the injected cells within a few minutes following the injection (data not shown) [17;18]. Despite this rapid nuclear accumulation, intact PO20-ONs could not be detected in the nuclei of the injected cells. This could be concluded from the R/G ratio of 0.3 ± 0.1. Also, a proper auto-correlation curve could not be registered from the red (acceptor) fluorescence fluctuations upon 488 nm excitation (Figure 9A, red line) while a good auto-correlation curve was obtained from the green (donor) fluorescence fluctuations (Figure 9A, green line). Subsequently, the concentration of the injected PO20-ONs was increased 11-fold by injecting a mixture of fluorescently labeled (2 µM) and non-labeled (20 µM) PO20-ONs in the cells. In that way the amount of fluorescent PO20-ONs was kept low enough to allow for proper auto-correlation analysis. As shown in Figure 9B, proper auto-correlation curves from both the green and red fluorescence fluctuations were obtained upon excitation at 488 nm, indicating that FRET occurred and thus intact PO20-ONs were present in the nuclei of the cells. Also, the R/G ratio of 1.1 ± 0.1 confirmed that intact PO20-ONs entered the nuclei when a larger amount of PO20-ONs was injected in the cytosol.

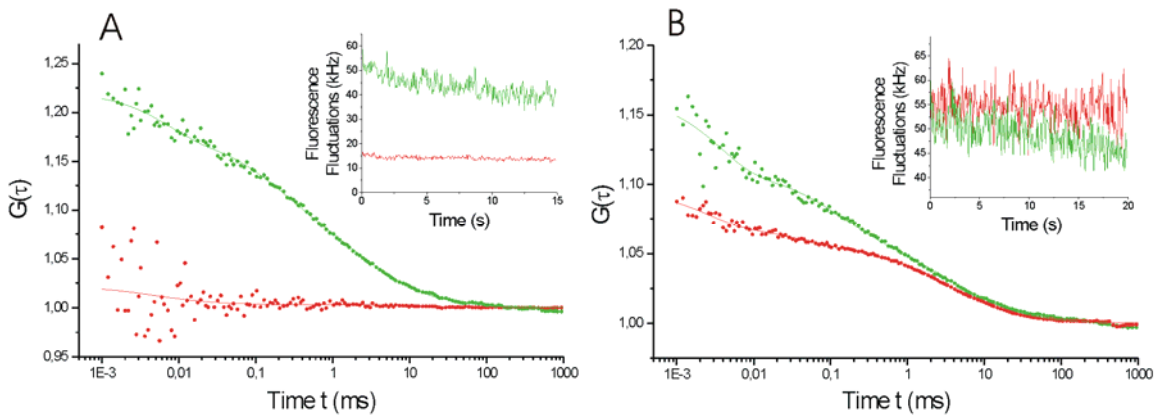

Figure 9. FCS measurements performed in the nucleus of A549 cells immediately after injection of (A) 2 µM fluorescently labeled PO20-ONs and (B) a mixture of 2 µM fluorescently labeled and 20 µM non-labeled PO20-ONs. Injections were performed in the cytoplasm of A459 cells. The graph shows the auto-correlation curves (dotted line) as derived from the green (rhodamine green, donor, green line) and red (Cy5, acceptor, red line) detector of the FCS instrument. The auto-correlation curves were best fitted with a dual-species fit (eq. 2) (solid line). The graph insert shows the green (green line) and red (red line) fluorescence fluctuations from which the auto-correlation curves were derived.

DISCUSSION

For some years now, antisense ONs are being investigated for the selective inhibition of various genes [1]. Regretfully, the therapeutic potential remains largely unrealized. Attempts to fundamentally explain the biological activity of nucleic acids loaded carriers, by studying their biophysical properties and cell biological behavior, are scarce although these studies are highly needed to allow the design of better delivery systems for nucleic acids. For that purpose, our laboratory uses advanced microscopy techniques like Fluorescence Correlation Spectroscopy [19-21]. In Chapter 3, we observed that PO-ONs in non-pegylated lipoplexes (LPXs) were well protected against enzymatic degradation when the LPXs were incubated in a DNase I solution. Although being protected against enzymatic degradation, we observed in this chapter that the nuclease sensitive PO-ONs delivered by non-pegylated liposomes did not show a biological effect, while the nuclease resistant PS-ONs did down-regulate the ICAM-1 protein expression (Figure 1). Subsequently, we followed the intracellular distribution and degradation of fluorescently double-labeled PO-ONs or PS-ONs delivered by DOTAP/DOPE liposomes by means of FCS and confocal imaging in order to explain the observed biological activity.

Explanation of the Biological Activity of Non-pegylated Lipoplexes Based on their Intracellular Fate and Structural Properties

Based on the mechanism of lipoplex formation as proposed in Chapter 3 and the intracellular fate and distribution of antisense ONs delivered by these lipoplexes as observed in this chapter, we propose below the intracellular pathway of non-pegylated liposomes containing PO- or PS-ONs in A549 cells, that can account for the obtainied antisense activity (Figure 10).

In a first step, the cationic LPXs settle on and electrostatically bind to the negatively charged cell membranes (Figure 10, step 1). It is widely accepted that liposomes predominantly enter cells by endocytosis [22-25]. Upon endocytosis of the DOTAP/DOPE liposomes loaded with fluorescent ONs, one would expect to see the endosomal vesicles as fluorescent dots in the cytoplasm of the transfected cells (Figure 10, step 2). Surprisingly, rather few cytoplasmic fluorescent dots were detected in the first hour following transfection. On the contrary, fluorescent nuclei were observed within the first hour after applying the LPXs to the A549 cells (Figure 3, 6 and 8). As the LPXs are too large to cross the pores of the nuclear membrane, the fluorescent nuclei suggest that the endosomal escape of the DOTAP/DOPE liposomes and release of the ONs in the cytosol of the A549 cells is a very

efficient process (Figure 10, step 3). A possible mechanism for endosomal escape of ON containing LPXs has been proposed by Zelphati and Szoka [26]. According to these authors, lipid contact occurs between cationic lipids from the LPXs and anionic lipids from the inner face of the endosomal membrane resulting in flip-flop of anionic lipids from the cytoplasmic face of the endosomal membrane. These anionic lipids laterally diffuse into the LPXs and form a charge neutralized ion-pair with the cationic lipids from the LPXs, which results in destabilization of the LPXs and displacement of the negatively charged ONs with their release into the cytoplasm of the cells. Recently, Gordon *et al.* demonstrated that anionic lipids in the endosomal membrane are not a primary prerequisite to trigger ON release [27]. On the contrary, neutral helper lipids in the delivery system, such as DOPE, seem to play a crucial role in improving the endosomal escape by adopting a hexagonal phase in the lumen of the endosomes that destabilizes the endosomal membrane [28;29]. Therefore, the presence of DOPE in the LPXs used in this chapter most likely explains the rapid endosomal escape that results in release of the ONs in the cytoplasm of the transfected cells.

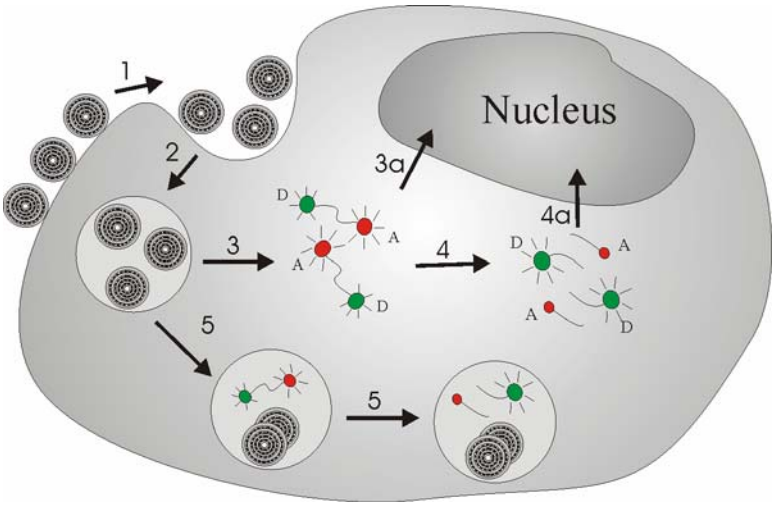

Figure 10. Proposed intracellular pathway of non-pegylated lipoplexes. (1) binding to the cell membrane, (2) internalization by endocytosis, (3) endosomal escape with release of the ONs in the cytoplasm, (3a) nuclear accumulation of intact ONs, (4) intracellular degradation of ONs, (4a) nuclear accumulation of degraded ONs and (5) degradation of the ONs in the endosomal compartment.

Several studies have reported that, once in the cytosol, free ONs readily accumulate in the nucleus [15;17;18]. By FCS, we observed that the ONs present in the nuclei were intact in the case of PS-ONs (Figure 10, step 3a), but degraded in the case of PO-ONs (Figure 10, step 4a). It is well known that PS-ONs are more resistant to degradation by nucleases. However, life times of PO-ONs in cells reported in literature vary from minutes to some hours [16;17;30;31]. In this chapter, we found that injected PO20-ONs were degraded within minutes when injected at low concentrations (2 μM), while intact PO20-ONs could be detected when the injected concentration was 11-fold higher. The fact that intact PO20-ONs

were not observed in the nuclei of the transfected cells, together with the observation that intact PO20-ONs were detected in the PO20-LPXs outside as well as inside the transfected cells, suggests that degradation occurs after release of the PO20-ONs from the DOTAP/DOPE liposomes (Figure 10, step 4). We indeed demonstrated in Chapter 3 that DOTAP/DOPE liposomes offer a good protection against enzymatic degradation to the PO-ONs they are carrying, as long as the PO-ONs remain complexed to their carrier [11]. Nevertheless, this chapter demonstrates that this protection against enzymatic degradation does not translate into a biological effect of the PO20-ONs due to the too efficient release and subsequent degradation of the PO20-ONs at the step of endosomal escape. We additionally observed that the nuclear fluorescence of PO20-ONs and PO40-ONs faded respectively within the first 2 hours and 4 hours after exposing PO20-LPXs and PO40-LPXs to the A549 cells (Figure 6-2h and Figure 8-4h). This probably reflects the diffusion of the shorter fluorescent degradation products out of the cells, as was already observed previously by Fisher *et al.* [16]. It should be noted that the fluorescent labels at the 3' and 5' end of the double-labeled ONs could interfere with the splicing activity of exonucleases. Therefore, the actual degradation of unlabeled PO-ONs is expected to occur even more rapidly.

In the case of phosphothioate ONs, intact PS20-ONs could be observed in the nuclei of the cells for at least 8 hours (Figure 3). This was no surprise as the more nuclease resistant PS20-ONs are not expected to degrade upon their release at the time of endosomal escape, thus creating a pool of intact PS20-ONs. This on its turn results in a longer time for PS20-ONs to bind to the target mRNA and to inhibit the targeted protein expression, which most likely explains why the nuclease resistant PS20-ONs could indeed establish an antisense effect. Although PS20-ONs did not degrade in the intracellular environment and are therefore not expected to spontaneously diffuse out of the cells, the fluorescence in the nuclei disappeared after more than 8 hours. Interestingly, there seemed to be a fluorescence shift from the nucleus to the cytoplasm of the cells (Figure 3-12h): the nuclear fluorescence faded while fluorescent dots (as seen by confocal imaging) and simultaneous green and red fluorescence peaks (as seen by FCS) appeared in the cytoplasm of the cells. The identity of the cytoplasmic granules is currently unknown, however, their appearance directly correlates with the dissipation of fluorescent PS20-ONs from the nucleus. This phenomenon has been observed previously by Fisher *et al.*, who suggested that intracellular PS-ONs could be exported from the cells by exocytosis [16]. In agreement with Fisher *et al.* we believe that the formation of these cytoplasmic granules, which apparently contain the fluorescent PS20-ONs that were previously present in the nucleus, could indicate that the cells display an export pathway to remove intact PS20-ONs out of the cells. It should be noted that nuclear bodies occurred in the nucleus before the apparent removal of the intact PS20-ONs from the nuclei of the cells. Since the formation of nuclear bodies is reported to mainly occur at higher

concentrations of PS-ONs [14-16], this could be the first step in exporting intact PS-ONs from the nuclei of the cells. Indeed, high PS-ONs concentrations could trigger ordening of PS-ONs in nuclear bodies that are then exported via the cytoplasm to the cellular membrane. Whether or not the formation of nuclear bodies is correlated with the export of PS-ONs from the cells is an important question that remains to be elucidated.

To our surprise, an increasing amount of fluorescent spots, which most likely represent endosomal vesicles, were detected in the cytoplasm of the cells transfected with PO40-LPXs at longer incubation times (see Figure 8-8h and 12h). The fluorescent spots persisted in the cytoplasm of the cells without the appearance of fluorescent nuclei, which indicates that endosomal escape of the LPXs with release of the PO40-ONs in the cytoplasm of the cells did not occur. Furthermore, upon increasing the incubation time from 8 till 12 hours, less (red colored) endosomal vesicles containing intact PO40-ONs were observed (compare the amount of intracellular red fluorescent dots in Figure 8B-8h and Figure 8B-12h), showing that degradation of the PO40-ONs took place. The question now raised is why DOPE appears to be unable to destabilize the endosomal membrane with release of the PO40-ONs in the cytoplasm of the cells. We have observed in Chapter 3 that PO40-ON containing DOTAP/DOPE liposomes, after being 4 hours in a buffer solution, spontaneously start to release their ONs in the surrounding environment, which we attributed to the fusion of neighbouring LPXs. It could well be that this lipoplex fusion also occurs in the endosomal compartment upon longer incubation times, thereby releasing PO40-ONs in the endosomes rather than in the cytoplasm of the cells (Figure 10, step 5). Consequently, the released PO40-ONs are entrapped and degraded in the endosomal compartment. In conclusion, DOPE is now apparently responsible for the destabilization of the lipids originating from the neighbouring LPXs, rather than the destabilization of the lipids originating from the endosomal membrane. Apart from LPXs fusion, the increasing amount of green fluorescent spots containing degraded PO40-ONs could also reflect the degradation of the LPXs by lysosomal enzymes.

Is there Potential in the Delivery of Nuclease Sensitive PO-ONs?

As described in the introduction, one approach to improve antisense activity of nucleic acids is to synthesize ONs with increased nuclease stability so that intracellular degradation should not be an issue [4]. However, modification of the ON backbone can introduce undesirable features such as solubility problems, delivery issues, lack of RNase H activation or simply the cost of synthesis [32]. Therefore, the development of cationic carriers that can efficiently deliver unmodified PO-ONs remains important and challenging. However, as observed in this chapter, cationic lipids are mainly useful in the delivery of nuclease resistant

ONs such as PS-ONs. Indeed, the efficient delivery of ONs at the time of endosomal escape does create a barrier for nuclease sensitive PO-ONs due to the rapid intracellular degradation of the naked PO-ONs, while the nuclease resistant PS-ONs remain intact. Therefore, carriers that could bring the PO-ONs as close as possible to the target mRNA or that allow the PO-ONs to establish an antisense effect while being encapsulated could be more suitable to deliver unmodified PO-ONs. One such carrier that could do the trick is the cationic polymer polyethyleneimine (PEI). In general it is believed that PEI escapes from the endosomes via a proton sponge mechanism [33;34]. The buffering capacity of PEI causes protons to be pumped in the endosomes, accompanied with an influx of Cl^- ions. This builds up the osmotic pressure which eventually causes the endosomes to rupture. The ON/PEI complexes are thus released in the cytosol of the cells as such, without release of the ONs at the step of the endosomal escape. In contrast to liposome/DNA complexes, PEI/DNA complexes can enter the nucleus as an associated complex [35]. Also, Pollard *et al.* found that, in contrast to cationic lipids, the dissociation of plasmid DNA from PEI was not necessary to establish a therapeutic effect [36]. This was again observed recently by Honoré *et al.* [37]. In a study employing oligonucleotides, Dheur *et al.* observed that PEI was able to improve the antisense activity of nuclease sensitive PO-ONs while cationic lipids were not [8]. We also observed that PO-ONs complexed with the cationic polymer *graft*-pDMAEMA (poly(2-dimethylamino)ethylmethacrylate bearing polyethyleneglycol chains) showed the same antisense effect as PS-ONs complexed with *graft*-pDMAEMA [7]. These results support the idea that cationic polymers could show more potential as non-viral gene delivery systems for unmodified PO-ONs when compared to cationic lipids.

ACKNOWLEDGEMENTS

Katrien Remaut is a Research Assistant of the Research Foundation - Flanders (Belgium). Niek Sanders and Kevin Braeckmans are Postdoctoral Fellows of the Research Foundation - Flanders (Belgium). The financial support of this institute is acknowledged with gratitude. All experimental data were collected at the Advanced Light Microscopy Facility at the European Molecular Biology Laboratory (EMBL), Heidelberg, Germany. The lab of Rainer Pepperkok is gratefully acknowledged for the support during the visit of Katrien Remaut at the EMBL. The authors would like to thank Leica Microsystems for continuous support of the Advanced Light Microscopy Facility.

REFERENCES

(1) Sazani, P.; Kole, R. Therapeutic potential of antisense oligonucleotides as modulators of alternative splicing. *J. Clin. Invest.* **2003**, 112, 481-486.

(2) Jabs, D. A.; Griffiths, P. D. Fomivirsen for the treatment of cytomegalovirus retinitis. *Am. J. Ophthalmol.* **2002**, 133, 552-556.

(3) Holmlund, J. T. Applying antisense technology - Affinitak (TM) and other antisense oligonucleotides in clinical development. *Ann. NY Acad. Sci.* **2003**, 1002, 244-251.

(4) Agrawal, S. Importance of nucleotide sequence and chemical modifications of antisense oligonucleotides. *Biochim. Biophys. Acta* **1999**, 1489, 53-68.

(5) Brown, D. A.; Kang, S. H.; Gryaznov, S. M.; Dedionisio, L.; Heidenreich, O.; Sullivan, S.; Xu, X.; Nerenberg, M. I. Effect of Phosphorothioate Modification of Oligodeoxynucleotides on Specific Protein-Binding. *J. Biol. Chem.* **1994**, 269, 26801-26805.

(6) Pedroso de Lima, M. C.; Simoes, S.; Pires, P.; Faneca, H.; Düzgünes, N. Cationic lipid-DNA complexes in gene delivery: from biophysics to biological applications. *Adv. Drug Deliver. Rev.* **2001**, 47, 277-294.

(7) Lucas, B.; Van Rompaey, E.; Remaut, K.; Sanders, N.; De Smedt, S.; Demeester, J. On the biological activity of anti-ICAM-1 oligonucleotides complexed to non-viral carriers. *J. Control. Release* **2004**, 96, 207-219.

(8) Dheur, S.; Dias, N.; Van Aerschot, A.; Herdewijn, P.; Bettinger, T.; Remy, J. S.; Helene, C.; Saison-Behmoaras, E. T. Polyethylenimine but not cationic lipid improves antisense activity of 3'-capped phosphodiester oligonucleotides. *Antisense Nucleic Acid Drug Dev.* **1999**, 9, 515-525.

(9) Shi, F.; Nomden, A.; Oberle, V.; Engberts, J. B. F. N.; Hoekstra, D. Efficient cationic lipid-mediated delivery of antisense oligonucleotides into eukaryotic cells: Down-regulation of the corticotropin-releasing factor receptor. *Nucleic Acids Res.* **2001**, 29, 2079-2087.

(10) Lucas, B.; Van Rompaey, E.; De Smedt, S. C.; Demeester, J.; Van Oostveldt, P. Dual-color FFS to study the complexation between poly-l-lysine and oligonucleotides. *Macromolecules* **2002**, 35, 8152-8160.

(11) Remaut, K.; Lucas, B.; Braeckmans, K.; Sanders, N. N.; Demeester, J.; De Smedt, S. C. Protection of oligonucleotides against nucleases by pegylated and non-pegylated liposomes as studied by Fluorescence Correlation Spectroscopy. *J. Control. Release* **2005**, 110, 209-223.

(12) Remaut, K.; Lucas, B.; Braeckmans, K.; Sanders, N. N.; De Smedt, S. C.; Demeester, J. FRET-FCS as a tool to evaluate the stability of oligonucleotide drugs after intracellular delivery. *J. Control. Release* **2005**, 103, 259-271.

(13) Jaaskelainen, I.; Sternberg, B.; Monkkonen, J.; Urtti, A. Physicochemical and morphological properties of complexes made of cationic liposomes and oligonucleotides. *Int. J. Pharm.* **1998**, 167, 191-203.

(14) Lorenz, P.; Baker, B. F.; Bennett, C. F.; Spector, D. L. Phosphorothioate antisense oligonucleotides induces the formation of nuclear bodies. *Mol. Biol. Cell* **1998**, 9, 1007-1023.

(15) Shoeman, R. L.; Hartig, R.; Huang, Y.; Grueb, S.; Traub, P. Fluorescence microscopic comparison of the binding of phosphodiester and phosphorothioate (antisense) oligodeoxyribonucleotides to subcellular structures, including intermediate filaments, the endoplasmic reticulum, and the nuclear interior. *Antisense Nucleic Acid Drug Dev.* **1997**, 7, 291-308.

(16) Fisher, T. L.; Terhorst, T.; Cao, X. D.; Wagner, R. W. Intracellular Disposition and Metabolism of Fluorescently-Labeled Unmodified and Modified Oligonucleotides Microinjected Into Mammalian-Cells. *Nucleic Acids Res.* **1993**, 21, 3857-3865.

(17) Leonetti, J. P.; Mechti, N.; Degols, G.; Gagnor, C.; Lebleu, B. Intracellular distribution of microinjected antisense oligonucleotides. *Proc. Natl. Acad. Sci. USA* **1991**, 88, 2702-2706.

(18) Chin, D. J.; Green, G. A.; Zon, G.; Szoka, F. C., Jr.; Straubinger, R. M. Rapid nuclear accumulation of injected oligodeoxyribonucleotides. *New Biologist* **1990**, 2, 1091-1100.

(19) De Smedt, S. C.; Remaut, K.; Lucas, B.; Braeckmans, K.; Sanders, N. N.; Demeester, J. Studying biophysical barriers to DNA delivery by advanced light microscopy. *Adv. Drug Deliver. Rev.* **2005**, 57, 191-210.

(20) Lucas, B.; Remaut, K.; Sanders, N. N.; Braeckmans, K.; De Smedt, S. C.; Demeester, J. Studying the intracellular dissociation of polymer-oligonucleotide complexes by dual color fluorescence fluctuation spectroscopy and confocal imaging. *Biochemistry* **2005**, 44, 9905-9912.

(21) Van Rompaey, E.; Engelborghs, Y.; Sanders, N.; De Smedt, S. C.; Demeester, J. Interactions between oligonucleotides and cationic polymers investigated by fluorescence correlation spectroscopy. *Pharm. Res.* **2001**, 18, 928-936.

(22) Shi, F.; Hoekstra, D. Effective intracellular delivery of oligonucleotides in order to make sense of antisense. *J. Control. Release* **2004**, 97, 189-209.

(23) Harashima, H.; Shinohara, Y.; Kiwada, H. Intracellular control of gene trafficking using liposomes as drug carriers. *Eur. J. Pharm. Sci.* **2001**, 13, 85-89.

(24) Zelphati, O.; Szoka, F. C., Jr. Intracellular distribution and mechanism of delivery of oligonucleotides mediated by cationic lipids. *Pharm. Res.* **1996**, 13, 1367-1372.

(25) Zuhorn, I. S.; Kalicharan, R.; Hoekstra, D. Lipoplex-mediated transfection of mammalian cells occurs through the cholesterol-dependent clathrin-mediated pathway of endocytosis. *J. Biol. Chem.* **2002**, 277, 18021-18028.

(26) Zelphati, O.; Szoka, F. C., Jr. Mechanism of oligonucleotide release from cationic liposomes. *Proc. Natl. Acad. Sci. USA* **1996**, 93, 11493-11498.

(27) Gordon, S. P.; Berezhna, S.; Scherfeld, D.; Kahya, N.; Schwille, P. Characterization of interaction between cationic lipid-oligonucleotide complexes and cellular membrane lipids using confocal imaging and fluorescence correlation spectroscopy. *Biophys. J.* **2005**, 88, 305-316.

(28) Fattal, E.; Couvreur, P.; Dubernet, C. "Smart" delivery of antisense oligonucleotides by anionic pH-sensitive liposomes. *Adv. Drug Deliver. Rev.* **2004**, 56, 931-946.

(29) Zuhorn, I. S.; Bakowsky, U.; Polushkin, E.; Visser, W. H.; Stuart, M. C. A.; Engberts, J. B. F. N.; Hoekstra, D. Nonbilayer phase of lipoplex-membrane mixture determines endosomal escape of genetic cargo and transfection efficiency. *Mol. Ther.* **2005**, 11, 801-810.

(30) Uchiyama, H.; Hirano, K.; Kashiwasake-Jibu, M.; Taira, K. Detection of Undegraded Oligonucleotides *in Vivo* by Fluorescence Resonance Energy Transfer. *J. Biol. Chem.* **1996**, 271, 380-384.

(31) Woolf, T. M.; Jennings, C. G. B.; Rebagliati, M.; Melton, D. A. The Stability, Toxicity and Effectiveness of Unmodified and Phosphorothioate Antisense Oligodeoxynucleotides in Xenopus Oocytes and Embryos. *Nucleic Acids Res.* **1990**, 18, 1763-1769.

(32) Hogrefe, R. I. An antisense oligonucleotide primer. *Antisense Nucleic Acid Drug Dev.* **1999**, 9, 351-357.

(33) Godbey, W. T.; Wu, K. K.; Mikos, A. G. Poly(ethylenimine) and its role in gene delivery. *J. Control. Release* **1999**, 60, 149-160.

(34) Bieber, T.; Meissner, W.; Kostin, S.; Niemann, A.; Elsasser, H. Intracelullar route and transcriptional competence of polyethylenimine-DNA complexes. *J. Control. Release* **2002**, 82, 441-454.

(35) Godbey, W. T.; Wu, K. K.; Mikos, A. G. Tracking the intracellular path of poly(ethylenimine)/DNA complexes for gene delivery. *Proc. Natl. Acad. Sci. USA* **1999**, 96, 5177-5181.

(36) Pollard, H.; Remy, J. S.; Loussouarn, G.; Demolombe, S.; Behr, J. P.; Escande, D. Polyethylenimine but not cationic lipids promotes transgene delivery to the nucleus in mammalian cells. *J. Biol. Chem.* **1998**, 273, 7507-7511.

(37) Honore, I.; Grosse, S.; Frison, N.; Favatier, F.; Monsigny, M.; Fajac, I. Transcription of plasmid DNA: Influence of plasmid DNA/polyethylenimine complex formation. *J. Control. Release* **2005**, 107, 537-546.

Chapter 6

INTRACELLULAR FATE AND BIOLOGICAL ACTIVITY OF ANTISENSE OLIGONUCLEOTIDES DELIVERED BY PEGYLATED LIPOSOMES

Parts of this chapter were published in:

Remaut, K.; Lucas, B.; Braeckmans, K.; Demeester, J.; De Smedt, S. C. *J. Control. Release* **2007**, 117, 256-266.

ABSTRACT

Liposomal vesicles have been widely investigated as carriers for the intracellular delivery of oligonucleotides (ONs). To avoid aspecific uptake by the reticulo endothelial system, 'pegylation' of the liposomes, by incorporating polyethyleneglycol (PEG) at the surface, has been an attractive strategy. While pegylation has a clear benefit on the systemic level, one could wonder whether pegylation also benefits the delivery efficacy of liposomes at the intracellular level. In this chapter, we followed the intracellular distribution of pegylated liposomes, with special attention to the integrity of the ONs they were carrying. We found that pegylated liposomes failed in protecting the phosphodiester ONs (PO-ONs) they carried, leading to rapid degradation of the PO-ONs in the endosomal compartment. Nuclease resistant phosphothioate ONs (PS-ONs) stayed intact in the intracellular environment. However, both for PO-ONs and PS-ONs, the PEG-chains at the surface of the pegylated liposomes inhibited the endosomal escape of the ONs. These intracellular findings explain why pegylated liposomes failed in establishing an antisense effect, both with nuclease sensitive PO-ONs and nuclease resistant PS-ONs.

Chapter 6

Intracellular Fate and Biological Activity of Antisense Oligonucleotides Delivered by Pegylated Liposomes

INTRODUCTION

The potential of antisense therapeutics lies in the simple mechanism where one needs only to know the sequence of the mRNA of interest to design the appropriate complementary oligonucleotide (ON) that can down-regulate the production of the corresponding protein. The antisense approach shows clear potential in the treatment of cancer and viral infections [1]. However, to adequately deliver antisense ONs into cells, the search for suitable delivery systems continues. Cationic liposomes are widely investigated as antisense ONs carriers. There is currently a fair idea on which parameters are crucial in the delivery of ONs by cationic liposomes [2]. First, the positive charge on the polar head group of the cationic lipids is important for binding the negatively charged ONs. Also, the liposome/ON complexes ('lipoplexes') ideally exhibit a net positive charge both to prevent their rapid aggregation and to promote their binding to the negatively charged cell membranes. Second, the features of the alkyl chains play an important role in the organization of the lipoplexes. To promote the endosomal escape of the lipoplexes, a cone-like lipid (with a small head group and expanding alkyl chains) should be incorporated in the liposomes. Cone-like lipids, such as dioleoylphosphatidylethanolamine (DOPE) can adopt a hexagonal phase that disturbs the endosomal membrane thereby provoking endosomal escape [3].

While a net positive charge may enhance cell membrane binding of the lipoplexes, it is well known that *in vivo* positively charged lipoplexes may bind to negatively charged serum components. This eventually leads to aggregation of the lipoplexes and opsonization by the reticulo endothelial system [4]. To overcome the rapid clearance of lipoplexes, polyethyleneglycol (PEG) bearing lipids have been incorporated in the liposomes to provide the lipoplexes with a PEG-shield at the surface. The so-called 'stealth' lipoplexes indeed

show a prolonged stability and circulation in the bloodstream [5]. Interestingly, our research group recently demonstrated that the pegylation of lipoplexes also positively influences their behavior in extracellular matrices like vitreous and sputum [6;7]. The pegylated lipoplexes retained their mobility in the vitreous, while the non-pegylated lipoplexes aggregate and get stuck in the collagen fiber network of the vitreous [6]. Also upon exposure to Cystic Fibrosis sputum the non-pegylated lipoplexes aggregate, which significantly decreases their gene transfection activity. On the contrary, pegylated lipoplexes retain their gene transfection activity after exposure to Cystic Fibrosis sputum [7].

Clearly, pegylation 'guides' lipoplexes in a more effective way through the extracellular compartments of the body. On the contrary, pegylation appears to decrease the transfection efficiency of lipoplexes once they go on to the intracellular level. Deshpande *et al.* reported that pegylation lowers the cellular interaction and uptake of the lipoplexes [8]. Song *et al.*, however, found that the cellular uptake of pegylated lipoplexes was unaltered and suggested that the inhibitory effect of pegylation is situated at the step of the endosomal escape [9]. Also in this chapter, we observed that pegylation lowers the transfection efficiency of DOTAP/DOPE liposomes carrying nuclease resistant phosphothioate ONs (PS-ONs) or nuclease sensitive phosphodiester ONs (PO-ONs).

For successful antisense delivery, the carriers should protect the ONs against extra- and intracellular nucleases. In Chapter 3, we found that PO-ONs complexed to non-pegylated liposomes were adequately protected against enzymatic degradation [10]. In Chapter 5, however, we observed that this protection against enzymatic degradation was not translated into a biological effect of the PO-ONs. This was attributed to the fact that the PO-ONs were rapidly degraded in the intracellular environment upon release of the non-pegylated liposomes [11]. Also in Chapter 3, we demonstrated that PO-ONs complexed to pegylated lipoplexes could still be degraded, demonstrating their accessibility to nucleases [10]. A major aim of this chapter was to elucidate how pegylation of lipoplexes influences their intracellular behavior and biological activity, with the focus on the intracellular degradation of the ONs they are carrying. Therefore, A549 cells were transfected with pegylated liposomes containing fluorescently double-labeled PO-ONs or PS-ONs and the intracellular distribution and degradation of the complexed ONs was followed by means of Fluorescence Correlation Spectroscopy (FCS) and confocal imaging.

MATERIALS AND METHODS

Materials

For the ICAM-1 antisense assay a non-labeled 20 mer phosphodiester oligonucleotide (PO20-ON; Isis1939: 5'-CCC-CCA-CCA-CTT-CCC-CTC-TC-3') and its phosphothioate analogue (PS20-ON) were used. As a control, a 20 mer phosphothioate ON without anti-ICAM-1 activity was used (5'GAG-ACT-TTC-ACT-TTT-CTC-TA 3'). In the FCS experiments and confocal imaging a fluorescent 40 mer phosphodiester ON (PO40-ON; 5'-GCC-GTC-TCT-GAC-TGC-TGA-TGA-CTA-CTA-TCG-TAT-AGT-GCG-G-3') and the fluorescent equivalent of PS20-ON were used. The fluorescent ONs were double-labeled with a rhodamine green fluorophore at the 3' end (λ_{ex} = 488 nm, λ_{em} = 532 nm) and a Cy5 fluorophore at the 5' end (λ_{ex} = 647 nm, λ_{em} = 670 nm). All ONs were purchased from Eurogentec (Seraing, Belgium) and were PAGE-purified by the supplier.

The cationic phospholipid DOTAP (N-(1-(2,3-dioleoyloxy)propyl)-N,N,N-trimethyl-ammoniumchloride), the neutral phospholipid DOPE (dioleoylphosphatidylethanolamine) and the pegylated (neutral) phospholipid DSPE-PEG (distearoylphosphatidylethanolamine (polyethyleneglycol 2000)) were purchased from Avanti® Polar Lipids (Alabaster, AL, USA).

Human lung carcinoma cells (A549 cells, ATCC number: CCL-185) (DSMZ, Braunschweig, Germany) were cultured in Dulbecco's modified Eagle's medium (DMEM) without phenol red (Gibco, Merelbeke, Belgium) containing 2 mM glutamine, 10% heat deactivated fetal bovine serum (FBS) and 1% penicillin-streptomycin at 37°C in a humidified atmosphere containing 5% CO_2.

Preparation of Liposomes and Lipoplexes

The pegylated and non-pegylated liposomes were prepared as described in Chapter 3. The hydrodynamic size and zeta potential of the pegylated and non-pegylated liposomes was routinely checked in 20 mM HEPES buffer (pH 7.4) by respectively dynamic light scattering (DLS, Malvern 4700, Malvern, Worcestershire, UK) and surface potential measurements (Zetasizer 2000, Malvern, Worcestershire, UK), as previously described [12], and equaled 128 $\pm$ 6 nm and +18 $\pm$ 3 mV for the pegylated liposomes and 126 $\pm$ 7 nm and +45 $\pm$ 4 mV for the non-pegylated liposomes.

For the preparation of lipoplexes, the ONs (stock solution in water) and the liposomes (stock solution in 20 mM HEPES, pH 7.4) were diluted in 'degradation buffer' (20 mM HEPES, 110 mM potassium acetate and 2 mM magnesium acetate, pH 7.4). The pegylated lipoplexes used in the FCS and confocal imaging experiments were prepared by mixing

15 µL of the pegylated liposome dispersion (400 µM for complexation with PO40-ONs or 200 µM for complexation with PS20-ONs) and 15 µL of fluorescently double-labeled PO40-ONs or PS20-ONs (2 µM), resulting in a +/- ratio of 5 (being the ratio of the number of positive charges, originating from the liposomes, to the number of negative charges, originating from the ONs). The resulting dispersion was vortexed for 10 seconds and the lipoplexes were allowed to equilibrate for 30 minutes at room temperature prior to use. Then, 120 µL DMEM was added before transferring the pegylated lipoplex dispersion to A549 cells grown to 90% confluency on glass-bottomed cover slips (Part No. PG-1.5-14-F, Glass bottom No. 1.5, MatTek Corporation). After 4 hours incubation at 37°C and 5% CO_2, the cells were washed and incubated further in DMEM containing 2 mM glutamine, 10% heat deactivated FBS and 1% penicillin-streptomycin. Confocal imaging and FCS measurements were performed 2, 4, 8, 12 and 24 hours after applying the pegylated lipoplex dispersion to the A549 cells as described below.

For the determination of the ICAM-1 antisense activity, pegylated or non-pegylated lipoplexes were prepared by mixing 80 µL of the pegylated or non-pegylated liposome dispersion (400 µM) and 80 µL of PO20-ONs, PS20-ONs or the control ON (4 µM), resulting in a +/- ratio of 5. The resulting dispersion was vortexed for 10 seconds and the lipoplexes were allowed to equilibrate for 30 minutes at room temperature prior to use. The antisense activity was determined as described in Chapter 5.

Confocal Imaging and Fluorescence Correlation Spectroscopy (FCS)

Confocal imaging and dual-color FCS experiments were performed on a LSM510 confocal laser scanning microscope equipped with a Confocor2 module (Carl Zeiss, Jena, Germany). The excitation light of the argon-ion laser (488 nm, 30 mW) and/or the helium-neon laser (633 nm, 5 mW) was reflected by a dichroic mirror (HFT 488/633) and focused through a Zeiss C-apochromat 40x, NA 1.2 water immersion objective into the sample. The fluorescence emission was re-collected by the same objective and split by another dichroic mirror (NFT 635) into the green detector (after passing a 505-550 bandpass filter) or into the red detector (after passing a 650 longpass filter). The fluorescence emission was detected by photon multipliers in the case of confocal imaging and avalanche photodiodes in the case of FCS.

In dual-color FCS measurements two ultrasensitive avalanche photodiode detectors monitor in time (typically for 5-10 seconds) respectively the red and green fluorescence in the detection volume of the microscope. The red and green fluorescence fluctuates as the dual-labeled molecules (ONs in this thesis) move in and out the detection volume. From these fluorescence intensity fluctuations auto-correlation curves can be derived that allow

calculating both the amount of fluorescent molecules in the detection volume and their diffusion time, being the average time it takes them to diffuse through the excitation volume. The dual-color FCS system was calibrated using rhodamine green based on the method of Schwille *et al.* [13].

To assure that we only analyzed vital cells, propidium iodide as a counterstain for dead cells was applied to the transfected cells immediately prior to microscopy. Before performing intracellular dual-color FCS measurements, first a confocal image of the cell was taken. Subsequently we indicated on the confocal image the locations in the cytoplasm and/or the nucleus where dual-color FCS measurements had to be performed. At these spots, the green and red fluorescence intensities were recorded with laser excitation set to 488 nm. From the fluorescence fluctuations, the ratio of the red to green fluorescence (R/G ratio) was calculated. The auto-correlation curves as obtained by the FCS instrument were not further analyzed.

Detection of Intact and Degraded ONs in A549 Cells

In the intact fluorescently double-labeled ONs, Fluorescence Resonance Energy Transfer (FRET) occurs between rhodamine green (donor fluorophore) and Cy5 (acceptor fluorophore) [14]. As illustrated in Figure 1, upon excitation at 488 nm laser light, in intact ONs the energy is transferred from the rhodamine green to the Cy5 fluorophore. This turns the ONs more red fluorescent while they become less green fluorescent. In other words, due to FRET the ratio of the red to green fluorescence (R/G ratio) increases and becomes higher than 1 in the ONs used in this thesis (see Table 1 in Chapter 5). When the ONs degrade, the distance between the both fluorophores increases and FRET no longer occurs (Figure 1). Hence, the R/G ratio drops (< 1) (see Table 1 in Chapter 5). To detect whether ONs were intact or degraded in the cells, the intracellular green and red fluorescence was determined by the detectors of both the FCS setup and the confocal microscope, using 488 nm excitation light as described above.

We showed in Chapter 2 that FRET occurs more efficiently in the double-labeled PO40-ONs than in the double-labeled anti-ICAM-1 PO20-ONs [14]. Consequently, monitoring the intracellular degradation of the PO40-ONs by FRET is more straightforward than following the degradation of the PO20-ONs. Therefore, in the intracellular confocal imaging and FCS measurements we preferred to make use of pegylated liposomes containing double-labeled PO40-ONs in stead of double-labeled PO20-ONs, although the PO40-ONs do not have an intracellular target. It should be noted, however, that the intracellular confocal imaging and FCS measurements on cells transfected with pegylated liposomes containing double-labeled PO20-ONs showed the same results as depicted for the PO40-ONs.

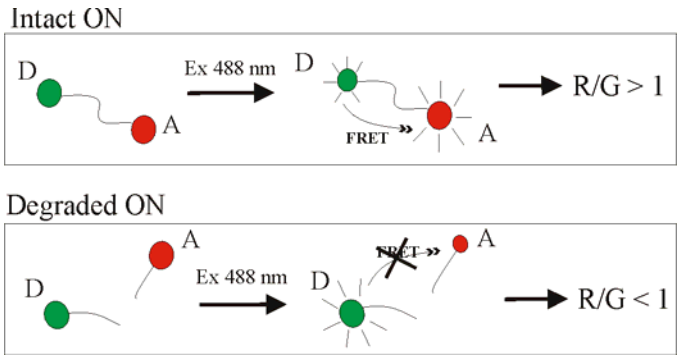

Figure 1. FRET as a tool to detect intact and degraded ONs upon excitation at 488 nm. (D) Rhodamine green, donor fluorophore, (A) Cy5, acceptor fluorophore and (R/G) ratio of the red to green fluorescence. In the intact ONs, FRET occurs which results in a R/G ratio that is higher than 1. When the ONs degrade, FRET no longer occurs and the R/G ratio drops to a value lower than 1.

RESULTS

Antisense Activity of PO-ONs and PS-ONs delivered by Pegylated and Non-Pegylated Liposomes

Figure 2 shows the antisense activity obtained using anti-ICAM-1 ONs with either a nuclease sensitive phosphodiester backbone (PO-ONs) or a nuclease resistant phosphothioate backbone (PS-ONs). When naked PO-ONs or PS-ONs were administered to the A549 cells, no antisense activity was observed. Indeed, the level of expression of the ICAM-1 protein equaled the one in the A549 cells that were treated with the naked control ONs. When PO-ONs or PS-ONs were complexed with non-pegylated liposomes, the PS-ONs but not the PO-ONs were able to down-regulate the ICAM-1 expression. Indeed, with the PS-ONs the ICAM-1 expression was about 45% lower than the one found in A549 cells treated with non-pegylated liposomes containing the control ONs. On the contrary, when PO-ONs or PS-ONs were complexed with pegylated liposomes, neither formulation was able to realize a substantial antisense effect: when compared to the ICAM-1 expression of A549 cells treated with pegylated liposomes containing the control ONs, the decrease in the ICAM-1 expression was less than 20%.

In Chapter 5, the biological activity of non-pegylated lipoplexes was correlated with the intracellular distribution and degradation of the delivered ONs, as studied by FCS and confocal imaging. In this chapter, we aimed to elucidate why pegylated liposomes failed in establishing an antisense effect, both with nuclease sensitive PO-ONs and nuclease resistant PS-ONs.

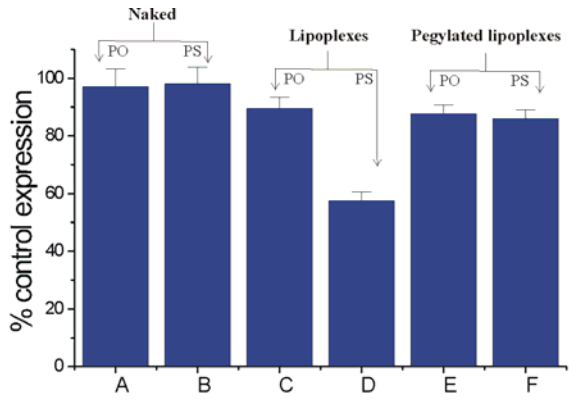

Figure 2. Antisense activity of (A) naked PO20-ONs, (B) naked PS20-ONs, (C, D) respectively PO20-ONs and PS20-ONs complexed to non-pegylated liposomes and (E, F) respectively PO20-ONs and PS20-ONs complexed to pegylated liposomes. The antisense activity is depicted as the percentage of ICAM-1 expression when compared to A549 cells that were treated with the corresponding formulation containing the control ONs (e.g. naked or complexed to non-pegylated or pegylated liposomes) as described in the Materials and Methods section. The +/- ratio of the lipoplexes was 5. The antisense activity represents the average of three independent experiments.

Intracellular Fate of PO-ONs Delivered by Pegylated Liposomes

A549 cells were transfected with pegylated liposomes containing double-labeled PO40-ONs (PO40-PEG-LPXs). The intracellular green and red fluorescence was studied by confocal imaging and the FCS setup, using 488 nm excitation light. In that case, the red fluorescence comes from excitation of the Cy5 fluorophores due to FRET.

Figure 3A-2h shows that fluorescent nuclei were not observed following the transfection of A549 cells with pegylated liposomes. When FCS measurements were performed in the nuclei of the cells, the fluorescence intensity equaled the autofluorescence of the nuclei (5-10 kHz), confirming the absence of PO40-ONs. Alternatively, mainly green fluorescent spots are observed in the cytoplasm of the transfected cells (Figure 3A-2h). Intracellular, red fluorescent spots do not appear, demonstrating the absence of FRET and thus the degradation of the PO40-ONs. Red fluorescence can, however, be clearly detected in the PO40-PEG-LPXs outside the A549 cells, flanking the plasma membrane (Figure 3B-2h). The discrepancy between the green fluorescence inside and the red fluorescence outside the cells can also be clearly seen in the merged image (Figure 3C-2h). From the fluorescence measured in the cytoplasm of the transfected cells (which was 10-100 fold higher than the autofluorescence of the cells) an average R/G ratio of 0.5 $\pm$ 0.1 was calculated. This in contrast to the average R/G ratio measured in the PO40-PEG-LPXs flanking the plasma membrane, which was 5.6 $\pm$ 0.6. Taken together, these observations suggest that the PO40-ONs degrade as soon as the pegylated lipoplexes have entered the cells.

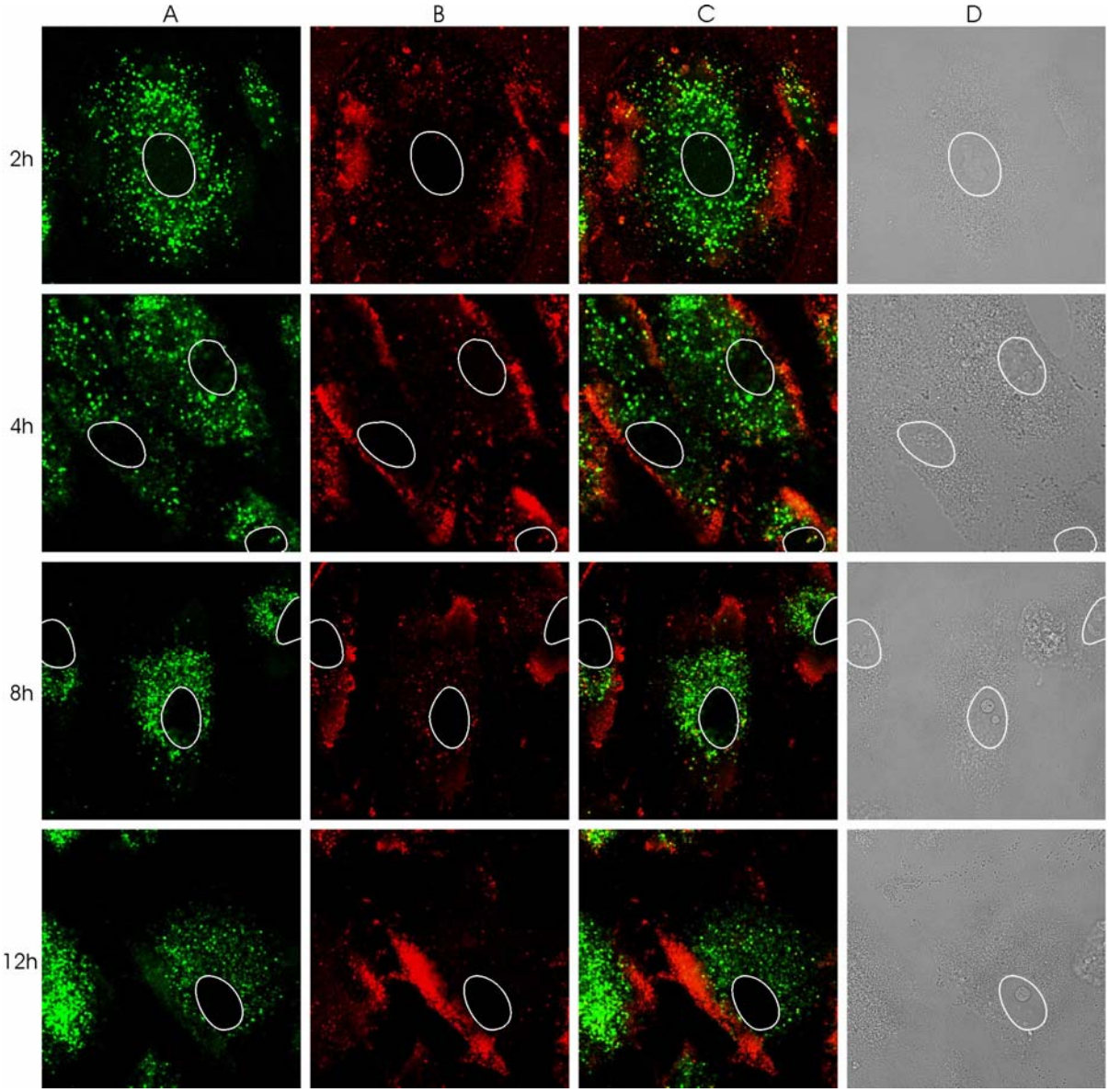

Figure 3. Green (A), red (B) and merged (C) confocal images of A549 cells respectively 2, 4, 8 and 12 hours after transfection with P040-PEG-LPXs. As excitation light of 488 nm was used, the red fluorescence in B comes from Cy5 excitation due to FRET. In the transmission images (D) a circle was drawn around the nuclei (as also around the non-fluorescent nuclei in A, B and C).

At longer incubation times the intracellular disposition did not change: green fluorescence was found in cytoplasmic dots, whereas red fluorescence could only be detected in the pegylated lipoplexes outside the cells (Figure 3A, B and C – 4, 8 and 12h). Also, free PO40-ONs were never detected in the nuclei of the transfected cells, as the fluorescence in the nuclei as detected by FCS never exceeded the autofluorescence of the cells. Since the detectors of the FCS instrument are highly sensitive and can even detect single molecules, this truly indicates that free PO40-ONs never reached the nuclei of the A549 cells.

Intracellular Fate of PS-ONs Delivered by Pegylated Liposomes

Subsequently, A549 cells were transfected with pegylated liposomes containing double-labeled PS20-ONs (PS20-PEG-LPXs). As for the PO40-PEG-LPXs, the intracellular green and red fluorescence was studied by confocal imaging and the FCS setup, using 488 nm excitation light (Figure 4). In that case, the red fluorescence comes from excitation of the Cy5 fluorophores due to FRET.

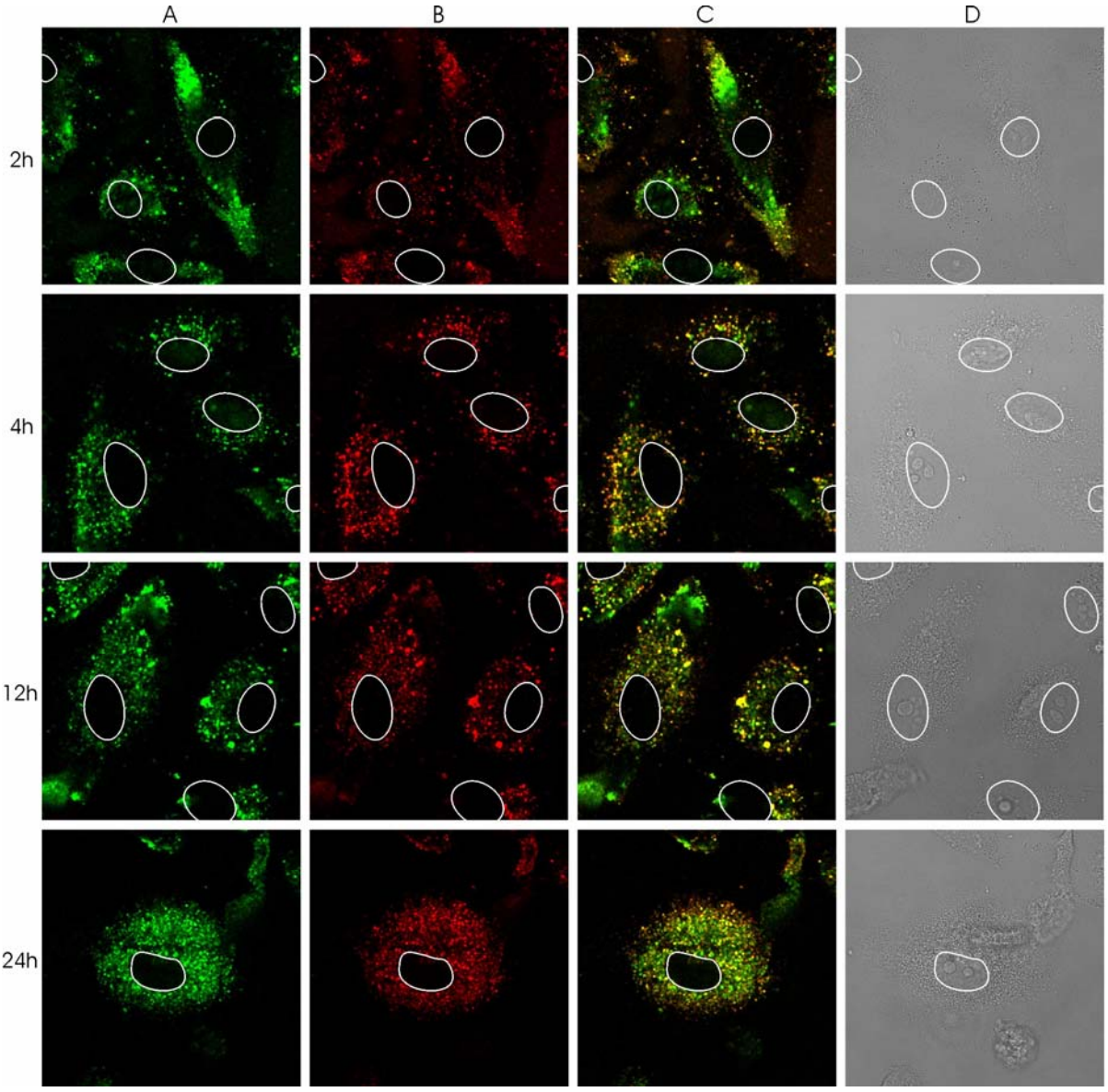

Figure 4. Green (A), red (B) and merged (C) confocal images of A549 cells respectively 2, 4, 12 and 24 hours after transfection with PS20-PEG-LPXs. As excitation light of 488 nm was used, the red fluorescence in B comes from Cy5 excitation due to FRET. In the transmission images (D) a circle was drawn around the nuclei (as also around the non-fluorescent nuclei in A, B and C).

When the A549 cells were transfected with PS20-PEG-LPXs, again no fluorescence was detected in the nuclei of the cells (Figure 4-2h). As for the PO40-ONs, FCS

measurements pointed out that the nuclear fluorescence equaled autofluorescence (5 to 10 kHz), confirming that the PS20-ONs delivered by the pegylated lipoplexes did not reach the nuclei of the cells. Instead, the fluorescence was mainly located in punctated structures in the cytoplasm of the cells. The amount of intracellular fluorescent vesicles increased when increasing the incubation time from 2 to 4 hours, indicating further intracellular uptake of the PS20-PEG-LPXs (Figure 4-2h and 4h). In contrast to PO40-ONs delivered by pegylated lipoplexes, the red fluorescent dots in Figure 4B and the yellow fluorescent dots in the merged image (Figure 4C) suggest that, at all incubation times, FRET occurs and the cytoplasmic structures contain intact PS20-ONs. This was confirmed by intracellular FCS measurements since the average R/G ratio as measured in the cytoplasm of the cells equaled 2.3 $\pm$ 0.3 which corresponds to intact PS20-ONs (see Table 1 in Chapter 5). The R/G ratio of intact PS-ONs reflects a lower FRET efficiency when compared to intact PO40-ONs (R/G 5.6 $\pm$ 0.6). This explains why the intact PS-ONs also appear in the green confocal image, while intact PO40-ONs mainly appear in the red confocal image. This also explains why intact PS-ONs appear yellow in the merged confocal image (Figure 4C) while the intact PO40-ONs appear bright red in the merged confocal image (Figure 3C). As for the PO40-ONs delivered by pegylated lipoplexes, the intracellular distribution of PS20-ONs delivered by pegylated lipoplexes did not change upon longer incubation times: green and red fluorescence was detected in cytoplasmic structures, whereas free PS20-ONs were not detected in the nuclei of the cells, not even 24 hours following the delivery of the PS20-ONs using pegylated liposomes.

DISCUSSION

A major aim in this chapter was to obtain a better insight in the intracellular path of ONs delivered by pegylated liposomes. Therefore, we determined the biological effect of the antisense molecules and their intracellular distribution and degradation when delivered by pegylated liposomes. To fully comprehend the effect of pegylation, the biological effect and the intracellular distribution and degradation of antisense molecules delivered by non-pegylated liposomes was also studied, as described in Chapter 5.

Explanation of the Biological Activity of Pegylated Lipoplexes Based on their Intracellular Fate and Structural Properties

In contrast to non-pegylated lipoplexes rather few studies, if any, describe the mechanism behind the formation of pegylated lipoplexes (PEG-LPXs). In Chapter 3, we

proposed a mechanism for the formation of PEG-LPXs in which the ONs are present on the outside of the pegylated lipoplexes, rather than on the inside. Based on the architecture of the PEG-LPXs we define below the intracellular pathway of pegylated liposomes containing PO-ONs or PS-ONs in A549 cells, which explains both their intracellular distribution and degradation as observed in Figure 3 and Figure 4 and their biological behavior as observed in Figure 2. The transfection pathway we propose for PEG-LPXs is depicted in Figure 5A.

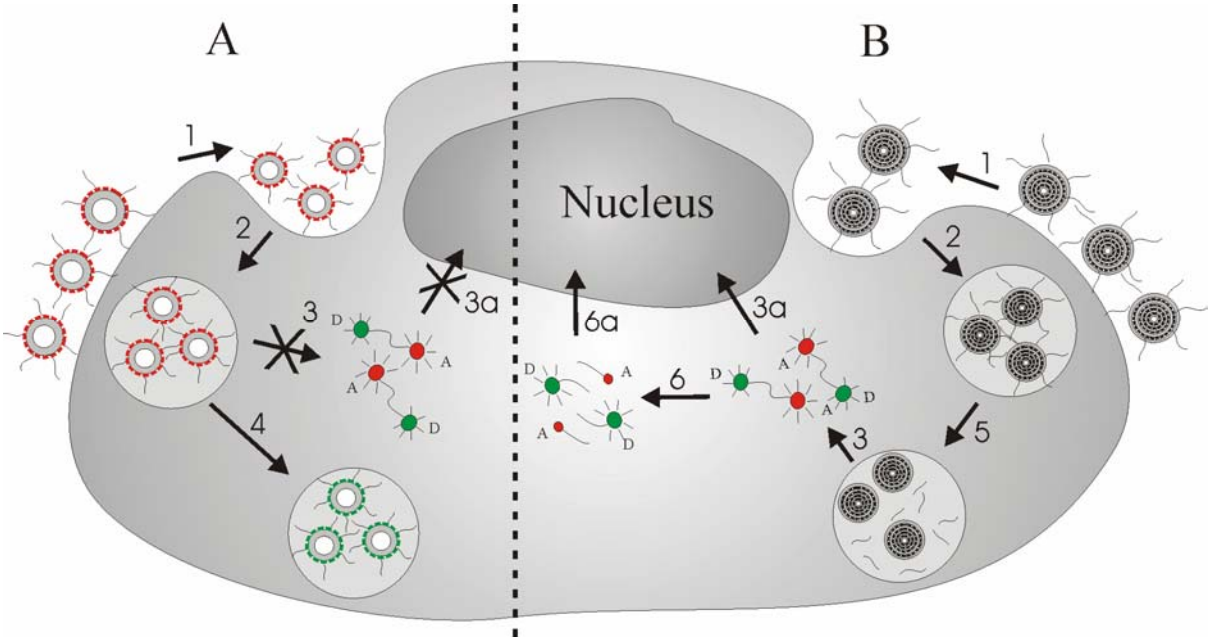

Figure 5. Proposed intracellular pathway of (A) pre-pegylated lipoplexes and (B) post-pegylated lipoplexes containing nuclease sensitive PO-ONs. (1) binding to the cell membrane, (2) internalization by endocytosis, (3) endosomal escape, (3a) nuclear accumulation of intact ONs, (4) degradation in the endosomal compartment, (5) de-pegylation in the endosomal compartment, (6) intracellular degradation of ONs and (6a) nuclear accumulation of degraded ONs.

As for non-pegylated lipoplexes (LPXs), the PEG-LPXs settle on the cell surface and are internalized by endocytosis (Figure 5A, step 1). The term endocytosis covers entry in the cell in a number of ways such as clathrin-dependent endocytosis, clathrin-independent endocytosis (e.g. non-coated vesicles and caveolae), phagocytosis and macropinocytosis. In contrast to LPXs, the endocytic mechanism that is involved in the uptake of the PEG-LPXs is not yet demonstrated. It could well be that the reduced charge of the PEG-LPXs influences the uptake pathway, however, the influence of charge on the mechanism of endocytosis remains to be elucidated. Following endocytosis, the PEG-LPXs are present in the early endosomes (Figure 5A, step 2), which can either recycle their cargo to the extracellular environment or mature to late endosomes. The late endosomes on their turn deliver their cargo to the lysosomes. As for the LPXs, the PEG-LPXs have to escape from the endosomal compartment and release their ONs in the cytoplasm of the cells in order to exert

an antisense effect. At this stage, however, the PEG-chains prevent close contact between the lipids from the PEG-LPXs and the endosomal membrane. Therefore, in contrast to LPXs, DOPE is not able to destabilize the endosomal membrane and the ONs are not released into the cytosol of the cells, precluding their delivery to the nucleus (Figure 5A, step 3 and 3a). Instead, the ONs remain entrapped in the endosomal compartment. As in PEG-LPXs the ONs are located at the surface and are thus unprotected against nucleases, the PO-ONs in the endosomes become degraded while the nuclease resistant PS-ONs remain intact (Figure 5A, step 4). The entrapment of the ONs in the endosomal compartment is in agreement with the fact that fluorescent nuclei were not observed in A549 cells transfected with PEG-LPXs (Figure 3 and 4) and explains why PEG-LPXs were not able to establish an antisense effect, neither with PO-ONs nor with PS-ONs (Figure 2). Furthermore, the intracellular degradation of PO-ONs could clearly be seen from the numerous green fluorescent dots in the cytoplasm in Figure 3, when compared to the green and red fluorescent dots that indicated the presence of intact PS-ONs in the cytoplasm of the cells in Figure 4. Since the PO-ONs remained intact in the pegylated lipoplexes outside the cells, this demonstrates that degradation only occurred after cellular entry of the PEG-LPXs. Up to our knowledge, this is the first time that the endosomal degradation of PO-ONs delivered by pegylated liposomes was demonstrated this clearly. Also, the observed intracellular behavior of PEG-LPXs agrees well with the mechanism for PEG-LPXs formation as proposed in Chapter 3.

Future Strategies in the Pegylation of Liposomes

The fact that PEG-chains at the surface of the PEG-LPXs prevent endosomal escape has been reported before by, among others, Meyer *et al.*, Shi *et al.* and Song *et al.* [9;15;16]. Up to our knowledge, we were the first, however, to demonstrate that the PO-ONs are not protected against degradation, even when complexed to the PEG-LPXs. Based on the relation between the 'pre-pegylated' lipoplex structure and the lack of protection against enzymatic degradation, we suggest that the following strategies could be of interest in the design of pegylated liposomes for ON delivery and other nucleic acids based therapeutics such as siRNA and plasmid DNA.

First, 'post-pegylation' should be considered to avoid degradation of the complexed ONs. LPXs should be prepared using non-pegylated liposomes (so that the ONs become entrapped between the lipid bilayers) with subsequent pegylation of the preformed LPXs. Second, the PEG-chains should be removable in the endosomal compartment in order to allow endosomal escape. Guo *et al.* calculated that lipid mixing could be initialized if the amount of PEG-lipid in the LPXs is less than 2.3 $\pm$ 0.6 mol% [17]. Therefore, lowering the

amount of PEG-lipid on the liposomes' surface could improve the endosomal escape and hence the biological activity of the ONs delivered by pegylated liposomes. To be able to remove the PEG-chains on the liposomes' surface two strategies are commonly used. One approach makes use of PEG-lipids where a pH sensitive group links the PEG to the lipid. The PEG chains are then removed in the endosomal compartment due to acidic-catalyzed hydrolysis [18-20]. Another approach is the use of exchangeable PEG-lipids such as PEG-ceramides [21]. The rate of PEG-ceramide removal from the LPXs depends on the size of the PEG moiety as well as on the acyl chain length. It should be noted that there is a possibility that 'post-pegylation' with removable PEG-derivates will not significantly improve the biological activity of PO-ONs complexed to cationic lipids. Indeed, as for the LPXs and the PEG-LPXs, the post-pegylated LPXs are expected to bind to the cell membrane and to be internalized by endocytosis (Figure 5B, step 1 and 2). Then, removal of the PEG-chains should occur in the endosomal compartment (Figure 5B, step 5). Subsequently, endosomal escape is expected to occur with release of the PO-ONs in the cytoplasm of the cells (Figure 5B, step 3). As this endosomal escape of the PO-ONs will be most likely followed by their rapid intracellular degradation (Figure 5B, step 6), mainly degraded PO-ONs are expected to accumulate in the nuclei of the cells (Figure 5B, step 6a). Therefore, it could well be that cationic lipids are mainly useful in the delivery of nuclease resistant ONs such as PS-ONs. However, the question of 'pre-pegylation' versus 'post-pegylation' of liposomes is also highly relevant towards the delivery of other nucleic acid based therapeutics such as siRNA and plasmid DNA.

ACKNOWLEDGEMENTS

Katrien Remaut is a Research Assistant of the Research Foundation - Flanders (Belgium). Kevin Braeckmans is a Postdoctoral Fellow of the Research Foundation - Flanders (Belgium). The financial support of the Research Foundation – Flanders and the BOF Ghent is acknowledged with gratitude. All experimental data were collected at the Advanced Light Microscopy Facility at the European Molecular Biology Laboratory (EMBL), Heidelberg, Germany. The lab of Rainer Pepperkok is gratefully acknowledged for the support during the visit of K. Remaut at the EMBL. The authors would like to thank Leica Microsystems for continuous support of the Advanced Light Microscopy Facility.

REFERENCES

(1) Sazani, P.; Kole, R. Therapeutic potential of antisense oligonucleotides as modulators of alternative splicing. *J. Clin. Invest.* **2003**, 112, 481-486.

(2) Audouy, S.; Hoekstra, D. Cationic lipid-mediated transfection in vitro and in vivo. *Mol. Membr. Biol.* **2001**, 18, 129-143.

(3) Zuhorn, I. S.; Bakowsky, U.; Polushkin, E.; Visser, W. H.; Stuart, M. C. A.; Engberts, J. B. F. N.; Hoekstra, D. Nonbilayer phase of lipoplex-membrane mixture determines endosomal escape of genetic cargo and transfection efficiency. *Mol. Ther.* **2005**, 11, 801-810.

(4) Audouy, S. A. L.; De Leij, L. F. M. H.; Hoekstra, D.; Molema, G. In vivo characteristics of cationic liposomes as delivery vectors for gene therapy. *Pharm. Res.* **2002**, 19, 1599-1605.

(5) Otsuka, H.; Nagasaki, Y.; Kataoka, K. PEGylated nanoparticles for biological and pharmaceutical applications. *Adv. Drug Deliver. Rev.* **2003**, 55, 403-419.

(6) Peeters, L.; Sanders, N. N.; Braeckmans, K.; Boussery, K.; de Voorde, J. V.; De Smedt, S. C.; Demeester, J. Vitreous: A barrier to nonviral ocular gene therapy. *Invest. Ophth. Vis. Sci.* **2005**, 46, 3553-3561.

(7) Sanders, N. N.; De Smedt, S. C.; Cheng, S. H.; Demeester, J. Pegylated GL67 lipoplexes retain their gene transfection activity after exposure to components of CF mucus. *Gene Ther.* **2002**, 9, 363-371.

(8) Deshpande, M. C.; Davies, M. C.; Garnett, M. C.; Williams, P. M.; Armitage, D.; Bailey, L.; Vamvakaki, M.; Armes, S. P.; Stolnik, S. The effect of poly(ethylene glycol) molecular architecture on cellular interaction and uptake of DNA complexes. *J. Control. Release* **2004**, 97, 143-156.

(9) Song, L. Y.; Ahkong, Q. F.; Rong, Q.; Wang, Z.; Ansell, S.; Hope, M. J.; Mui, B. Characterization of the inhibitory effect of PEG-lipid conjugates on the intracellular delivery of plasmid and antisense DNA mediated by cationic lipid liposomes. *Biochim. Biophys. Acta* **2002**, 1558, 1-13.

(10) Remaut, K.; Lucas, B.; Braeckmans, K.; Sanders, N. N.; Demeester, J.; De Smedt, S. C. Protection of oligonucleotides against nucleases by pegylated and non-pegylated liposomes as studied by Fluorescence Correlation Spectroscopy. *J. Control. Release* **2005**, 110, 209-223.

(11) Remaut, K.; Lucas, B.; Braeckmans, K.; Sanders, N. N.; Demeester, J.; De Smedt, S. C. Delivery of phosphodiester oligonucleotides: Can DOTAP/DOPE liposomes do the trick? *Biochemistry* **2006**, 45, 1755-1764.

(12) Lucas, B.; Van Rompaey, E.; De Smedt, S. C.; Demeester, J.; Van Oostveldt, P. Dual-color FFS to study the complexation between poly-l-lysine and oligonucleotides. *Macromolecules* **2002**, 35, 8152-8160.

(13) Schwille, P.; Meyer-Almes, F.; Rigler, R. Dual-Color Fluorescence Cross-Correlation spectroscopy for multicomponent diffusional analysis in solution. *Biophys. J.* **1997**, 72, 1878-1886.

(14) Remaut, K.; Lucas, B.; Braeckmans, K.; Sanders, N. N.; De Smedt, S. C.; Demeester, J. FRET-FCS as a tool to evaluate the stability of oligonucleotide drugs after intracellular delivery. *J. Control. Release* **2005**, 103, 259-271.

(15) Meyer, O.; Kirpotin, D.; Hong, K.; Sternberg, B.; Park, J. W.; Woodle, M. C.; Papahadjopoulos, D. Cationic liposomes coated with polyethylene glycol as carriers for oligonucleotides. *J. Biol. Chem.* **1998**, 273, 15621-15627.

(16) Shi, F.; Wasungu, L.; Nomden, A.; Stuart, M. C. A.; Polushkin, E.; Engberts, J. B. F. N.; Hoekstra, D. Interference of poly(ethylene glycol)-lipid analogues with cationic-lipid-mediated delivery of oligonucleotides; role of lipid exchangeability and non-lamellar transitions. *Biochem. J.* **2002**, 366, 333-341.

(17) Guo, X.; Mackay, J. A.; Szoka, F. C. Mechanism of pH-triggered collapse of phosphatidylethanolamine liposomes stabilized by an ortho ester polyethyleneglycol lipid. *Biophys. J.* **2003**, 84, 1784-1795.

(18) Masson, C.; Garinot, M.; Mignet, N.; Wetzer, B.; Mailhe, P.; Scherman, D.; Bessodes, M. pH-sensitive PEG lipids containing orthoester linkers: new potential tools for nonviral gene delivery. *J. Control. Release* **2004**, 99, 423-434.

(19) Guo, X.; Szoka, F. C. Steric stabilization of fusogenic liposomes by a low-pH sensitive PEG-diortho ester-lipid conjugate. *Bioconjug. Chem.* **2001**, 12, 291-300.

(20) Boomer, J. A.; Inerowicz, H. D.; Zhang, Z. Y.; Bergstrand, N.; Edwards, K.; Kim, J. M.; Thompson, D. H. Acid-triggered release from sterically stabilized fusogenic liposomes via a hydrolytic dePEGylation strategy. *Langmuir* **2003**, 19, 6408-6415.

(21) Rejman, J.; Wagenaar, A.; Engberts, J. B. F. N.; Hoekstra, D. Characterization and transfection properties of lipoplexes stabilized with novel exchangeable polyethylene glycol-lipid conjugates. *BBA-Biomembr.* **2004**, 1660, 41-52.

Chapter 7

INFLUENCE OF PLASMID DNA TOPOLOGY ON THE TRANSFECTION PROPERTIES OF DOTAP/DOPE LIPOPLEXES

Parts of this chapter were published in:

Remaut, K.; Sanders, N. N.; Fayazpour, F.; Demeester, J.; De Smedt, S. C. *J. Control. Release* **2006**, 115, 335-343.

ABSTRACT

Plasmid DNA (pDNA) can occur in the compact supercoiled (SC) form, the relaxed open circular (OC) form and the linearized form. In this chapter, we investigated the transfection efficiency of SC, OC and linearized pDNA complexed to DOTAP/DOPE liposomes in Vero cells. Only DOTAP/DOPE liposomes containing SC pDNA showed protein expression while DOTAP/DOPE liposomes loaded with OC or linearized pDNA failed. First we wondered whether the better transfection properties of the SC pDNA containing lipoplexes could be due to a better transcription of SC pDNA in the nuclei of the cells. However, microinjecting naked SC, OC or linearized pDNA in the nuclei of the Vero cells revealed that the transcription efficiency was mainly dependent on the intranuclear concentration of the pDNA, rather than on the pDNA topology. Upon microinjecting comparable concentrations of the pDNA topologies in the cytoplasm, however, the SC topology resulted in a significantly higher transfection, especially in cells that underwent cell division in the period after injection. It appears that, when compared to OC and linearized pDNA, SC pDNA is better suited to reach the nuclei of the cells. When compared to OC pDNA, the nearly two times more rapid diffusion of the SC topology could account for these observations. For the equally rapidly diffusing linearized pDNA, however, most likely the additional susceptibility towards enzymatic degradation by exonucleases explains the superior transfection efficiencies of the SC topology.

Chapter 7

Influence of Plasmid DNA Topology on the Transfection Properties of DOTAP/DOPE Lipoplexes

INTRODUCTION

Gene therapy aims to replace defective genes with the scope to enhance the production of certain proteins. Efficient gene delivery requires the uptake of the plasmid DNA (pDNA) in the target cell, release of the pDNA into the cytoplasm and transport to the nucleus where transcription takes place.

It has been reported that intracellular degradation of the pDNA significantly limits the gene transfer efficiency [1]. There are only a few studies, however, that deal with the nature and the extent of pDNA degradation in the cytosol of the cells. Lechardeur *et al.* estimated the apparent half-life of double-stranded DNA in the cytosol of HeLa cells between 50 and 90 minutes, while Pollard *et al.* showed that the delivery of pDNA in COS-7 and A549 cells was prevented by Ca^{2+}-sensitive nucleases [2;3]. Whether or not the nature of intracellular degradation is similar in different cell types is not clear, mainly due to the limited research in this area. Intracellular degradation is not the only factor influencing the transfection efficiency. Kreiss *et al.* observed that the transfection efficiency depends on the size of the pDNA, making it easier for smaller pDNA copies [4]. This hypothesizes that smaller pDNA copies may diffuse more efficiently through the cytosol to the perinuclear region and/or more efficiently translocate into the nucleus via the pores of the nuclear membrane. Lukacs *et al.* showed that DNA fragments up to 100 bp moved freely in the cytosol of HeLa cells. Upon increasing the pDNA size, the mobility started to decrease and the pDNA fragments became completely immobile in the case of 2000 bp and more [5]. Also, the nuclear membrane is reported as a major barrier in pDNA delivery [6;7]. In non-dividing cells, nuclear import and export takes places via the nuclear pore complexes (NPCs). These NPCs have a cutoff value

of about 9 nm for passive diffusion, which can be enlarged to about 30 nm for active transport mediated by nuclear localization signals (NLS) [8]. The passage of larger pDNA fragments through the nuclear pores can be enhanced by the coupling of a NLS signal to the pDNA, although the nuclear import remains low [9]. The nuclear entry of pDNA is, however, greatly enhanced upon cell division, when the nuclear membrane is temporarily disassembled [10]. Understanding how and to what extent the different intracellular barriers limit the transfection efficiency of pDNA is important to determine strategies to enhance the gene transfer.

Most studies employing pDNA for the transfection of cells use supercoiled (SC) pDNA. Purified pDNA indeed mainly occurs in the compact SC form. It can, however, be converted to open circular (OC) and linearized pDNA by respectively a single- and double-stranded break in the SC pDNA. Up to our knowledge there is only one study, by Cherng *et al.*, that compared the transfection efficiencies of respectively SC, OC and linearized pDNA [11]. Cherng *et al.* delivered the different pDNA topologies with the cationic polymer pDMAEMA and observed that SC pDNA yielded higher transfection efficiencies than its OC or linearized analogue. An explanation for these observations was, however, not given. In this chapter, we were interested to evaluate whether SC pDNA also generated better transfection efficiencies than its OC or linearized analogue when delivered by cationic DOTAP/DOPE liposomes, which is indeed the case. We additionally aimed to understand why SC pDNA is the best topology to transfect cells. Therefore, the degradation and diffusion of the SC, OC and linearized pDNA was evaluated by respectively gel electrophoresis and FCS measurements. Also, the gene expression efficiency was evaluated after microinjecting the different pDNA topologies in the nucleus or the cytoplasm of the cells.

MATERIALS AND METHODS

Plasmid DNA

The gWIZ™ GFP (green fluorescent protein) encoding plasmid (5799 bp) was purchased from Gene Therapy Systems INC. (San Diego, USA). Plasmid DNA was extracted from *E. coli* using the Qiagen plasmid Mega kit (Qiagen Benelux B.V., Venlo, The Netherlands). The pDNA concentrations were determined by UV spectrophotometry at 260 nm. SC pDNA was converted to OC by incubating the SC form for 48 hours at 60°C. To convert the SC pDNA to linearized pDNA, the restriction enzyme XmnI, which has 1 recognition site in a non-encoding region of the gWIZ™ GFP plasmid, was used according to

the manufacturers instructions (Promega, Madison, USA). The topology (SC, OC or linearized) of the pDNA was routinely checked by 1% agarose gel electrophoresis.

Preparation of Liposome/pDNA Complexes

SC, OC or linearized pDNA was complexed to cationic DOTAP/DOPE liposomes. The cationic phospholipid DOTAP (N-(1-(2,3-dioleoyloxy)propyl)-N,N,N-trimethyl-ammoniumchloride) and the neutral phospholipid DOPE (dioleoylphosphatidylethanolamine) were purchased from Avanti® Polar Lipids (Alabaster, AL, USA). The liposomes contained DOTAP and DOPE in a 1:1 molar ratio and were prepared as described in Chapter 3. The hydrodynamic size and zeta potential of the resulting cationic liposomes was routinely checked by respectively dynamic light scattering (DLS, Malvern 4700, Malvern, Worcestershire, UK) and surface potential measurements (Zetasizer 2000, Malvern, Worcestershire, UK), as previously described [12], and equaled respectively 126 $\pm$ 7 nm and +45 $\pm$ 4 mV.

Upon mixing positively charged liposomes with negatively charged pDNA, spontaneously liposome/pDNA complexes (lipoplexes) were formed. The lipoplexes were prepared by mixing equal volumes of a liposome dispersion (5 mM) and a pDNA solution (0.7 µg/µL). The resulting dispersion was vortexed for 10 seconds and the lipoplexes were allowed to equilibrate for 30 minutes at room temperature prior to use. The lipoplexes had a +/- ratio of 2.5, being the ratio of the number of positive charges (originating from the liposomes) to the number of negative charges (originating from the pDNA). Before transferring the lipoplexes to the Vero cells, the lipoplex dispersions were 1:100 diluted in Dulbecco's modified Eagle's medium (DMEM).

Transfection of Vero Cells

Vero cells (African green monkey kidney cells, ATCC number: CCL-81) were cultured in DMEM without phenol red (Gibco, Merelbeke, Belgium) containing 2 mM glutamine, 10% heat deactivated fetal bovine serum (FBS) and 1% penicillin-streptomycin (culture medium) at 37°C in a humidified atmosphere containing 5% CO_2. Prior to transfection, 2.5 x 10^4 cells/cm² were seeded in a 24-well plate and incubated until 80% confluency. Then, the cells were washed twice with phosphate buffer saline (PBS) (Gibco, Invitrogen, Merelbeke, Belgium) and incubated for 4 hours with 500 µL of the above mentioned lipoplex dispersion. After 4 hours, the lipoplexes were removed and the cells were washed twice with PBS. Consequently the cells were incubated for 24 hours in culture medium to allow the production of the GFP. Then, the cells were washed twice with PBS and 100 µL trypsin-EDTA was added to each well to detach the cells from the surface of the wells. After 10

minutes incubation at 37°C, 600 µL PBS was added to each well and the detached cells were transferred into disposable acrylic cuvets. On these samples the fluorescence (due to GFP expression) was measured using excitation and emission wavelengths of respectively 470 and 520 nm, with an Aminco Bowman® Series 2 spectrofluorometer (Spectronic instruments, NY, USA). As a blanc, 100 µL trypsin-EDTA + 600 µL PBS was used.

Microinjection Experiments

Microinjection experiments were performed with a Femtojet® microinjector and an Injectman® NI 2 micromanipulator (Eppendorf, Hamburg, Germany) coupled to a LSM510 confocal laser scanning microscope. Vero cells were grown to 80% confluency on glass-bottomed cover slips (Part No. PG-1.5-14-F, Glass bottom No. 1.5, MatTek Corporation). Injections were performed in the cytoplasm or nucleus of Vero cells, using 0.1, 1, 10 or 100 µg/mL SC, OC or linearized pDNA in water. Injection solutions were supplemented with 2 mg/mL 70 kDa TRITC-dextran to identify the site of injection. After respectively 4 and 24 hours the number of GFP expressing cells was counted and compared to the total number of injected cells. For each concentration and topology, about 100 cells were injected in the nucleus or in the cytoplasm. GFP and TRITC were detected with a SPOT Insight CCD Camera (Diagnostic Instruments) coupled to an epi-fluorescence Eclipse TE300D microscope (Nikon, Japan).

Degradation of SC, OC and Linearized pDNA

pDNA was degraded by incubating pDNA solutions with different concentrations of DNase I (Pulmozyme®, 1 unit/µL, Genentech) or DNase II (bovine spleen, type V, E.C. 3.1.22.1, 4.7 units/µL, Sigma-Aldrich). The pDNA solutions (5 µg/mL) were prepared in a 'degradation buffer' (20 mM HEPES, 110 mM potassium acetate and 2 mM magnesium acetate, pH 7.4) or an acidic buffer (40 mM acetic acid and 60 mM potassium acetate, pH 4.7) for degradation experiments with respectively DNase I and DNase II. 200 µL aliquots of the pDNA solutions were placed in a water bath at 37°C and 2 µL of a chosen enzyme dilution was added. After the appropriate incubation time, the pDNA aliquots were placed on ice and the DNase I or DNase II enzyme was inhibited by addition of 800 µL freshly prepared 'inhibitor solution' (0.1 M iodoacetate, 50 mM EDTA and 10 mM Tris-HCl, pH 7.5). For degradation in cytosolic cell extract, pDNA solutions (5 µg/mL) were mixed with an equal volume of cytosolic cell extract. The cytosolic cell extract was prepared as described in Chapter 2 [13].

Agarose Gel Electrophoresis

To visualize the degradation of pDNA, the pDNA solutions were loaded onto a 1% agarose gel and electrophoresed at 80 V for 45 minutes in TBE buffer (10.8 g/L Tris-base, 5.5 g/L boric acid and 5.8 g/L EDTA, pH 8). Therefore, 35 µL of the pDNA samples was mixed with 5 µL of 'loading buffer' (50% sucrose solution in TBE). pDNA was stained after the run with ethidium bromide and visualized with UV illumination. The agarose gels were further analyzed using ImageJ (Rasband, W.S., ImageJ, U. S. National Institutes of Health, Bethesda, Maryland, USA, http://rsb.info.nih.gov/ij/, 1997-2006).

Fluorescence Correlation Spectroscopy (FCS)

The diffusion coefficient of SC, OC and linearized pDNA was determined by Fluorescence Correlation Spectroscopy (FCS). Therefore, the different pDNA topologies were labeled with Cy5 using the *Label* IT® Cy™5 labeling kit (Mirus Bio Corporation, Madison, USA). To prevent conversion from the SC to OC or linearized forms, the labeling reaction was performed overnight at room temperature. The labeled pDNA was purified by ethanol precipitation, according to the instructions of the manufacturer.

To measure the diffusion coefficient by FCS, the fluorescence intensity fluctuations, caused by the diffusion of fluorescently labeled molecules through the excitation volume of a microscope, are registered. From these fluorescence intensity fluctuations an auto-correlation curve can be derived [14]. The auto-correlation curves $G(\tau)$ were analyzed with the Confocor2 software to calculate the diffusion time τ_t, being the average time the fluorescently labeled molecules need to migrate through the detection volume of the FCS instrument. The auto-correlation curves were always analyzed using both a single-species fit (equation 1 in Chapter 5) and a dual-species fit (equation 2 in Chapter 5) and the sense analysis was retained based on the appearance of the residuals of the fit. From the calculated diffusion time τ_t the diffusion coefficient D was calculated using equation 4 (see Chapter 1).

The FCS experiments were performed on a LSM510 confocal laser scanning microscope equipped with a Confocor2 module (Carl Zeiss, Jena, Germany) using 1 ng/µL Cy5 labeled pDNA solutions. The excitation light of a helium-neon laser (633 nm, 5 mW) was reflected by a dichroic mirror (HFT 488/633) and focused through a Zeiss C-apochromat 40x, NA 1.2 water immersion objective into the sample. The Cy5 fluorescence emission was recollected by the same objective and split by another dichroic mirror (NFT 635) into the red detector (after passing a 650 longpass filter). The fluorescence intensity fluctuations were typically measured for 5 runs of 10 seconds. The FCS instrument automatically generated auto-correlation curves from the registered fluorescence intensity fluctuations. The FCS system was calibrated using rhodamine green based on the method of Schwille *et al.* [15].

RESULTS

Transfection Properties of SC, OC and Linearized pDNA Delivered by Cationic DOTAP/DOPE Liposomes

Figure 1 shows the GFP expression in Vero cells treated with lipoplexes containing respectively SC, OC and linearized pDNA. Only lipoplexes containing SC pDNA resulted in GFP expression. When the lipoplexes contained OC or linearized pDNA, no GFP expression was observed. When DNase I was added to the lipoplexes containing SC pDNA the GFP expression remained, indicating that the lipoplexes well protected the SC pDNA they carried. When naked pDNA was used, no GFP expression was obtained. This was expected as the negatively charged pDNA needs a carrier to efficiently gain access to the intracellular environment.

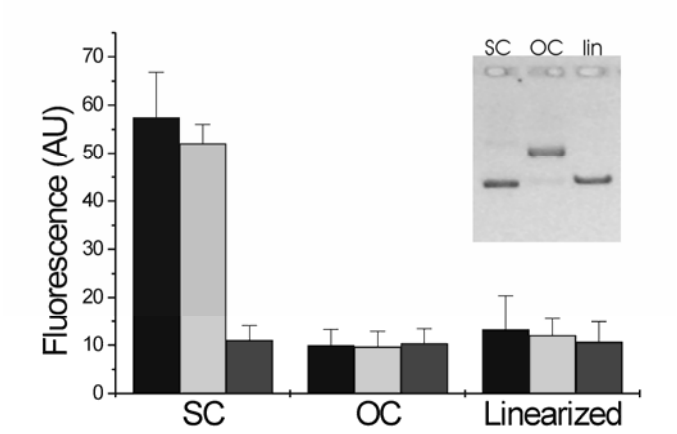

Figure 1. Transfection of Vero cells using respectively SC, OC and linearized pDNA. The Vero cells were exposed to respectively lipoplexes (black bars), lipoplexes to which DNase I was added (light gray bars) and naked pDNA (dark gray bars). The fluorescence is a measure for the expression of the GFP protein. The graph insert shows the outcome of agarose gel electrophoresis on the SC, OC and linearized pDNA samples used in this chapter.

Nuclear Injection of SC, OC and Linearized pDNA

To see whether the nuclear machinery behaves differently with regard to SC, OC and linearized pDNA, the different pDNA topologies were injected in the nuclei of cells and the percentage of GFP expressing cells was counted, respectively 4 and 24 hours after the injection.

Figure 2A and 2B are two examples of Vero cells, successfully injected in the nucleus, that showed GFP expression. When SC or OC pDNA was injected in the nucleus, the percentage of GFP expressing cells was independent on the pDNA topology but did

depend on the concentration of the injected pDNA (Figure 2C). pDNA concentrations of 100, 10 and 1 µg/mL yielded GFP expression in about 90% of the injected cells while the efficiency dropped to about 40% when only 0.1 µg/mL was used. Linearized pDNA (Figure 2C) yielded a slightly lower percentage of GFP expressing cells 4 hours after intranuclear injection when compared to SC and OC pDNA. However, 24 hours after the injection the GFP expression efficiency equaled the efficiency obtained in cells injected with SC or OC pDNA. It should be noted that at higher pDNA concentrations the percentage of GFP expressing cells remained the same. However, the higher the pDNA concentration the brighter the fluorescence of the cells, indicating more GFP expression (data not shown).

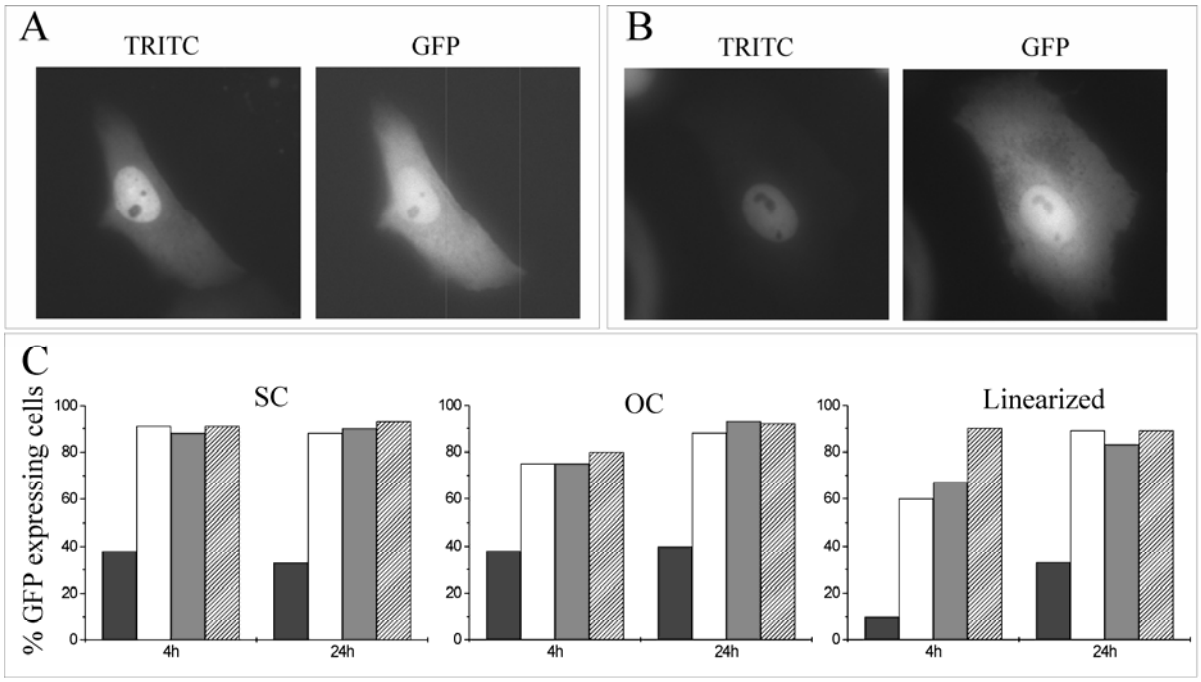

Figure 2. (A and B) Microscopy images of GFP expressing Vero cells which were injected in the nucleus with a pDNA solution containing TRITC-dextran. The TRITC-image points out the site of injection, while the GFP-image points out expression of the pDNA. (C) % of Vero cells expressing GFP respectively 4 and 24 hours after nuclear injection of SC, OC or linearized pDNA. The concentrations of the injected pDNA solutions were 0.1 µg/mL (black bars), 1 µg/mL (white bars), 10 µg/mL (gray bars) or 100 µg/mL (striped bars).

Cytoplasmic Injection of SC, OC and Linearized pDNA

To express GFP, pDNA has to translocate from the cytoplasm into the nucleus of the cells. To see whether SC, OC and linearized pDNA transfect differently after arrival in the cytosol, the pDNA topologies were injected in the cytoplasm of the cells. Respectively 4 and 24 hours after the injection, the GFP expressing cells were counted (Figure 3).

When the GFP expression was evaluated 4 hours after the cytoplasmic injection, only a few of the cells injected with SC or OC pDNA but not with linearized pDNA expressed GFP and only if the highest DNA concentration was used (e.g. 100 µg/mL) (Figure 3C, 4h). This indicates that only few pDNA copies entered the nucleus within this time.

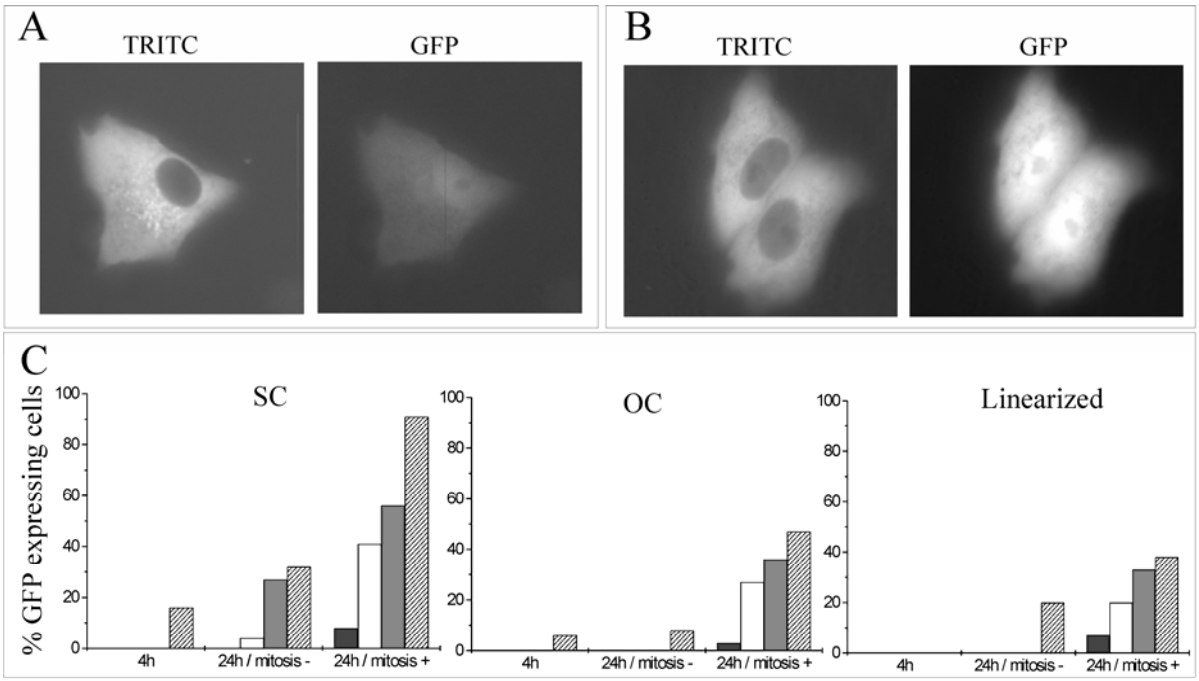

Figure 3. (A and B) Microscopy images of GFP expressing Vero cells which were injected in the cytoplasm with a pDNA solution containing TRITC-dextran, respectively before (A) and after (B) cell division. The TRITC-image points out the site of injection, while the GFP-image points out expression of the pDNA. (C) % of Vero cells expressing GFP respectively 4 and 24 hours after cytoplasmic injection of SC, OC or linearized pDNA. After 24 hours, we discriminated between cells that had not divided (24h/mitosis -) and cells that underwent a cell division (24h/mitosis +). The concentrations of the injected pDNA solutions were 0.1 μg/mL (black bars), 1 μg/mL (white bars), 10 μg/mL (gray bars) or 100 μg/mL (striped bars).

24 hours after the injection GFP expression was observed in both non-divided (e.g. Figure 3A) and divided (e.g. Figure 3B) cells. Importantly, in the non-divided cells SC pDNA was the most efficient in reaching the nucleus (Figure 3C, 24h/mitosis -). For all pDNA topologies, at all concentrations used, a higher number of cells expressed GFP if the cells divided in the 24 hours following the injection (Figure 3C, 24h/mitosis +). Like in non-divided cells, in divided cells SC pDNA resulted in the highest percentage of GFP expressing cells, followed by OC and linearized pDNA. Importantly, cytoplasmic injection of 100 μg/mL SC pDNA solution resulted in GFP expression in 90% of the divided cells, thus reaching the level as observed upon nuclear injection (Figure 2C). With OC and linearized pDNA, this high transfection efficiency was not observed. It should be emphasized that the higher GFP expression by cytosolic SC pDNA delivered by microinjection is in line with the superior transfection properties of SC DNA delivered by lipoplexes as observed in Figure 1.

Degradation of SC pDNA in Cytoplasmic Vero Cell Lysate

To understand why DOTAP/DOPE lipoplexes containing SC pDNA transfect better than the ones containing OC or linearized pDNA, it is important to know if after release from the cationic liposomes in the cytosol SC pDNA remains supercoiled for a sufficiently long

time. Indeed, if SC pDNA would be rapidly converted into OC or linearized pDNA, the SC topology itself could not explain the difference in GFP expression by lipoplexes containing respectively SC, OC and linearized pDNA. SC pDNA can be converted into OC and/or linearized pDNA, depending on the cut profile of the nucleases predominantly present in the cytoplasm of Vero cells. Nucleases which break single-strands will convert SC to OC pDNA while nucleases which break double-strands will convert SC to linearized pDNA.

Figure 4 shows the degradation profile of SC pDNA upon addition of respectively DNase I, DNase II and cytoplasmic Vero cell lysate. DNase I is known to cut only one strand of the double-stranded DNA at a time, thus converting SC pDNA to OC pDNA [16]. Successive single-stranded breaks in the OC pDNA eventually results in the formation of linearized pDNA as can be clearly followed in Figure 4A. On the contrary, DNase II simultaneously cuts both strands of the double-stranded DNA [17;18]. This results in the conversion of SC pDNA into linearized pDNA, without the OC intermediate as can be seen in Figure 4B. Figure 4C shows the degradation of SC pDNA in cytoplasmic Vero cell lysate. We observed that the SC pDNA slowly disappears, accompanied by an increase in the amount of OC pDNA. This allows to conclude that the nucleases in the cytoplasm of Vero cells predominantly exhibit a DNase I-like cut mechanism, resulting in single-stranded breaks in the pDNA. Therefore, upon degradation in the cytoplasm of Vero cells, SC pDNA will initially be converted into the OC topology.

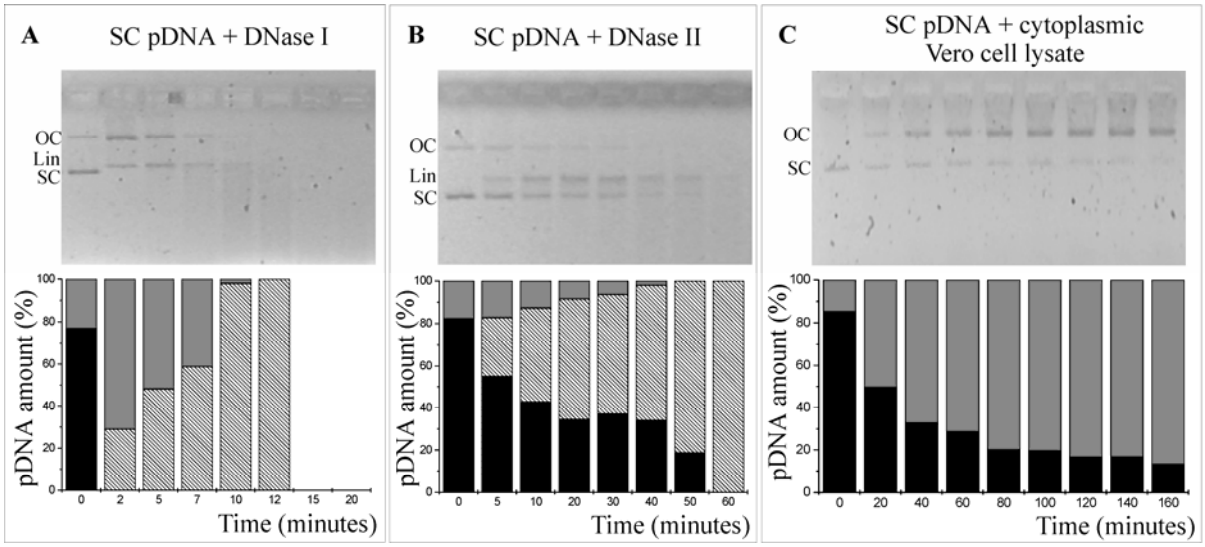

Figure 4. Degradation profiles of SC pDNA upon addition of (A) 0.02 Units DNase I, (B) 0.05 Units DNase II or (C) cytoplasmic Vero cell lysate. The % SC (black bars), OC (gray bars) or linearized (striped bars) pDNA was determined from the agarose gel using Image J.

Degradation of SC pDNA by DNase I

Figure 4A shows that SC pDNA converts into OC pDNA within the first two minutes under the influence of 0.02 Units of DNase I. Since the nucleases in the cytoplasmic Vero cell lysate exhibit a DNase I-like cut mechanism, we were interested to follow the turnover of SC pDNA into the OC topology at a DNase I concentration lower than in Figure 4A. When 2×10^{-4} Units DNase I were used, SC pDNA remained detectable on the agarose gel for 15 minutes after addition of the DNase I enzyme (Figure 5A, black bars). Also, SC pDNA clearly converted into OC pDNA (Figure 5A, gray bars). When $1x\ 10^{-3}$ Units DNase I were used, the SC pDNA was already degraded within the first two minutes (Figure 5B, black bars). Upon longer incubation times, the OC pDNA was further degraded into linearized pDNA, a phenomenon that could only be detected using the higher DNase I concentration (Figure 5B, striped bars). Comparing Figure 5 and Figure 4C, we can conclude that the DNase I-like nuclease activity in the cytoplasm of Vero cells is rather moderate. Indeed, although a substantial part of the SC pDNA molecules have been converted into the OC topology after 1 hour, a significant number of SC pDNA molecules remain to exist in the cytoplasmic Vero cell lysate.

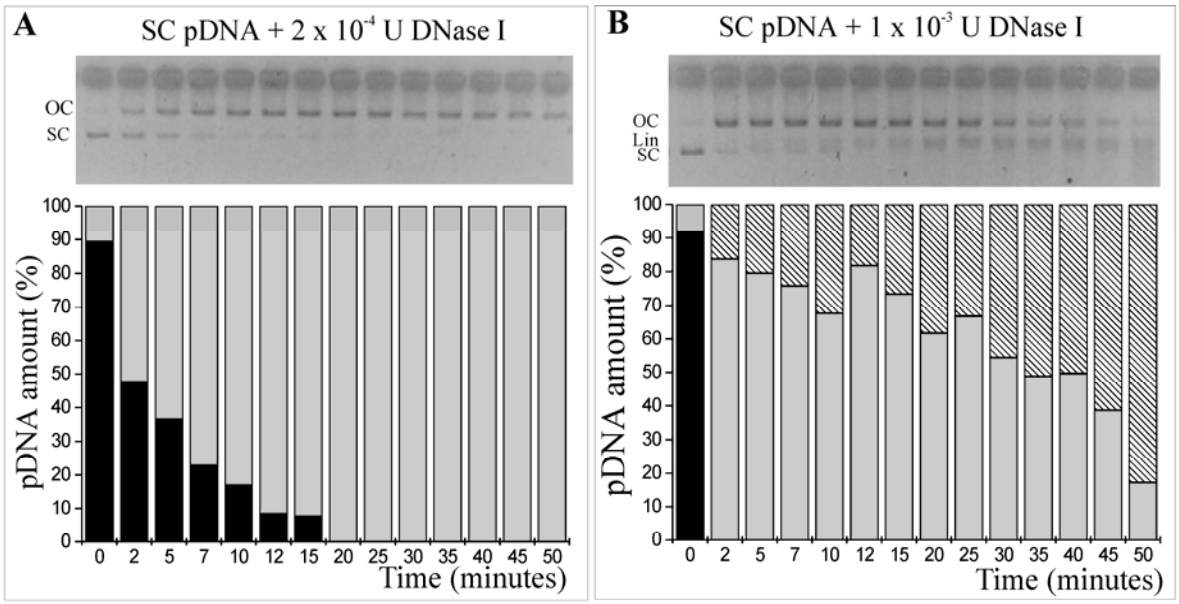

Figure 5. Degradation of SC pDNA using (A) 2×10^{-4} and (B) 1×10^{-3} Units DNase I. The % of SC (black bars), OC (gray bars) and linearized (striped bars) pDNA was calculated from the agarose gel using Image J.

Size of SC, OC and Linearized pDNA

Besides degradation, also the size of the pDNA may influence the amount of intact pDNA that reaches the cell nucleus. Using the Stokes-Einstein equation, the size of the different pDNA topologies was determined from their diffusion coefficient as measured in

buffer by FCS. Figure 6 shows the auto-correlation curves. They were best fitted with a dual-species fit, which indicates that the Cy5 labeled pDNA solutions contained two populations with a distinct diffusion coefficient, namely slowly diffusing Cy5 labeled pDNA molecules and rapidly diffusing remaining free Cy5 fluorophores. SC and linearized pDNA had a similar diffusion coefficient of respectively $1.91 \pm 0.06 \times 10^{-12}$ m²/s and $1.86 \pm 0.04 \times 10^{-12}$ m²/s (the black and green auto-correlation curves in Figure 6A almost completely overlap), while OC pDNA diffused about 1.8 times slower with a diffusion coefficient of $1.05 \pm 0.02 \times 10^{-12}$ m²/s (the red auto-correlation curve in Figure 6A declines more slowly). The slower diffusion of OC pDNA indicates a larger hydrodynamic radius as calculated from the Stokes-Einstein equation, namely 207 ± 4 nm when compared to 114 ± 4 nm and 117 ± 3 nm for respectively SC and linearized pDNA.

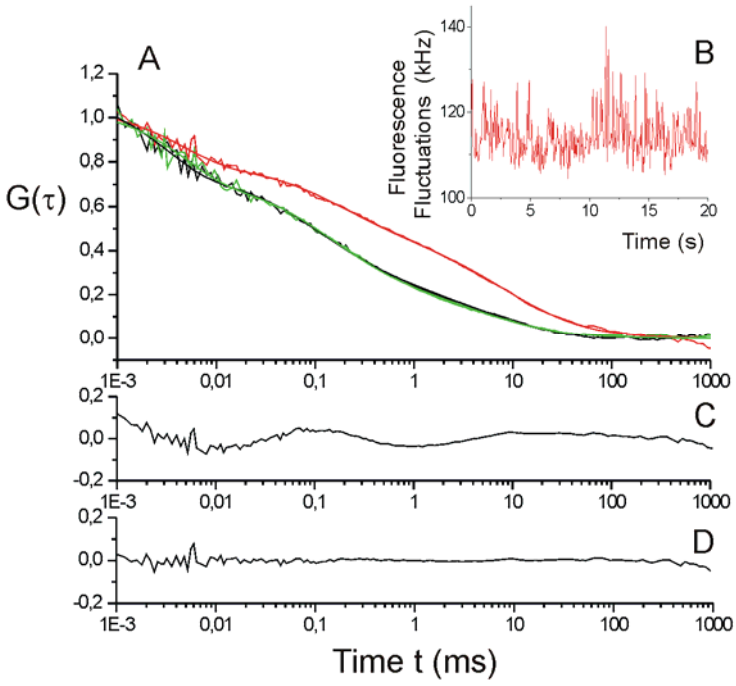

Figure 6. (A) Auto-correlation curves and dual-species fit as obtained from FCS measurements on Cy5-labeled SC (black), OC (red) or linearized (green) pDNA. Representative fluorescence fluctuations are shown in (B). (C) and (D) show the residuals of the fit after fitting the auto-correlation data of OC pDNA with respectively a single-species fit (C) and a dual-species fit (D). The residuals of the fit for SC or linearized pDNA were similar as for OC pDNA and show that the data were best fitted with a dual-species fit.

DISCUSSION

Plasmid DNA can occur in the compact supercoiled (SC) form, the relaxed open circular (OC) form and a linearized form. Although all three pDNA topologies have the same primary structure, we observed that SC pDNA complexed to cationic DOTAP/DOPE

liposomes yields significantly higher transfection than its OC or linearized analogue. Also Cherng *et al.* has observed that SC pDNA results in better transfection than OC or linearized pDNA upon delivery of the pDNA using the cationic polymer pDMAEMA [11]. Understanding why cationic liposomes with SC pDNA transfect better may help us in further improving the outcome of (non-viral) pDNA therapies.

One hypothesis to explain the better transfection properties of SC pDNA containing lipoplexes could be that SC pDNA is more efficiently transcribed than OC and linearized pDNA. However, upon injection of the different pDNA topologies in the nuclei of Vero cells we found that the concentration of the pDNA rather than the pDNA topology determined the level of GFP expression (Figure 2C). Indeed, the nuclear microinjection experiments showed that there is no substantial difference in transfection efficiency of SC, OC and linearized pDNA at comparable intranuclear concentrations, especially at longer incubation times. The reason for the lower level of GFP expression by lipoplexes containing OC and linearized pDNA should thus be found outside the cell nuclei, namely in the cytoplasmic barriers that prevent OC and linearized pDNA, and to a lesser extent SC pDNA, to reach and enter the cell nucleus in an intact way.

The amount of pDNA that reaches the cells nucleus is influenced by the amount of pDNA that is present in the cytoplasm of the cells. Indeed, Figure 3C shows that for all the pDNA topologies, the amount of GFP expressing cells increases upon microinjection of higher concentrations of pDNA in the cytoplasm of the cells. The higher expression by SC pDNA containing lipoplexes, compared to the ones containing OC or linearized pDNA (Figure 1), could be due to a higher cytosolic concentration of pDNA when SC pDNA lipoplexes are used. This on its turn could result from a higher intracellular uptake of the SC/lipoplexes and/or a better release of the SC topology from the lipoplexes in the cytoplasm of the cells. However, even at comparable intracellular concentrations, naked SC pDNA appears to be more efficient in reaching the nuclear machinery from the cytoplasmic compartment when compared to naked OC and linearized pDNA (Figure 3C). Indeed, microinjecting the same concentration of SC, OC and linearized pDNA in the cytosol of the Vero cells yields higher transfection efficiencies when SC pDNA is used, both in non-divided and divided cells. This indicates that not only the intracellular concentration upon delivery, but also the topology of the pDNA in the cytosol influences the gene expression efficiency. The fact that SC pDNA, present in the cytosol, shows better transfection may result from (a) a better stability of SC pDNA in the cytoplasm of the cells, (b) a faster diffusion of SC pDNA towards the nuclei of the cells and/or (c) a more efficient entry into the nuclei of the cells.

Up to our knowledge, the turnover of SC, OC and linearized pDNA into 'non-transfecting' degradation products is not well documented. In other words, it is unclear whether, when SC pDNA is used, biologically active DNA remains present in the cytosol for a

significant long time. We observed that the nucleases in the cytosolic cell extract of Vero cells predominantly degrade SC pDNA into the OC topology, thus revealing a single-stranded cut mechanism. It should be emphasized that one single-stranded cut is sufficient to relax SC pDNA to OC pDNA, while OC pDNA needs successive single-stranded breaks to be converted into linearized pDNA. For example, Figure 5B shows that in buffer with 1 x 10^{-3} Units DNase I it takes only 2 minutes for SC pDNA to be converted into the OC topology, while it takes a significantly longer time for OC pDNA to further degrade into linearized pDNA. From this point of view, SC pDNA has a shorter half-life (when defined as keeping its topology) when compared to OC pDNA. It is, however, important to note that while the presence of the SC topology guarantees transcriptionally active pDNA molecules, the OC topology does not necessarily imply that the pDNA remained transcriptionally active. Successive single-stranded breaks in the OC pDNA sequence could indeed affect the transcription efficiency without affecting the pDNA topology. Unfortunately, at the moment it is unclear how many single-stranded cuts the OC pDNA can bear before it becomes transcriptionally inactive.

Lechardeur *et al.* estimated the apparent half-life of SC pDNA between 50 and 90 minutes [2]. This is well in agreement with the disappearance of SC pDNA in the presence of cytoplasmic Vero cell lysate as observed from agarose gel electrophoresis in Figure 4C. The SC pDNA molecules (which need only a single nuclease attack to convert to OC) remained detectable on the agarose gel for a substantial time, thus indicating only a moderate nuclease activity in the cytoplasm of the Vero cells. As SC pDNA molecules are not immediately degraded in the cytoplasm of Vero cells, we hypothesize that the better transfection efficiency of SC pDNA (when compared to OC and linearized pDNA) may be related to a faster diffusion of SC pDNA towards the nuclei of the cells and/or a more efficient entry into the nuclei of the cells during the time SC pDNA molecules remain present in the cytoplasm of the Vero cells.

It has been shown that higher transfection efficiencies are achieved with smaller pDNA molecules [4;19], which was attributed to a better diffusion through the cytoplasm of the cells or an enhanced uptake through the nuclear pore complexes. One could suggest that the more compact SC pDNA could more easily pass the pores in the nuclear membrane. From diffusion measurements, however, we calculated a hydrodynamic radius of about 210 nm for the OC pDNA and about 115 nm for the SC and linearized topologies. When compared to the maximal size of the nuclear pore complexes, which is about 30 nm in the case of active transport, it seems rather unlikely that either one of the pDNA topologies used in this chapter could make it through the nuclear pore complexes. There are, however, several studies which demonstrate that larger DNA fragments (> 2000 bp) can make it through the nuclear pore complexes [20-22]. The effect of the pDNA topology on the

translocation of the pDNA molecules has not been reported before. We observed that SC pDNA is apparently more efficient in passing the nuclear pore complexes than OC or linearized pDNA, since SC pDNA and to a lesser extent OC and linearized pDNA generated GFP expression in at least some of the non-divided cells injected in the cytoplasm (Figure 3C (4h and 24h, mitosis -)).

An important observation was that the transfection efficiency significantly increased upon cell division of the cells injected in the cytoplasm (Figure 3C), a phenomenon which has been reported before [6;23]. During cell division, the nuclear membrane of a parent cell is temporarily broken down and restored in the two daughter cells. This gives the pDNA in the parent cell the opportunity to be enclosed in the nuclear environment of the two daughter cells without the need to pass the nuclear pore complexes. Nuclear injections pointed out that the level of GFP expression is dependent on the amount of pDNA in the nucleus rather than on the pDNA topology. Also, Figure 3C (24h/mitosis +) pointed out that following microinjection in the cytosol, SC pDNA is the most efficient in generating GFP expression. Together, these observations indicate that a higher amount of intact SC pDNA molecules is able to enter the nucleus upon cell division, when compared to OC and linearized pDNA. In our opinion this indicates that more SC pDNA was present around the nucleus at the time of cell division, what on its turn suggests that SC pDNA more easily makes its way to the perinuclear region, when compared to the OC or linearized pDNA topology.

The actin cytoskeleton, which has an estimated mesh size of about 100-150 nm, is suggested as the principle determinant of size-dependent DNA mobility [24]. It has indeed been shown that larger DNA fragments (> 2000 basepares) are largely immobile in the cytoplasm of cells [5]. The calculated hydrodynamic radius of OC pDNA used in this chapter was about 210 nm, thus possibly larger than the mesh size of the actin cytoskeleton. In the case of OC pDNA, the lower amount of GFP expressing cells upon cell division could result from an obstructed diffusion of the OC pDNA towards the perinuclear region. SC and linearized pDNA (~ 115 nm) should be equally able to diffuse to the perinuclear region. The stretched linearized pDNA may, however, become more entangled in the actin network slowing down its movement. Also, linearized pDNA is additionally accessible to exonucleases. Both factors could explain why linearized pDNA, when compared to SC pDNA, results in a lower transfection upon cytoplasmic injections (Figure 3C).

Passive diffusion of pDNA molecules through the actin cytoskeleton may not be the only way to reach the perinuclear region. A recent study by Vaughan *et al.* has suggested that the diffusion of pDNA through the cytoplasm is mediated by microtubules, with the involvement of dynein as motor protein [25]. Possibly, SC pDNA makes better use of this transport pathway due to a better diffusion towards the microtubules and/or an increased binding to the microtubules. Also, Salman *et al.* demonstrated that nuclear localization signal

(NLS) peptides improve the transport of the NLS-containing cargo to the nucleus by dynein-dependent motion along microtubules [26]. This, in our opinion, demonstrates the importance of the microtubules in the transfection process, since higher transfection by NLS-coupled pDNA [9;27;28] could actually result from an increased pDNA concentration in the perinuclear region due to this NLS-mediated transport along the microtubules.

When non-viral gene delivery systems are used to deliver plasmid DNA to the intracellular environment, it is clear that the time and place of release of the pDNA will play an important role in generating a therapeutic outcome. Ideally, the delivery system should release the pDNA close to the nuclear membrane. Since the translocation of the pDNA to the cell nucleus is greatly enhanced upon cell division, the time between release of the pDNA and cell division should be as short as possible to avoid degradation of the pDNA in the waiting period. Therefore, delivery systems where the release of pDNA is triggered by cell division could greatly enhance the transfection efficiency. Another approach could be to develop delivery systems that become entrapped in the cell nucleus during cell division and release their pDNA directly in the cell nucleus afterwards. Recently, our laboratory developed nanogels that show potential for that purpose [29]. The biodegradable dextran-based nanogels are designed to slowly degrade in the intracellular environment, thereby releasing their cargo. Ideally, the degradation properties of the nanogels should be such that not yet degraded nanogels become entrapped in the cell nucleus during cell division, followed by degradation of the nanogels and release of the pDNA directly in the cell nucleus. Whether or not such non-viral pDNA carriers will significantly improve the transfection remains to be elucidated.

ACKNOWLEDGEMENTS

N.N. Sanders is a Postdoctoral Fellow of the Research Foundation - Flanders (Belgium). The financial support of this institute is acknowledged with gratitude. FCS measurements were performed at the Advanced Light Microscopy Facility at the European Molecular Biology Laboratory (EMBL), Heidelberg, Germany. The lab of Rainer Pepperkok is gratefully acknowledged for the support during the visit of K. Remaut at the EMBL. Annika De Roo is gratefully acknowledged for here assistance in the practical experiments.

REFERENCES

(1) Glasspool-Malone, J.; Steenland, P. R.; McDonald, R. J.; Sanchez, R. A.; Watts, T. L.; Zabner, J.; Malone, R. W. DNA transfection of macaque and murine respiratory tissue is greatly enhanced by use of a nuclease inhibitor. *J. Gene Med.* **2002**, 4, 323-332.

(2) Lechardeur, D.; Sohn, K. J.; Haardt, M.; Joshi, P. B.; Monck, M.; Graham, R. W.; Beatty, B.; Squire, J.; O'Brodovich, H.; Lukacs, G. L. Metabolic instability of plasmid DNA in the cytosol: a potential barrier to gene transfer. *Gene Ther.* **1999**, 6, 482-497.

(3) Pollard, H.; Toumaniantz, G.; Amos, J. L.; Avet-Loiseau, H.; Guihard, G.; Behr, J. P.; Escande, D. Ca2+-sensitive cytosolic nucleases prevent efficient delivery to the nucleus of injected plasmids. *J. Gene Med.* **2001**, 3, 153-164.

(4) Kreiss, P.; Cameron, B.; Rangara, R.; Mailhe, P.; Aguerre, C. O.; Airiau, M.; Scherman, D.; Crouzet, J.; Pitard, B. Plasmid DNA size does not affect the physicochemical properties of lipoplexes but modulates gene transfer efficiency. *Nucleic Acids Res.* **1999**, 27, 3792-3798.

(5) Lukacs, G. L.; Haggie, P.; Seksek, O.; Lechardeur, D.; Freedman, N.; Verkman, A. S. Size-dependent DNA mobility in cytoplasm and nucleus. *J. Biol. Chem.* **2000**, 275, 1625-1629.

(6) Escriou, V.; Carrière, M.; Bussone, F.; Wils, P.; Scherman, D. Critical assessment of the nuclear import of plasmid during cationic lipid-mediated gene transfer. *J. Gene Med.* **2001**, 3, 179-187.

(7) James, M. B.; Giorgio, T. D. Nuclear-associated plasmid but not cell-associated plasmid is correlated with transgene expression in cultured mammalian cells. *Mol. Ther.* **2000**, 1, 339-346.

(8) Ribbeck, K.; Görlich, D. Kinetic analysis of translocation through nuclear pore complexes. *EMBO J* **2001**, 20, 1320-1330.

(9) Ludtke, J. J.; Zhang, G.; Sebestyen, M. G.; Wolff, J. A. A nuclear localization signal can enhance both the nuclear transport and expression of 1 kb DNA. *J. Cell Sci.* **1999**, 112, 2033-2041.

(10) Brunner, S.; Sauer, T.; Carotta, S.; Cotten, M.; Saltik, M.; Wagner, E. Cell cycle dependence of gene transfer by lipoplex, polyplex and recombinant adenovirus. *Gene Ther.* **2000**, 7, 401-407.

(11) Cherng, J. Y.; Schuurmans-Nieuwenbroek, N. M. E.; Jiskoot, W.; Talsma, H.; Zuidam, N. J.; Hennink, W. E.; Crommelin, D. J. A. Effect of DNA topology on the transfection efficiency of poly((2-dimethylamino)ethyl methacrylate)-plasmid complexes. *J. Control. Release* **1999**, 60, 343-353.

(12) Lucas, B.; Van Rompaey, E.; De Smedt, S. C.; Demeester, J.; Van Oostveldt, P. Dual-color FFS to study the complexation between poly-l-lysine and oligonucleotides. *Macromolecules* **2002**, 35, 8152-8160.

(13) Remaut, K.; Lucas, B.; Braeckmans, K.; Sanders, N. N.; De Smedt, S. C.; Demeester, J. FRET-FCS as a tool to evaluate the stability of oligonucleotide drugs after intracellular delivery. *J. Control. Release* **2005**, 103, 259-271.

(14) Schwille, P. Fluorescence correlation spectroscopy and its potential for intracellular applications. *Cell Biochem. Biophys.* **2001**, 34, 383-408.

(15) Schwille, P.; Meyer-Almes, F.; Rigler, R. Dual-Color Fluorescence Cross-Correlation spectroscopy for multicomponent diffusional analysis in solution. *Biophys. J.* **1997**, 72, 1878-1886.

(16) Sanders NN, De Smedt SC, Demeester J: Deoxyribonuclease I, in McGrath BM, Walsh G (eds): Therapeutic Enzymes. Boca Raton, Taylor & Francis Group, 2006, pp 97-116.

(17) Overbo, K.; Myrnes, B. Deoxyribonuclease II from the Icelandic scallop (Chlamys islandica): Isolation and partial characterization. *Comp. Biochem. Phys. B* **2006**, 143, 315-318.

(18) Ikeda, S.; Takata, N. Deoxyribonuclease II purified from Euglena gracilis SM-ZK, a chloroplast-lacking mutant: comparison with porcine spleen deoxyribonuclease II. *Comp. Biochem. Phys. B* **2002**, 131, 519-525.

(19) Darquet, A. M.; Rangara, R.; Kreiss, P.; Schwartz, B.; Naimi, S.; Delaere, P.; Crouzet, J.; Scherman, D. Minicircle: An improved DNA molecule for in vitro and in vivo gene transfer. *Gene Ther.* **1999**, 6, 209-218.

(20) Dean, D. A. Import of plasmid DNA into the nucleus is sequence specific. *Exp. Cell Res.* **1997**, 2330, 293-302.

(21) Branden, L. J.; Mohamed, A. J.; Smith, C. I. A peptide nucleic acid-nuclear localization signal fusion that mediates nuclear transport of DNA. *Nature Biotechnol.* **1999**, 17, 784-787.

(22) Boulikas, T. Nuclear localization signal peptides for the import of plasmid DNA in gene therapy. *Int. J. Oncol.* **1997**, 301-309.

(23) Wilke, M.; Fortunati, E.; Van Den Broek, M.; Hoogeveen, A. T.; Scholte, B. J. Efficacy of a peptide-based gene delivery system depends on mitotic activity. *Gene Ther.* **1996**, 1133-1142.

(24) Dauty, E.; Verkman, A. S. Actin cytoskeleton as the principal determinant of size-dependent DNA mobility in cytoplasm. *J. Biol. Chem.* **2005**, 280, 7823-7828.

(25) Vaughan, E. E.; Dean, D. A. Intracellular trafficking of plasmids during transfection is mediated by microtubules. *Mol. Ther.* **2006**, 13, 422-428.

(26) Salman, H.; Abu-Arish, A.; Oliel, S.; Loyter, A.; Klafter, J.; Granek, R.; Elbaum, M. Nuclear localization signal peptides induce molecular delivery along microtubules. *Biophys. J.* **2005**, 89, 2134-2145.

(27) Aronsohn, A. I.; Hughes, J. A. Nuclear localization signal peptides enhance cationic liposome-mediated gene therapy. *J. Drug Target.* **1997**, 5, 163-169.

(28) Zanta, M. A.; Belguise, V. P.; Behr, J. P. Gene delivery: A single nuclear localization signal peptide is sufficient to carry DNA to the cell nucleus. *Proc. Natl. Acad. Sci. USA* **1999**, 96, 91-96.

(29) Van Thienen, T. G.; Lucas, B.; Flesch, F. M.; van Nostrum, C. F.; Demeester, J.; De Smedt, S. C. On the synthesis and characterization of biodegradable dextran nanogels with tunable degradation properties. *Macromolecules* **2005**, 38, 8503-8511.

SUMMARY AND GENERAL CONCLUSIONS

SUMMARY AND GENERAL CONCLUSIONS

Several disorders originate from the presence or absence of specific proteins. In antisense therapy, short oligonucleotides (ONs) with a sequence complementary to the target mRNA are administered with the aim to inhibit the production of disease-causing proteins. In this way for example viral infections and cancer can be treated by the inhibition of vital proteins in the viral reproduction process or specific oncogenes respectively. Gene therapy aims to induce protein production by the administration of plasmid DNA (pDNA) that encodes the desired protein. This finds its application in DNA vaccinations or the treatment of genetic disorders such as Cystic Fibrosis. For gene therapy to be successful, the nucleic acids should reach the cytoplasm (in the case of ONs) or the nucleus (in the case of pDNA) of the target cells. Also, the nucleic acids should remain intact as their sequence is necessary to maintain their biological activity.

The broad application of antisense and gene therapy is mainly limited by delivery problems of the nucleic acids. Indeed, naked nucleic acids are prone to degradation, poorly taken up by the target cells or do not reach their target cells at all. Several viral and non-viral vectors are under investigation for the advanced delivery of nucleic acids. Viral vectors provide high transfection efficiencies but can possibly evoke severe immune responses. Non-viral vectors are less expensive, easier and safer to make, but suffer from the limited current transfection efficiencies. As described in **Chapter 1**, non-viral carriers aim to help the nucleic acids to enter their target cells, escape from the endosomal compartment and reach the cytoplasm or the nucleus of the cells. Also, they should protect the nucleic acids against enzymatic degradation during the different steps of the delivery process. In this thesis, we especially focused on the latter barrier: we aimed to elucidate the role of the intracellular degradation of the nucleic acids in limiting their therapeutic effect.

There are only limited methods that allow to follow the on site degradation of nucleic acids in living cells. In **Chapter 2**, we evaluated the use of an advanced light microscopy technique, namely Fluorescence Correlation Spectroscopy (FCS), for that purpose. FCS makes use of very sensitive avalanche photodiode detectors to determine the amount of fluorescently (e.g. green or red) labeled molecules in a small confocal volume and their diffusion characteristics. In 'dual-color' Fluorescence Cross-Correlation Spectroscopy (FCCS), also the amount of fluorescently double-labeled molecules (e.g. green and red) can

be determined. We aimed to apply FCCS to follow the degradation of fluorescently double-labeled ONs by a decrease in the amount of double-labeled molecules when degradation takes place. Also, the shorter degradation products were expected to move more rapidly through the detection volume of the FCS instrument. 20 mer and 40 mer phosphodiester ONs (PO20-ONs or PO40-ONs) and 20 mer phosphothioate ONs (PS20-ONs) were double-labeled with a rhodamine green fluorophore at the 3' end and a Cy5 fluorophore at the 5' end. The degradation of the ONs was followed in buffer after the addition of DNase I, DNase II and cytosolic cell extract, or after microinjecting the ONs in the cytoplasm of living cells. Rather surprisingly, dual-color FCCS was not able to accurately determine the amount of double-labeled ONs in the solution. From the fluorescence fluctuation profiles as registered by the FCS instrument, it could be concluded that Fluorescence Resonance Energy Transfer (FRET) occurred between the rhodamine green and the Cy5 fluorophores. Upon excitation of the rhodamine green, donor fluorophore, part of the excitation energy is transferred to the Cy5, acceptor fluorophore. This results in a decrease of the rhodamine green fluorescence and an increase in the Cy5 fluorescence when compared to the situation in which FRET does not occur. An important condition for proper FCCS measurements is that the fluorescence of one fluorophore is not influenced by the presence or absence of the other fluorophore. In the case of FRET, however, this condition is not fulfilled explaining why FRET between the both fluorophores disturbed the applicability of dual-color FCCS to monitor the time-dependent degradation of the double-labeled ONs.

The occurrence of FRET seemed, however, useful to determine the integrity of the double-labeled ONs in a different way. An important condition for FRET is the close proximity of the rhodamine green, donor fluorophore and the Cy5, acceptor fluorophore, as occurs in the intact ONs. When the ONs are degraded, this condition is no longer fulfilled. The degradation of the ONs and thus the disappearance of FRET could be easily followed by monitoring the ratio of the red, donor fluorescence to the green, acceptor fluorescence (R/G ratio) upon excitation of the rhodamine green fluorophore. The ultrasensitive detectors of the FCS instrument proved to be very accurate in measuring the green and red fluorescence intensities, both in buffer and in living cells. Furthermore, FCS allows monitoring the fluorescence intensities originating from a single molecule. Therefore, the R/G ratio can also be determined in these situations where the concentration of the fluorescent molecules is too low to be detected by conventional fluorescence microscopy, as could occur upon the intracellular delivery of the double-labeled ONs by non-viral gene delivery systems.

In a next step, FCS was applied to study the protection against enzymatic degradation of the double-labeled ONs upon complexation with non-viral carriers such as cationic liposomes and cationic polymers. Upon mixing these cationic carriers with the negatively charged ONs, spontaneously interpolyelectrolyte complexes are formed due to

electrostatic interactions. These complexes are aimed at increasing the uptake and delivery of the ONs in the target cells. Furthermore, the complexed ONs should be protected against enzymatic degradation during the different steps of the delivery process. In **Chapter 3**, double-labeled PO40-ONs were complexed with respectively non-pegylated and pegylated cationic liposomes and their protection against enzymatic degradation was followed by means of the R/G ratio as determined by FCS. Pegylation by the coupling of polyethyleneglycol (PEG) at the surface of the liposomes is a frequently used strategy to improve the extracellular behavior of DNA/liposome complexes (lipoplexes). Pegylation of lipoplexes prevents their aggregation and subsequent opsonization by the reticulo endothelial system thereby preventing their clearance from the bloodstream. Pegylation, however, appears to decrease the efficiency of lipoplexes at the intracellular level. In Chapter 3 we found that pegylation also influences the protection against enzymatic degradation that non-pegylated and pegylated lipoplexes offer to the ONs they are carrying. Non-pegylated lipoplexes initially adequately protected the complexed ONs against enzymatic degradation. This agrees with the mechanism of lipoplex formation as can be found in literature. In a first step, negatively charged ONs bind to the surface of the cationic liposomes. This triggers fusion of different liposomes, resulting in the formation of multilamellar particles in which the ONs are entrapped between the lipid bilayers from the individual liposomes (see Chapter 3, Figure 11A). The ONs are thus shielded from the environment in which the nucleases are present. However, the protection of the ONs against enzymatic degradation decreased as a function of the incubation time (a few hours) of the lipoplexes. From the fluorescence fluctuation profiles, as registered by the FCS instrument, it became obvious that non-pegylated lipoplexes aggregate during prolonged incubation times, accompanied by the gradual release of the ONs as a function of time (see Chapter 3, Figure 8). Therefore, it could be concluded that not the complexed ONs, but the slowly released ONs became accessible to degradation by nucleases.

When pegylated liposomes were used to complex the ONs, initially, a substantial fraction of the ONs became degraded immediately upon exposure of the pegylated lipoplexes to nucleases. This points out that, in contrast to non-pegylated liposomes, the ONs were still accessible to nucleases when complexed to pegylated liposomes. In literature, almost no information is available regarding the mechanism behind the formation of pegylated lipoplexes. Based on experimental evidence, we proposed a mechanism for pegylated lipoplex formation that can account for the observed degradation of the complexed ONs (see Chapter 3, Figure 11B). As occurs in the formation of non-pegylated lipoplexes, the anionic ONs are expected to bind to the cationic surface of the pegylated liposomes due to electrostatic interactions. The PEG-chains at the surface, however, most likely prevent the fusion of different pegylated liposomes and thus the encapsulation of the ONs between

successive lipid-bilayers originating from the individual pegylated liposomes. Therefore, the ONs remain unprotected at the surface of the pegylated liposomes, still accessible to nucleases in the surrounding environment.

Cationic polymers form another class of widely studied non-viral gene delivery systems. Polyethyleneimine (PEI) is such a cationic polymer that is considered as a promising candidate for antisense delivery. Pegylation of PEI is an attractive strategy to improve the solubility of the PEI/DNA complexes (polyplexes), decrease their cytotoxicity and to prevent their aggregation and clearance from the bloodstream. In **Chapter 4** we evaluated whether pegylation of PEI influenced the protection of ONs against enzymatic degradation as offered by the PEI polymers. Therefore, double-labeled PO40-ONs were complexed to respectively PEI and polyethyleneglycol-polyethyleneimine (PEG-PEI) polymers and their protection against enzymatic degradation was followed by means of the R/G ratio as determined by FCS. Both PEI and PEG-PEI initially adequately protected the complexed ONs against enzymatic degradation as more than 70% of the ONs remained intact upon exposing the polyplexes to nucleases. This protection was maintained in the PEI polyplexes during the 30 hours incubation time. In PEG-PEI polyplexes, however, eventually up to 70% of the complexed ONs became degraded during the 30 hours incubation time. As was observed for the cationic lipid-based carriers in Chapter 3, pegylation thus also seemed to decrease the protection efficiency of the cationic polymer-based carriers that were studied in Chapter 4. Again an explanation could be found in the proposed mechanism of complex formation between the ONs and the pegylated and non-pegylated PEI polymers. The polyplexes essentially consist of a core containing multiple ONs and multiple polymer chains, held together by electrostatic interactions. In the case of PEG-PEI, this core is additionally surrounded by a shield of PEG-chains. It seems that both for PEI and PEG-PEI, a fraction of the complexed ONs is situated at the edge of the polyplexes' core, as could be deduced from the initial degradation of the ONs upon exposing the polyplexes to nucleases. In the case of PEG-PEI, however, more ONs seem to become accessible to nucleases as a function of the incubation time. It can be expected that the electrostatic interactions which keep the ONs and the polymer-chains together are constantly broken and reformed, resulting in a continuous reorganization of the polyplexes' core. During this process, ONs from the inner part of the core can supposedly relocate to the edge of the polyplexes' core, where they can interact with nucleases in the surrounding environment. From the fluorescence fluctuation profiles, as registered by the FCS instrument, it could be concluded that the ONs are bound less tightly by the PEG-PEI polymers, when compared to the PEI polymers. As the electrostatic interactions between the ONs and the PEG-PEI polymers seem to be more easily disturbed, this could indicate that the reorganization of the PEG-PEI polyplexes is more pronounced when compared to the PEI polyplexes, leading to more frequent occasions

for the ONs to relocate to the edge of the PEG-PEI polyplexes' core, where they subsequently become the subject of enzymatic degradation.

Chapter 3 and Chapter 4 pointed out that FCS is a valuable tool to study the protection of ONs against enzymatic degradation, both with lipid-based and polymer-based gene delivery systems. Some caution was needed, however, in the interpretation of the R/G ratio derived from the complexed ONs. Upon complexation, multimolecular complexes are formed by the association of different double-labeled ONs and different non-labeled cationic lipids or polymers in the lipoplexes and polyplexes, respectively. Due to the compaction of the ONs, FRET may not only occur between both fluorophores of an individual ON, but possibly also between fluorophores originating from different neighbouring ONs in the complexes. In this case, however, the R/G ratio is not representative for the amount of intact ONs in the complexes as FRET may also occur when the neighbouring ONs are degraded. Another phenomenon that may occur, is the quenching of the rhodamine green and Cy5 fluorescence upon compaction of the ONs, as was seen for the PEI and PEG-PEI polyplexes (see Chapter 4, Figure 4). The nearly complete disappearance of the green and red fluorescence in the polyplexes made the R/G ratio meaningless as a measure for the amount of intact complexed ONs. Both for the lipid-based and polymer-based gene delivery systems as studied in this thesis, the R/G ratio of the complexed ONs was thus no longer correlated with their integrity. When the ONs were displaced from the lipoplexes and polyplexes by the addition of respectively sodiumdodecylsulfate (SDS) and dextran sulfate, however, the correlation between the R/G ratio and the ONs' integrity was restored. Therefore, the ONs were always released from the complexes (after a certain incubation time and inhibition of the nucleases) before interpretation of the R/G ratio.

An important question in this thesis was to what extent the degradation of the DNA molecules, delivered by non-viral carriers, was responsible for limiting their biological effect. In **Chapter 5** we determined the biological activity of ONs with a nuclease sensitive phosphodiester backbone (PO-ONs) or a nuclease resistant phosphothioate backbone (PS-ONs) upon delivery with non-pegylated liposomes. We found that the liposomes failed in generating an antisense effect with PO-ONs, while they succeeded with the chemically modified PS-ONs. The protection of the PO-ONs against enzymatic degradation in the non-pegylated lipoplexes as observed in Chapter 3, did thus not translate into a biological effect of the PO-ONs. In order to explain these observations, double-labeled PO-ONs and PS-ONs were complexed to non-pegylated liposomes and their intracellular distribution and degradation was followed by means of FCS and confocal imaging. Lipoplexes were efficiently taken up by the cells by endocytosis. Consequently, the lipoplexes were present in endosomal vesicles, from which they should escape in order to prevent their degradation in the lysosomal compartment. Also, the complexed ONs should be released in the cytoplasm

of the cells to allow them to execute their antisense effect. Confocal imaging demonstrated that the endosomal escape of the lipoplexes was accompanied by the efficient release of both the PO-ONs and the PS-ONs into the cytoplasm of the cells. Furthermore, the released ONs rapidly accumulated into the cell nucleus. Both FRET imaging and the R/G ratio as determined by FCS pointed out that the released PO-ONs were rapidly degraded, while intact PS-ONs could be detected during at least 8 hours following their delivery. As the complexed PO-ONs seemed to remain intact in the intracellular environment, this pointed out that degradation only occurred after release of the PO-ONs from the non-pegylated lipoplexes. Therefore, we concluded that the protection against enzymatic degradation of PO-ONs as offered by non-pegylated liposomes did not translate into a biological effect due to the too efficient release and subsequent degradation of the PO-ONs at the step of the endosomal escape of the lipoplexes. In the case of PS-ONs, the ONs are not degraded upon release at the time of the endosomal escape, creating a pool of intact, biologically active PS-ONs.

Both PO-ONs and PS-ONs failed in generating an antisense effect when pegylated liposomes were used as a delivery system. In **Chapter 6** the intracellular distribution and degradation of the double-labeled PO-ONs and PS-ONs was followed by FCS and confocal imaging upon their administration to the target cells using pegylated liposomes. As observed for the non-pegylated lipoplexes, the pegylated lipoplexes were efficiently internalized by endocytosis. The pegylated lipoplexes, however, did not succeed in protecting the PO-ONs against enzymatic degradation in the endosomal compartment. This agrees with the structural properties of the pegylated lipoplexes as proposed in Chapter 3, where the ONs are situated at the surface of the pegylated liposomes, unshielded from nucleases present in the intracellular environment. One could thus conclude that degradation of the PO-ONs is responsible for the lack of biological activity. The PS-ONs, however, also failed in generating an antisense effect, although both FCS and confocal imaging clearly demonstrated that the PS-ONs remained intact in the intracellular environment. An explanation for the lack of biological activity could be found in the endosomal escape of the pegylated lipoplexes that failed to occur. The PEG-chains at the surface of the pegylated lipoplexes can be hold responsible for the inhibition of the endosomal escape. It is indeed known that interaction between the lipids from the lipoplexes and the lipids from the endosomal membrane plays an important role in the destabilization of the endosomal membrane and the subsequent release of the complexed DNA molecules in the cytoplasm of the cells. The PEG-chains at the lipoplexes' surface, however, prevent these lipid-lipid interactions. As a consequence, the delivered ONs are trapped in the endosomal compartment, separated from their biological target in the cytoplasm or the nucleus of the cells. This explains why both PO-ONs and PS-ONs failed in generating an antisense effect. The inhibitory effect of pegylation at the

step of the endosomal escape can be overcome by reversible pegylation, where the PEG-chains leave the surface of the lipoplexes in the endosomal compartment. The rapid intracellular degradation of the PO-ONs, however, raises the concern that suitable delivery systems for PO-ONs may not be found. Also, with the recent discovery of small interfering RNA (siRNA), the future interest in antisense therapy with ONs may be questioned. siRNAs are small, double-stranded RNA molecules that, via the 'RNA induced silencing complex' (RISC), result in a very efficient down-regulation of the targeted protein expression. Also, double-stranded siRNAs seem to be much more resistant against enzymatic degradation in the intracellular environment, when compared to the single-stranded PO-ONs. Although the delivery problems with siRNA and antisense ONs are essentially the same, the siRNA field makes rapid progress. This while antisense ONs, that have already been studied for many years, resulted in only a few (rather inefficient) antisense therapeutics that are actually on the market. The increased efficiency of siRNAs, however, also comes with the increased risk of off-target effects. Therefore, it remains to be seen if the therapeutic potential of siRNA will live up to its promise, leaving the well known antisense ONs behind.

In contrast to antisense therapy, gene therapy with plasmid DNA (pDNA) aims to induce novel genes or repair mal-functioning genes. As the sequence of the pDNA is crucial to allow the expression of the encoded proteins, pDNA should remain intact during the delivery process. pDNA can occur in the compact supercoiled (SC) form, the relaxed open circular (OC) form and the linearized form. In **Chapter 7**, we found that mainly the SC topology resulted in gene expression upon delivery with non-pegylated liposomes. Nuclear injections of the different pDNA topologies proved that not the pDNA topology, but rather the concentration of pDNA in the nucleus determined the transcription efficiency. Upon injection in the cytoplasm, however, both the pDNA concentration as well as the topology determined the transfection efficiency. Gene expression was most efficient when using SC pDNA at the highest injection concentration. Furthermore, the amount of transfected cells drastically increased when the cells divided in the period following the injection, indicating that the nuclear membrane was an important barrier in pDNA delivery. As more SC pDNA molecules seemed to reach the nucleus upon cytoplasmic injections, we questioned if a difference in degradation of the pDNA topologies could account for these observations. SC pDNA, however, was degraded at least as rapidly as the OC or the linearized form. In a next step, the diffusion characteristics of the different pDNA topologies were investigated by FCS. The nearly two times slower diffusing OC topology could explain why the faster diffusing SC pDNA molecules were more efficient in reaching the cell nucleus. The diffusion of the linearized pDNA topology did, however, not differ from that observed for the SC pDNA molecules. Therefore, in the case of linearized pDNA, the additional susceptibility towards exonucleases most likely explains the lower transfection efficiency when compared to the SC

form. The observation that nuclear accumulation of pDNA is greatly enhanced during cell division raises the idea that non-viral gene delivery systems that optimally guide their pDNA to the nucleus of the daughter cells during the process of cell division could greatly enhance the level of gene expression. Furthermore, the delivery system should protect the pDNA against enzymatic degradation in the period before cell division occurs. An interesting strategy could be to develop DNA nanoparticles that are entrapped in the nuclei of the daughter cells during cell division. Indeed, after nuclear entrapment, the DNA nanoparticles are expected to release their pDNA directly in the cell nucleus of the daughter cells, thereby avoiding degradation of the pDNA in the cytoplasm and overcoming the need to pass the nuclear membrane.

This thesis demonstrated that FCS measurements can be applied to answer the question why particular non-viral carriers are suitable to induce a biological effect while other carriers fail. Since FCS measurements are performed in a limited confocal volume, many times smaller than the dimensions of a single cell, it mainly generates information on the specific intracellular situation in a well-defined compartment of the cell. This in contrast to conventional microscopy or the more recently developed Single Particle Tracking (SPT) which map the intracellular pathways throughout the entire intracellular environment. It is expected that the combination of conventional microscopy with advanced microscopy systems such as FCS and SPT, each with their own advantages and limitations, will continue to guarantee further breakthroughs in the complex study of the intracellular behavior of non-viral DNA/carrier complexes. The increasing knowledge on the intracellular barriers in antisense- and gene therapy is expected to contribute on its turn to the rational design of a new generation of ‘intelligent’ gene delivery systems.

SAMENVATTING EN ALGEMEEN BESLUIT

SAMENVATTING EN ALGEMEEN BESLUIT

Een waaier van aandoeningen vindt zijn oorsprong in de aan- of afwezigheid van bepaalde proteïnen. Gentherapie wenst op de oorzaak van deze aandoeningen in te werken door de productie van dergelijke proteïnen respectievelijk te inhiberen of te stimuleren. In antisense therapie worden korte, enkelstrengige DNA moleculen (oligonucleotiden (ONs)) toegediend die de juiste sequentie bevatten om de productie van het ongewenste proteïne te verhinderen. Zo kunnen bijvoorbeeld virale infecties worden behandeld door levensnoodzakelijke virale proteïnen stil te leggen. Ook kunnen bepaalde kankers bestreden worden via de inhibitie van kankerspecifieke proteïnen. Bij gentherapie met plasmide DNA (pDNA) worden circulaire, dubbelstrengige DNA moleculen toegediend die de genetische informatie bevatten voor de productie van het gewenste proteïne. Dit vindt zijn toepassing in onder andere DNA vaccinaties en de behandeling van genetische defecten zoals Cystische Fibrose. Aangezien zowel ONs als pDNA inwerken op cellulair niveau, waar de genetische informatie zich bevindt, dienen ze binnenin de doelcellen te geraken vooraleer ze hun functie kunnen uitoefenen. Bovendien dienen deze DNA moleculen intact te blijven aangezien hun sequentie noodzakelijk is voor het bekomen van het gewenste therapeutische effect.

De huidige toepasbaarheid van antisense- en gentherapie wordt voornamelijk gelimiteerd door toedieningsproblemen: naakte DNA moleculen zijn onderhevig aan afbraak, bereiken hun doelcellen niet of worden slechts in geringe mate opgenomen. Verscheidene virale en niet-virale dragers worden onderzocht voor de geavanceerde toediening van DNA moleculen. Alhoewel virale dragers voor een efficiënte toediening van DNA moleculen zorgen, vertonen ze problemen zoals het mogelijks opwekken van een ernstige immuunrespons. Niet-virale dragers daarentegen zijn veiliger en gemakkelijker in gebruik, maar blijken tot op heden onvoldoende efficiënt in het bekomen van een therapeutisch effect. Zoals werd besproken in **Hoofdstuk 1**, wordt van de ideale niet-virale drager verwacht dat hij efficiënt wordt opgenomen in de doelcellen en zijn DNA moleculen vrijstelt in het cytoplasma (voor ONs) of in de kern (voor pDNA) van de cellen. Bovendien dienen de DNA moleculen beschermd te worden tegen afbraak gedurende het volledige toedieningsproces. Het is voornamelijk deze laatste stap die het onderwerp vormt van dit proefschrift: we wensten te achterhalen in welke mate de afbraak van DNA moleculen aan de basis ligt van het uitblijven van een therapeutisch effect.

Er zijn slechts een gering aantal methoden die toelaten om de afbraak van DNA moleculen te volgen in levende cellen. Daarom werd in **Hoofdstuk 2** de bruikbaarheid van Fluorescentie Correlatie Spectroscopie (FCS) nagegaan voor deze toepassing. FCS is een techniek die gebruik maakt van zeer gevoelige fluorescentie detectoren teneinde het aantal fluorescent (voorbeeld groen of rood) gemerkte moleculen in een klein volume te bepalen samen met hun diffusietijd. In 'twee-kleuren' Fluorescentie Cross-correlatie Spectroscopie (FCCS) kan bovendien het aantal dubbel fluorescent (groen en rood) gemerkte moleculen worden bepaald. FCCS kan dus worden aangewend om de afbraak van dubbel fluorescent gemerkte ONs te volgen aan de hand van een daling van het aantal dubbel fluorescent gemerkte deeltjes. Bovendien kan er worden verwacht dat de kleinere degradatieproducten een snellere diffusie vertonen. 20 of 40 basenparen lange ONs met een nuclease gevoelige phosphodiester ruggengraat (PO20-ONs of PO40-ONs) of 20 basenparen lange ONs met een nuclease resistente phosphothioate ruggengraat (PS20-ONs) werden dubbel fluorescent gemerkt met een rhodamine groen fluorofoor (groene fluorescentie) op hun 3' uiteinde en een Cy5 fluorofoor (rode fluorescentie) op hun 5' uiteinde. De afbraak van de ONs werd onderzocht in buffer na incubatie met de nucleasen DNase I, DNase II, in cytosolisch celextract en in levende cellen na micro-injectie in het cytoplasma. Tot onze verbazing was 'twee-kleuren' FCCS niet in staat om het aantal dubbel fluorescent gemerkte ONs in oplossing accuraat te bepalen. Uit de analyse van de geregistreerde groene en rode fluorescentie kon worden afgeleid dat Fluorescentie Resonantie Energie Transfer (FRET) optrad tussen het rhodamine groen en het Cy5 fluorofoor. Bij FRET wordt na excitatie van het rhodamine groen, donor fluorofoor een deel van de excitatie energie overgedragen naar het Cy5, acceptor fluorofoor. Dit resulteert in een daling van de groene fluorescentie en een stijging van de rode fluorescentie ten opzichte van de situatie waarin FRET niet optreedt. Een belangrijke vereiste voor FCCS is dat de fluorescentie van het ene fluorofoor niet wordt beïnvloed door de aan- of afwezigheid van het andere fluorofoor. Dit verklaart waarom in het geval van FRET tussen beide fluoroforen FCCS niet geschikt bleek te zijn om het aantal intacte, dubbel fluorescent gemerkte ONs te volgen in functie van de tijd.

Het optreden van FRET in de dubbel fluorescent gemerkte ONs bleek echter op een andere manier geschikt om de afbraak van de ONs te volgen. Een belangrijke voorwaarde voor FRET is dat de beide fluoroforen zich in elkaars nabijheid bevinden. Wanneer de ruggengraat van de ONs degradeert, is aan deze voorwaarde echter niet meer voldaan. De afbraak van de ONs, en dus het verdwijnen van FRET, kon gemakkelijk gevolgd worden aan de hand van de verhouding tussen de rode (acceptor) fluorescentie en de groene (donor) fluorescentie (R/G ratio) in functie van de tijd bij excitatie van het rhodamine groen fluorofoor. De gevoelige detectoren van het FCS instrument bleken zeer geschikt om de groene en rode fluorescentie intensiteiten te bepalen en dit zowel in buffer als na micro-injectie van de ONs

in levende cellen. FCS biedt bovendien het voordeel dat de fluorescentie van een enkele molecule kan worden gedetecteerd. Hierdoor kan de R/G ratio ook bepaald worden in die situaties waar de intracellulaire concentratie van fluorescent gemerkte moleculen te laag is om te worden gedetecteerd met conventionele FRET microscopie, zoals het geval kan zijn na intracellulaire toediening van ONs met niet-virale dragers.

In een volgende stap werd FCS aangewend om de bescherming van dubbel fluorescent gemerkte ONs na te gaan wanneer deze zijn gebonden aan niet-virale dragers zoals kationische lipide-partikels (liposomen) of kationische polymeren. Wanneer deze kationische dragers worden gemengd met de negatief geladen ONs, worden spontaan complexen gevormd door elektrostatische interacties. Deze complexen hebben als doel de opname en vrijgave van de ONs in de doelcellen te verhogen. Bovendien dienen de ONs, gebonden aan de niet-virale drager, beschermd te worden tegen afbraak in de extracellulaire en intracellulaire omgeving. In **Hoofdstuk 3** werd de bescherming van ONs nagegaan na complexatie met kationische liposomen die frequent worden gebruikt in het kader van antisense therapie. Hiertoe werden dubbel fluorescent gemerkte PO40-ONs gecomplexeerd met zowel gepegyleerde als niet-gepegyleerde liposomen en werd hun afbraak gevolgd aan de hand van de R/G ratio met behulp van FCS. Pegylatie, door koppeling van polyethyleenglycol (PEG) aan het oppervlak van de liposomen, is een frequent aangewende strategie om de extracellulaire eigenschappen van lipide/DNA complexen (lipoplexen) te verbeteren. Pegylatie van lipoplexen verhindert hun aggregatie en opsonisatie door het reticulo endotheliaal systeem, wat hun circulatietijd in de bloedbaan doet toenemen. Op intracellulair niveau blijkt pegylatie echter een aantal negatieve invloeden te hebben, zoals het verminderen van de endosomale vrijstelling van de gepegyleerde lipoplexen. In Hoofdstuk 3 konden we waarnemen dat pegylatie ook een invloed heeft op de bescherming tegen degradatie die gepegyleerde en niet-gepegyleerde liposomen bieden aan de gecomplexeerde ONs. Niet-gepegyleerde liposomen vertoonden initieel een goede bescherming van de gecomplexeerde ONs tegen afbraak, hetgeen overeenkomt met het in de literatuur beschreven mechanisme van lipoplex formatie. Na binding van de ONs aan de kationische liposomen induceren de ONs het samensmelten van verschillende niet-gepegyleerde liposomen. Dit resulteert in de vorming van multilamellaire lipoplexen waarin de ONs gevangen zitten tussen de opeenvolgende lipide-dubbellagen van de individuele liposomen (zie Hoofdstuk 3, Figuur 11A). Bijgevolg worden de gecomplexeerde ONs afgeschermd van de omgeving waarin de nucleasen zich bevinden. We konden echter vaststellen dat de bescherming van de ONs tegen afbraak afnam naarmate de incubatietijd (enkele uren) van de lipoplexen toenam. Aan de hand van de fluorescentie fluctuaties, zoals geregistreerd met het FCS instrument, kon worden aangetoond dat niet-gepegyleerde lipoplexen aggregeren in functie van de tijd met een graduele vrijstelling van de ONs tot

gevolg (zie Hoofdstuk 3, Figuur 8). Dit bracht ons tot de conclusie dat niet de gecomplexeerde ONs, maar eerder de vrijgestelde ONs toegankelijk werden voor afbraak door nucleasen.

In het geval van gepegyleerde liposomen toonde de daling van de R/G ratio in functie van de tijd aan dat een groot deel van de gecomplexeerde ONs onmiddellijk werd afgebroken na blootstelling van de lipoplexen aan nucleasen. Dit duidt erop dat, in tegenstelling tot de niet-gepegyleerde lipoplexen, de ONs in gepegyleerde lipoplexen nog steeds toegankelijk zijn voor afbraak door nucleasen. In de literatuur is zo goed als geen informatie terug te vinden betreffende het mechanisme van complexvorming tussen ONs en gepegyleerde liposomen. We stelden echter een mechanisme voor betreffende de formatie van gepegyleerde lipoplexen dat de substantiële initiële afbraak van de gecomplexeerde ONs kan verklaren (zie Hoofdstuk 3, Figuur 11B). Naar analogie met de niet-gepegyleerde liposomen kan worden verondersteld dat de ONs in eerste instantie aan het oppervlak van de gepegyleerde liposomen binden. De aanwezigheid van de PEG-ketens aan het oppervlak verhindert echter de versmelting van verschillende gepegyleerde liposomen, met als gevolg dat de insluiting van ONs tussen opeenvolgende lipide-dubbellagen van de gepegyleerde liposomen wordt voorkomen. Bijgevolg blijven de ONs onbeschermd aan het oppervlak van de individuele gepegyleerde liposomen, waar ze nog steeds in contact kunnen komen met de omgeving waarin de nucleasen zich bevinden.

Naast kationische liposomen worden ook vaak kationische polymeren aangewend als niet-virale drager in antisense therapie. Een frequent onderzocht kationisch polymeer is polyethyleenimine (PEI). Ook voor PEI is pegylatie een veel voorkomende strategie om de oplosbaarheid te bevorderen, de cytotoxiciteit te verminderen en de aggregatie in de bloedstroom met klaring van de PEI/DNA complexen (polyplexen) te vermijden. In **Hoofdstuk 4** werd geëvalueerd in welke mate de bescherming van de gecomplexeerde ONs tegen enzymatische afbraak wordt beïnvloed door pegylatie van PEI. Hiertoe werden dubbel fluorescent gemerkte PO40-ONs gecomplexeerd met zowel gepegyleerde als niet-gepegyleerde PEI polymeren en werd hun afbraak gevolgd aan de hand van de R/G ratio met behulp van FCS. Zowel PEI als PEG-PEI vertoonden initieel een goede bescherming van de ONs tegen enzymatische afbraak: meer dan 70% van de gecomplexeerde ONs bleef intact in de aanwezigheid van nucleasen. In de PEI polyplexen werd deze bescherming behouden gedurende de 30 uren incubatietijd met het DNase I enzym. In de PEG-PEI polyplexen werd uiteindelijk tot 70% van de gecomplexeerde ONs afgebroken gedurende de 30 uren incubatietijd. Naar analogie met de lipide-gebaseerde niet-virale dragers, bleek pegylatie dus ook de beschermende eigenschappen van polymeer-gebaseerde niet-virale dragers te verminderen. Opnieuw kon een verklaring worden gevonden in de complexvorming tussen ONs en PEI en PEG-PEI polymeren. De polyplexen bestaan in

essentie uit een kern waarin verschillende ON-strengen en verschillende polymeerketens door elektrostatische interacties bij elkaar worden gehouden. In het geval van PEG-PEI, wordt deze kern bovendien omgeven door een mantel van PEG-ketens. De initiële degradatie van de gecomplexeerde ONs wijst erop dat een fractie van de gecomplexeerde ONs zich aan de rand van de polyplex kern bevindt, zowel in PEI als in PEG-PEI gebaseerde polyplexen. In het geval van PEG-PEI blijken echter meerdere ONs toegankelijk te worden voor enzymatische afbraak in de loop van het incubatieproces. Er kan verwacht worden dat de elektrostatische interacties tussen de ONs en de polymeerketens in de polyplexen continu kunnen verbroken en terug aangegaan worden, met een voortdurende reorganisatie van de polyplex kern tot gevolg. Tijdens dit proces kunnen intacte ONs uit het binnenste van de polyplex kern vermoedelijk relokaliseren naar het oppervlak van de kern waar ze bijgevolg toegankelijk worden voor enzymatische afbraak. Een grondige analyse van de fluorescentie fluctuatieprofielen, zoals geregistreerd met het FCS instrument, duidde erop dat de ONs minder ‘sterk’ gebonden zijn in de kern van de PEG-PEI polyplexen. Aangezien de elektrostatische interacties tussen PEG-PEI polymeren en ONs gemakkelijker kunnen verbroken worden, kan dit verklaren waarom een groter deel van de gecomplexeerde ONs tijdens het incubatieproces naar het oppervlak van de polyplex kern relokaliseert, waar ze vervolgens kunnen worden afgebroken door nucleasen.

Zowel in Hoofdstuk 3 als 4 werd aangetoond dat FCS uitermate geschikt is om de bescherming van ONs tegen enzymatische afbraak na te gaan en dit zowel met lipide-gebaseerde als met polymeer-gebaseerde niet-virale dragers. Enige voorzichtigheid was echter geboden bij de interpretatie van de R/G ratio van de gecomplexeerde ONs. Bij complexatie werden multimoleculaire complexen gevormd door associatie van vele dubbel fluorescent gemerkte ONs en vele liposomen of polymeerketens in respectievelijk de lipoplexen en de polyplexen. Door de compactie van de ONs in de complexen bleek het mogelijk dat FRET niet enkel optrad tussen de fluoroforen van een enkele ON-streng, maar ook tussen naburig gecomplexeerde ONs. In dit geval kon FRET dus ook optreden wanneer de fluoroforen van gedegradeerde ONs zich in elkaars nabijheid bevonden. Bijgevolg was het FRET signaal en dus de R/G ratio niet meer representatief voor het aantal intacte ONs in de complexen. Een ander fenomeen dat optrad ten gevolge van de compactie van de ONs was de onvoorziene uitdoving van de fluorescentie van het rhodamine groen en het Cy5 fluorofoor, zoals werd waargenomen voor de PEI-gebaseerde en PEG-PEI gebaseerde polyplexen (zie Hoofdstuk 4, Figuur 4). Het nagenoeg volledig wegvallen van het groene en rode fluorescent signaal zorgde ervoor dat de correlatie tussen de berekende R/G ratio en het al dan niet aanwezig zijn van intacte ONs in de polyplexen volledig verloren ging. Zowel voor lipide-gebaseerde als voor polymeer-gebaseerde niet-virale dragers bleek de R/G ratio van de gecomplexeerde ONs dus niet langer representatief te zijn voor hun integriteit.

Wanneer de ONs echter van de lipoplexen of polyplexen werden vrijgesteld door toevoeging van respectievelijk sodiumdodecylsulfaat (SDS) of dextraan sulfaat, kon de R/G ratio van de vrijgestelde ONs opnieuw aangewend worden om hun afbraak te evalueren. Daarom werden de ONs steeds vrijgesteld van de complexen (na een bepaalde inwerktijd en inhibitie van de aanwezige nucleasen) vooraleer de R/G ratio werd bepaald.

Een belangrijke vraag in dit proefschrift was in welke mate de afbraak van DNA moleculen aan de basis ligt van het uitblijven van een therapeutisch effect. In **Hoofdstuk 5** werd de biologische activiteit nagegaan van nuclease gevoelige PO-ONs en nuclease resistente PS-ONs na toediening met niet-gepegyleerde liposomen. We stelden vast dat enkel PS-ONs gecomplexeerd met niet-gepegyleerde liposomen in staat waren de productie van het doelwit proteïne te verminderen. De bescherming van PO-ONs tegen enzymatische afbraak door niet-gepegyleerde liposomen, zoals aangetoond in Hoofdstuk 3, bleek dus niet te resulteren in een biologisch effect. Om deze waarnemingen te verklaren werden, na toediening van de ONs aan de cellen met niet-gepegyleerde liposomen, de intracellulaire vrijgave en afbraak van dubbel fluorescent gemerkte PO-ONs en PS-ONs gevolgd met behulp van FCS en confocale microscopie. Niet-gepegyleerde lipoplexen werden efficiënt in de cellen opgenomen door endocytose. Aangezien na endocytose de lipoplexen aanwezig zijn in endosomale vesikels, dienden de lipoplexen uit de endosomen te ontsnappen om degradatie in de lysosomen te vermijden. Bovendien dienden de ONs te worden vrijgegeven in het cytoplasma om hun therapeutisch effect te kunnen uitoefenen. We stelden vast dat de endosomale vrijgave van niet-gepegyleerde lipoplexen gepaard ging met een efficiënte vrijgave van zowel de PO-ONs als de PS-ONs in het cytoplasma van de cellen. De vrijgestelde ONs accumuleerden vervolgens snel in de celkern. Uit zowel confocale microscopie als uit de R/G ratio kon worden afgeleid dat de vrijgestelde ONs snel werden afgebroken in het geval van PO-ONs, terwijl intacte PS-ONs gedetecteerd werden gedurende minstens 8 uur volgend op hun toediening met niet-gepegyleerde lipoplexen. Aangezien de nog gecomplexeerde PO-ONs grotendeels intact bleken te zijn, wees dit erop dat de degradatie slechts plaats vond na hun intracellulaire vrijgave van de niet-gepegyleerde lipoplexen. Niettegenstaande de goede bescherming tegen afbraak in de niet-gepegyleerde lipoplexen bleek de snelle degradatie van de vrijgestelde PO-ONs dus aan de oorsprong te liggen van het uitblijven van een antisense effect. Dit in tegenstelling tot de vrijgestelde PS-ONs, die voldoende lang intact bleven in het intracellulaire milieu om een biologisch effect teweeg te brengen.

Wanneer de antisense activiteit van PO-ONs en PS-ONs werd nagegaan na toediening met gepegyleerde liposomen, bleken de PO-ONs, noch de PS-ONs de productie van het doelwit proteïne te doen afnemen. Naar analogie met Hoofdstuk 5 werd in **Hoofdstuk 6** de intracellulaire vrijgave en afbraak van dubbel fluorescent gemerkte PO-ONs

en PS-ONs nagegaan na toediening met gepegyleerde liposomen. Zoals niet-gepegyleerde lipoplexen werden de gepegyleerde lipoplexen efficiënt opgenomen in de cellen door endocytose. De gepegyleerde lipoplexen bleken echter niet in staat de PO-ONs te beschermen tegen degradatie in de intracellulaire omgeving. Dit komt overeen met de vooropgestelde opbouw van gepegyleerde lipoplexen in Hoofdstuk 3, waarbij de PO-ONs zich aan het oppervlak van de gepegyleerde liposomen bevonden en bijgevolg nog steeds toegankelijk waren voor intracellulaire nucleasen. De afbraak van PO-ONs in het intracellulair milieu zou dus aan de basis kunnen liggen van het uitblijven van een antisense effect. Met de nuclease resistente PS-ONs werd er echter ook geen antisense effect vastgesteld, alhoewel FCS en confocale microscopie duidelijk aantoonden dat de PS-ONs intact bleven in de intracellulaire omgeving. Een verklaring voor het uitblijven van een antisense effect kon worden gevonden in het niet optreden van de endosomale vrijgave van de gecomplexeerde ONs. Bijgevolg bleven de ONs, aanwezig in de endosomale vesikels, afgeschermd van hun therapeutisch doelwit dat zich in het cytoplasma of de kern van de cellen bevindt. De PEG-ketens aan het oppervlak van de gepegyleerde lipoplexen zijn verantwoordelijk voor het verhinderen van de endosomale vrijstelling van de gecomplexeerde ONs. Het is bekend dat het contact tussen de lipiden van de lipoplexen en de lipiden van de endosomale membraan een belangrijke factor is voor de verstoring van de endosomale membraan met vrijstelling van de gecomplexeerde DNA moleculen in het cytoplasma tot gevolg. De PEG-ketens aan het oppervlak van de gepegyleerde liposomen voorkomen echter deze lipide-lipide interacties waardoor ze de cytoplasmatische vrijgave van de gecomplexeerde ONs verhinderen. Dit verklaart waarom zowel nuclease gevoelige PO-ONs als nuclease resistente PS-ONs niet in staat waren een antisense effect teweeg te brengen na toediening met gepegyleerde liposomen. Het inhiberend effect van de PEG-ketens op de endosomale vrijstelling kan worden overkomen door gebruik te maken van reversibele pegylatie, waarbij de PEG-ketens het oppervlak van de liposomen verlaten in de endosomale vesikels. De snelle intracellulaire afbraak van PO-ONs doet echter de vraag rijzen of het al bij al mogelijk is om geschikte toedieningssystemen te ontwikkelen die de PO-ONs in staat zullen stellen een antisense effect uit te voeren. Bovendien kan met de recente opgang van het smal interferentie RNA (siRNA) de toekomst van antisense ONs in het algemeen worden in vraag gesteld. siRNAs zijn kleine, dubbelstrengige RNA moleculen die met behulp van het ‘RNA induced silencing complex’ (RISC) zeer efficiënt de expressie van een doelwit proteïne kunnen stil leggen. Bovendien blijken dubbelstrengige RNA moleculen vele malen stabieler in de intracellulaire omgeving dan de enkelstrengige PO-ONs. Alhoewel de toedieningsproblemen met siRNA in essentie dezelfde zijn als met antisense ONs, blijkt het siRNA veld een veel snellere vooruitgang te boeken. Dit terwijl het therapeutisch potentieel van antisense ONs reeds vele jaren wordt onderzocht, met slechts

enkele (bovendien weinig efficiënte) klinische toepassingen tot gevolg. Door hun grotere effectiviteit vertonen siRNAs echter ook meerdere neveneffecten zoals het inwerken op andere proteïnen dan het beoogde doelwit proteïne. Hierdoor valt nog af te wachten of de therapeutische mogelijkheden van het siRNA zullen ingelost worden en of de reeds lang gekende antisense ONs naar de achtergrond zullen verdwijnen.

Naast inhibitie van de productie van proteïnen met antisense therapie vindt gentherapie met plasmide DNA (pDNA) zijn toepassing in die situaties waar men bepaalde proteïnen intracellulair wenst aan te maken. Aangezien de sequentie van het toegediende pDNA de noodzakelijke informatie voor de productie van het gewenste proteïne bevat, is het van belang dat de pDNA moleculen intact blijven tijdens het toedieningsproces. De dubbelstrengige pDNA moleculen kunnen voorkomen in een supercoiled vorm (SC), een open circulaire vorm (OC) of in een lineaire vorm. In **Hoofdstuk 7** werd vastgesteld dat voornamelijk de SC vorm resulteert in de productie van het gewenste proteïne na toediening van de verschillende pDNA vormen aan cellen met niet-gepegyleerde liposomen. Nucleaire injecties van de verschillende pDNA vormen toonden aan dat, eens in de kern, de pDNA concentratie en niet de pDNA topologie de efficiëntie van de proteïne productie bepaalde. Bij injectie in het cytoplasma bleek echter zowel de concentratie als de pDNA topologie een rol te spelen: voornamelijk de hoogst geïnjecteerde pDNA concentraties resulteerden in proteïne productie, waarbij de SC pDNA topologie het meest efficiënt bleek. De efficiëntie nam bovendien sterk toe in cellen die een celdeling ondergingen in de periode na injectie, wat erop wijst dat de nucleaire membraan een grote barrière is in de toediening van pDNA moleculen. Aangezien de SC pDNA topologie het meest efficiënt bleek in het bereiken van de celkern, werd met behulp van gel electroforese nagegaan of een verschil in afbraak aan de oorsprong zou kunnen liggen van het hogere aantal SC pDNA moleculen dat de celkern bereikte. SC pDNA bleek echter minstens even snel af te breken als de OC of lineaire vorm. Vervolgens werden, met behulp van FCS, de diffusie-eigenschappen van het pDNA nagegaan. De nagenoeg twee maal tragere diffusie van de OC vorm in vergelijking met de SC vorm zou kunnen verklaren waarom SC pDNA efficiënter is in het bereiken van de celkern dan OC pDNA. Het lineaire pDNA vertoonde echter dezelfde diffusietijd als zijn SC analoog. In het geval van lineair pDNA diende de lagere efficiëntie ten opzichte van de SC vorm vermoedelijk gezocht te worden in de extra afbraak van het lineair pDNA door exonucleasen. De aanwijzingen dat pDNA moleculen zich, tijdens de celdeling, op efficiënte wijze een toegang verschaffen tot de celkern doen vermoeden dat niet-virale dragers die hun pDNA, tijdens de celdeling, optimaal in de kernen van de dochtercellen binnenloodsen, de efficiëntie van gentherapie sterk zouden kunnen doen toenemen. Verder blijft de vereiste dat het pDNA, in de periode die de celdeling voorafgaat, maximaal dient beschermd te worden tegen afbraak in het cytoplasma. Een interessante strategie zou bijgevolg kunnen zijn om

DNA nanopartikels te ontwikkelen die tijdens de celdeling worden ingesloten in de celkern van de dochtercellen, waarna ze rechtstreeks hun pDNA kunnen vrijstellen in de celkern van de dochtercellen. Hierdoor zou zowel de afbraak van het pDNA in het cytoplasma als de barrière van het nucleaire membraan kunnen vermeden worden.

Dit proefschrift toonde aan dat FCS metingen kunnen aangewend worden in de vraag waarom een bepaalde niet-virale drager al dan niet geschikt is om een biologisch effect teweeg te brengen. Aangezien FCS metingen uitgevoerd worden in een zeer beperkt volume, vele malen kleiner dan de dimensies van een cel, wordt voornamelijk informatie bekomen over de specifieke intracellulaire situatie in een welbepaald celcompartiment. Dit in tegenstelling tot conventionele microscopische beeldvorming of het recent ontwikkelde Single Particle Tracking (SPT) die de intracellulaire processen in een volledige cel in beeld brengen. Er wordt verwacht dat de combinatie van conventionele microscopie met geavanceerde microscopie systemen zoals FCS en SPT, elk met hun specifieke voor- en nadelen, in de toekomst verdere doorbraken zal blijven verzekeren in de complexe studie van het intracellulair gedrag van DNA/drager complexen. Onze verwachting is dat de toenemende kennis betreffende de intracellulaire barrières in antisense- en gentherapie op haar beurt zal bijdragen tot het rationeel ontwerpen van een nieuwe generatie van ‘intelligente’ DNA toedieningssystemen.

CURRICULUM VITAE

CURRICULUM VITAE – KATRIEN REMAUT

PERSONALIA

Surname:	REMAUT
First name:	KATRIEN
Nationality:	Belgian
Place & date of birth:	Ghent, November 10th 1978
Marital status:	married
Private address:	Prinsenhof 105 9000 Ghent, Belgium
Tel. :	(+32) 9 329 93 65
Professional address:	Laboratory of General Biochemistry and Physical Pharmacy Ghent University Harelbekestraat 72 9000 Ghent Belgium
Tel.:	(+32) 9 264 80 78
Fax. :	(+32) 9 264 81 89
E-mail:	katrien.remaut@ugent.be
URL :	www.biofys.ugent.be

LANGUAGE

Dutch:	mother tongue
English:	fluent
French:	good

DEGREES

2 July 1998:	Diploma of the First Cycle Pharmacist with the Greatest Distinction, Ghent University
29 June 2001:	Pharmacist with the Greatest Distinction, Ghent University

AWARDS & SCHOLARSHIPS

29 June 2001:	Graduation Award 'Bank van Breda'
Feb 2003:	Awarded an International Travel Scholarship from the FIP Foundation For Education and Research to present a poster at the Winter Symposium & 11th International Symposium on Recent Advances in Drug Delivery Systems, Salt Lake City, Utah, USA
July 2003:	Highlights of student posters Award at the 30th Annual Meeting of the Controlled Release Society in Glasgow, Scotland, July 19-23, 2003
Oct 2004:	Winner of the AIO competition at the FIGON Dutch Medicines Days, 7-8 October 2004, Lunteren, The Netherlands
Jan – Feb 2005:	Funds from the Research Foundation Flanders for stay abroad at the ALMF, EMBL, Heidelberg, Germany

PUBLICATIONS IN JOURNALS OR BOOKS WITH PEER REVIEW

Remaut, K., Sanders, N., De Geest, B.G., Braeckmans, K., Demeester, J. and De Smedt, S.C. Material challenges for extracellular, cytoplasmatic and nuclear delivery of nucleic acids. *Mat. Sci. Eng. R.* **2007**, invited review, submitted.

Remaut, K., Lucas, B., Raemdonck, K., Demeester, J. and De Smedt, S.C. Can we better understand the intracellular behavior of DNA nanoparticles by Fluorescence Correlation Spectroscopy. *J. Control. Release* **2007**, in press.

Remaut, K., Lucas, B., Raemdonck, K., Braeckmans, K., Demeester, J. and De Smedt, S.C. Protection of oligonucleotides against enzymatic degradation by pegylated and non-pegylated branched polyethyleneimine. *Biomacromolecules* **2007**, in press.

Braeckmans, K., **Remaut, K.,** Vandenbroucke, R., Demeester, J. and De Smedt, S.C. Line FRAP with the confocal laser scanning microscope for diffusion measurements in small regions of 3-D samples. *Biophysical J.* **2007**, 92, 2172-2183.

Remaut, K., Lucas, B., Braeckmans, K., Demeester, J. and De Smedt, S.C. Pegylation of liposomes favours the endosomal degradation of the phosphodiester oligonucleotides they are carrying. *J. Control. Release* **2007**, 117, 256-266.

Remaut, K., Sanders, N.N., Fayazpour, F., Demeester, J. and De Smedt, S.C. Influence of plasmid DNA topology on the transfection properties of DOTAP/DOPE lipoplexes. *J. Control. Release* **2006**, 115, 335-343.

Raemdonck, K., **Remaut, K.,** Lucas, B., Sanders, N.N., Demeester, J. and De Smedt, S.C. In situ analysis of single-stranded and duplex siRNA integrity in living cells. *Biochemistry* **2006**, 45, 10614-10623.

Van Drooge, D., Braeckmans, K., Hinrichs W.L.J., **Remaut, K.,** De Smedt S.C. and Frijlink H.W. Characterization of the mode of incorporation of lipophilic compounds in solid dispersions at the nano-scale using Fluorescence Resonance Energy Transfer (FRET). *Macromol. Rapid. Comm.* **2006**, 27, 1149-1155.

Braeckmans, K., Stubbe, B.G., **Remaut, K.**, Demeester, J. and De Smedt, S.C. Anomalous photobleaching in fluorescence recovery after photobleaching measurements due to excitation saturation - a case study for fluorescein. *J. Biomed. Opt.* **2006**, 11, 044013.

Remaut, K., Lucas, B., Braeckmans, K., Sanders, N.N., Demeester, J. and De Smedt, S.C. On the delivery of phosphodiester oligonucleotides: can DOTAP/DOPE liposomes do the trick? *Biochemistry* **2006**, 45, 1755-1764.

Remaut, K., Lucas, B., Braeckmans, K., Sanders, N.N., Demeester, J. and De Smedt, S.C. Protection of oligonucleotides against nucleases by pegylated and non-pegylated liposomes as studied by Fluorescence Correlation Spectroscopy. *J. Control. Release* **2005**, 110, 212-226.

Lucas, B., **Remaut, K.**, Sanders, N.N., Braeckmans, K., De Smedt, S.C. and Demeester, J. Studying the intracellular dissociation of polymer-oligonucleotide complexes by dual color fluorescence fluctuation spectroscopy and confocal imaging. *Biochemistry* **2005**, 44, 9905-9912.

Lucas, B., **Remaut, K.**, Sanders, N.N., Braeckmans, K., De Smedt, S.C. and Demeester, J. Towards a better understanding of the dissociation behavior of liposome-oligonucleotide complexes in the cytosol of cells. *J. Control. Release* **2005**, 103, 435-450.

Remaut, K., Lucas, B., Braeckmans, K., Sanders, N.N., De Smedt, S.C. and Demeester, J. FRET-FCS as a tool to evaluate the stability of oligonucleotides drugs after intracellular delivery. *J. Control. Release* **2005**, 103, 259-271.

De Smedt, S.C, **Remaut, K.**, Lucas, B., Braeckmans, K., Sanders, N.N. and Demeester, J. Studying biophysical barriers to DNA delivery by advanced fluorescence microscopy. *Adv. Drug Deliver. Rev.* **2005**, 57, 191-210.

Lucas, B., **Remaut, K.**, Braeckmans, K., Haustraete, J., De Smedt, S.C. and Demeester, J. Studying pegylated DNA complexes by dual color fluorescence fluctuation spectroscopy. *Macromolecules* **2004**, 37, 3832-3840.

Lucas, B., Van Rompaey, E., **Remaut, K.**, Sanders, N., De Smedt, S.C. and Demeester, J. On the biological activity of anti-ICAM-1 oligonucleotides complexed to non-viral carriers. *J. Control. Release* **2004**, 96, 207-219.

ABSTRACTS IN JOURNALS OR BOOKS WITH PEER REVIEW

Remaut, K., Lucas, B., Braeckmans, K., Sanders, N.N., De Smedt, S.C. and Demeester, J. Fluorescence energy transfer to study the degradation of double-labeled oligonucleotides. *J. Control. Release* **2005**, 101, 352-354.

Lucas, B.L., **Remaut, K.,** De Smedt, S.C. and Demeester, J. Studies on the intracellular release of genetic drugs from pharmaceutical carriers. *J. Control. Release* **2005**, 101, 402-405.

Cornelissen, B., **Remaut, K.,** Kersemans, V., Oltenfreiter, R., Burvenich, I. and Slegers, G. 123I-EGF internalisation in tumour cells in vitro is inhibited by farnesyltransferase inhibitor therapy: possible target for early therapy response prediction. *Eur. J. Nucl. Med. Mol. I.* **2004**, 31, S391-S391.

Lucas, B.L., **Remaut, K.,** De Smedt, S.C. and Demeester, J. Studies on the intracellular release of genetic drugs from pharmaceutical carriers. *Abstr. Paper. Am. Chem. Soc.* **2003**, 266, U177-U177.

Lucas, B.L., **Remaut, K.,** De Smedt, S.C. and Demeester, J. Studies on the intracellular release of genetic drugs from pharmaceutical carriers. *Biochemistry* **2003**, 42, 8631-8632.

ABSTRACTS OF LECTURES WITH ACTIVE CONTRIBUTION

Fluorescence Resonance Energy Transfer to study the degradation of double labelled oligonucleotides.
***Remaut, K.,** Lucas, B., Braeckmans, K., Sanders, N.N., De Smedt, S.C. and Demeester, J.
11th Forum of Pharmaceutical Sciences (8-9 May 2003, Spa, Belgium)

Fluorescence Correlation Spectroscopy to study the degradation of double labelled oligonucleotides.
***Remaut, K.,** Lucas, B., Braeckmans, K., Sanders, N.N., De Smedt, S.C. and Demeester, J.
Biopharmacy Day (23 May 2003, Utrecht, the Netherlands)

Towards a better understanding of the intracellular behaviour of nanoscopic drug particles.
De Smedt, S.C., Lucas, B., ***Remaut, K.,** Sanders, N.N, Braeckmans, K. and Demeester, J.
European Workshop on Fluorescence Correlation Spectroscopy techniques (24-25 March 2005, Le Kremlin Bicetre, France). Invited.

ABSTRACTS OF LECTURES WITHOUT ACTIVE CONTRIBUTION

Studies on the intracellular release of genetic drugs from pharmaceutical carriers.
*Lucas, B., **Remaut, K.,** De Smedt, S.C., Vandenbroucke, R. and Demeester, J.
8th annual meeting of the American Society of Gene Therapy (1-5 June 2005, St Louis, USA)

New drug delivery opportunities for micro- and nanogels?
*De Smedt, S.C., De Geest, B.G., Van Thienen, T., **Remaut, K.** and Demeester, J.
6th International Conference and workshop on Cell culture and in vitro models for drug absorption and delivery (1-10 March 2006, Saarbrucken, Germany). Invited.

Studies on the intracellular release of genetic drugs from pharmaceutical carriers.
*Lucas, B., **Remaut, K.,** Sanders, N.N., Braeckmans, K., De Smedt, S.C. and Demeester, J.
Focus on Microscopy (9-12 April 2006, Perth, Australia)

Fluorescence recovery after photobleaching with the confocal laser scanning microscope for mobility measurements in 3-D samples.
*Braeckmans, K., Peeters, L., **Remaut, K.,** Sanders, N., De Smedt, S.C. and Demeester, J.
Focus on Microscopy (9-12 April 2006, Perth, Australia)

In situ analysis of single-stranded and duplex siRNA integrity in living cells.
*Raemdonck, K., **Remaut, K.,** Lucas, B., Sanders, N.N., Demeester, J. and De Smedt, S.C.
Spring Meeting of the Belgian-Dutch Biopharmaceutical Society (22 May 2006, Beerse, Belgium)

Can we better understand the intracellular behaviour of nucleic acid containing nanoparticles by fluorescence correlation spectroscopy?
*De Smedt, S.C., Lucas, B., **Remaut, K.,** Raemdonck, K., Braeckmans, K., Sanders, N.N. and Demeester, J.
Nanomedicine and Drug Delivery Symposium (8-10 October 2006, Ohama, Nebraska, USA). Invited.

Wanted and unwanted properties of surface-pegylated nucleic acid nanoparticles.
*De Smedt, S.C., Peeters, L., Lentacker, I., **Remaut, K.,** Sanders, N.N. and Demeester, J.
13th International Symposium on Recent Advances in Drug Delivery Systems (26-28 February 2007, Salt Lake City, Utah, USA)

ABSTRACTS OF POSTERS WITH ACTIVE CONTRIBUTION

Studies on the intracellular release of genetic drugs from pharmaceutical carriers.
*Lucas, B., **Remaut, K.,** Sanders, N.N., Braeckmans, K., De Smedt, S.C. and Demeester, J.
Winter Symposium & 11th International Symposium on Recent Advances in Drug Delivery Systems (3-6 March 2003, Salt Lake City, Utah, USA)

FRET to study the degradation of double labelled oligonucleotides.
***Remaut, K.,** Lucas, B., Braeckmans, K., Sanders, N.N., De Smedt, S.C. and Demeester, J.
30th Annual Meeting of the Controlled Release Society (19-23 July 2003, Glasgow, Scotland)
8th European Symposium on Controlled Drug Delivery (7-9 April 2004, Noordwijk aan Zee, the Netherlands)
RNAi Europe (18-19 October 2004, London, Great Britain)

Fluorescence Correlation Spectroscopy to study the degradation of oligonucleotides, both naked and complexed to cationic carriers.
***Remaut, K.,** Lucas, B., Braeckmans, K., Sanders, N.N., De Smedt, S.C. and Demeester, J.
First young scientist day (19 May 2005, Ghent, Belgium)
Biopharmacy Day (20 May 2005, Ghent, Belgium)
9th European Symposium on Controlled Drug Delivery (5-7 April 2006, Noordwijk aan Zee, the Netherlands)

Real-time monitoring of single-stranded and duplex short interfering RNA integrity inside living cells.
*Raemdonck, K., **Remaut, K.,** Lucas, B., Sanders, N.N., Demeester, J. and De Smedt, S.C.
9th European Symposium on Controlled Drug Delivery (5-7 April 2006, Noordwijk aan Zee, the Netherlands)

ABSTRACTS OF POSTERS WITHOUT ACTIVE CONTRIBUTION

Towards a better understanding of the intracellular behaviour of nanoscopic drug particles.
*De Smedt, S.C., Lucas, B., **Remaut, K.,** Sanders, N.N., Braeckmans, K. and Demeester, J.
32nd Annual Meeting & Exposition of the Controlled Release Society (18-22 June 2005, Miami, Florida, USA)

Real-time monitoring of short interfering RNA (siRNA) integrity inside living cells.
*Raemdonck, K., **Remaut, K.,** De Smedt, S.C. and Demeester, J.
RNAi europe (28-29 September 2005, Amsterdam, the Netherlands)

Real-time monitoring of single-stranded and duplex short interfering RNA integrity inside living cells.
*Raemdonck, K., **Remaut, K.,** Lucas, B., Sanders, N.N., Demeester, J. and De Smedt, S.C.
9th Annual Meeting of the American Society of Gene Therapy (31 May – 4 June 2006, Baltimore, USA)
33rd Annual meeting of the controlled release society (22-26 July 2006, Vienna, Austria)
13th International Symposium on Recent Advances in Drug Delivery Systems (26-28 February 2007, Salt Lake City, Utah, USA)

*presenting author

RESEARCH VISITS

1-6 July 2002: Personal microinjection course under guidance of Dr. R. Pepperkok and Dr. A. Girod at the Advanced Light Microscopy Facility (ALMF), EMBL, Heidelberg, Germany.

1-12 March 2004: Collaboration with the laboratory of Dr. R. Pepperkok at the Advanced Light Microscopy Facility (ALMF), EMBL, Heidelberg, Germany.

Jan – Feb 2005 : Collaboration with the laboratorium of Dr. R. Pepperkok at the Advanced Light Microscopy Facility (ALMF), EMBL, Heidelberg, Germany.